

UNCLASSIFIED

AD 296 753

*Reproduced
by the*

**ARMED SERVICES TECHNICAL INFORMATION AGENCY
ARLINGTON HALL STATION
ARLINGTON 12, VIRGINIA**



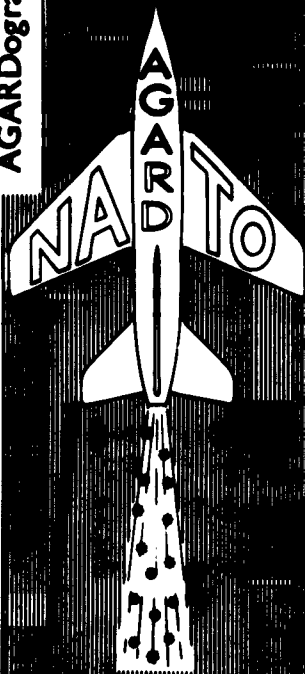
UNCLASSIFIED

NOTICE: When government or other drawings, specifications or other data are used for any purpose other than in connection with a definitely related government procurement operation, the U. S. Government thereby incurs no responsibility, nor any obligation whatsoever; and the fact that the Government may have formulated, furnished, or in any way supplied the said drawings, specifications, or other data is not to be regarded by implication or otherwise as in any manner licensing the holder or any other person or corporation, or conveying any rights or permission to manufacture, use or sell any patented invention that may in any way be related thereto.

296 753

CATALOGUE BY ASI/A 296 753

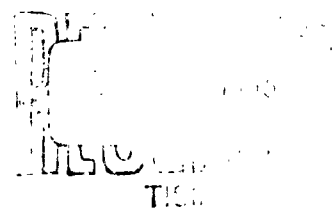
AGARDograph 64



AGARDograph 64

AGARDograph

A REVIEW OF MEASUREMENTS
ON AGARD CALIBRATION MODELS



NO. OTS NOVEMBER 1961

FOR AGARD REPRODUCTION

NORTH ATLANTIC TREATY ORGANIZATION
ADVISORY GROUP FOR AERONAUTICAL RESEARCH AND DEVELOPMENT
(ORGANISATION DU TRAITE DE L'ATLANTIQUE NORD)

A REVIEW OF MEASUREMENTS ON AGARD CALIBRATION MODELS

Editor:

R. Hills

Aircraft Research Association, Bedford, England

This is one of a series of Wind Tunnel AGARDographs concerned with wind tunnel design, operation, and test techniques. Professor Wilbur C. Nelson of the University of Michigan is the editor of the Series.

SUMMARY

An analysis has been made of measurements in various wind tunnels of AGARD Calibration Models A, B, C, D and E. The analysis has shown considerable scatter of results, particularly at transonic speeds, on Models B and C. When transition is fixed on the models, scatter is reduced and, where possible, reference curves are given to enable comparison to be made with any future tests.

SOMMAIRE

Une analyse a été faite des mesures effectuées dans de différentes souffleries sur les maquettes d'étalonnage A, B, C, D et E de l'AGARD. L'analyse a démontré un écart important dans les résultats obtenus, tout particulièrement aux vitesses transsoniques, sur les maquettes B et C. Lorsque le point de transition est fixé sur les maquettes, l'écart diminue; dans les cas où il a été possible, on a donné des courbes de référence, pour permettre d'établir une comparaison avec les résultats de tous essais futurs.

533.6.072

3b8b

CONTENTS

	Page
SUMMARY	111
SONNAIRE	111
GENERAL INTRODUCTION	v
PART I	
TESTS ON AGARD MODEL A by R. Nills	1
PART II	
A REVIEW OF MEASUREMENTS ON AGARD CALIBRATION MODEL B IN THE TRANSONIC SPEED RANGE by H. Valk and J.N. van der Zwaan	35
PART III	
A REVIEW OF MEASUREMENTS ON AGARD CALIBRATION MODEL B IN THE MACH NUMBER RANGE FROM 1.4 TO 8 by J.P. Hartsuiker	95
PART IV	
A REVIEW OF MEASUREMENTS ON AGARD CALIBRATION MODEL C IN THE TRANSONIC SPEED RANGE by H. Valk	137
PART V	
TESTS ON AGARD MODEL D by R. Nills	213
PART VI	
TESTS ON AGARD MODEL E by R. Nills	229

GENERAL INTRODUCTION

The need for comparison of different wind tunnel facilities was recognized as early as the nineteen twenties when the same airship model was tested in many of the wind tunnels in the world. This international programme was successful in highlighting some differences between these wind tunnels and reducing the uncertainty of comparison of results from different sources. Since in the period 1940-1950 a large number of new tunnels and new types of tunnels were built, a similar programme of comparative tests was suggested in 1952 by the Wind Tunnel and Model Testing Panel of AGARD, meeting in Rome, Italy. It was thought that models suitable for testing in supersonic tunnels would be particularly useful to determine the degree of variation in test results between the different tunnels and would enable the effects of changes in Reynolds number, turbulence, model size and model tolerances to be investigated.

Two models were selected at the 1952 meeting. AGARD Calibration Model A is a body of revolution designed by N.A.S.A. and designated by them as RM 10. This model had already been tested extensively in the U.S.A. and its drag characteristics were shown to be sensitive to boundary layer transition and the model was thus useful for comparisons based on drag results. It was intended that the model should be tested with and without stabilizing fins so that wind tunnel results could be compared with free-flight tests.

AGARD Model B is a configuration consisting of a delta wing mounted on a cylindrical body of revolution. The wing has a 4% thickness/chord ratio bi-convex section and the planform is an equilateral triangle. This model was selected as being suitable for the measurement of overall forces, particularly in supersonic tunnels.

At the Panel meeting in Paris in 1954, it was agreed to add a third calibration model - AGARD C. This model is identical to Model B except that the body is extended aft and a fin with a T-tail mounted on the top added. It was hoped that the addition of a horizontal tail surface would make it easier to detect reflected shock waves, since these would alter the pitching moment due to the tailplane. It was therefore thought that this model would be most suitable for tests in the transonic speed range.

AGARD Calibration Model D was agreed upon at the Panel meeting in Ottawa, Canada, in 1955. This model is an elementary wing alone designed to check comparative derivative measurements in low speed tunnels. It was thought that this model would provide a means of checking the different types of testing methods and mechanisms used in dynamic stability measurements. A similar model for dynamic stability tests in supersonic tunnels consisting of a thin delta with sharp leading and trailing edge was agreed later as AGARD Model F.

In view of the recent rapid development of various forms of testing in the hypersonic speed range, it was suggested that a hemisphere should be designated as AGARD Calibration Model E for testing in such facilities. Measurements of pressure distributions, stagnation temperature, heat transfer and normal aerodynamic coefficients should be compared.

In this AGARDograph, the results on the various models have been collected and analysed. A large number of tests have been done on Models A, B and C and a few tests on Models D and E. No tests have yet been reported on AGARD Model F. Detailed conclusions have been included in each section, but it is worthwhile summarizing the main points here.

The tests on Model B in the supersonic tunnels show on the whole reasonable agreement. The scatter of results obtained on Models B and C in various transonic facilities is larger than might have been hoped and is more than the figures which have been quoted for experimental accuracy. In a few cases the scatter may be due to inaccuracies in measuring techniques, but the major differences are probably due to changes in the state of the boundary layer. It was realized soon after the calibration models were specified that consistent results would only be obtained if transition was fixed near the leading edge of the wings and the nose of the body. Many of the tests have, however, been made with transition not fixed and these results, as might be expected, show the most scatter, not only of drag and base pressure but also of lift and pitching moments. Results with transition fixed are in general more consistent, but are still not as good as might be expected. Where possible, reference curves have been given in this report for the transition-fixed condition so that a comparison with any individual set of results can be made.

The tests have shown the importance of checking flow inclination and flow curvature in all parts of the working section of a wind tunnel. Lift and pitching moment were not always zero on the symmetrical Model B at zero incidence. Model C showed even larger discrepancies because changes in the flow over the base of the body caused changes in the flow angle over the tailplane, adding to any similar changes in flow angle at the tailplane due to the tunnel flow inclination.

The transonic tests on Models B and C have not shown any consistent effects near Mach number 1.0 of interference from the walls of the tunnels and it has not been possible to examine the comparative merits, for example, of slotted and perforated walls. It is evident that a different type of model is required for a test of this nature.

Only four tests have been reported on dynamic stability models at low speeds and few conclusions can be drawn. The two models proposed for this type of test should prove valuable in the future in checking the efficiency of various types of rigs which are being developed for dynamic stability measurements.

Hypersonic test facilities are now coming into operation fairly rapidly but there are not sufficient tests on hemispheres available yet to provide very much comparative data. The review which has been made here can only be regarded as a preliminary one and many more results should be forthcoming in the next year or so.

R. Hills

November 1961

PART I

TESTS ON AGARD MODEL A

by

R. Hills

Aircraft Research Association, Bedford, England

SUMMARY

An analysis has been made of various wind tunnel, flight and range measurements on a slender body of revolution. The tests covered a range of Reynolds numbers from 1×10^6 to 140×10^6 and Mach numbers from 0.85 to 6.9. With transition fixed near the nose of the body, the measurements of drag in the various facilities show reasonable agreement but, with a smooth model, there are wide variations due to differing transition positions.

CONTENTS

	Page
SUMMARY	2
LIST OF TABLES	4
LIST OF FIGURES	4
NOTATION	6
1. INTRODUCTION	7
2. RANGE OF TESTS	7
3. MODELS AND MEASUREMENTS	7
4. RESULTS AND DISCUSSION	8
4.1 Model Without Fins	8
4.2 Base Pressure Drag	8
4.3 Forebody Drag	10
4.4 Forebody Pressure Drag	10
4.5 Skin Friction	10
4.6 Drag with Fins	11
4.7 Lift and Pitching Moment	12
5. CONCLUSIONS	12
REFERENCES	13
TABLES	16
FIGURES	18

LIST OF TABLES

		Page
Table I	Details of Models	16
Table II	Miscellaneous Measurements of the Drag of AGARD Model A with Fins	17

LIST OF FIGURES

Fig.1	General configuration of AGARD Model A	18
Fig.2	AGARD Model A. Comparison of measured total drag coefficients	19
Fig.3(a)	Variation of critical sting length with Reynolds number (Fig.6 of Ref.27)	20
Fig.3(b)	Base-pressure coefficients as a function of sting diameter (Fig.7 of Ref.27)	21
Fig.3(c)	Variation of base-pressure coefficients with Reynolds number (Fig.11 of Ref.27)	22
Fig.4	AGARD Model A. Variation of base pressure with Mach number for three Reynolds numbers	23
Fig.5	AGARD Model A. Variation of forebody drag with Reynolds number (Ref.4)	24
Fig.6(a)	AGARD Model A. Variation of forebody drag with Mach number at two Reynolds numbers	25
Fig.6(b)	AGARD Model A. Variation of forebody drag with Mach number at $R = 4 \times 10^6$	26
Fig.7	AGARD Model A. Forebody pressures. Comparison of estimates and experiments	27
Fig.8(a)	AGARD Model A. Friction drag against Reynolds number at $M = 1.6$	28
Fig.8(b)	AGARD Model A. Friction drag against Reynolds number. $M = 2.0$ and 2.5	29
Fig.8(c)	AGARD Model A. Friction drag against Reynolds number. $M = 3.0$ to 7.0	30

		Page
Fig.9	AGARD Model A with fins. Variation of drag with transition location	31
Fig.10(a)	AGARD Model A. Variation of lift slope with Mach number	32
Fig.10(b)	AGARD Model A. Variation of centre of pressure with Mach number	33
Fig.11	AGARD Model A with fins. Variation of lift slope and centre of pressure	34

NOTATION

A	body frontal area
A_b	body base area
C_{Db}	base drag coefficient, $= - (A_b/A) C_{pb}$
C_{DF}	forebody drag coefficient, $= C_{DT} - C_{Db}$
C_{Df}	forebody friction drag coefficient, $= C_{DF} - C_{Dp}$
C_{Dp}	forebody pressure drag coefficient
C_{DT}	total drag coefficient, $= D/(qA)$
C_f	flat plate skin friction coefficient
C_p	specific heat at constant pressure
C_{pb}	base pressure coefficient relative to free stream static pressure, $= (p_b - p)/q$
C_L	lift coefficient, $= L/(\frac{1}{2}\rho V^2 A)$
D	measured drag
d_b	body base diameter
d_s	sting diameter at body base
k	coefficient of heat conduction
l	length of body
M	Mach number
q	dynamic pressure, $= \frac{1}{2}\rho V^2$
R	Reynolds number based on body length
T_1	temperature at outer edge of boundary layer
T_w	temperature at body wall
α	angle of incidence (degrees)
μ	coefficient of viscosity
ω	exponent in viscosity-temperature relationship (i.e. $\mu \propto T^\omega$)

TESTS ON AGARD MODEL A

1. INTRODUCTION

AGARD Model A is a slender body of revolution which was selected as a suitable calibration model for testing and checking supersonic wind tunnels. As NACA RM 10 body, this model was tested in a number of wind tunnels and in flight before it was selected as an AGARD calibration model.

Some collections and analyses of results have already been made². In this paper this work has been used extensively to provide a comprehensive summary on all the work done on this model to-date.

2. RANGE OF TESTS

Figure 1 gives the details of the model. Most of the tunnel tests have been made on the model without fins and a single flight test has also been made on a sting-supported model without fins. Other flight tests were made on self-powered rocket models with fins and range tests have been made on finned models.

The tests have been made over a range of Reynolds numbers from 1×10^6 to 40×10^6 in tunnels and 12×10^6 to 140×10^6 for free-flight models. Mach numbers covered ranges from 1.5 to 6.9 in tunnels and 0.85 to 4 in flight.

3. MODELS AND MEASUREMENTS

A full description of the tunnels and models used is given in the various references and is not repeated here. An attempt has, however, been made in Table I to summarize the most important details. The AGARD specification for the ratio of sting diameter to base diameter, as shown in Figure 1, was not published until after many of the tests noted here were made and the different values used in different tunnel tests may well alter the results. This is discussed in further detail later.

In some cases, details of the construction and surface roughness of the model have been given^{2,4}. The model finishes were of high standard, in general, and it is unlikely that difference of finish between models has had any large effect on the results. Transition was fixed in a number of tests by strips of carborundum powder near the nose of the model. One test in a range was made with transition fixed by machined grooves on the nose of the model.

In the flight measurements with fins, the standard method of Doppler radar was used to obtain velocity and telemetered signals from a pressure cell and a longitudinal accelerometer gave base pressure and total drag. In the fin-off flight tests, the forces were measured on the model with a sting balance, the readings being transmitted to the ground by telemetering.

Skin friction has been measured in a few cases both in flight^{12,13} and in the NACA 4 ft and 9 in. tunnels² by rake surveys of the total pressures through the

boundary layer. To obtain the skin friction drag, an estimated temperature gradient through the boundary layer was used, as discussed in Reference 2.

Forebody pressure drag has been measured in some tunnel tests by integrating the pressure distribution measured at a number of orifices (12 to 240 in number) in the model. In some cases several rows of orifices were used; in other tests the model was rotated about a longitudinal axis and a number of sets of readings was taken.

One set of tests has been made on a half-model⁷ mounted on the wall of the tunnel. The half-model was displaced from the tunnel wall by a shim, to allow for the boundary layer thickness. Tests at $M = 1.57$ showed that this shim had to be about three times the boundary layer displacement thickness to give a drag on the half-model comparable with that on a complete model measured in the same tunnel. For Mach numbers of 1.8 and 2, the half-model gave good agreement with a complete model with a shim of about twice the boundary layer displacement thickness.

4. RESULTS AND DISCUSSION

4.1 Model Without Fins

A plot of the measured total drag coefficient from a representative set of results at varying Reynolds number and Mach number is shown in Figure 2 (taken from Reference 4). There is obviously a very considerable scatter in these results and further detailed analysis is necessary.

The results with transition fixed are much less scattered than the main body of data, but unfortunately there are not enough tests with transition fixed to enable any comprehensive analysis to be done using only these results. To compare the results, the total drag has been separated into base drag, forebody pressure drag (i.e., total pressure drag) and skin friction drag.

4.2 Base Pressure Drag

Most of the tests have been made with a sting diameter from 0.58 to 0.72 of the base diameter rather than the recommended 0.49. In one set of recent AEDC tests (Reference 27*), a comprehensive range of sting diameter to base diameter and length of parallel sting to base diameter was tested. Some early NASA tests in the 4 ft x 4 ft tunnel at $M = 1.59$ suggested that for turbulent flow over the model there should be no change in the base pressure due to sting taper, provided that there was a parallel length of sting 2.5 times the base diameter downstream of the base. In the AEDC tests a critical sting length was defined as the length for which there was no further change of base pressure with increase of parallel sting length. Figure 3(a) shows this critical length plotted against Mach number for three Mach numbers and includes an indication of the Reynolds number at which the flow over the base becomes turbulent. The curves marked as "Wake Unstable" at $M = 2.0$ and 3.0 were in regions where a small change in Reynolds number produced a rapid increase in base pressure,

* This Report was received after the main body of the analysis in this note was completed and results from it have not been included in all the figures.

although it appeared that sting interference was a minimum. No explanation of this effect has been given. These results show that the AGARD specification is satisfactory for the transition free case at $R \geq 1.3 \times 10^6$ for $M = 2.0$, $R \geq 2.3 \times 10^6$ at $M = 3.0$ and $R \geq 3.1 \times 10^6$ at $M = 4.0$. At $M = 5.0$, it was not possible to find an interference-free sting length in the range tested ($l_s/d_b = 1$ to 6 and $R = 1$ to 2.7×10^6).

A similar examination of the effect of sting diameter is shown in Figure 3(b) (from Reference 27). This shows two distinct curves for laminar and turbulent flow. For the turbulent case, the base pressure appears to level off to a constant value for the smallest diameter tested ($0.3 d_b$), but for the specified value of 0.5 there is still some interference present at $M = 2.0$ to 4.0. The variation for the turbulent case for $0.35 \leq d_s/d_b \leq 0.66$ is only 0.015 in base pressure coefficient. For the laminar case, the curves show an increase with decrease of sting diameter and no interference-free sting diameter can be determined. However, the variation of base pressure is small for sting diameters of over $0.5 d_b$.

The general shape of the change of base pressure with Reynolds number, with transition free, is illustrated by Figure 3(c) (from Reference 27). When the Reynolds number is low there is a laminar boundary layer over the whole body and extending into the wake. Under these conditions the base pressure is very small. As the Reynolds number increases, the transition to turbulent flow moves forward in the wake to the base of the body and the base pressure decreases rapidly. The minimum value of base pressure occurs when the transition to turbulent flow is at the base of the body. Thereafter, as the transition point moves forward on the body, the base pressure increases slightly, probably until the transition is at the nose of the body. After this point a further increase of Reynolds number only results in a small further change in base pressure.

With the transition fixed at the nose of the body, the one curve on Figure 3(c) at $M = 2.0$ confirms the results of Reference 2 that the base pressure is nearly constant over the Reynolds number range from 2×10^6 up to 10^7 . Above $R = 10^7$ there is a slight decrease with further increase of Reynolds number.

Figure 4 attempts to summarize all the results of base pressure plotted against Mach number for three different Reynolds numbers. No correction has been made for sting diameter in these results and, since in all cases the sting diameter is higher than the recommended, $-C_{pb}$ is probably about 0.01 too high compared with results for the recommended sting diameter of 0.49. This difference is fairly small compared with the scatter of the results.

At a Reynolds number of approximately 30×10^6 the flight test, which covers a large range of Mach number, agrees well with the few tunnel tests which have been made at high Reynolds number and, as shown in Reference 3, it is in good agreement with the estimates of base pressure based on the theoretical work of Love¹⁸. At the lower Reynolds numbers, the transition-fixed results show little change and reasonable agreement between the different tunnels. The natural transition results are, however, very scattered. At $R = 4 \times 10^6$ and $M = 2$, for example, C_{pb} can range from -0.02 to -0.12 and its value is obviously dependent on the transition position on the body, which can vary in different tunnels for the same Reynolds number and Mach number.

4.3 Forebody Drag

The forebody drag is obtained by subtracting the base drag due to base pressure from the total drag. It is shown plotted against Reynolds number for one set of tests in Figure 5 and against Mach number for various Reynolds numbers in Figures 6(a) and 6(b). At the highest Reynolds number the tunnel results are all in reasonable agreement and, though transition was not fixed in these cases, it is probably near the nose of the models. The flight test, which was also made at high Reynolds number, shows an appreciable lower value for drag throughout the Mach number range. As pointed out in Reference 6, this is probably due to a more rearward position of transition in flight, where the appreciable heat transfer to the model will have the effect of stabilizing the boundary layer. Tunnel experiments were made with a body which could be heated or cooled²² and the results confirmed the theoretical estimates of the stabilizing effect of heat transfer.

At the lower Reynolds numbers there is considerably more scatter on the results, which must be due to variation of transition position. With the transition fixed forward the results are in reasonable agreement, but there is not sufficient information, particularly at the higher Mach numbers, to draw mean curves accurately. Unfortunately no observations of transition position were made in the tunnel tests and so further correlation of the forebody drag is not possible.

4.4 Forebody Pressure Drag

Figure 7 shows the measured forebody pressure drag compared with various estimates, including one made by using characteristics from Reference 3, two from Reference 8, using the estimates of Fraenkel⁹ and Lighthill's second-order theory, and one made from the generalized curves of Reference 11 (also based on Fraenkel's work). Near $M = 1.5$, all the estimates and measurements agree reasonably well but, at higher Mach numbers, there are appreciable differences between the estimates, amounting to as much as ± 0.01 on C_{Dp} over the Mach number range from 3 to 4. Unfortunately there are not at present sufficient experimental results, particularly in the Mach number range 3 to 5, to check the estimates.

4.5 Skin Friction

By subtracting the forebody pressure drag from the forebody total drag, the skin friction drag, C_{Df} , can be obtained. Where possible the measured value of forebody pressure drag has been used, but if this is not available the value given by the generalized curves of Reference 11 (Fig. 7) has been taken. Figures 8(a)-(c) show the results plotted against Reynolds number. These curves are similar to those given in Reference 7, but, in that report, the forebody pressure drag as given by slender-body theory was used. For comparison the skin friction drag on a flat plate is also shown. For the incompressible laminar skin friction on a flat plate, the Blasius formula $C_f = 1.328/\sqrt{R}$ has been used, with a compressible flow correction using Young's formula¹⁷

$$\frac{C_f}{C_{f1}} = \left(1 + 0.365 (\gamma - 1) M^2 \sigma^{\frac{\omega-1}{2}} \right)^{\frac{\omega-1}{2}}$$

where a mean value of $\sigma = \mu C_p / k = 0.72$ and $\omega = 8/9$ were taken, so that

$$\frac{C_f}{C_{f1}} = (1 + 0.1239 M^2)^{-0.0555}$$

For a turbulent boundary layer, the incompressible skin friction formula due to Prandtl and Schlichting has been used:

$$C_f = \frac{0.455}{(\log R)^{2.58}}$$

with a correction to compressible flow due to Young¹⁸

$$\frac{C_f}{C_{f1}} = \frac{T_1}{T_w} \left(\frac{\log R}{\log R + (2 + \omega) \log(T_1/T_w)} \right)^{2.58}$$

where, with zero heat transfer,

$$\frac{T_1}{T_w} = \left(1 + \frac{\gamma - 1}{2} M_1^2 \sigma^{1/3} \right)^{-1}$$

and values for $\sigma = 0.72$ and $\omega = 8/9$ have been taken.

For the AGARD Model A, the drag coefficient is based on body frontal area and $C_{Df} = 36.3 C_f$. No allowance has been made for the increase in skin friction due to increase in velocities round a body compared with a flat plate.

Over the Mach number range from 1.6 to 2.5, the results (Figures 8(a) and (b)) show very good agreement between flat plate skin friction and the measurements on the body. At higher Mach numbers the agreement is not quite so satisfactory.

This method of plotting the results shows clearly the Reynolds number range for transition from laminar to turbulent flow on the bodies and, on Figures 8(a) and 8(c), the transition Reynolds number on a 10° cone in some of the tunnels is also shown. These transition Reynolds numbers are very close to the Reynolds number at which forward movement of transition occurs on the AGARD Model A.

The measurements of skin friction made on the AGARD Model A body with a rake^{12,13} in flight over a Mach number range from 1.5 to 3.0, have shown very good agreement with van Driest's theory¹⁹ for turbulent skin friction when the effects of heat transfer are included. In this Mach number range this theory gives values of turbulent skin friction 5% to 8% above the formula quoted here. This difference between the theories is within the experimental error in the measurements.

4.6 Drag with Fins

Few detailed tests have been done on the model with fins. In Reference 10 some of the results available have been analysed and some results are given from range firings

of models where the transition position could be estimated from schlieren photographs. Some tests were also made with a screw thread type of trip near the nose of the model to locate the transition forward. The variation of total drag with transition location could then be obtained and Figure 9 (from Reference 10) shows the results at $M = 1.6$ and $R = 3 \times 10^6$ and $M = 3$ and $R = 5 \times 10^6$. There is a reasonable overall agreement between the range results and the tunnel tests.

Further results on the drag of the model with fins are given in Reference 2 over a range of Mach numbers up to 3, including free-flight tests, and at $M = 6.9$ in Reference 8. Some tabulated results are included in Table II, but further analysis is not really possible because so few comparisons are available.

4.7 Lift and Pitching Moment

The lift curves for the body alone are non-linear and Figure 10(a) shows the results expressed as a ratio C_L/a for a range of incidence. There is a reasonable agreement between the various different results over a wide range of R from 3×10^6 to 30×10^6 . The effects of transition cannot be evaluated, as its position was not recorded in these tests.

Figure 10(b) shows the corresponding curves for the variation of centre of pressure in terms of body length. Figure 11 gives the corresponding curves with fins. The number of results is rather limited but, again, there is a fair agreement among them.

5. CONCLUSIONS

- (i) The total drag measurements on the AGARD Model A show considerable scatter of results in various tunnels.
- (ii) Base pressure measurements show a consistent set of results at high Reynolds number (20 to 30×10^6), but at lower Reynolds number there are large differences and the pressure is dependent on the thickness and state of the boundary layer near the base of the body. If the transition is fixed at the nose, the base pressure is reasonably independent of Reynolds number from about 2×10^6 up to 10^7 and only decreases slowly at higher Reynolds number.
- (iii) Pressure distribution measurements give a forebody pressure drag in good agreement with the various theoretical estimates for $M = 1.5$ to 2 , but at higher Mach numbers there are few experimental results.
- (iv) The skin friction drag is in very good agreement with flat plate skin friction for both laminar and turbulent boundary layers over the Mach number range 1.6 to 2.5 but in not quite such good agreement at the higher Mach numbers.
- (v) At Mach numbers in the range $1.6 - 2.5$ the transition Reynolds number on the AGARD Model A is close to that on a 10^0 cone.
- (vi) While a test with a smooth model is a useful check of the transition Reynolds number of a tunnel, the transition should be fixed near the nose of the model if comparison of results with other tunnels is required.
- (vii) Lift and pitching moment measurements with and without fins show reasonable agreement in results from various tunnels.

REFERENCES

1. A. G. A. R. D. *Wind Tunnel Calibration Models. AGARD Specification 2, September 1958.*
2. Evans, Albert, J. *The Zero-Lift Drag of a Slender Body of Revolution (NACA RM-10 Research Model) as Determined from Tests in Several Wind Tunnels and in Flight at Supersonic Speeds. NACA Report 1160, 1954.*
3. Piland, R. O. *Drag Measurements on a 1/6 Scale, Finless, Sting-Mounted NACA RM-10 Missile in Flight at Mach Numbers from 1.1 to 4.04, Showing Some Reynolds Number and Heating Effects. NACA RM L54H09, October 1954.*
4. Schueler, C. J.
Strike, W. T. *An Investigation of the Lift, Drag, and Pitching-Moment Characteristics of AGARD Calibration Models A and B. Arnold Engineering Development Center, AEDC-TN-55-34, February 1956.*
5. Schueler, C. J. *Lift, Drag and Pitching-Moment Characteristics of AGARD Calibration Models A and B at Mach Numbers 3.98 and 4.98. Arnold Engineering Development Center, AEDC-TN-57-9, May 1957.*
6. Schueler, C. J. *AGARD Tests - Comparison of Wind Tunnel and Free Flight Results. Presented at 7th Meeting of the Supersonic Tunnel Association, Redstone Arsenal, Huntsville, Alabama, April 1957.*
7. van der Bliek, J. A. *Drag Measurements on AGARD Model A in the N.A.E. 30 x 16 in. Wind Tunnel and Comparison with Other Data. National Research Council of Canada, N.R.C. Laboratory Report LR-233, November 1958.*
8. McCauley, W. D.
Feller, W. V. *An Investigation of the Characteristics of the NACA RM-10 (With and Without Fins) in the Langley Hypersonic Tunnel at a Mach Number of 6.9. NACA RM L54I03, 1954.*
9. Fraenkel, L. E. *Curves for Estimating the Wave Drag of Some Bodies of Revolution, Based on Exact and Approximate Theories. ARC 15,685, Current Paper 136, 1953.*
10. Carros, R. J.
James, C. S. *Some New Drag Data on the NACA RM-10 Missile and a Correlation of the Existing Drag Measurements at $M = 1.6$ and 3.0. NACA TN 3171, 1954.*
11. Royal Aeronautical
Society *Aerodynamics Data Sheets. Royal Aeronautical Society Volume 1, Bodies S.02.03 Series.*

12. Maloney, J.P. *Drag and Heat Transfer on a Parabolic Body of Revolution (NACA RM-10) in Free Flight to Mach Number 2 with Both Constant and Varying Reynolds Number and Heating Effects on Turbulent Skin-Friction.* NACA RM L54D06, 1954.
13. Swanson, A.G.
et alii *Flight Measurements of Boundary-Layer Temperature Profiles on a Body of Revolution (NACA RM-10) at Mach Numbers from 1.2 to 3.5.* NACA TN 4061, 1957.
14. Chapman, D.R. *An Analysis of Base Pressure at Supersonic Velocities and Comparison with Experiment.* NACA Report 1051, 1951.
15. Love, E.S. *The Base Pressure at Supersonic Speeds on Two-Dimensional Airfoils and Bodies of Revolution Having Turbulent Boundary Layers.* NACA RM L53C02, 1953.
16. Czarnecki, K.R.
Sinclair, A.R. *A Note on the Effect of Heat Transfer on Peak Pressure Rise Associated with Separation of Turbulent Boundary-Layer on a Body of Revolution (NACA RM-10) at a Mach Number of 1.61.* NACA TN 3997, 1957.
17. Howarth, L.
(Editor) *Modern Developments in Fluid Dynamics. Chapter X, Vol.I, High Speed Flow* by A.D. Young, Oxford University Press, 1953.
18. Young, A.D. *The Calculation of the Profile Drag of Aerofoils and Bodies of Revolution at Supersonic Speeds.* College of Aeronautics, Cranfield, Report No.73.
19. van Driest, E.R. *Turbulent Boundary Layers in Compressible Fluids.* Journal of the Aeronautical Sciences, Volume 18, March 1951, p.145.
20. Chauvin, L.T.
Malonfy, J.P. *Turbulent Convective Heat-Transfer Coefficients Measured from Flight Tests of Four Research Models (NACA RM-10) at Mach Numbers from 1.0 to 3.6.* NACA RM L54L15, 1955.
21. Chauvin, L.T.
de Moreas, C.A. *Correlation of Supersonic Convective Heat-Transfer Coefficients from Measurements of the Skin Temperature of a Parabolic Body of Revolution (NACA RM-10).* NACA TN 3623, 1956 (supersedes NACA RM L51A18, 1951).
22. Czarnecki, K.R.
Sinclair, A.R. *An Investigation of the Effects of Heat Transfer on Boundary-Layer Transition on a Parabolic Body of Revolution (NACA RM-10) at a Mach Number of 1.61.* NACA Report 1240, 1955.
23. Hoffman, S. *Free Flight Tests to Determine the Power-On and Power-Off Pressure Distribution and Drag of the NACA RM-10 Research Vehicle at Large Reynolds Numbers Between Mach Numbers of 0.8 and 3.0.* NACA RM L55H02, 1955.

24. Nicolaides, J.D.
Karpov, B.G. *On the Free Flight Drag Determination of a Finned Configuration (FM-10) Flying at Critical Reynolds Numbers. Aberdeen Ballistic Laboratory Memorandum Report 751, December 1953.*
25. Mottard, E.J.
Loposer, J.D. *Average Skin-Friction Drag Coefficients from Tank Tests of a Parabolic Body of Revolution (NACA RM-10). NACA Report 1161, 1954.*
26. Tate, R.E.
Taylor, A.L. *An Investigation of the Axial-Force Characteristics of a Parabolic Body of Revolution (NACA RM-10) at Various Reynolds Numbers and at Mach Numbers 1.50, 1.73, 2.00, 2.23 and 2.50. Convair Ordnance Aeronautical Laboratory OAL/CM 840, May 1955.*
27. Schueler, C.J. *Comparison of the Aerodynamic Characteristics of AGARD Model A from Tests in 12 in. and 40 in. Supersonic Wind Tunnels. Arnold Engineering Development Center, AEDC-TN-61-8, February 1961.*

TABLE I

Details of Models

Facility	Ref.	Model Length (in.)	Sting d_s/d_b	Mach Number	Reynolds Number $\times 10^{-6}$	T ^a	Measurements		Fins	
							Force	Pressure	With	Without
NACA 4 ft x 4 ft	2	50	0.579	1.6	2 - 40	F & N	X	-	-	X
NACA 4 ft x 4 ft	2	42.05	0.60	1.59	1.8 - 4.5	F	-	X	-	X
NACA 4 ft x 4 ft	2	42.05	0.36	1.59	2.6 - 4.5	N	X	-	X	-
NACA 8 ft x 6 ft	2	73	0.66	1.49 - 1.98	30	N	X	X	X	X
NACA 9 in. x 9 in.	2	9	0.589	1.62 - 2.41	1 - 11	F & N	X	X	-	X
NACA 9 in. x 9 in.	2	7.325	0.49	1.62	2.66	N	X	-	X	-
NACA 1 ft x 3 ft	2	12.21	?	1.52 - 1.98	8.6 - 12.4	N	X	X	-	X
NACA Flight	2	146.5	0	0.85 - 2.5	36 - 140	N	X	-	X	-
NACA Flight	2	73.25	0	0.85 - 2.5	15 - 80	N	X	-	X	-
NACA Flight	3	24.42	0.722	1.0 - 4.0	15 - 48	N	X	-	-	X
NACA 9 in. x 9 in.	3	?	?	4.0	14 - 20	N	X	-	-	X
AEDC 12 in. x 12 in.	4	16.37	0.66 & 0.31	2.0 - 4.0	4 - 27	N	X	-	-	X
AEDC 12 in. x 12 in.	5	16.37	0.66	3.98, 4.98	1.5 - 7	N	X	-	-	X
NAE 30 in. x 16 in.	7	12.20	0.82	1.3 - 2.0	4 - 4.5	N	X	-	-	X
NACA 11 in. x 11 in.	8	12.21	?	6.9	1.7 - 4.5	N	X	-	X	X
NACA 11 in. x 11 in.	8	10	0.60	6.9	4	N	-	X	-	X
NACA Range	10	3.06	0	1.6, 3.0	3, 5	F & N	X	-	X	-
EBL Range	11	9.60	0	1.8 - 3.2	10 - 18	N	X	-	X	-
Convair 27 in. x 19 in.	12	12.2	0.65 & 0.49	1.5 - 2.5	6 - 8.9	F & N	X	-	X	X
Norway 8 in. x 8 in.	-	8	0.49	1.92	5.6	N	X	-	X	X

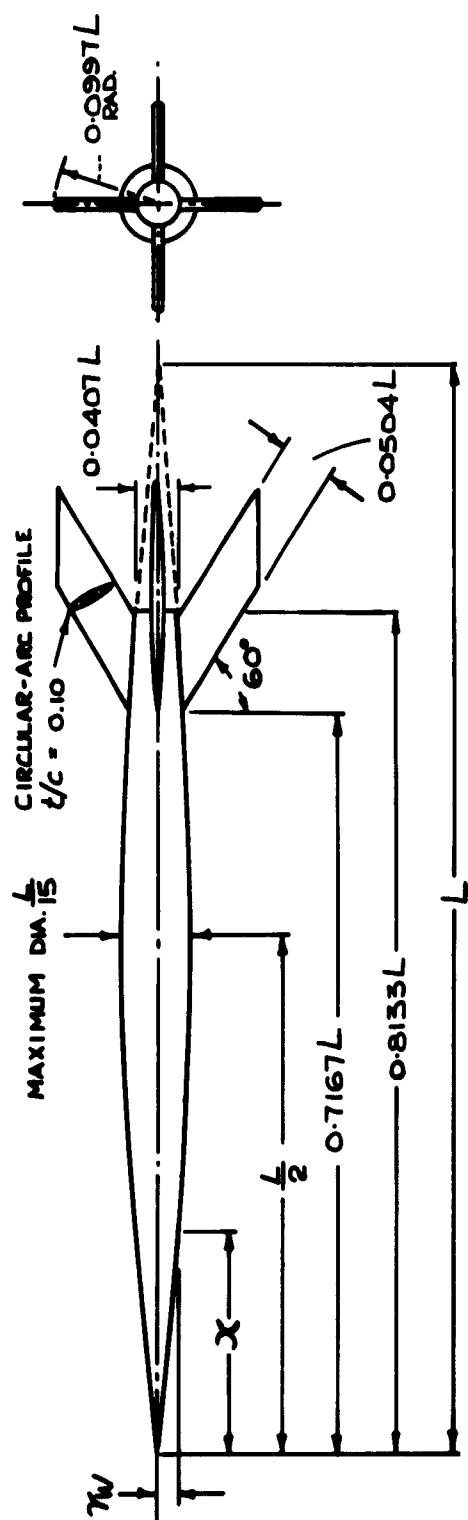
^aT - Transition, F - Fired near nose, N - Natural

TABLE II

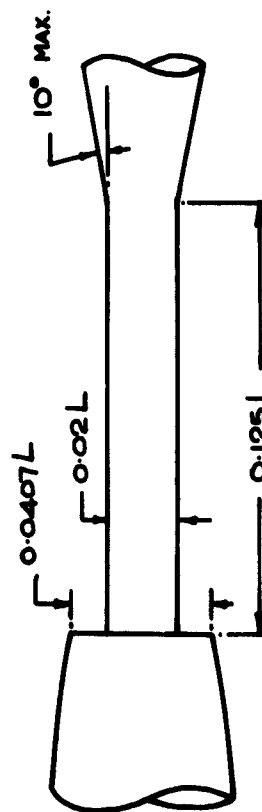
Miscellaneous Measurements of the Drag of AGARD Model A with Fins

Ref.		M	1.4	1.6	2.0	2.5	3.0				
2	NACA* Flight 146.5 in. models	$10^{-6}R$ C_{DT} C_{Db}	100 0.265 0.04	150 0.25 0.045	20 0.23 0.045	50 0.207 0.044	- - -				
2	NACA† Flight 73.2 in. models	$10^{-6}R$ C_{DT} C_{Db}	27-50 0.23 0.025	35-60 0.225 0.030	50-75 0.205 0.025	85 0.203 0.025	- - -				
23	NACA Flight	$10^{-6}R$ C_{DT} C_{Db}			83 0.222 0.037	93 0.205 0.035	107 0.185 0.032				
		M	1.77	1.78	1.81	2.34	2.37	2.44	3.21	3.21	3.22
24	Aberdeen BRL Range	$10^{-6}R$ Laminar area(%) C_{DT}	9.9 5 0.295	9.9 5 0.276	9.9 78 0.245	12.9 45 0.231	12.9 45 0.234	12.9 84 0.231	17.8 14 0.221	17.8 75 0.200	17.8 85 0.200
		M	6.9	6.9	6.9	6.9	6.9	6.9	6.9		
8	NACA 11 in. Hyper- sonic Tunnel	$10^{-6}R$ C_{DT}	1.8 0.145	2.1 0.134	2.6 0.125	3.0 0.119	3.75 0.113	3.9 0.110	4.4 0.106		

* Results from several models, $M < 2$, scatter of 0.01 on C_{DT} † Results from several models, $M < 2$, scatter of 0.015 on C_{DT} and 0.01 on C_{Db}



$$\text{BODY PROFILE } r_v = \frac{x}{1.5} \left(1 - \frac{x}{L}\right)$$



STING DETAIL

Fig.1 General configuration of AGARD Model A

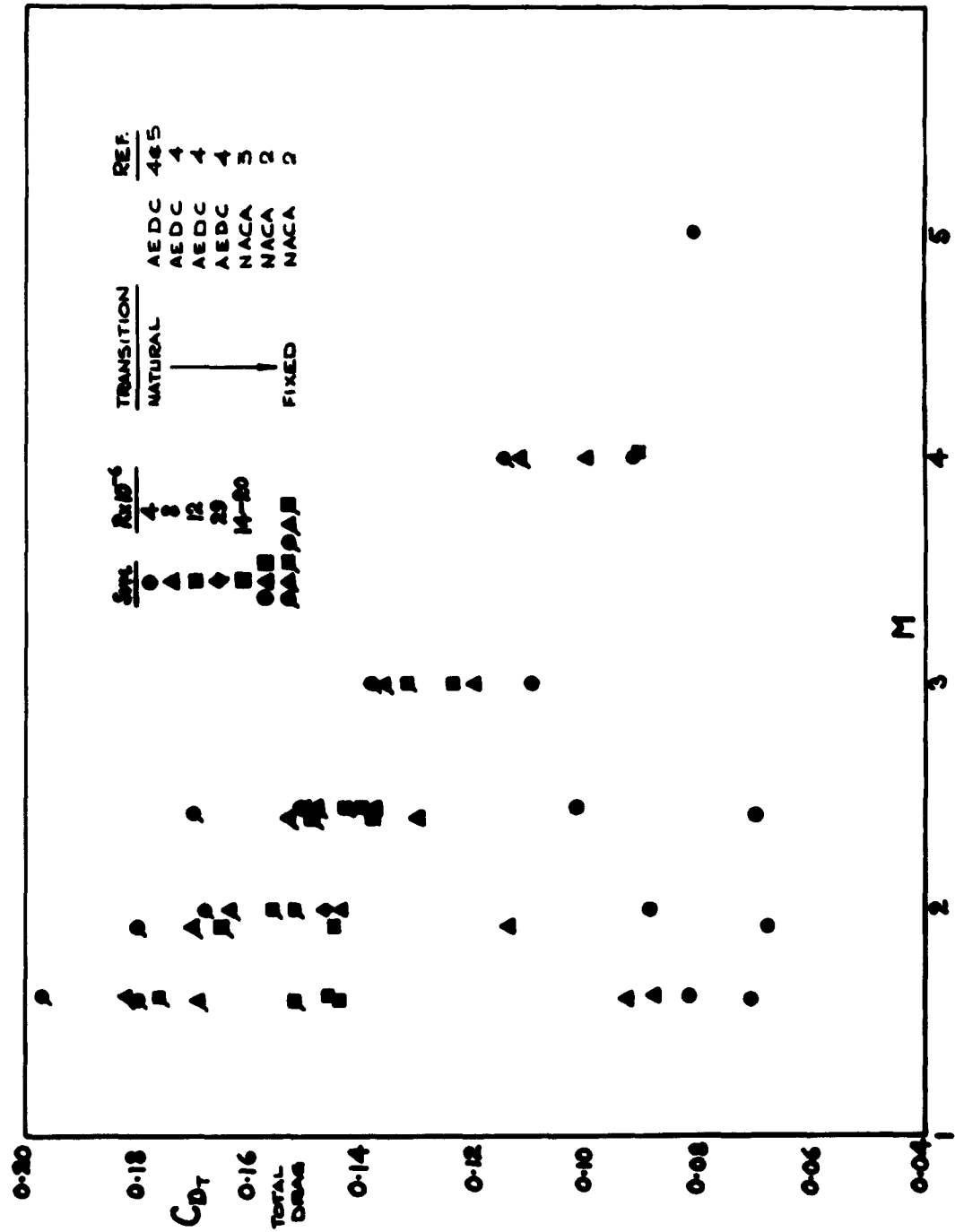


Fig. 2 AGARD Model A. Comparison of measured total drag coefficients

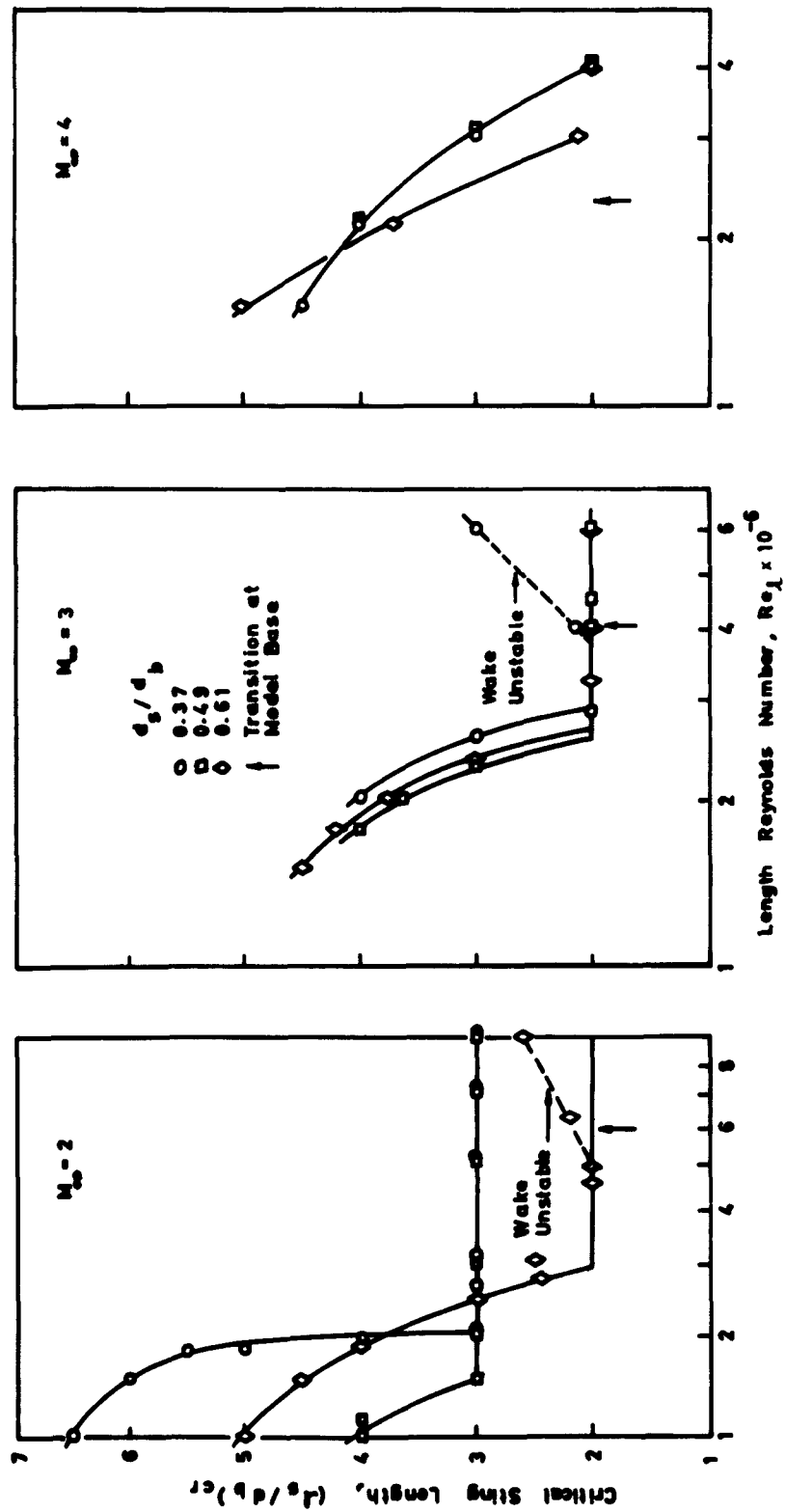


Fig.3(a) Variation of critical sting length with Reynolds number
(Fig.6 of Ref.27)

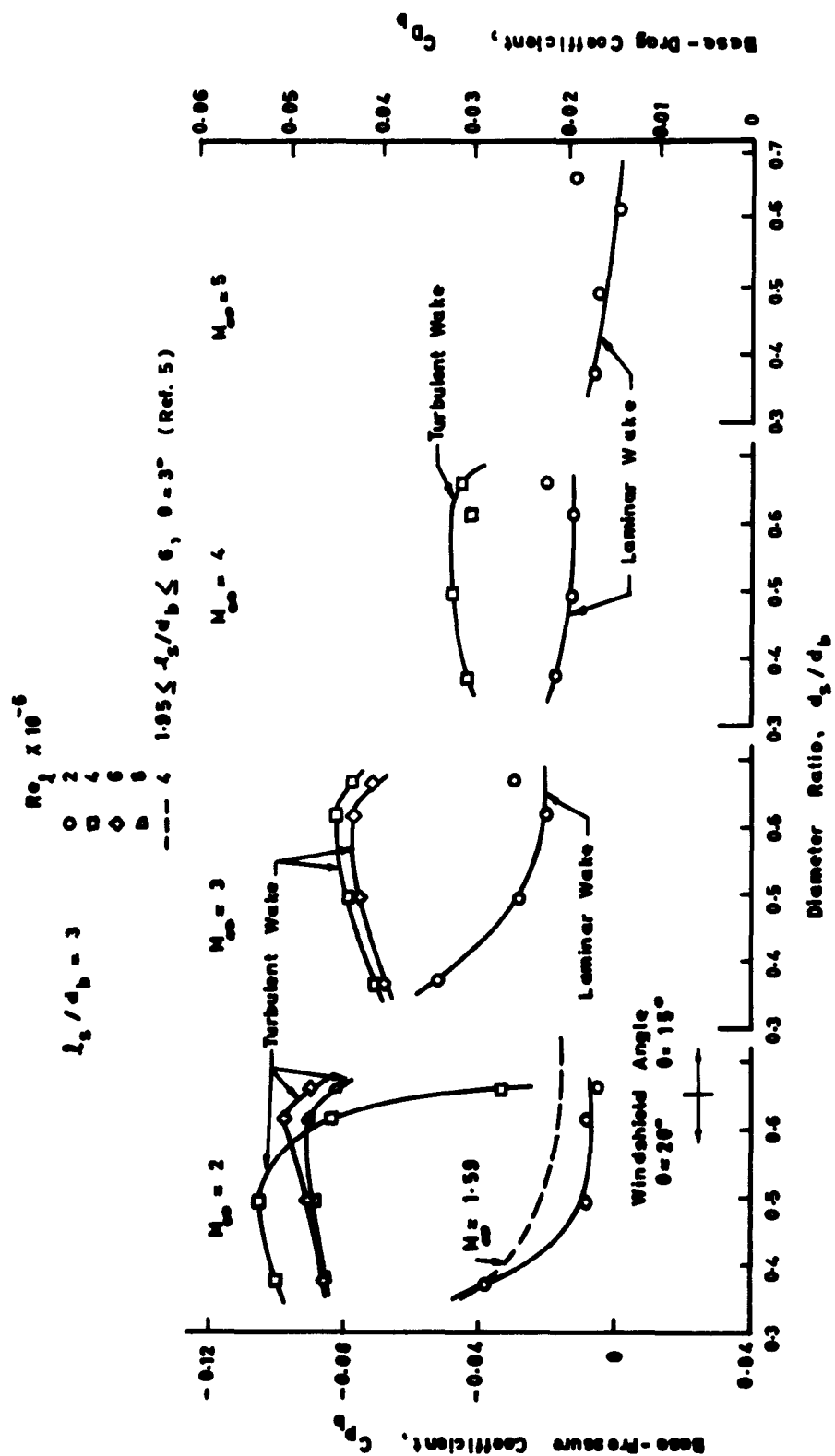


Fig.3(b) Base-pressure coefficients as a function of sting diameter
(Fig.7 of Ref.27)

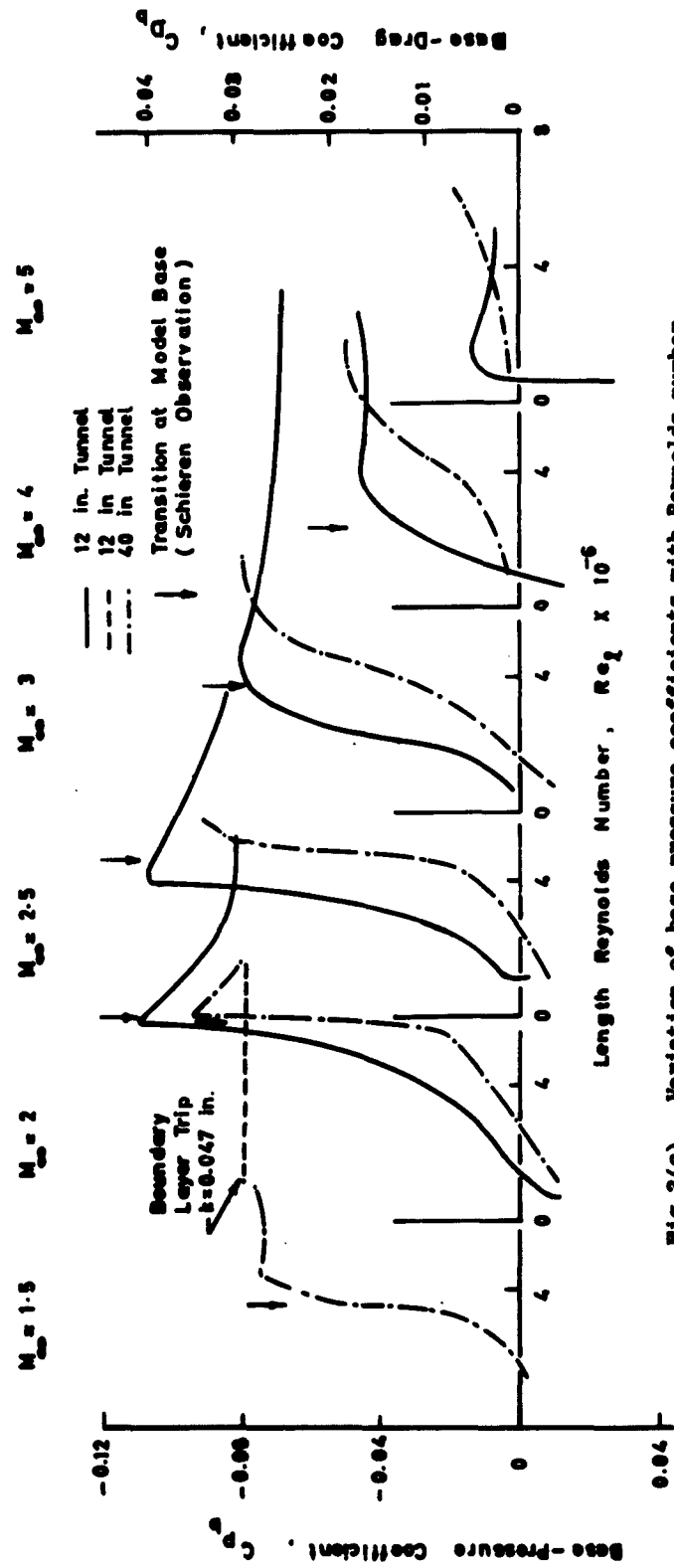


Fig.3(c) Variation of base-pressure coefficients with Reynolds number
(Fig.11 of Ref.27)

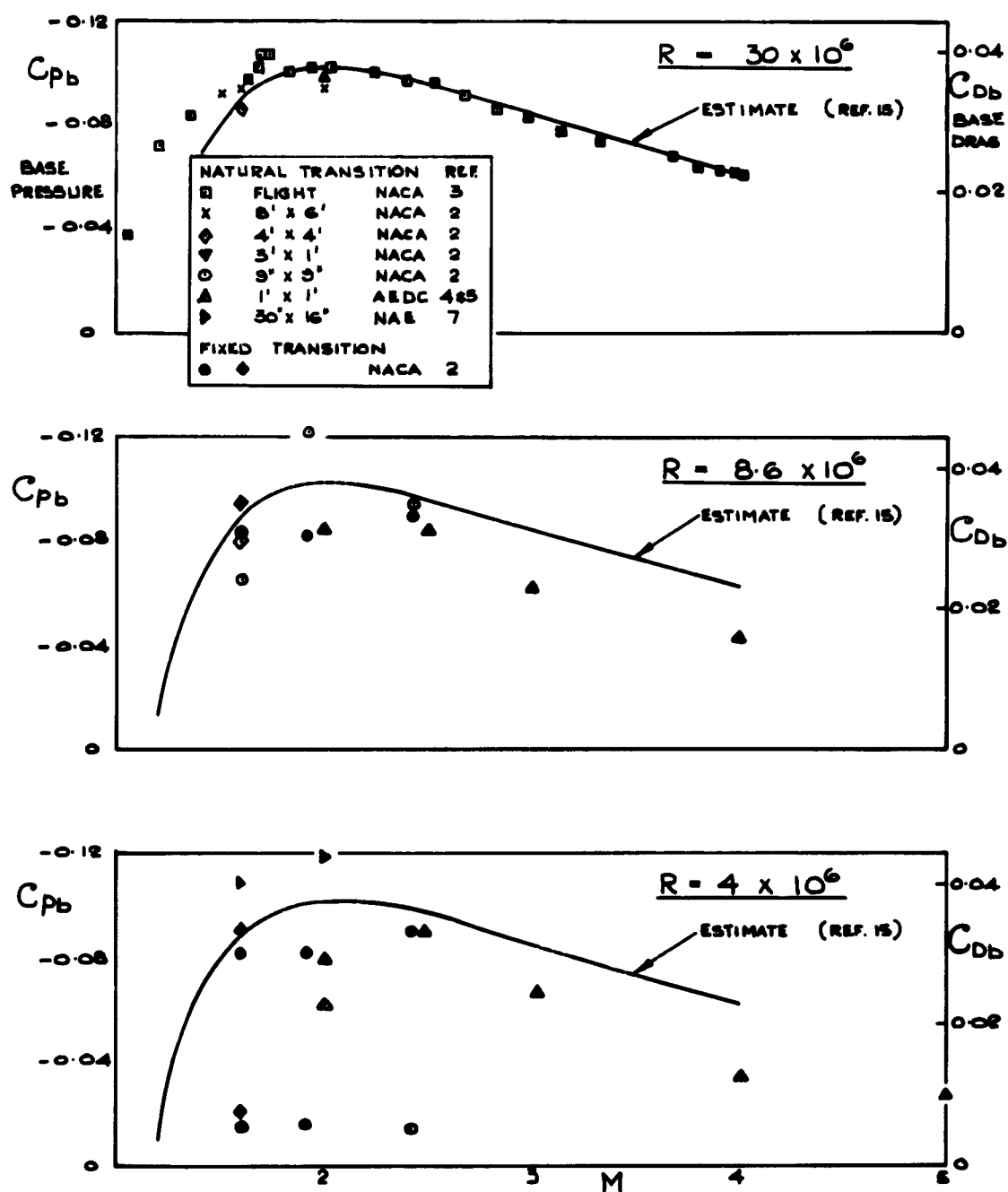


Fig.4 AGARD Model A. Variation of base pressure with Mach number for three Reynolds numbers

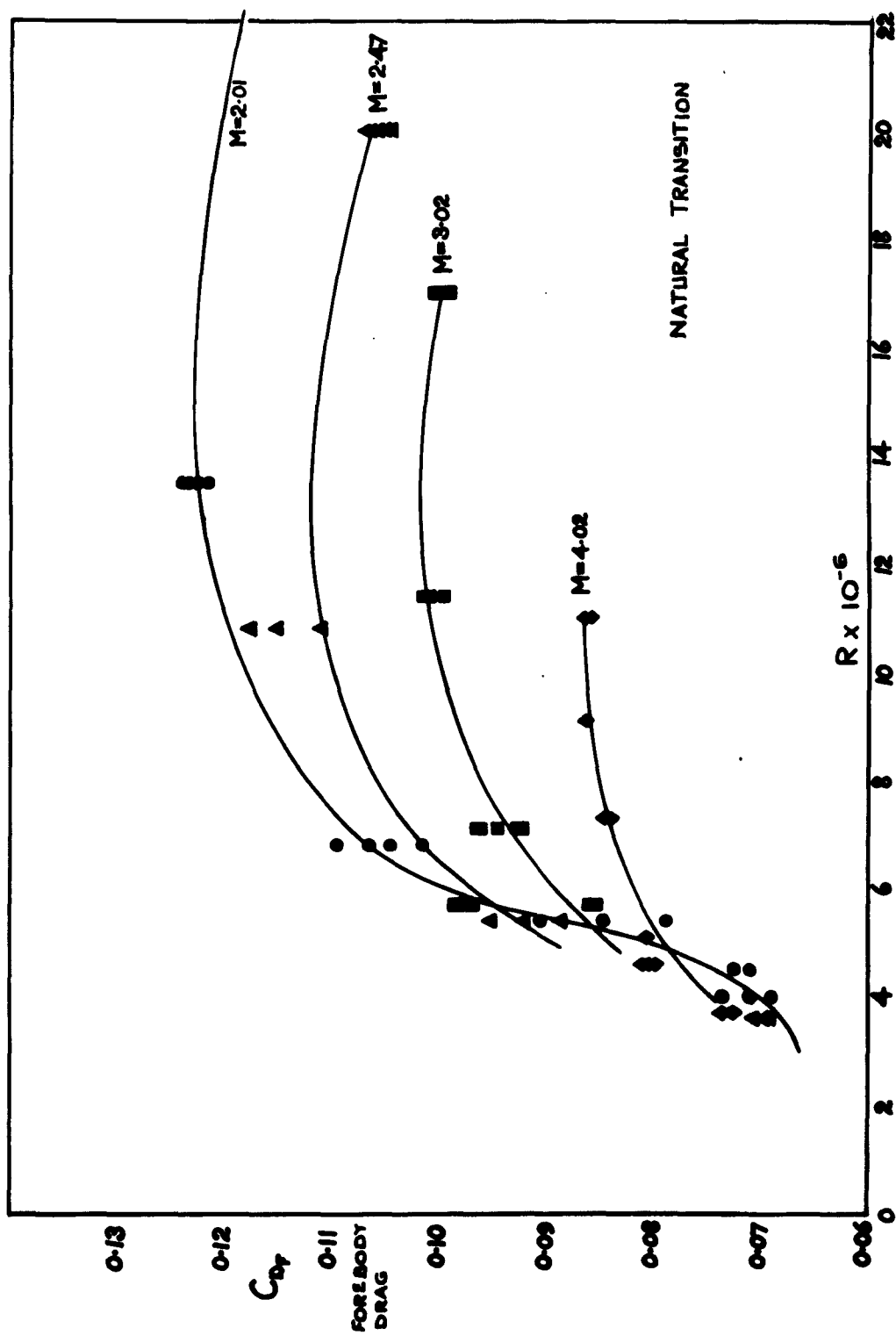


Fig.5 AGARD Model A. Variation of forebody drag with Reynolds number (Ref.4)

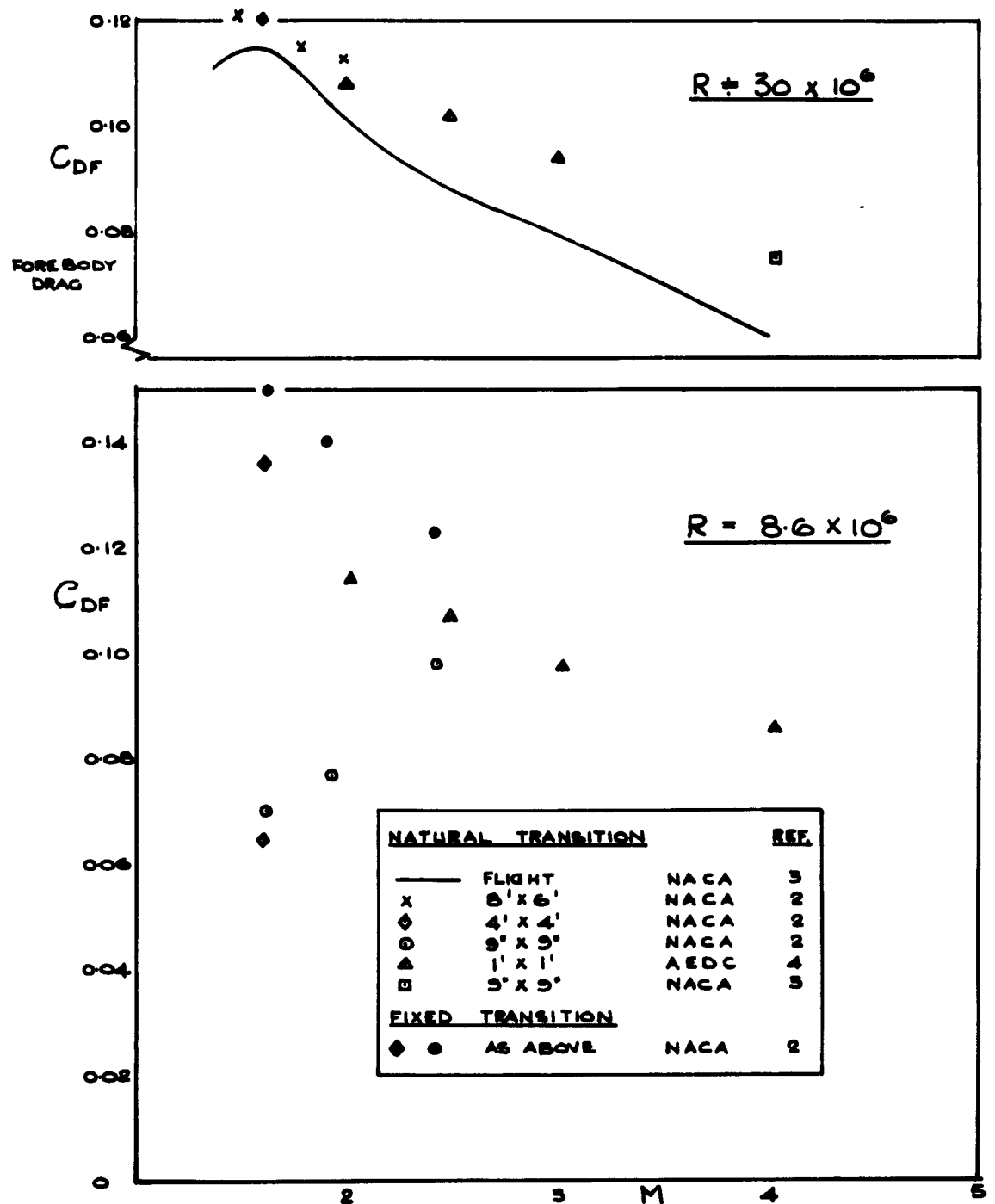
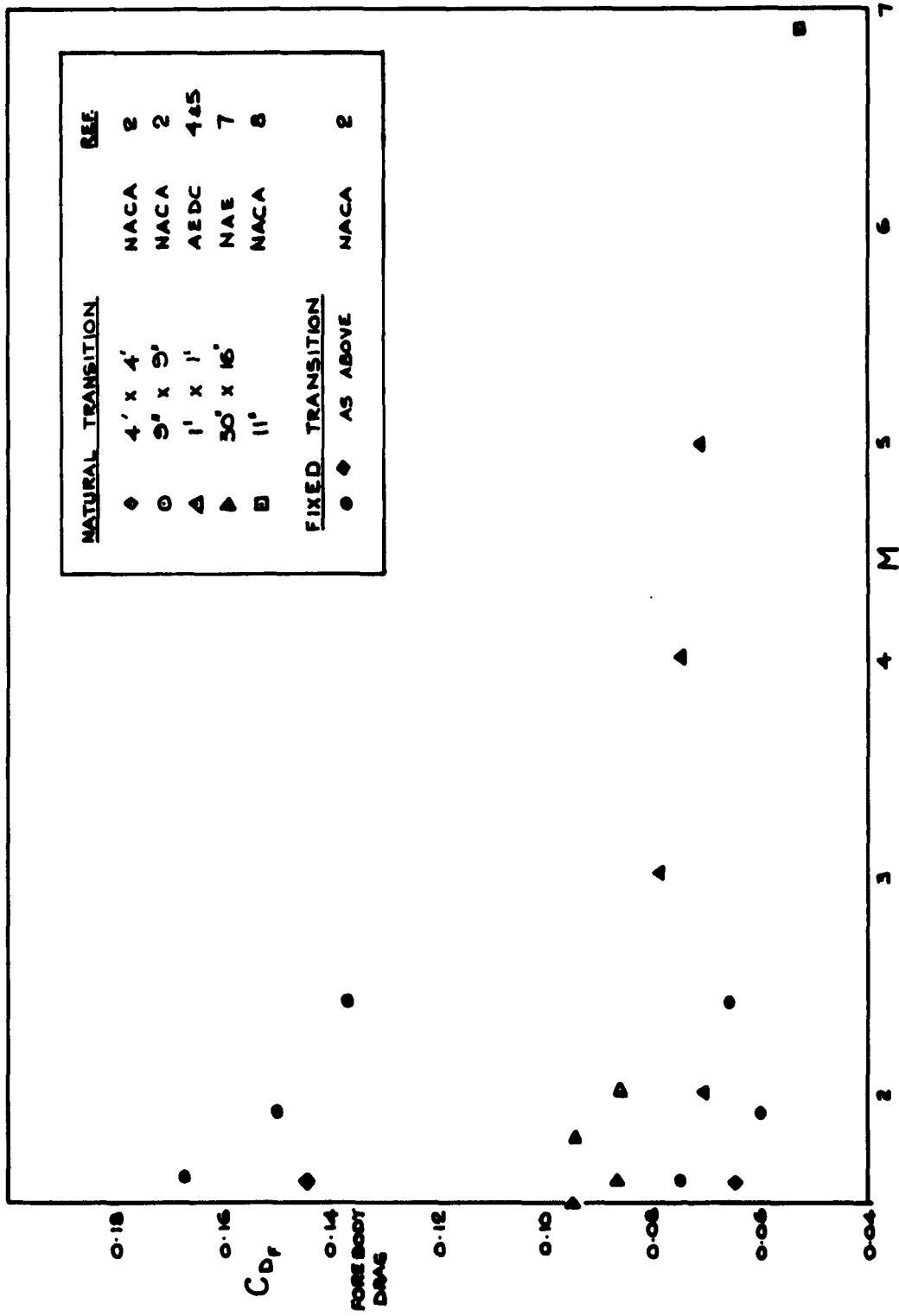


Fig.6(a) AGARD Model A. Variation of forebody drag with Mach number at two Reynolds numbers

Fig. 6(b) AGARD Model A. Variation of forebody drag with Mach number at $R = 4 \times 10^6$

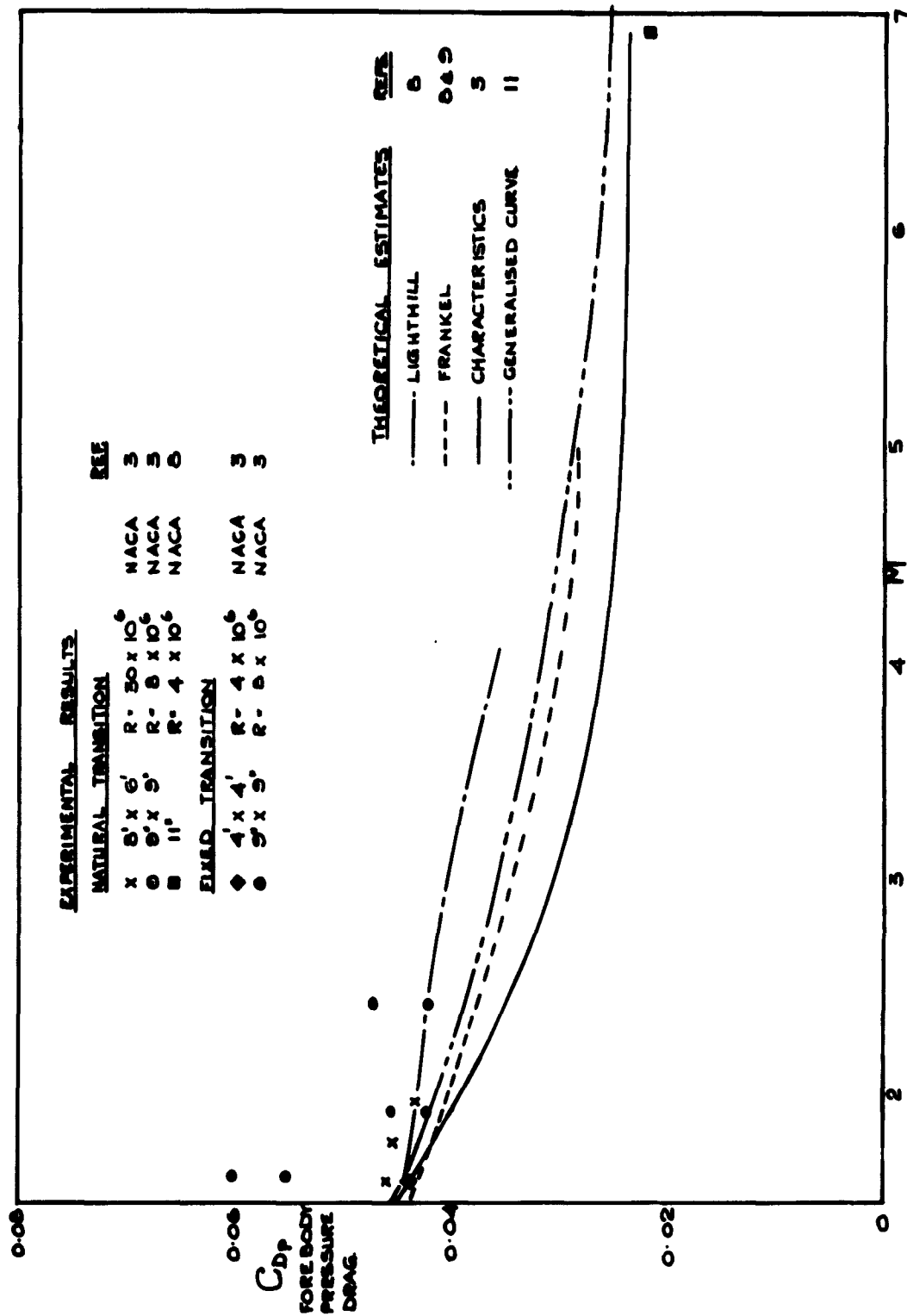


Fig.7 AGARD Model A. Forebody pressures. Comparison of estimates and experiments

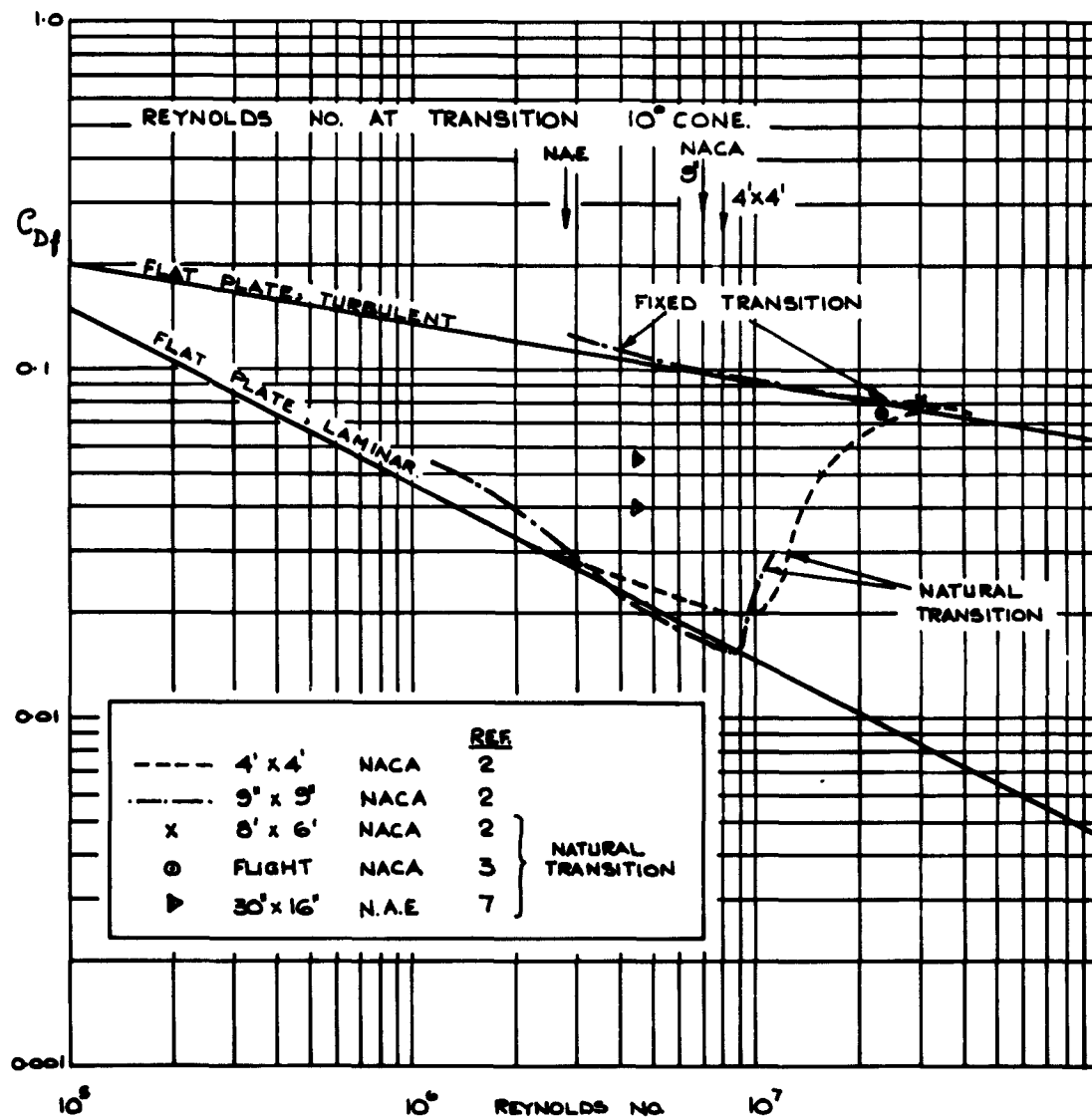


Fig.8(a) AGARD Model A. Friction drag against Reynolds number at $M = 1.6$

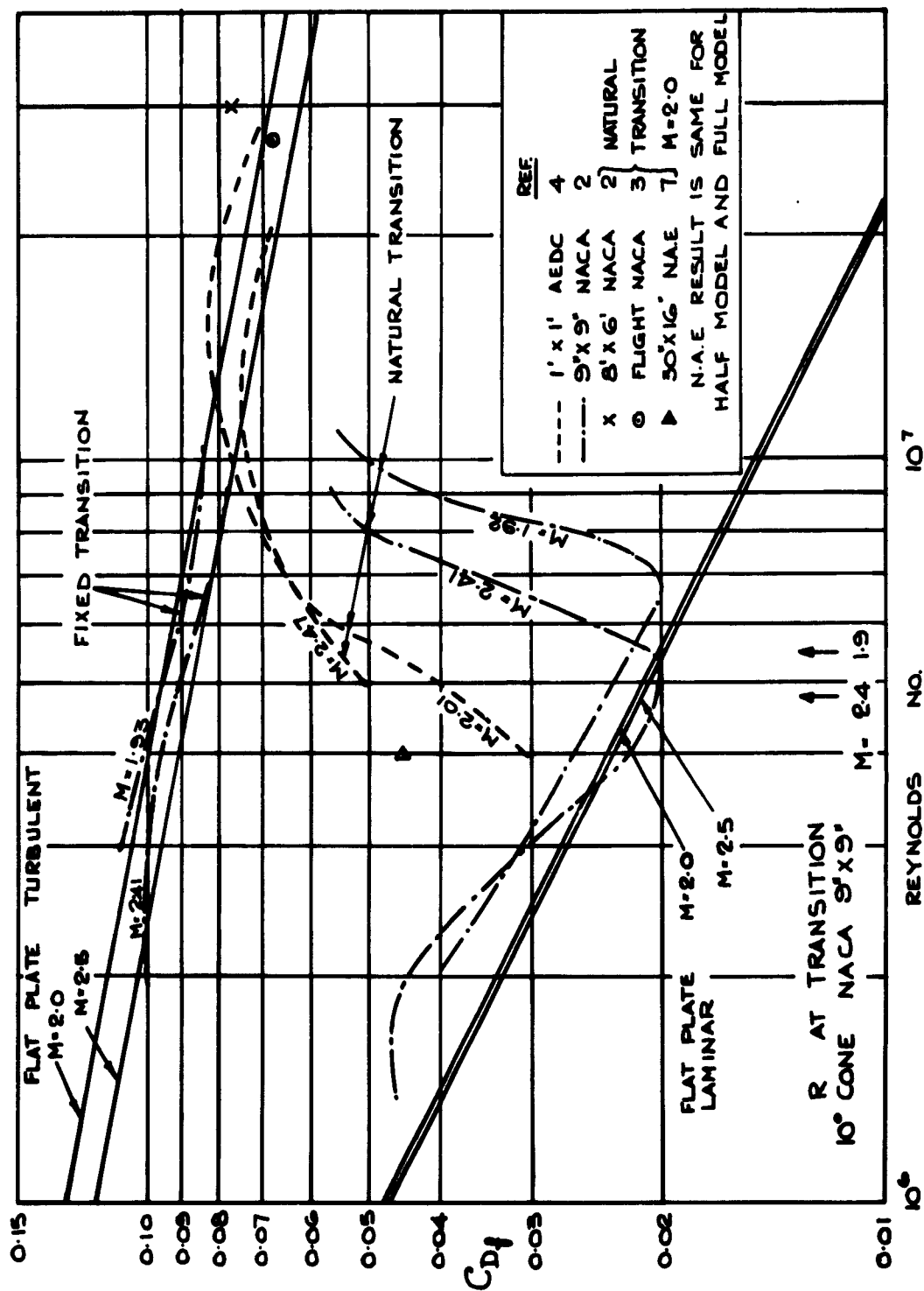


Fig. 8(b) AGARD Model A. Friction drag against Reynolds number. $M = 2.0$ and 2.5

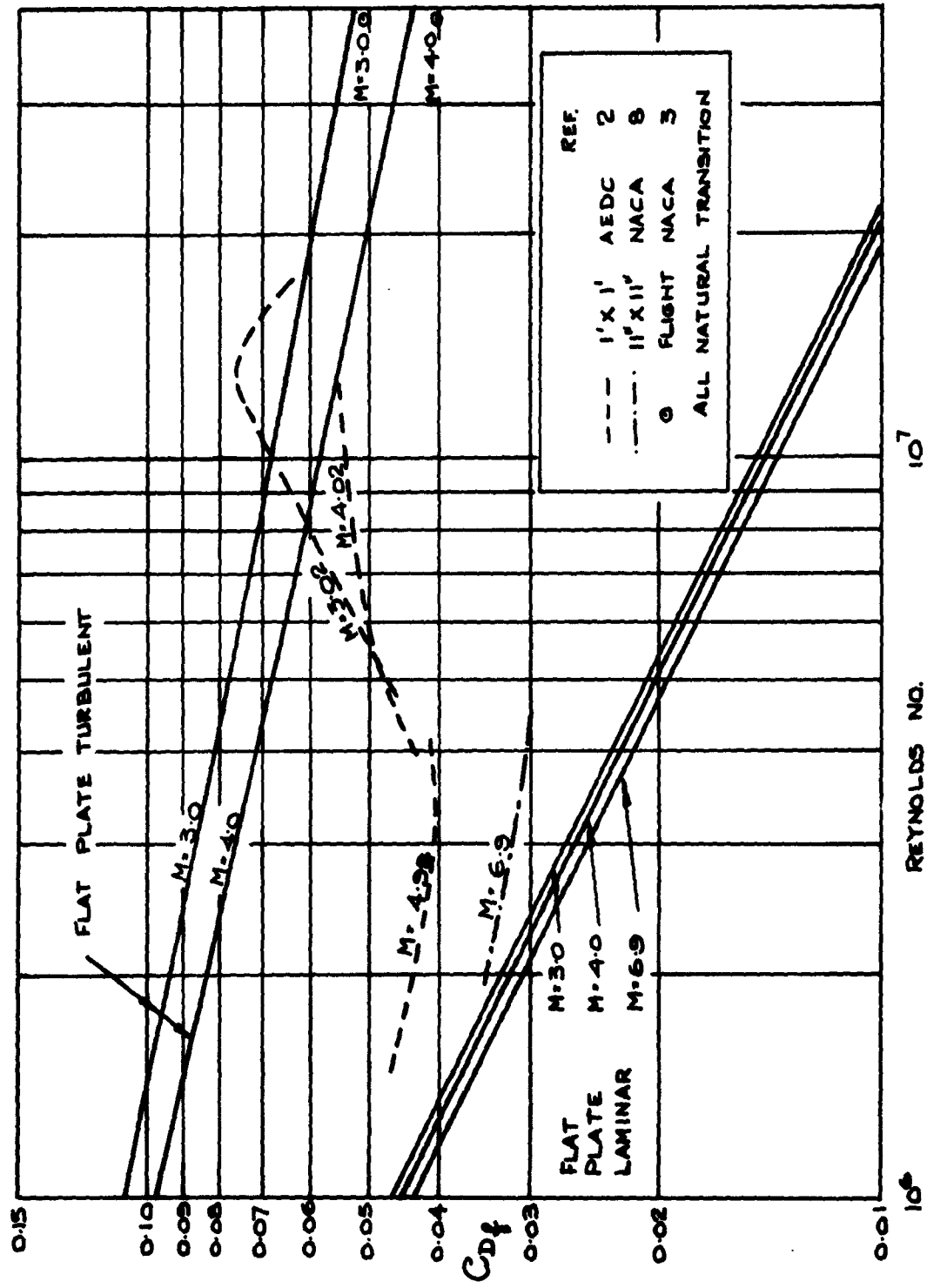


Fig. 8(c) AGARD Model A. Friction drag against Reynolds number. $M = 3.0$ to 7.0

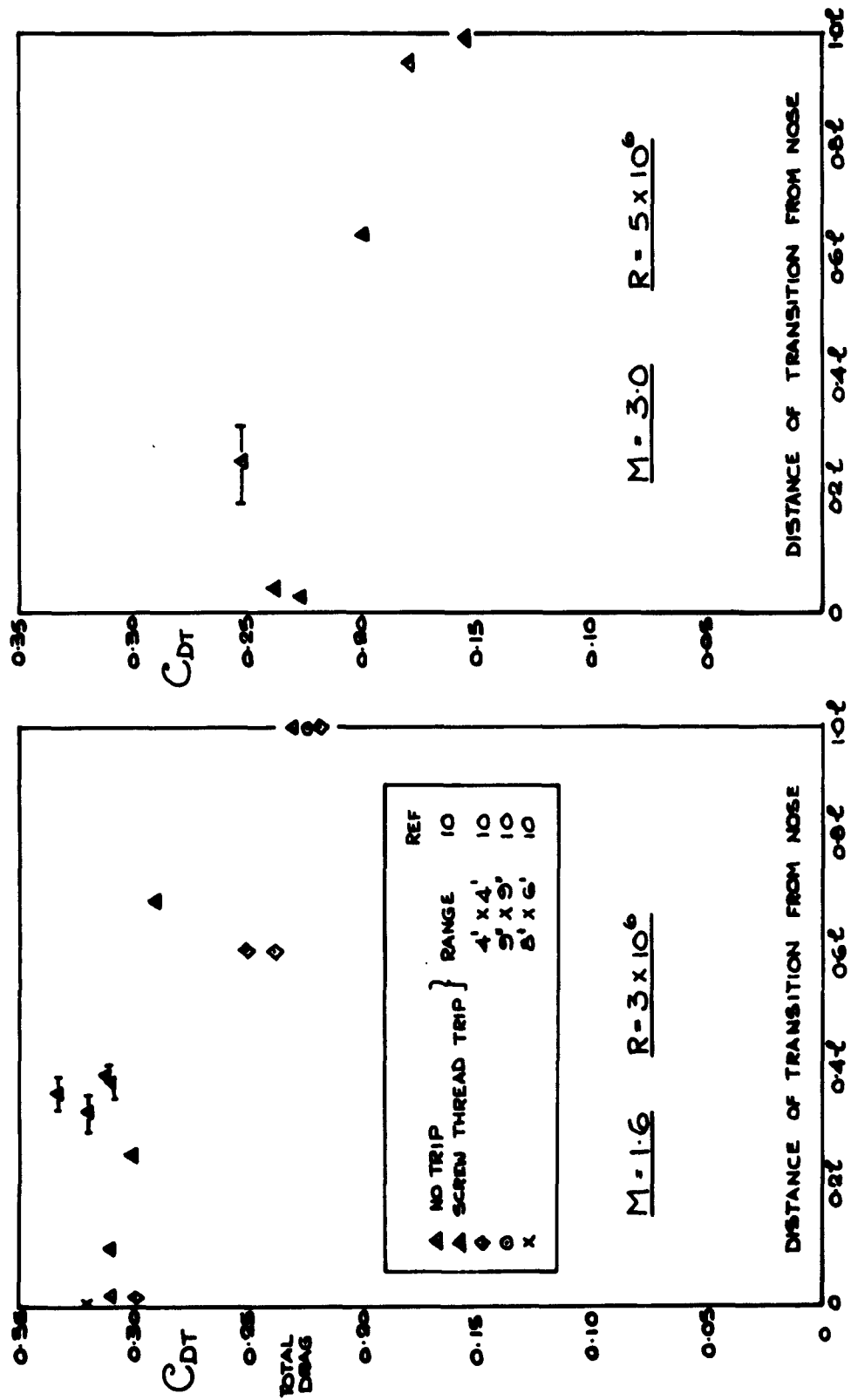


Fig. 9 AGARD Model A with fins. Variation of drag with transition location

$\alpha = 2^\circ \ 4^\circ \ 6^\circ$						REF.
\triangle	\triangle	\triangle	1' x 1'	$R = 4 \text{ to } 20 \times 10^6$	AEDC.	445
\square	\square	\square	11"	$R = 4 \times 10^6$	NACA	8
\circ			8' x 6'	$R = 30 \times 10^6$	NACA	8
\diamond			4' x 4'	$R = 36 \times 10^6$	NACA	8
∇	∇		8' x 8'	$R = 56 \times 10^6$	NORWAY	UNPUBLISHED

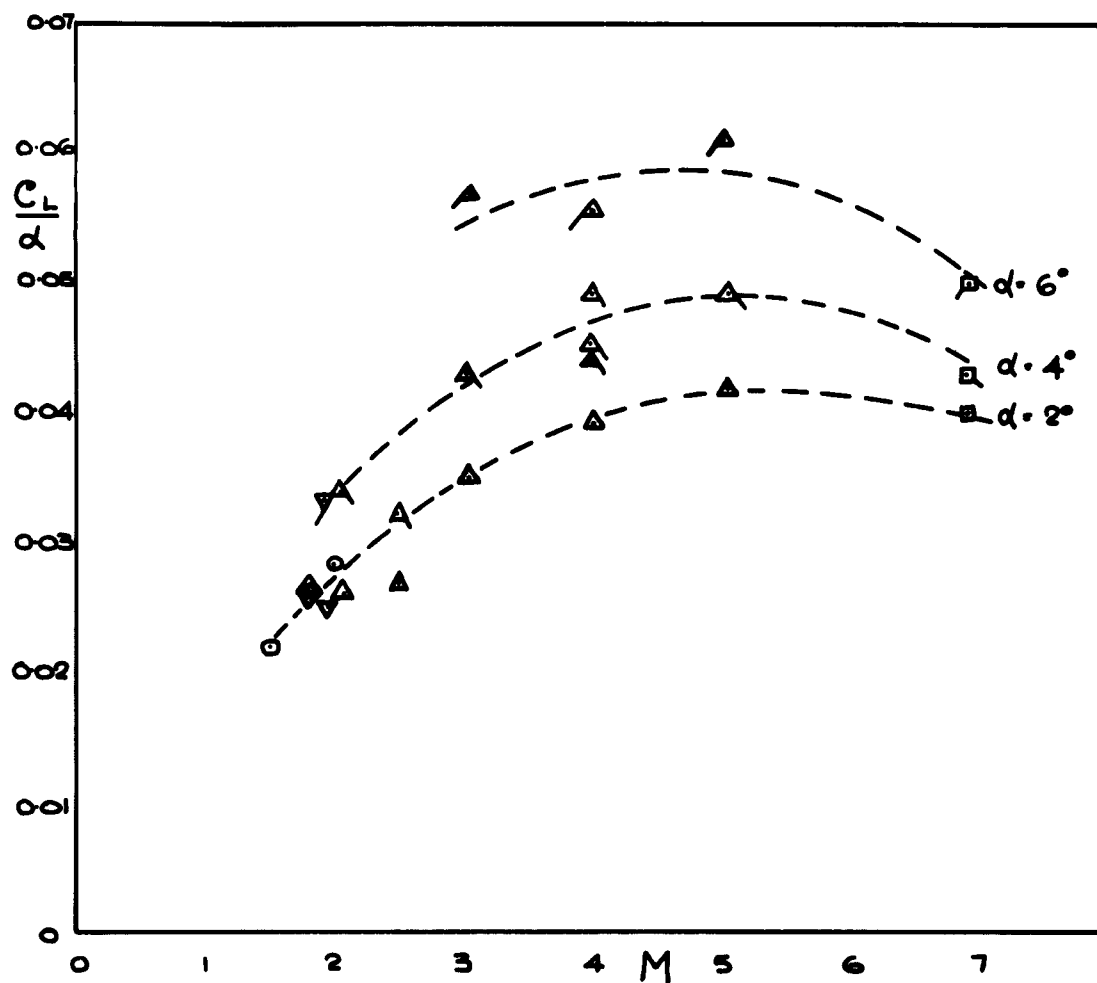


Fig.10(a) AGARD Model A. Variation of lift slope with Mach number

$\alpha = 2^\circ \quad 4^\circ \quad 6^\circ$						REF.
Δ	Δ	Δ	1' x 1'	$R = 4 \text{ to } 20 \times 10^6$	NACA	4 & 5
\square	\square	\square	11"	$R = 4 \times 10^6$	NACA	8
\circ	\circ	\circ	8' x 6'	$R = 30 \times 10^6$	NACA	8
∇	∇	∇	8" x 8"	$R = 5.6 \times 10^6$	NORWAY	UNPUBLISHED

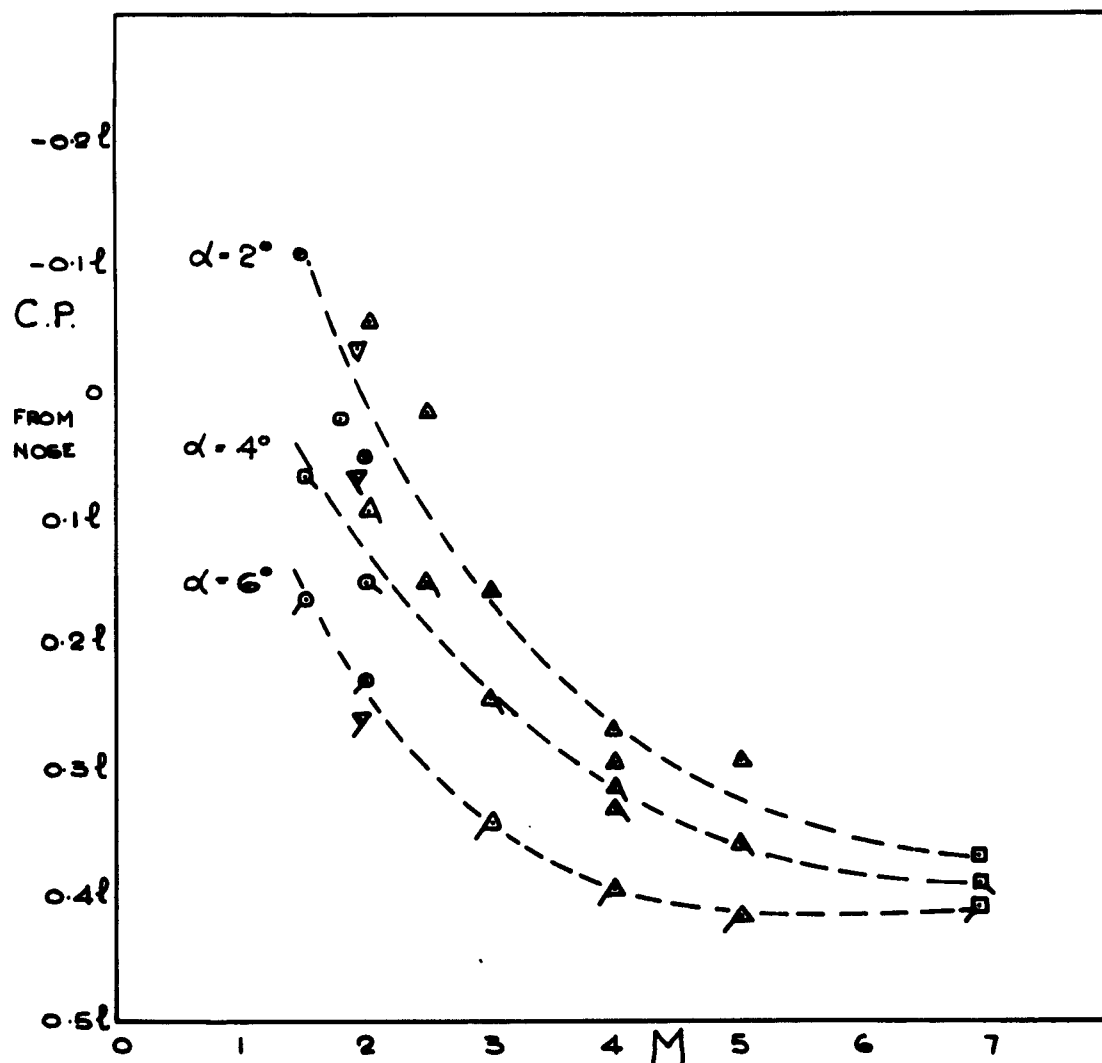


Fig.10(b) AGARD Model A. Variation of centre of pressure with Mach number

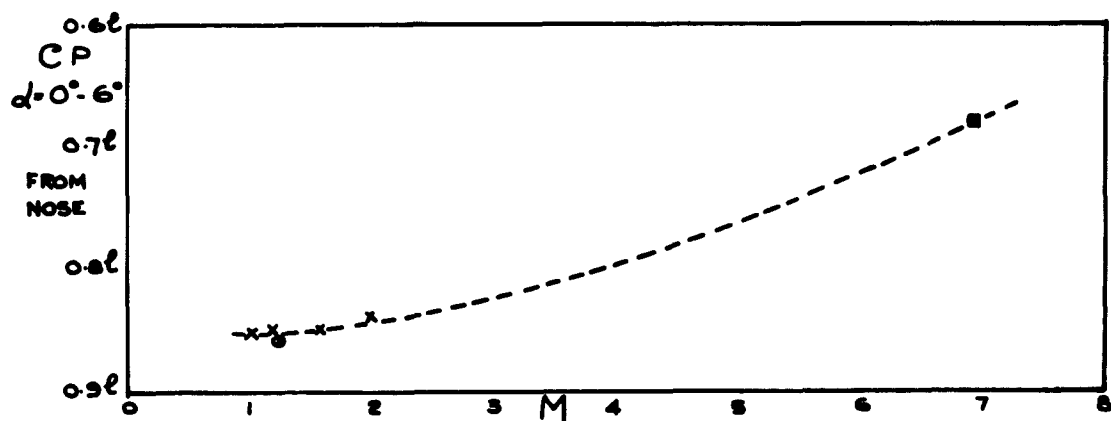
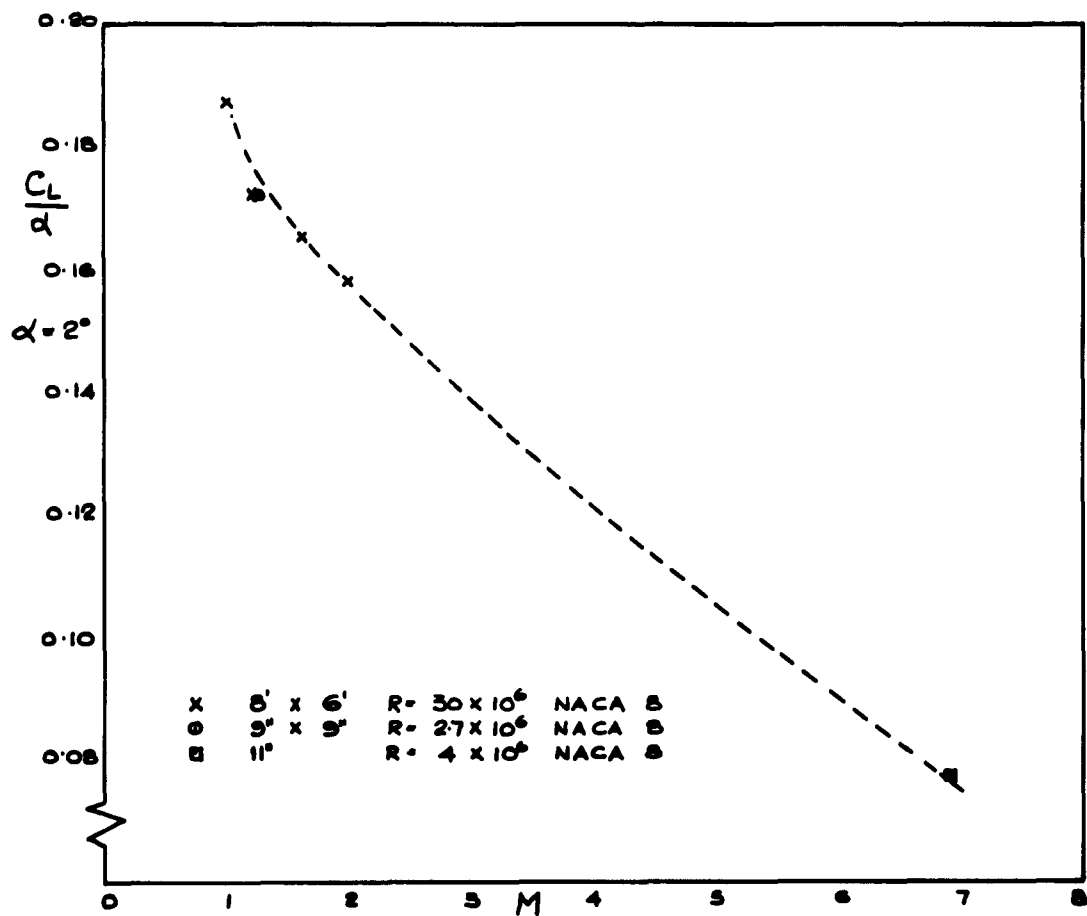


Fig.11 AGARD Model A with fins. Variation of lift slope and centre of pressure

PART II

**A REVIEW OF MEASUREMENTS ON AGARD CALIBRATION MODEL B
IN THE TRANSONIC SPEED RANGE**

by

H. Valk and J.H. van der Zwaan

Nationaal Lucht- en Ruimtevaartlaboratorium, Amsterdam

SUMMARY

This report contains a survey and a comparison of the results from tests with AGARD Calibration Model B at Mach numbers between 0.7 and 1.3. The available data include tests in different wind tunnels, at different Reynolds numbers and blockage percentages for models with and without fixed transition.

The results from different sources show many discrepancies; some of these can be explained. A first effort is made to establish reference curves, to facilitate further comparison.

CONTENTS

	Page
SUMMARY	36
LIST OF TABLES	38
LIST OF FIGURES	38
NOTATION	40
1. INTRODUCTION	43
2. APPARATUS	43
2.1 Test Facilities	43
2.2 Model	43
2.3 Model Support	44
3. RESULTS AND DISCUSSION	44
3.1 General	44
3.2 Lift	45
3.3 Lift-Curve Slope	47
3.4 Moment	48
3.5 Neutral Point	49
3.6 Forebody Drag	50
3.7 Base Drag	51
4. CONCLUSIONS	52
REFERENCES	53
TABLES	55
FIGURES	58

LIST OF TABLES

		Page
Table I	General Data on Models and Facilities	55
Table II	Accuracy and Repeatability of the Measurements, as Stated in the References	57

LIST OF FIGURES

Fig.1	AGARD Model B	58
Fig.2	Reynolds number, based on mean aerodynamic chord, versus Mach number	59
Fig.3	Lift coefficient versus Mach number for all available tests	60
Fig.4	Lift curve slope at $C_L = 0$ versus Mach number for all available tests	61
Fig.5	Pitching moment versus Mach number for all available tests	62
Fig.6	Neutral point at $C_L = 0$ versus Mach number for all available tests	63
Fig.7	Forebody drag coefficients versus Mach number for all available tests	64
Fig.8	Base drag coefficient versus Mach number for all available tests	64
Fig.9	Reference curves for lift coefficient versus Mach number	65
Fig.10a-j	Comparison of data with reference curves for lift	66 - 70
Fig.11	Reference curve for lift curve slope at $C_L = 0$ versus Mach number	71
Fig.12a-o	Comparison of data with reference curve for lift-curve slope at $C_L = 0$	72 - 74
Fig.13	Examples of lift-curve slope variation with angle of attack	75
Fig.14	Reference curves for pitching moment coefficient versus Mach number	76

		Page
Fig.15a-i	Comparison of data with reference curves for pitching moment	77 - 81
Fig.16	Reference curve for neutral point at $C_L = 0$ versus Mach number	82
Fig.17a-l	Comparison of data with reference curve for neutral point at $C_L = 0$	83 - 86
Fig.18	Skin friction drag at $M = 0.8$ as a function of Reynolds number, based on c_{av}	87
Fig.19a-c	Reference curve for transonic drag rise at $C_L = 0$ and general comparison	88
Fig.20a-l	Comparison of data with reference curve for transonic drag rise	89 - 91
Fig.21a-k	Base drag coefficient at $C_L = 0$ versus Mach number	92 - 94

NOTATION

A_b	body base area
b	wing span
B	test section width
\bar{c}	mean aerodynamic chord, $= 2.309 D$
c_{av}	average geometric chord of wing-body combination, $= \frac{\text{wetted area of wing-body combination}}{2(b - D) + \pi D} = 1.50 \bar{c}$
C_{Db}	base drag coefficient, $= -(A_b/S)C_{pb}$
C_{Df}	forebody drag coefficient, $= \frac{\text{forebody drag}}{qS} = C_{Dt} - C_{Db}$
ΔC_{Df}	transonic drag rise coefficient, $= C_{Df} - (C_{Df})_{M=0.8}$
C_f	skin-friction drag coefficient, $= \frac{\text{skin-friction drag}}{q \times \text{half wetted area}}$
C_{Dt}	total drag coefficient
C_L	lift coefficient, $= \text{lift}/(qS)$
$C_{L\alpha}$	lift curve slope, $= dC_L/d\alpha$
C_m	pitching moment coefficient about 50% of mean aerodynamic chord (mrc), $= \text{moment}/(qS\bar{c})$
C_{pb}	base pressure coefficient relative to free stream static pressure, $= (p_b - p)/q$
d	sting diameter
D	body diameter
H	test section height
l	length of straight portion of sting
L	length of body, $= 8.5 D$
M	Mach number
mrc	moment reference centre, 50% of mean aerodynamic chord

p	free stream static pressure
p_b	base pressure
q	free stream dynamic pressure, $= \frac{1}{2} \rho V^2$
r	local body radius
Re	Reynolds number based on \bar{c}
Re'	Reynolds number based on c_{av}
S	total wing area, $= 6.928 D^2$
V	free-stream velocity
x	distance along body axis
X_{mrc}	distance of mrc aft of model nose in body diameters, $= 5.943$
X_{np}	distance of neutral point at $C_L = 0$ aft of model nose in body diameters, $= X_{mrc} - (\bar{c}/D)(dC_m/dC_L)_{C_L = 0}$
α	angle of attack
θ	cone angle of sting
ρ	free stream density

A REVIEW OF MEASUREMENTS ON AGARD CALIBRATION MODEL B IN THE TRANSONIC SPEED RANGE

1. INTRODUCTION

AGARD Calibration Model B is an ogive-cylinder with a delta wing, originally designed for the calibration of supersonic wind tunnels, but it is often also used for calibrating transonic wind tunnels.

This report contains a comparison of the results at Mach numbers between 0.7 and 1.3.

The available data were taken from References 1-11. These data were obtained in tests in different wind tunnels, at different Reynolds numbers and blockage percentages for models with and without fixed transition. Table I shows that there are twenty-two different tests to be compared, including two free-flight tests.

2. APPARATUS

2.1 Test Facilities

In so far as they are known, the most significant data of the test section such as size, wall shape and open percentage, are shown in Table I. Further details of the test facilities are given in Reference 1-12 and will not be repeated here.

2.2 Model

AGARD Calibration Model B is a configuration consisting of a wing and body combination. The wing is a delta in the form of an equilateral triangle with a span four times the body diameter. The body is a cylindrical body of revolution with an ogive nose. The model is shown in Figure 1 and is more fully described in Reference 13.

The model sizes of the various tests in relation to the test section sizes are given in Table I.

In a number of tests the transition of the boundary layer was fixed by trip wires on the body at 1.5 body diameters aft of the nose and on the upper and lower surfaces of the wing at 15% of the chord. Two tests (A4 and C2) were made with fixed transition by grit transition strips. Fixed transition on the body in test A4 was omitted. The diameter of the trip wires is given in Table I.

The nose of the model used for the tests B1, B2 and B3 was slightly different from the prescribed form. The difference, however, was quite small so that no influence on the measurements is to be expected.

Two tests (F1 and F2) were executed as half-model tests. A shim was used to keep the model out of the tunnel-wall boundary layer.

In the two flight tests (H1 and H2) the model was equipped with two vertical stabilization fins.

2.3 Model Support

The ultimate specification of the sting dimensions, given in Reference 13, was published after the completion of many tests, and a number of different sting configurations were used. The sting dimensions for the various tests are given in Table I.

3. RESULTS AND DISCUSSION

3.1 General

On analysing the data, it should be borne in mind that in most cases the AGARD calibration models were tested when the various wind tunnels had only just been put into operation and that, since then, modifications and improvements have been made without the models being re-tested. Moreover, the data were often reported in preliminary form and might not have been checked carefully in all cases. Hence the data presented are not necessarily the best results that the tunnels are capable of producing.

In this report the analysis of the data is confined to a Mach number range of 0.7 to 1.3. The Reynolds numbers of the various tests are represented in Figure 2. The mean aerodynamic chord is taken as the reference length.

Lift, lift-curve slope, moment, neutral point, forebody drag and base drag are compared. The coefficients are plotted against Mach number in Figures 3-8. Obviously there is a considerable scatter in these results.

The factors which may, in general, affect the data are

- (i) instrument errors,
- (ii) tunnel-wall interference,
- (iii) other imperfections of the tunnel flow,
- (iv) sting interference,
- (v) imperfections of the model,
- (vi) Reynolds number and the method of fixing boundary layer transition.

The available information does not permit evaluation of all these factors. This holds especially for (i), (iii) and (v). As far as (i) and, to a certain extent, (iii) are concerned, the available information on accuracy and repeatability is shown in Table II. It is evident that this information is not sufficient to separate the influence of the accuracy of the measurements from the other factors. In general very little is known about the influence of the factors (i), (iii) and (v) on the

measurements under consideration. Unless stated otherwise in this report it has been assumed that the effect of these factors is small enough to justify an attempt to correlate the discrepancies with the factors (ii), (iv) and (vi).

The first aim of the procedure followed in the detailed analysis was to try to take into account the factors (ii), (iv) and (vi) in the form of certain suitable parameters and thus to select corresponding results. Wherever this procedure succeeded, so-called 'reference curves' were established and the other data were compared with these curves. On the other hand, in certain cases the reverse procedure was adopted, namely to select the data which show conformity and to try to derive conclusions from this fact.

It is well recognized by the authors that the analysis presented in this report is not complete. In many cases the explanation of the observed facts is lacking. However, it was thought to be worth making the results at this stage available to those interested in the AGARD calibration model program. The results, even in the present form, may prove useful for certain purposes. From contacts with some institutes the authors received comments which are also incorporated in the report.

Finally, it may be stated that the aerodynamic forces are in themselves 'integrated' effects. This makes it difficult to reach detailed conclusions. The analysis would doubtless have been facilitated if the more direct effects had also been measured by taking pressure measurements and schlieren pictures, etc. An extension of the calibration program in this direction would be greatly welcomed.

3.2 Lift

For all the tests the lift coefficient was plotted against Mach number for three different values of angle of attack, 0° , 4° and 8° . At higher angles of attack insufficient data are available.

It is to be expected that corresponding results will be found for those tests where the tunnel wall interference is sufficiently small and where no considerable scale effects are present. The effect of a difference in sting configuration may be considered negligible.

A rough theoretical estimate of the tunnel wall influence on lift for this model showed that large effects are not likely, in view of the fact that the wing area is relatively small. Therefore, as a starting point, the data were gathered from the tests with fixed transition and with natural transition at high Reynolds number. These tests* are A3, A4, B2, B3, C2, C3, C4, D2 and F2. These tests showed agreement with the exception of C3, C4 and F2. Figure 9 shows the results for A3, A4, B2, B3, C2 and D2, together with reference curves which are representative for the group. This correspondence is taken as the basis for a further analysis.

In Figure 10 a comparison of all data with the reference curves (dotted lines) is given. It is obvious that the results selected to compose the reference curves show good agreement with these curves (Figs. 10c, 10d, 10e and 10g). The results of B2 and

* No C_L data are available for D4 and H2.

B3 approach the reference curves even more closely, if a correction is made for the effect of asymmetry which is shown in the results at zero degrees. Although a trip was used in test D2, the discrepancies at higher angles of attack may be due to the low Reynolds number: possibly the trip wire diameter was too small to be effective. For the rest it is not thought that at the present stage more can be said about the differences within this group.

The following table gives the main characteristics from the viewpoint of tunnel wall interference of the selected results.

Test	Model Blockage %	Wall	
		Type	Open %
A3, A4	1.15	4 perf.	6
B2, B3	0.17	4 slotted	11
C2	0.20	4 perf.	-
D2	0.50	4 perf.	8

So the foregoing conclusion means that, within the limits presented in the table, no wall interference effects can be traced. This result, together with a study of Table I, leads to the assumption that significant wall interference effects need not be expected either for the test A2 (same wall system as for A3, A4; 0.01% blockage ratio), B1 (same wall system and blockage ratio as for B2, B3), C3 (same wall system and blockage ratio as for C2) and D1 (same wall system and blockage ratio as for D2)*. So it is appropriate to study the results of these with respect to possible scale effects.

In the results of test A2 (Fig.10b) there is a remarkable 'bump' apparent between $M = 0.9$ and $M = 1.0$. A similar effect is shown in B1 (Fig.10d) and, to a less extent, in C2 (Fig.10e).

The results of C3 are entirely different from the reference curves. These differences are not thought to be of aerodynamical origin, the more so because for C3 and C2 the same model was tested in the same wind tunnel with only a different method of fixing boundary layer transition.

The differences between D1 and D2 (Fig.10g) can only be correlated with the influence of the trip wire.

As a conclusion for the group A2, B1, C3 and D1 it may be said that on the one hand certain scale effects seem to be present; on the other hand it is likely that some experimental imperfections exist.

Finally the results of A1, C4, E1, F1, F2 and G1 have to be considered, being the tests for which neither tunnel wall interference nor scale effect can be excluded at first sight.

* No C_L data are available for C1, D3, D4.

In view of the fact that the blockage ratio is 2.5% and the Reynolds number fairly high, it is appropriate to ascribe the discrepancies of test A1 (Fig.10a) to wall interference. Tunnels designed to provide the least interference over a wide range of transonic Mach numbers behave somewhat like an open-jet tunnel at Mach numbers near one. Therefore the indicated Mach number should be corrected (decreased) as a function of model size.

For C4 (Fig.10f) it is assumed, as was done for C3, that the large difference from the reference curve is of non-aerodynamic origin.

For E1 (Fig.10h) the 'official' curves were obtained by taking the mean value of two tests. The latter of the two was executed with a re-wired balance. The results of this test alone show a much better agreement with the reference curve.

The data for F1 and F2 (Fig.10i) are consistently lower than the reference curve. This result agrees well with the general features of half-model testing, as discussed in more detail in Reference 14. It is mentioned in this report that typical values of the lift curve slope for half-models of some wing-body configurations were around 10% lower than the corresponding values for complete models.

Discrepancies are present in the results of test G1 (Fig.10j). The origin of this may be found in the fact that the test was made in an open-jet tunnel. It is likely that, at least for the highest Mach number (0.99), a considerable positive correction is needed.

3.3 Lift-Curve Slope

The lift-curve slope is taken at $C_L = 0$. The same tests as in Section 3.2 were used in composing the reference curve, including tests D4 and H2 of which no data were available for the C_L comparison. These results and the reference curve are shown in Figure 11. The dotted line in this figure represents a curve giving theoretical values taken from Reference 11. The calculation for the curve of Reference 11 was derived from Reference 15. The agreement is very good. A comparison of all the data with the reference curve (dotted line) is given in Figure 12.

At first sight it may be considered superfluous to study the lift-curve slope, since the C_L curves for $\alpha = 4^\circ$, as shown in Figure 10, already represent the mean value of $C_{L\alpha}$ in the region between 0° and 4° . However, in several tests at certain Mach numbers, there is a change in lift-curve slope in the region of zero angle of attack, while the overall character of the C_L - α curve is not changed. These effects are evident in tests B1 and B3 at Mach numbers between 0.9 and 1.0 and in C2 at Mach numbers around 1.0. Typical examples are shown in Figure 13. In several other tests this tendency of change in lift-curve slope is also apparent, but a smooth line was drawn in the reference curves, because the discrepancies were considered to be within the accuracy of the measurements. In Figure 12 the results are shown as they are given in the original reports.

In Figure 11 the reference curve reflects mainly the overall value of the lift-curve slope, represented by the dotted lines in Figure 13. This makes it clear that the reference curve is in fair agreement with the reference curve for lift at $\alpha = 4^\circ$ (Fig.9).

Apart from the effect just mentioned, only the following comparisons are made with regard to lift-curve slope:

Test C3 also shows a marked change of $C_{L\alpha}$ in the region of $\alpha = 0$. While here the overall value is higher than the reference curve, as shown in Figure 10f, the local value given in Figure 12g is quite near the reference curve.

For C1 (Fig.12g), D3 (Fig.12k), and H2 (Fig.12o) no data on lift were available; only the lift-curve slope was known.

3.4 Moment

It was intended to follow the same procedure as in Section 3.2 to obtain reference curves. After preliminary observations, however, it appeared that only three of the selected tests, A4, B2 and B3, show corresponding results up to a Mach number of 1.10. With so few data the reference curves should be handled with great care. However, for a simple mutual comparison the reference curve, apart from the interpretation which may be given to it, will be used.

In accordance with the specification of Reference 13, the moment reference centre is taken at 50% of the mean aerodynamic chord. The data have been plotted against Mach number for $C_L = 0, 0.2$ and 0.4 . The reference curves at these lift coefficients are represented in Figure 14. In Figure 15 the available results are compared.

Among the many discrepancies which can be seen in Figure 15, the following are noteworthy:

The tests A2 (Fig.15b), C2 (Fig.15e), D1 (Fig.15g) and, to some extent, B1 (Fig.15d), C4 (Fig.15f) show a bump in the curves at Mach numbers between 0.9 and 1.0. A similar bump, but in the opposite direction, is found in the lift curves of tests A2, B1 and C2 (Section 3.2). When a smooth curve is drawn through all the points, except those in the Mach number range mentioned, it is seen that the bump means an increase in lift and a decrease in moment, so that the extra lift must act downstream of the moment reference centre. For C4 the same effect can be demonstrated, though less clearly, for the lift curve. For D1 the effect is present if the supersonic values of the moment for D1 and D2 are brought to the same level.

As was the case for the lift, test A1 (Fig.15a) shows a large deviation from the reference curves. Again this may be due to a tunnel-wall interference effect.

In contrast with what was said in Section 3.2, tests C2 and C3 (Fig.15e) give the same results, though different from the reference curves.

Test C4 (Fig.15f) agrees much better with the reference curves than was the case for the lift.

Tests D1 and D2 (Fig.15g) differ markedly from the reference curves.

It may be concluded from the results given in Reference 7 (test E1) that the re-wiring of the balance had hardly any effect on the moment. Accordingly the C_m curve (Fig.15h) is in good agreement with the reference curve.

Up to a Mach number of 1.05 test F2 (Fig.15i) shows a good agreement. As is revealed in Reference 8, the data in the range $M = 1.0$ to $M = 1.35$ must be excluded, as they are affected by shock-wave reflection phenomena.

3.5 Neutral Point

The study of the neutral point is in fact the study of dC_m/dC_L . In this report the position of the neutral point is given in body diameters aft of the model nose and only the position at $C_L = 0$ is studied.

By means of the tests A3, A4, B2, B3 and C2 it was possible to determine the reference curve. As a check on the latter, a curve giving theoretical values is available. This curve was taken from Reference 11, in which it was derived from Reference 15. Both curves and the results of the selected tests are represented in Figure 16.

The reference curve agrees very closely with the reference curve for the moment at $C_L = 0.2$ (Fig.14). This agreement supports the moment reference curve, which was based only on A4, B2 and B3.

Much the same as was the case for the comparison between lift-curve slope and lift, disagreement between the moment at $C_L = 0.2$ and the neutral point at $C_L = 0$ will reveal non-linearities in the slope of the C_m-C_L curves. This is clearly the case for test B1. For some of the other tests, such as B3, the effect is present but less marked, or the non-linearity is spread over a wider range of C_L .

Figure 17 shows the comparison of all the available data with the reference curve. For several of the tests, there is a striking correspondance between the deviations from the reference curve for the neutral point and the lift-curve slope, namely for test A1 (Figs.17a and 12a), B1 (Figs.17d and 12d), C2 (Figs.17e and 12h), F1 and F2 (Figs.17j and 12m), and to a less extent A2 (Figs.17b and 12b), B3 (Figs.17d and 12f) and C1 (Figs.12g and 17e). If in these tests the value of $C_{L\alpha}$ at a given Mach number is greater (respectively smaller) than the value of the reference curve, the value X_{np} is also greater (respectively smaller) than the reference curve value. The resulting change in dC_m/dC_L indicates that the extra (positive or negative) lift, with regard to the reference curve lift, is acting downstream of the moment reference centre. This result is a confirmation of the same conclusion arising from the lift-moment comparison for $\alpha \approx 4^\circ$ and $\alpha \approx 8^\circ$ (Section 3.4).

The other tests showed only the following points:

For C1, D3, D4, G1 and H2, neutral point data exist though no moment data for $C_L = 0.2$ and 0.4 were available.

D3 and D4 (Fig.17h) show marked discrepancies.

The agreement for G1 (Fig.17k) is very good.

For H2 (Fig.17l) a general agreement with the reference curve exists.

Test C3 (Fig.17e) gives about the same results as C2, which corresponds with the results of the moment comparison.

3.6 Forebody Drag

The forebody drag is obtained by subtracting the drag due to the base from the total drag. Because the aft end of the body is entirely cylindrical, the forebody drag may be expected to be independent of the sting configuration. In this paper the forebody drag is observed only at $C_L = 0$.

The drag characteristics as a function of Reynolds number permit an interesting comparison with the skin-friction drag of a flat plate. From pressure measurements at the N.L.L. on the body of the AGARD Model C, it has been concluded that, up to a Mach number of 0.8, there is no pressure drag of any significance for the body. It is expected that the contribution of the wing to the pressure drag is also negligible. So it can be assumed that the forebody drag at $M = 0.8$ represents the subsonic skin-friction drag. A comparison such as is shown in Figure 18 can be made. Here the C_{Df} values measured for the model have been converted into a skin-friction coefficient C_f , using one-half of the wetted area of the complete model as a reference instead of the wing area. For the Reynolds number, a problem arises as to what reference length should be used in order to compare the wing-body combination with a simple rectangular flat plate. An average geometric chord for the complete wing and body combination, c_{av} , was chosen, and it appeared to be 1.5 times the mean aerodynamic chord. The measured drag points with free transition clearly exhibit the influence of Reynolds number on the transition from laminar to turbulent boundary layer. The results with fixed transition agree very well with the dotted line. The latter represents the calculated skin-friction drag, if it is assumed that the boundary layer before the transition wire is entirely laminar and aft of the wire entirely turbulent*. The general tendency of Figure 18 is that the scatter in the subsonic values of the forebody drag is for the most part due to Reynolds effect.

In that case it is possible to eliminate the Reynolds effect in the following analysis by subtracting the forebody drag at $M = 0.8$ from the drag at the other Mach numbers. What remains is a comparison of the 'transonic drag rise', the ΔC_{Df} .

From Figure 19 it is to be seen that the results of several tests can be subdivided into three categories, which show mutually corresponding results. The first category (Fig. 19a) contains the tests A2, H1 and H2. The model dimensions of test A2 are very small in relation to the test section sizes, so that the test can be considered to be interference free. Tests H1 and H2 were made in free flight†. The curve drawn through the measured points of these tests can be assumed to represent the interference-free transonic drag rise and is therefore taken as the reference curve.

A number of tests, namely B1, B2 and B3 and C2, C2 and C3 show corresponding results (Fig. 19b), but the trend of the transonic drag rise is flatter than for the

* Of H1 only the total drag was known; the forebody drag was computed by subtracting the base drag of H2 from the total drag. The pressure drag of the stabilization fins of H1 and H2 was neglected, since the fins are very thin.

† No correction has been made for compressibility effects which, at this Mach number, are negligible.

reference curve. The two groups B and C have been performed in test sections with completely different wall systems; only the blockage ratio of the models is about the same (0.17% and 0.20% respectively). Tests A3 and A4, related to again another wall system and having a considerably higher blockage ratio (1.15%), show the same trend. Two tests, A1 and C4, show the same tendency but to a greater extent. Test A1 has been performed with a similar wall system as A3 and A4; test C4 is related to the same wall system as C1, C2 and C3. The blockage ratio for this category is 2.5% and 1.6% respectively. Generally, it may be said that a higher blockage ratio gives a flatter trend of the transonic drag rise.

In Figure 20 a comparison of all the available data with the reference curve is given and the following points are noticeable:

The transonic drag rise of the tests C1, C2 and C3 (Fig.20e) show a flat part in the curve at $M = 1.04$. This is probably due to a tunnel-wall interference effect, more of which will be said in Section 3.7.

From Figure 20g it appears that tests D1 and D2 (blockage ratio 0.5%) give results which agree with the reference curve. Test D3 and D4 (blockage ratio 0.7%) give differing results (Fig.20h), but agreement is very good if the two curves are shifted with respect to each other over a Mach number range of 0.03.

The transonic drag rise of test E1 (Fig.20i) does not agree very well, but the total drag results of repeated runs are identical, while the base drag results are different. So the base drag results, and therefore the forebody drag results, must be considered suspect.

In pursuance of the contact with N.R.C., the drag data of tests F1 and F2 in the range $M = 1.0$ and $M = 1.35$ must be excluded, as they are affected by shock reflections. The blockage ratio of F1 and F2 is 0.6%, which is considerably lower than is the case for tests A1 and C4. Up to a Mach number of 1.05, however, the results (Fig.20j) show the same tendency as the curve in Figure 19c (high blockage ratio). This may be due to the fact that there is only one slotted liner, located on the tunnel side wall directly opposite to the side wall on which the half-model is mounted.

The transonic drag rise characteristic of test G1 (Fig.20k) does not show an obvious compressibility effect.

3.7 Base Drag

In Figure 8 a survey is given of all the available base drag data for $C_L = 0$ and there is obviously considerable scatter. Apart from wave reflections, the effect of which will be apparent in a limited region of supersonic Mach numbers, the important parameters for the base drag are Reynolds number and sting geometry. The effect of Reynolds number can be large, if the transition of the boundary layer occurs near or in the mixing region downstream of the base. For the tests under consideration it may be expected that the transition already occurs on the body, with the possible exception of test D3 (see Fig.18). For D3, however, no base drag data are available. Since, in the other tests, the boundary layer becomes turbulent at a certain distance before the base, it may be expected that the influence of the

Reynolds number is not very pronounced. So, it is logical to compare the results of those tests which duplicated the sting geometry, as specified in Reference 13, most closely. Unfortunately these tests, A1, A2, A3, A4, B1, B2 and B3, do not show mutual agreement.

It should be noticed here that, apart from the factors mentioned, the tunnel operating conditions may have a large influence on the base pressure. In transonic wind tunnels the Mach number distribution can be drastically affected by variation in tunnel pressure ratio. Thus changes in tunnel pressure ratio can be expected to affect base drag measurements, especially when the model is large and its base is situated in the aft part of the test section. No data on this were available. However, the tests with the largest blockage ratios (A1, A3, A4, C4 and E1) are the most suspect.

Furthermore, there exists a reasonable doubt of the results of the following tests:

C4, because an entirely different sting was used;

E1, because the base drag measurements were doubtful, as mentioned in Section 3.6;

F1 and F2, because these are for a half-model without sting and because, in the range $M = 1.0$ to $M = 1.35$, the measurements are affected by shock reflections, as already mentioned;

G1, because the base drag is considerably lower than in one of the other tests.

From this it is evident that a reliable reference curve cannot be found. Therefore the results of Figure 8 are represented individually in Figure 21 and only one further comment remains.

Although the sting geometry is different, agreement was found between the results of the tests B1, B2 and B3 (Fig.21d) and C1, C2 and C3 (Fig.21e). Furthermore, there is, for the tests C1, C2 and C3 at $M = 1.05$, a point lying completely outside the curve. This may be due to a shock wave reflection, which hits the base. It does not seem to be a reflection of the bow wave, but the suggestion is ventured that a shock wave comes from the leading edge of the test support and reaches the model after being reflected by the opposite wall. At $M = 1.02$ this reflection hits the model further forward on the wing. This may be an explanation of the flat part in the transonic drag rise curve and possibly also of the irregularities at this Mach number for the data on lift, lift-curve slope, moment, and neutral point.

4. CONCLUSIONS

The paper analyses the results of tests at transonic speeds in various wind tunnels on the AGARD Calibration Model B. It has been generally found that the agreement between the results is worse than the experimenter would expect. On the other hand the agreement between the results of some of the tests allows the establishment of reference curves that to a certain extent represent the current results, and which have been used to facilitate a further comparison. An exception is made for the base drag data where no correlation is evident.

The data points that disagree form curves that are sometimes different in value, at other times different in trend. Detailed explanation of the discrepancies cannot be given, but in general the following conclusions can be drawn:

Part of the scatter, and even some of the largest differences, are very probably caused by imperfections in the measurements.

The scatter seems to be partly due to Reynolds number. Therefore it is desirable to test at sufficiently high Reynolds number or with fixed transition in order to obtain results that are suitable for comparison of the qualities of the wind tunnels.

In general, differences in the subsonic values of the forebody drag coefficient can be traced as the influence of the Reynolds number or of the methods, if any, of fixing transition of the boundary layer.

The model does not seem to be very sensitive to tunnel-wall interference. This conclusion applies especially to the lift interference, because the wing area is small with respect to the model size.

REFERENCES

1. Milillo, J.R.
Chevalier, H.L. *Test Results of the AGARD Calibration Model B and a Modified AGARD Model C in the AEDC Transonic Model Tunnel.* Arnold Engineering Development Center, AEDC-TN-57-6, May 1957.
2. Milillo, J.R. *Transonic Tests of an AGARD Model B and a Modified Model C at 0.01 percent Blockage.* Arnold Engineering Development Center, AEDC-TN-58-48, August 1958.
3. Dick, R.S. *Tests in the PWT 16 ft Transonic Circuit of an AGARD Model B and a Modified Model C at 1.15 percent Blockage.* Arnold Engineering Development Center, AEDC-TN-59-32, April 1959.
4. Schreiber, B. *A Compilation of Data from Tests of AGARD Models B and C in the Boeing Wind Tunnels.* Boeing, Seattle, Document D 2-5360.

5. Tate, S.E. *Performance of AGARD Calibration Models With and Without Transition Control in the Cornell 8-foot Transonic Wind Tunnel; Part I, AGARD B Models.* Cornell Aeronautical Laboratories, CAL WTO-362, January 1958.

6. O.N.E.R.A. *Caractéristiques Transsoniques des Maquettes AGARD B et C - Essais de l'ONERA.* ONERA Fiche Doc.176.

7. Wykes, R.C.
Fisher, R.A. *An Investigation of the Lift, Drag and Pitching Moment Characteristics of AGARD Calibration Models B and C at the Ohio State University Transonic Wind Tunnel.* North American Aviation Inc. Report 57 H-618, 1957.

8. Laberge, J.G. *Half-Model Measurements of Longitudinal Force and Moment Characteristics of AGARD Model B at Subsonic and Supersonic Speeds.* National Research Council of Canada, NRC Can. LR-267, December 1959.

9. Wedemeyer, E. *Drei-Komponentenmessungen am AGARD-Eichmodell B im AVA-Hochgeschwindigkeitskanal.* AVA, Göttingen, Report 58-02, June 24, 1958.

10. Piland, R.O. *The Zero-Lift Drag of a 60° Delta-Wing-Body Combination (AGARD Model 2) Obtained from Free-Flight Tests Between Mach Numbers of 0.8 and 1.7.* NACA TN 3081, April 1954.

11. Mitchell, J.L. *Rocket Model Investigation of the AGARD Model B Configuration by the NACA Langley Laboratory.* NACA Memorandum, February 7, 1957.

12. Wykes, R.C. *Test and Model Information for Transonic and Supersonic Wind Tunnel Tests of Sting Mounted, AGARD Calibration Models B and C at the Ohio State University 12 in. x 12 in. Wind Tunnel and at the North American Aviation, Inc. Supersonic Aerodynamic Laboratory (SAL) 16 in. x 16 in. Wind Tunnel.* North American Aviation Inc. Report 56 H-274, June 28, 1956.

13. A.G.A.R.D. *Wind Tunnel Calibration Models.* AGARD Specification 2, September 1958.

14. van der Blik, J.A. *Notes on Half-Model Testing in Wind Tunnels.* National Research Council of Canada, NRC Can. LR-235, January 1959.

15. Nielsen, J.N.
et alii *Lift and Pitching-Moment Interference between a Pointed Cylindrical Body and Triangular Wings of Various Aspect Ratios at Mach Numbers of 1.50 and 2.02.* NACA TN 3795, December 1956.

Test	Ref.	Institute	Wind Tunnel			
			Name	Test Section		
				Size	Walls	Open %
A1	1	A.E.D.C.	Transonic Model Tunnel	1 x 1 ft ²	4 perf.*	6
A2	2	A.E.D.C.	PWT Transonic Circuit	16 x 16 ft ²	4 perf.*	6
A3	3	A.E.D.C.	PWT Transonic Circuit	16 x 16 ft ²	4 perf.*	6
A4	3	A.E.D.C.	PWT Transonic Circuit	16 x 16 ft ²	4 perf.*	6
B1	4	Boeing	Transonic Wind Tunnel	8 x 12 ft ²	4 slotted	11
B2	4	Boeing	Transonic Wind Tunnel	8 x 12 ft ²	4 slotted	11
B3	4	Boeing	Transonic Wind Tunnel	8 x 12 ft ²	4 slotted	11
C1	5	C.A.L.	Transonic Wind Tunnel	8 x 8 ft ²	4 perf.	-
C2	5	C.A.L.	Transonic Wind Tunnel	8 x 8 ft ²	4 perf.	-
C3	5	C.A.L.	Transonic Wind Tunnel	8 x 8 ft ²	4 perf.	-
C4	5	C.A.L.	Transonic Wind Tunnel	8 x 8 ft ²	4 perf.	-
D1	6	O.N.E.R.A.	Soufflerie Courneuve	0.28 x 0.28 m ²	4 perf.	8
D2	6	O.N.E.R.A.	Soufflerie Courneuve	0.28 x 0.28 m ²	4 perf.	8
D3	6	O.N.E.R.A.	Soufflerie S 5 Chalais	0.2 x 0.3 m ²	2 slotted	-
D4	6	O.N.E.R.A.	Soufflerie S 5 Chalais	0.2 x 0.3 m ²	2 slotted	-
E1	7	O.S.U.	Transonic Wind Tunnel	12 in. x 12 in.	4 perf.	-
F1	8	N.A.E.	High Speed Wind Tunnel	30 in. x 16 in.	1 slotted†	3
F2	8	N.A.E.	High Speed Wind Tunnel	30 in. x 16 in.	1 slotted†	3
G1	9	A.V.A.	Hochgeschwindigkeitkanal	0.75 x 0.75 m ²	open jet	100
H1	10	N.A.C.A.				
H2	11	N.A.C.A.				

1

B : test section width
H : test section height
L : model length
b : wing span

D : body diameter
d : sting diameter
l : length of straight portion of s
 θ : cone angle of sting

TABLE I

General Data on Models and Facilities

Section		Model					Sting			Reynolds Number Range ($\times 10^{-6}$)	Remarks
		L/H	b/H	Blockage %	Transition	Same Model	d/D	l/D	$\theta/2$		
Walls	Open %										
4 perf.*	6	1.4	0.65	2.5	Natural	}	0.488	3.0	5.6°	1.6-2	} Model nose slightly different
4 perf.*	6	0.09	0.04	0.01	Natural		0.488	3.0	5.6°	0.7-1.2	
4 perf.*	6	0.95	0.45	1.15	Natural	}	0.50	3.08	1.11°	8.5-12	
4 perf.*	6	0.95	0.45	1.15	0.025 in.		0.50	3.08	1.11°	8.5-12	
4 slotted	11	0.40	0.13	0.17	Natural	}	0.483	2.98	2.94°	2.9-3.4	
4 slotted	11	0.40	0.13	0.17	0.006 in.		0.483	2.98	2.94°	2.9-3.4	
4 slotted	11	0.40	0.13	0.17	0.014 in.		0.483	2.98	2.94°	2.9-3.4	
4 perf.	-	0.40	0.19	0.2	Natural	}	0.50	1.5	-	1.7	
4 perf.	-	0.40	0.19	0.2	Grit		0.50	1.5	-	1.7	
4 perf.	-	0.40	0.19	0.2	0.015 in.		0.50	1.5	-	1.7	
4 perf.	-	1.06	0.50	1.6	0.015 in.		-	-	-	4.6	Sting configuration different
4 perf.	8	0.60	0.29	0.5	Natural	}	0.60	2.2	4°	0.92	
4 perf.	8	0.60	0.29	0.5	0.07 mm		0.60	2.2	4°	0.92	
2 slotted	-	0.85	0.27	0.7	Natural		0.60	2.2	4°	0.33	
2 slotted	-	0.85	0.27	0.7	0.07 mm		0.60	2.2	4°	0.33	
4 perf.	-	0.89	0.42	1.12	Natural		0.40	~5	-	1.3-1.8	
slotted†	3	0.51	0.23	0.6	Natural	}				1.4-1.6	Half model
slotted†	3	0.51	0.23	0.6	0.020 in.					1.4-1.6	Half model
open jet	100	0.67	0.31	0.6	Natural		0.30	2.7	step	1.7-2.0	
					Natural					1.0-1.5	Free flight
					Natural					5.3-11	Free flight

- no data available

•

• Inclined holes

† Right portion of sting

sting

† Slotted wall opposite the side wall on which the half-model is mounted

2

TABLE II

Accuracy and Repeatability of the Measurements, as Stated in the References

Test	ΔM	$\Delta \alpha$	ΔC_L	ΔC_m	ΔC_{Dt}	ΔC_{Df}	ΔC_{Db}	Remarks
A1	± 0.002	$\pm 0.10^\circ$	± 0.0140	± 0.0020	-	± 0.0040	± 0.0005	$0.70 \leq M \leq 1.15$
A1	± 0.006	$\pm 0.10^\circ$	± 0.0100	± 0.0010	-	± 0.0020	± 0.0002	$1.20 \leq M \leq 1.50$
A2	± 0.003	$\pm 0.30^\circ$	± 0.0150	± 0.0050	-	± 0.0060	± 0.0020	$0.70 \leq M \leq 1.15$
A2	± 0.006	$\pm 0.30^\circ$	± 0.0100	± 0.0020	-	± 0.0030	± 0.0010	$1.20 \leq M \leq 1.50$
A3, A4	± 0.003	$\pm 0.05^\circ$	± 0.0040	± 0.0020	-	± 0.0030	± 0.0003	$0.70 \leq M \leq 1.10$
A3, A4	± 0.006	$\pm 0.05^\circ$	± 0.0040	± 0.0020	-	± 0.0030	± 0.0003	$1.20 \leq M \leq 1.60$
B1, B2, B3	-	-	-	-	-	-	-	
C1, C2, C3	-	$\pm 0.10^\circ$	± 0.0021	± 0.0008	-	± 0.0003	-	
C4	-	$\pm 0.10^\circ$	± 0.0037	± 0.0006	-	± 0.0008	-	
D1, D2	-	-	-	-	-	-	-	
D3, D4	-	-	-	-	-	-	-	
E1	-	$\pm 0.01^\circ$	± 0.0050	± 0.0050	± 0.0010	-	± 0.0015	
F1, F2	± 0.020	$\pm 0.02^\circ$	± 0.0050	± 0.0007	± 0.0020	-	± 0.0002	
G1	-	-	-	-	-	-	-	
H1, H2	-	-	-	-	-	-	-	

- no data available

Notes, taken from the references:

1. The accuracy of the data of tests A1, A2, A3 and A4 has been determined by combining the errors in the balance read-out system, base pressure and stream parameters by a method based on a 95% level and a normal error distribution.
2. For C1, C2 and C3 the testing procedure resulted in the repetition of at least one model attitude during each run, from which an estimate was made of the repeatability.
3. The values for test E1 are based on repeatability.
4. The values of tests F1 and F2 are examples of typical uncertainties.

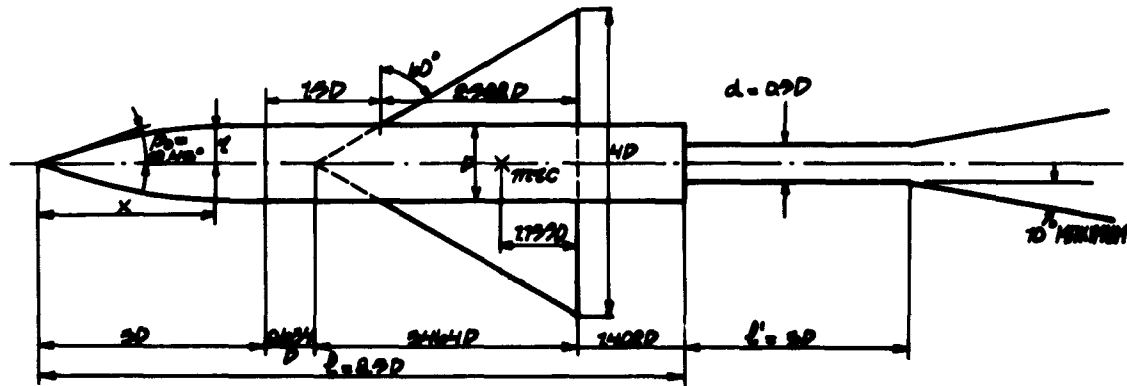


Fig.1 AGARD Model B

Wing profile : symmetrical circular arc section. Thickness ratio = 0.04

Nose profile : length 3 D. Equation of curve $r = \frac{x}{3} \left[1 - \frac{1}{9} \left(\frac{x}{D} \right)^2 + \frac{1}{54} \left(\frac{x}{D} \right)^3 \right]$

Radii of nose and wing leading edges should be D/500.

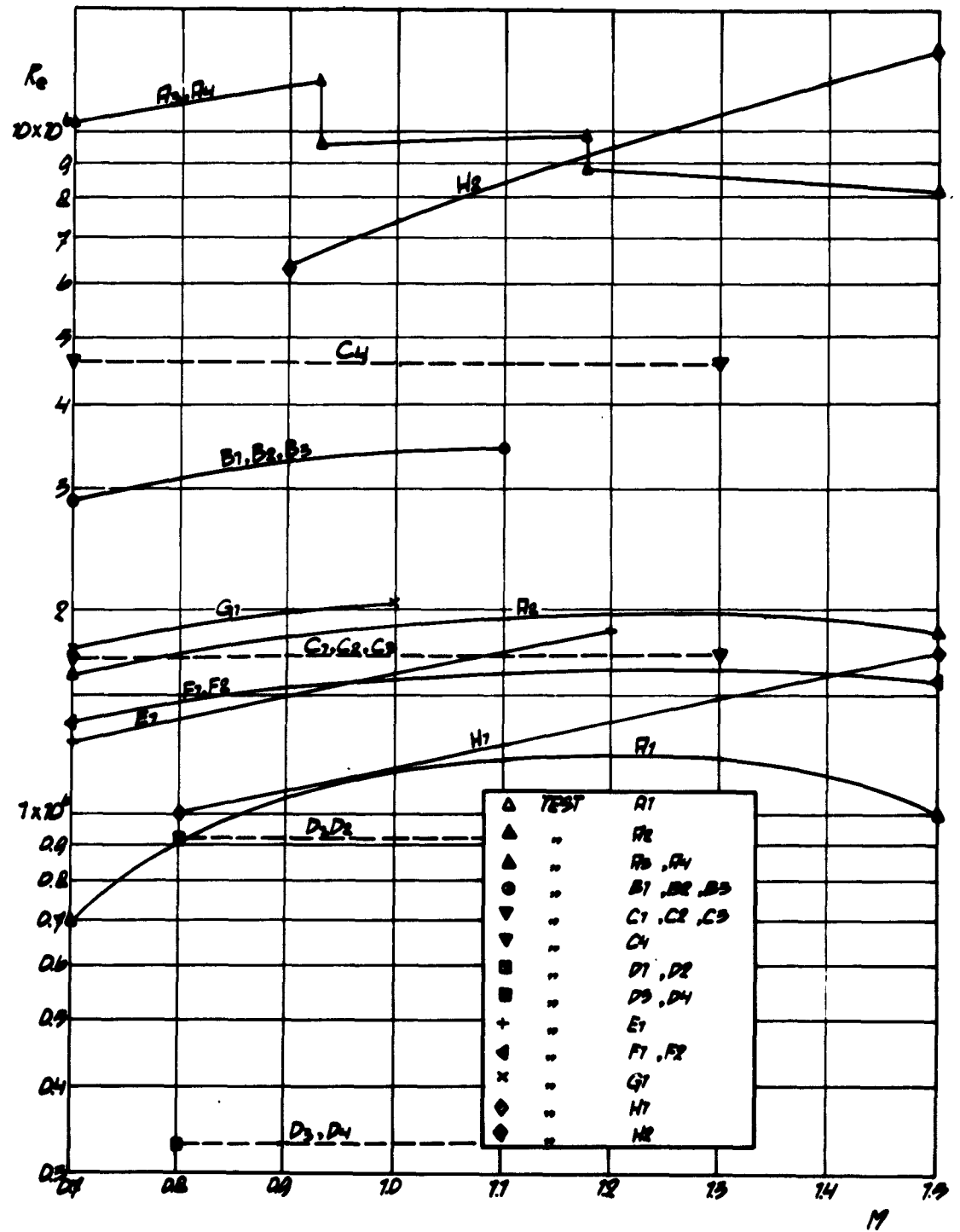


Fig.2 Reynolds number, based on mean aerodynamic chord, versus Mach number

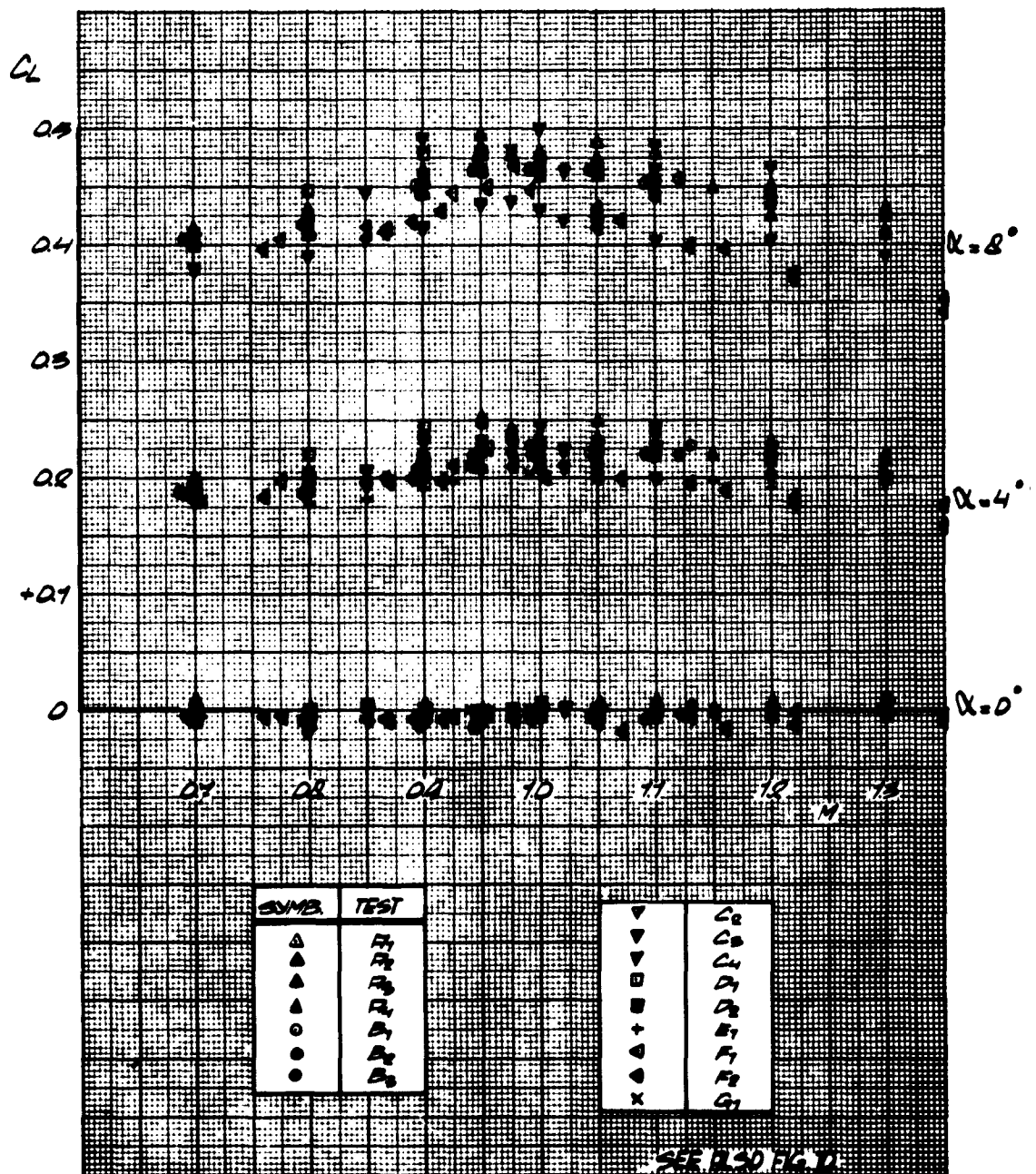


Fig.3 Lift coefficient versus Mach number for all available tests

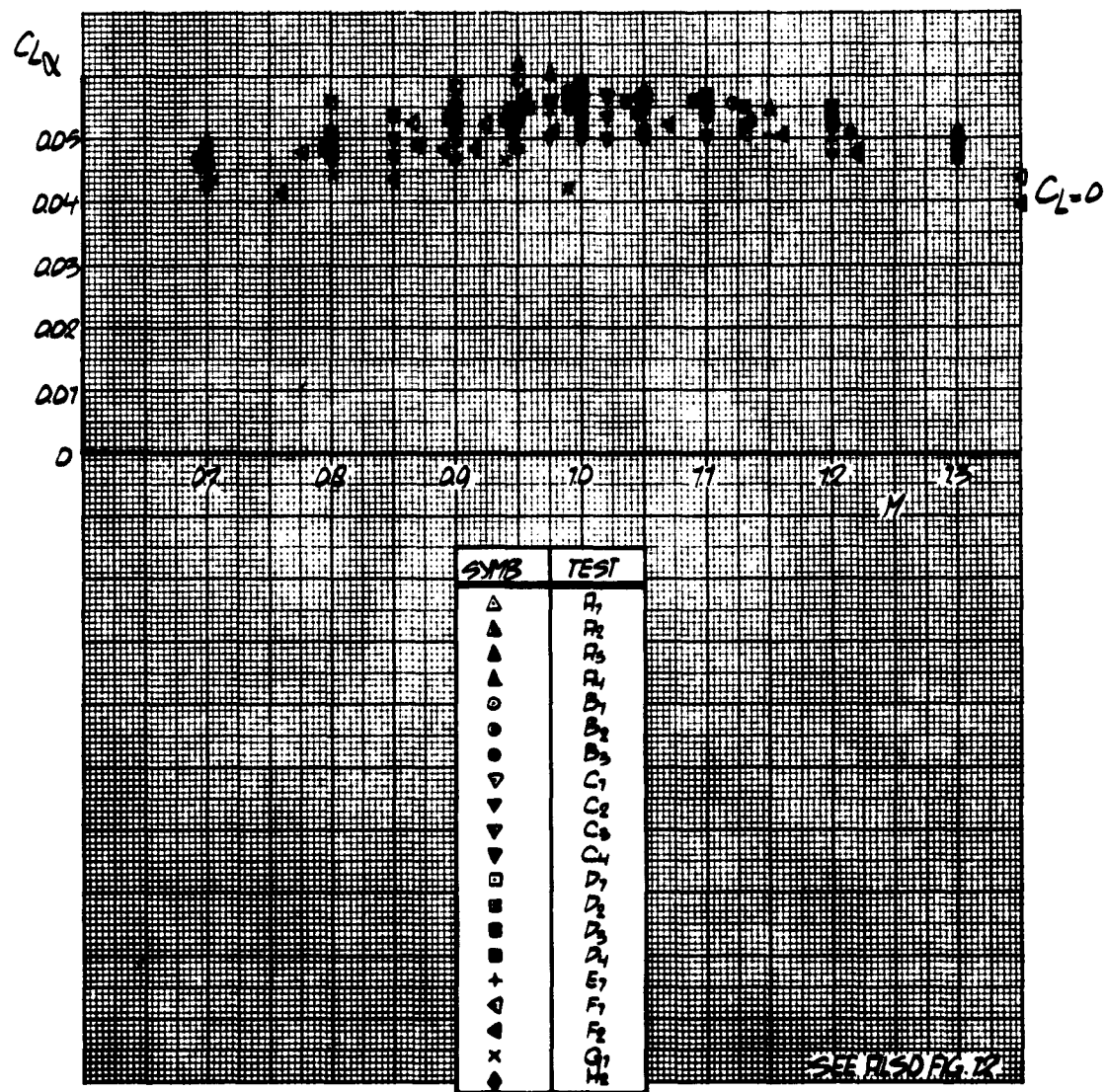


Fig.4 Lift curve slope at $C_L = 0$ versus Mach number for all available tests

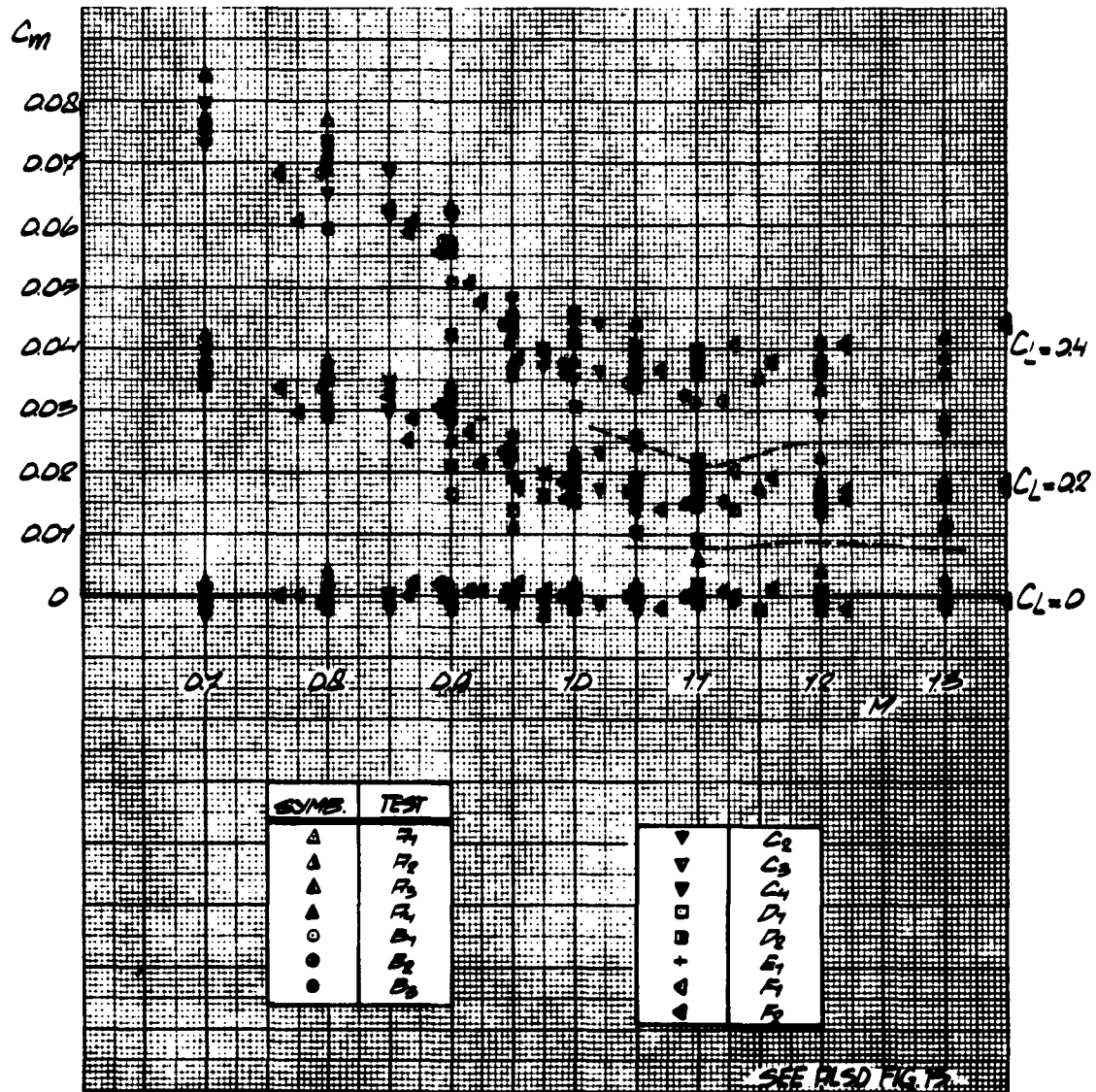


Fig. 5 Pitching moment versus Mach number for all available tests

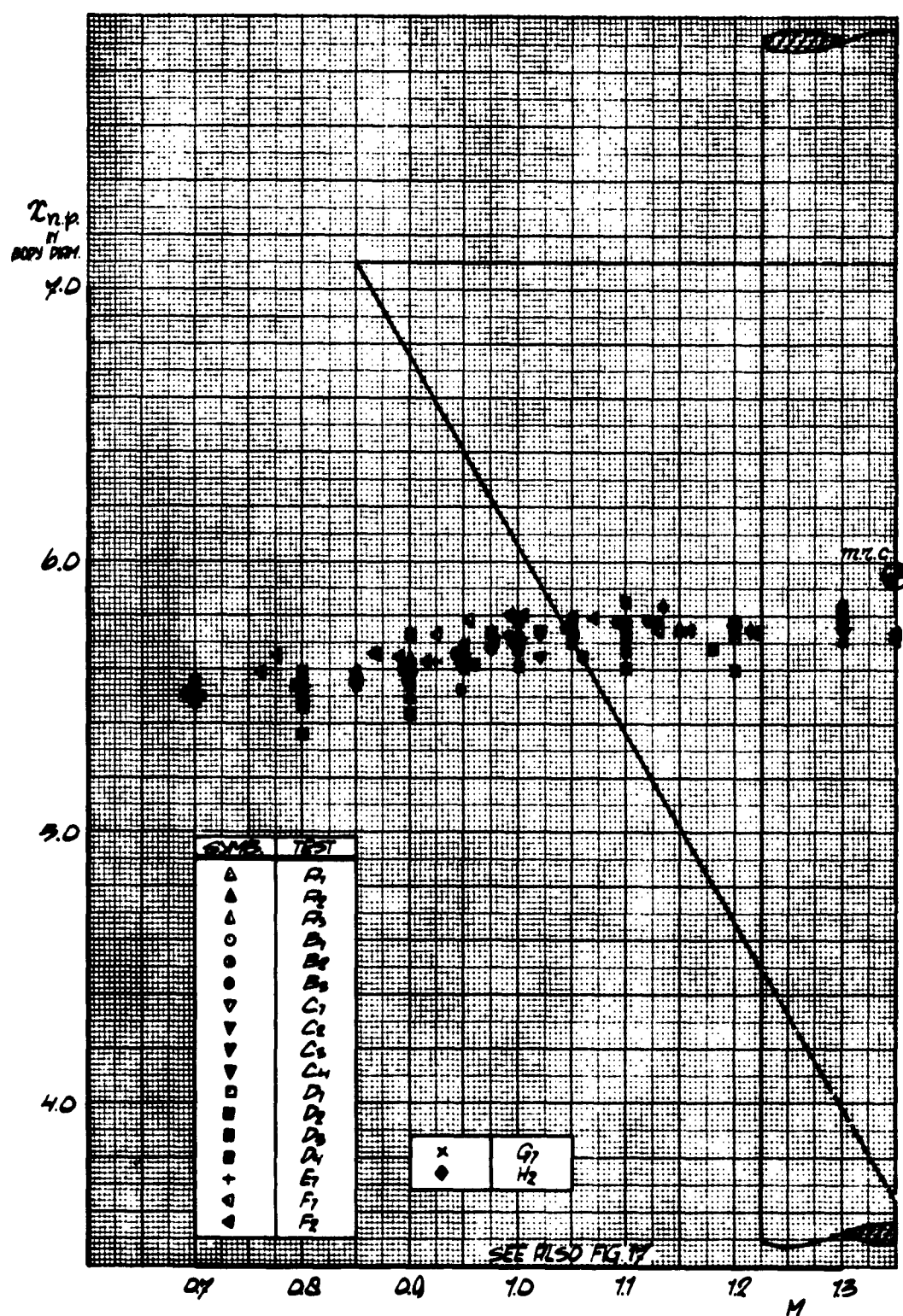


Fig. 6 Neutral point at $C_L = 0$ versus Mach number for all available tests

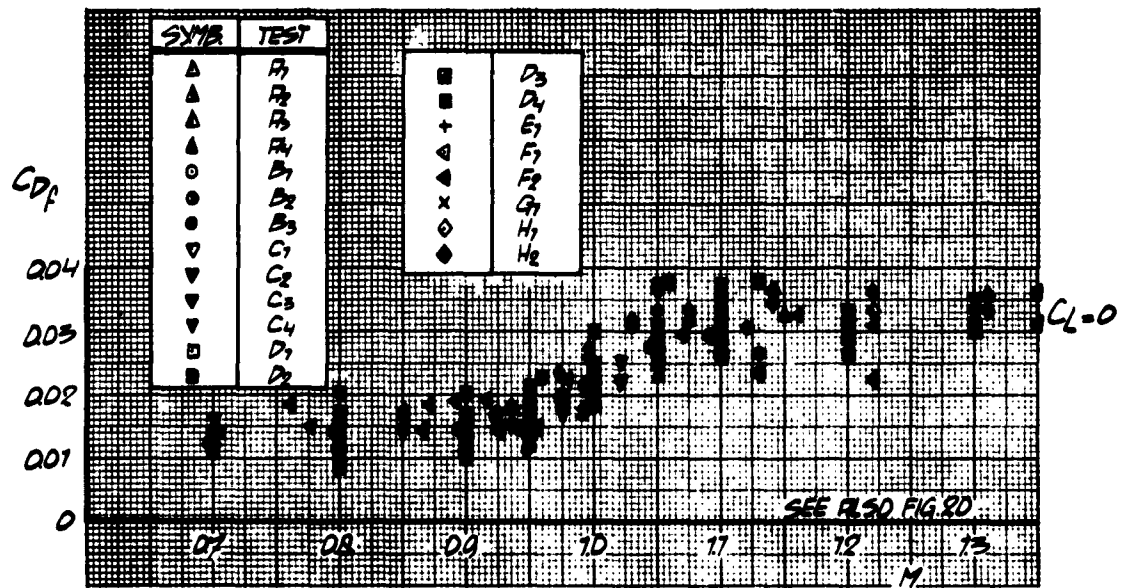


Fig. 7 Forebody drag coefficients versus Mach number for all available tests

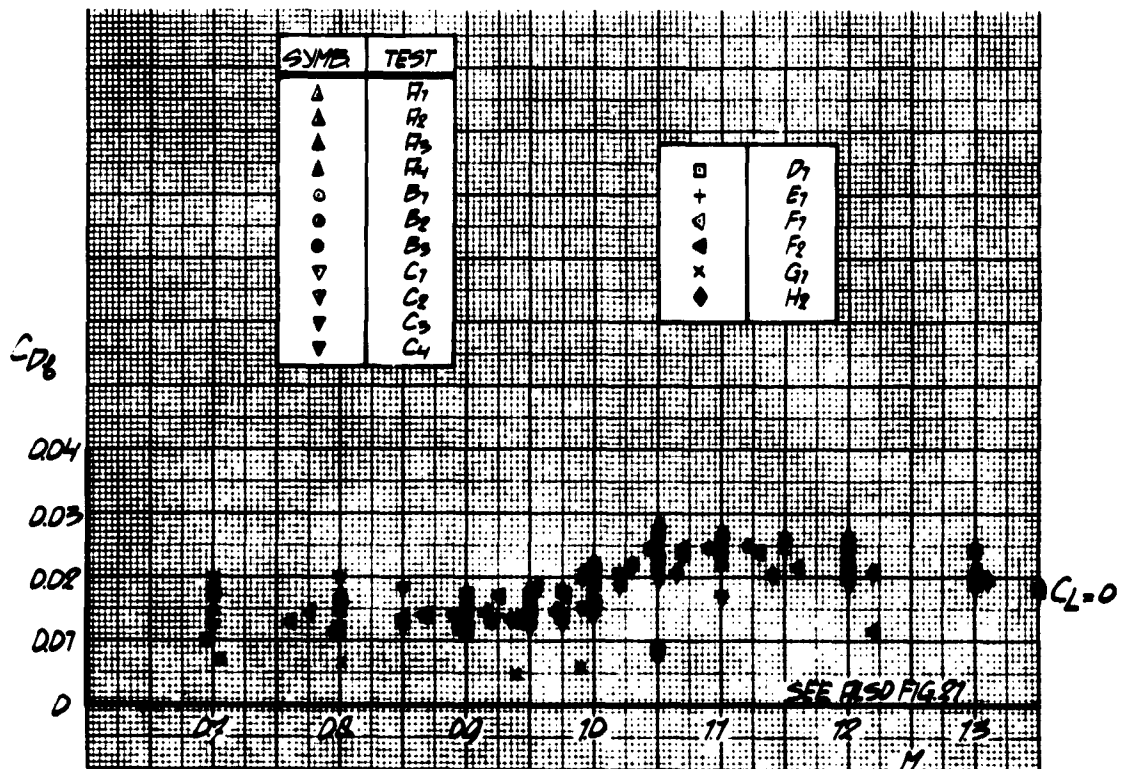


Fig. 8 Base drag coefficient versus Mach number for all available tests

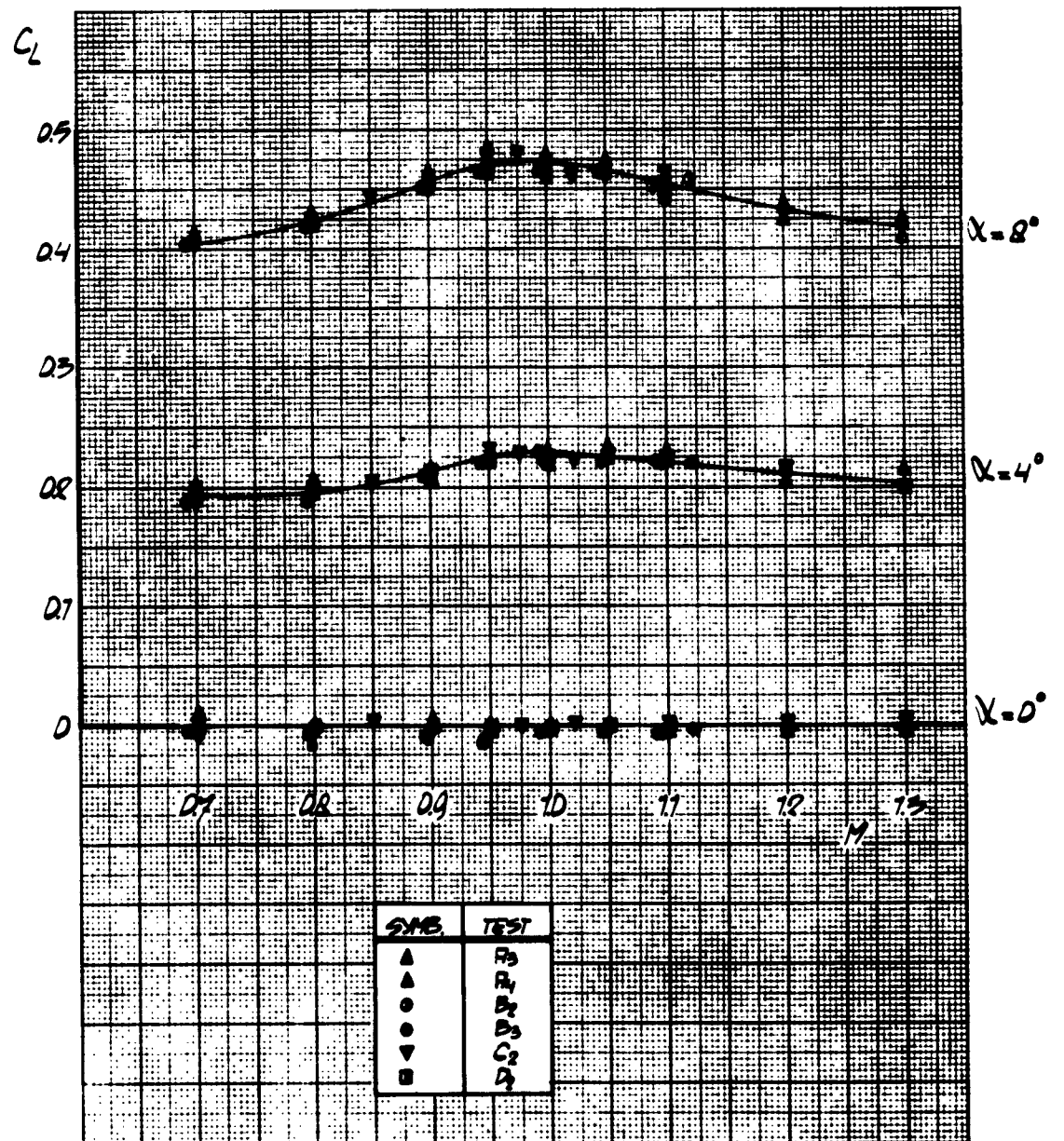


Fig.9 Reference curves for lift coefficient versus Mach number

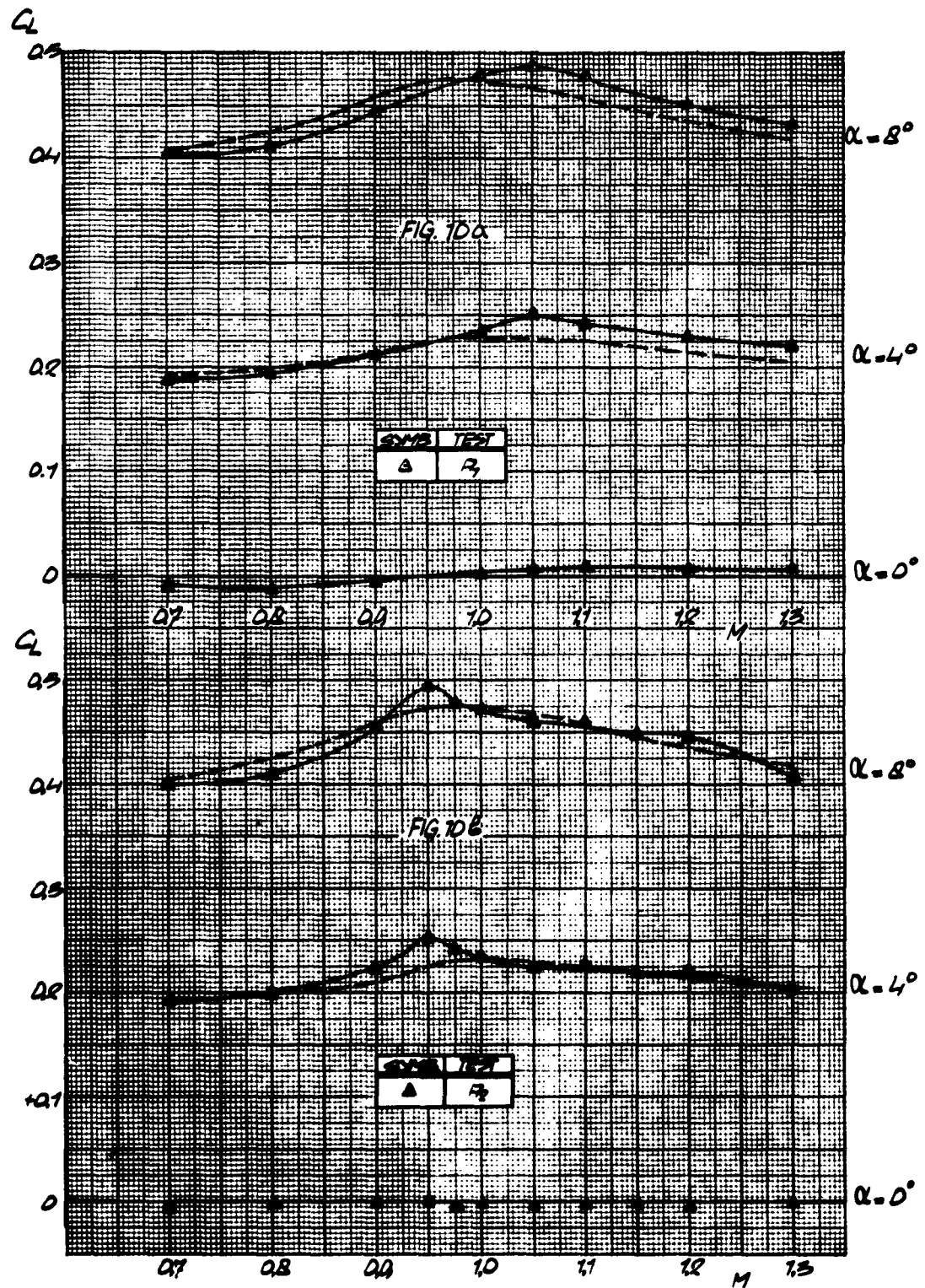


Fig.10 Comparison of data with reference curves for lift

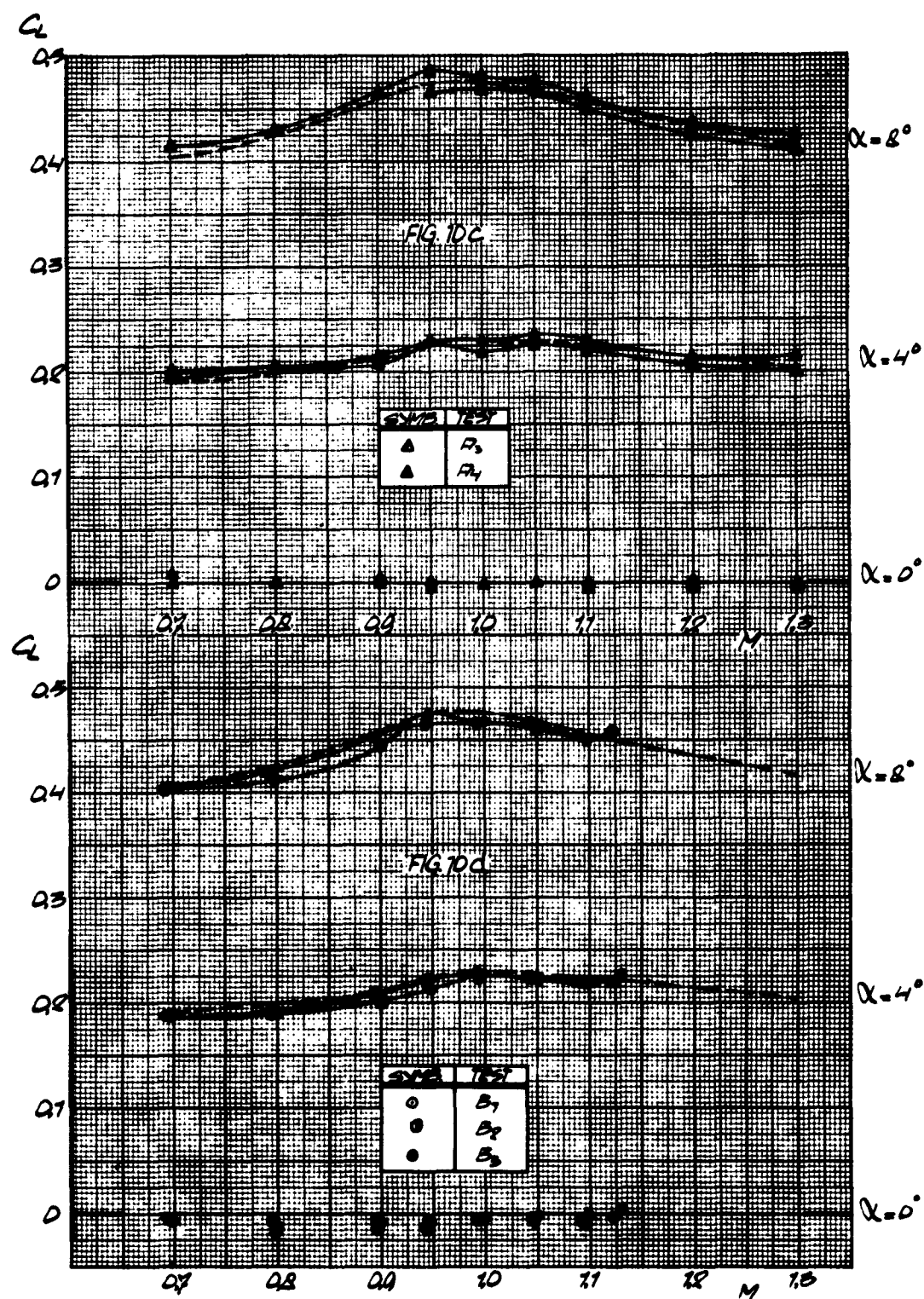


Fig.10 Comparison of data with reference curves for lift (continued)

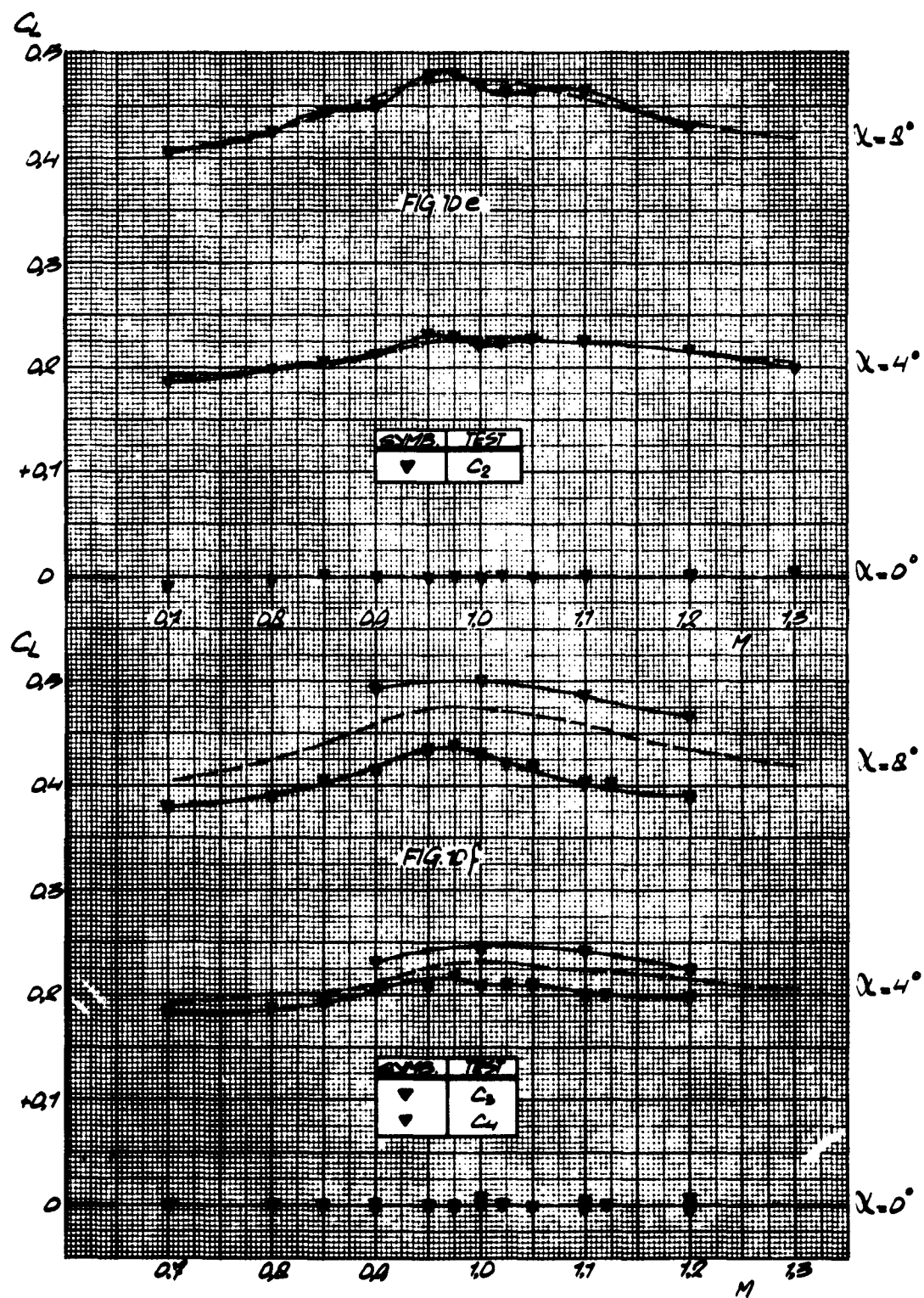


Fig.10 Comparison of data with reference curves for lift (continued)

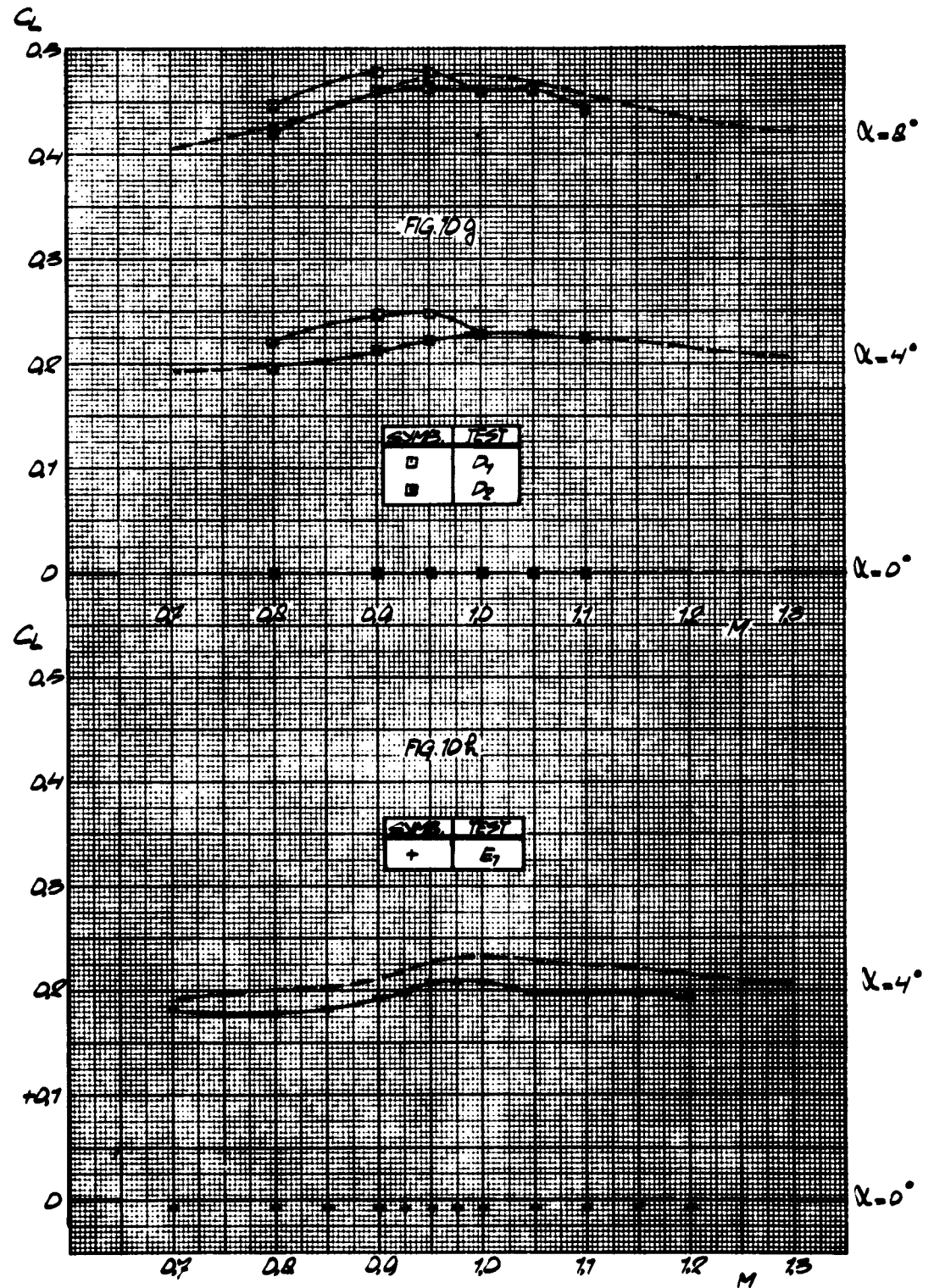


Fig.10 Comparison of data with reference curves for lift (continued)

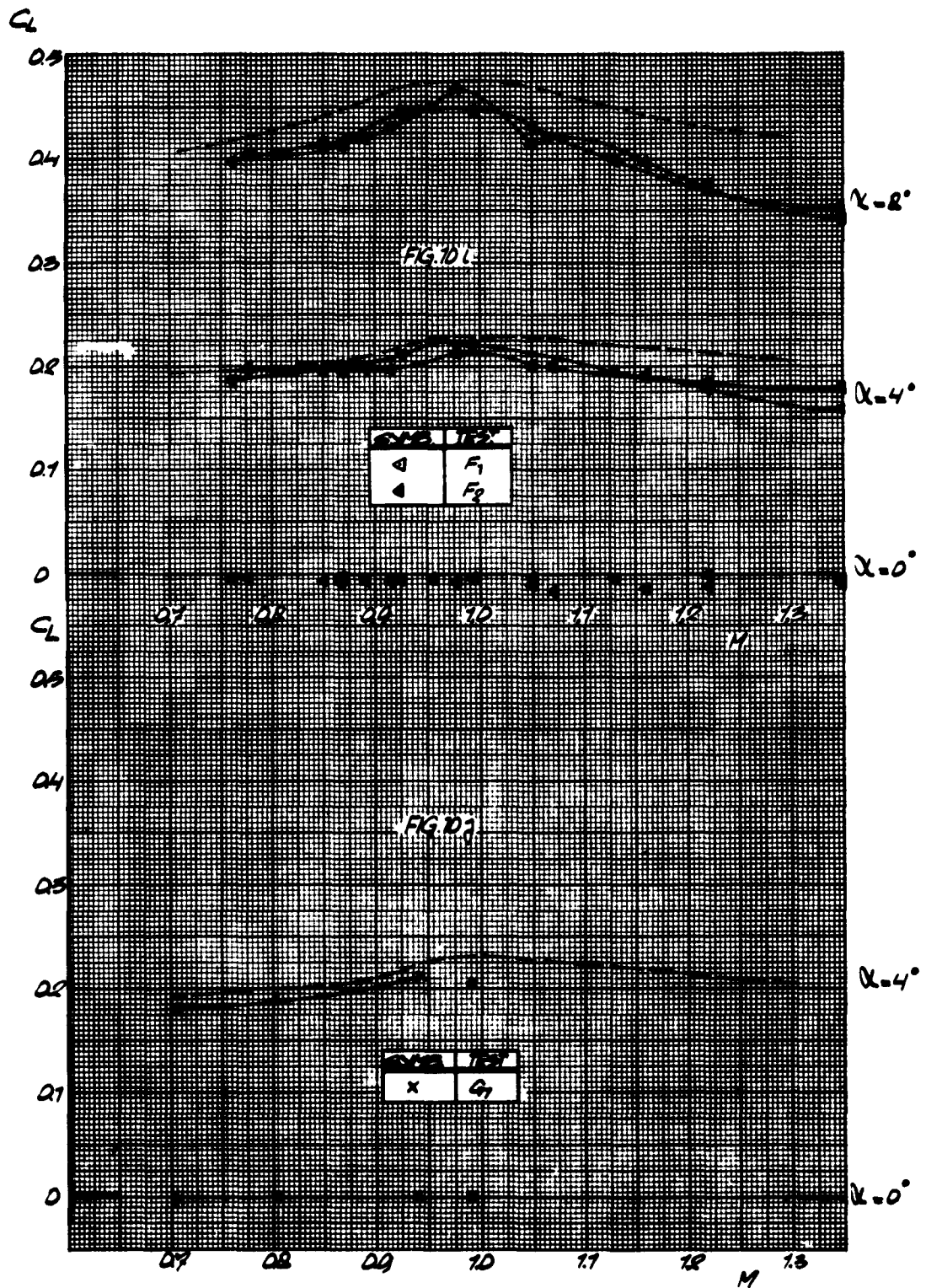


Fig.10 Comparison of data with reference curves for lift (continued)

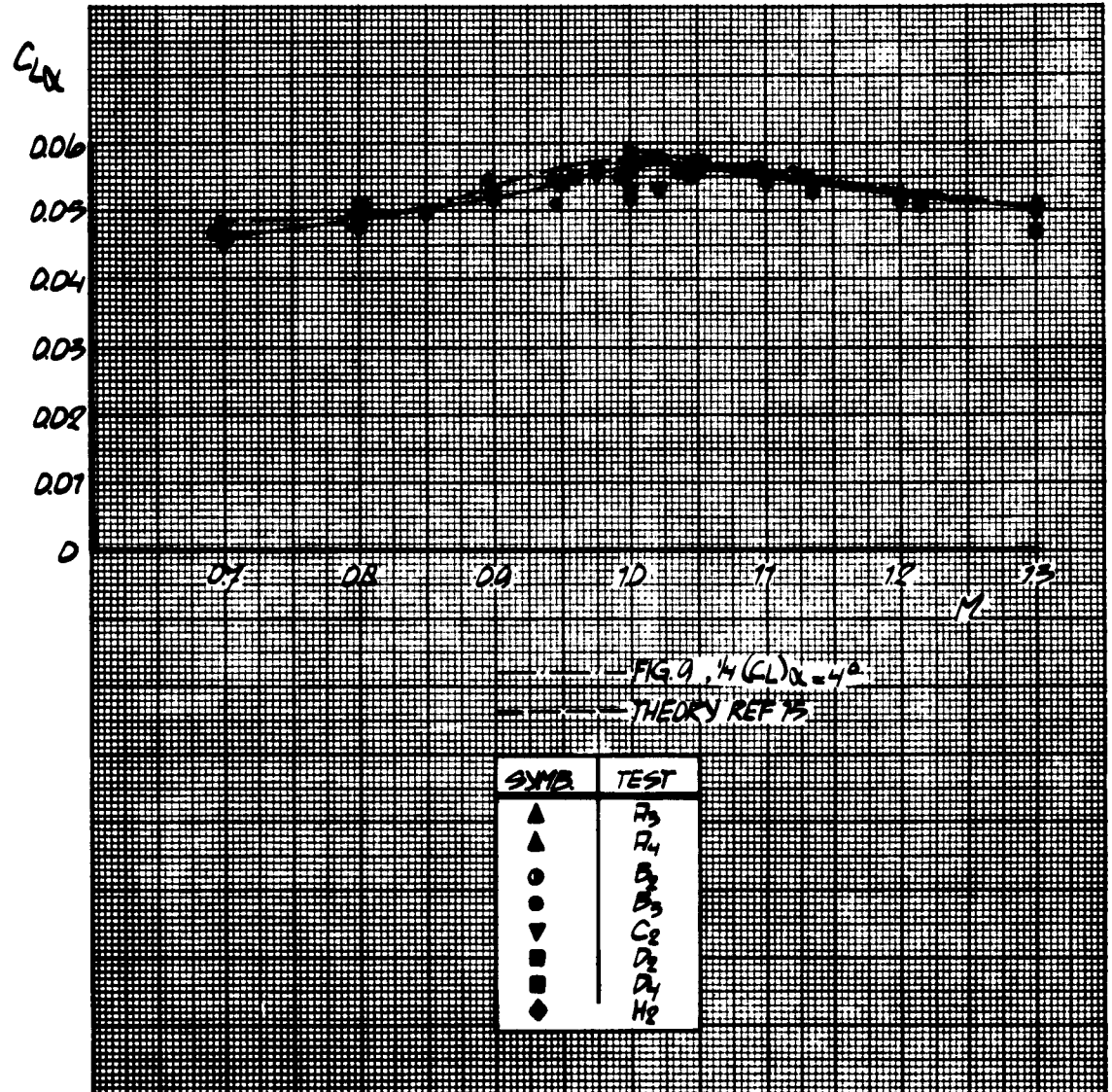


Fig.11 Reference curve for lift curve slope at $C_L = 0$ versus Mach number

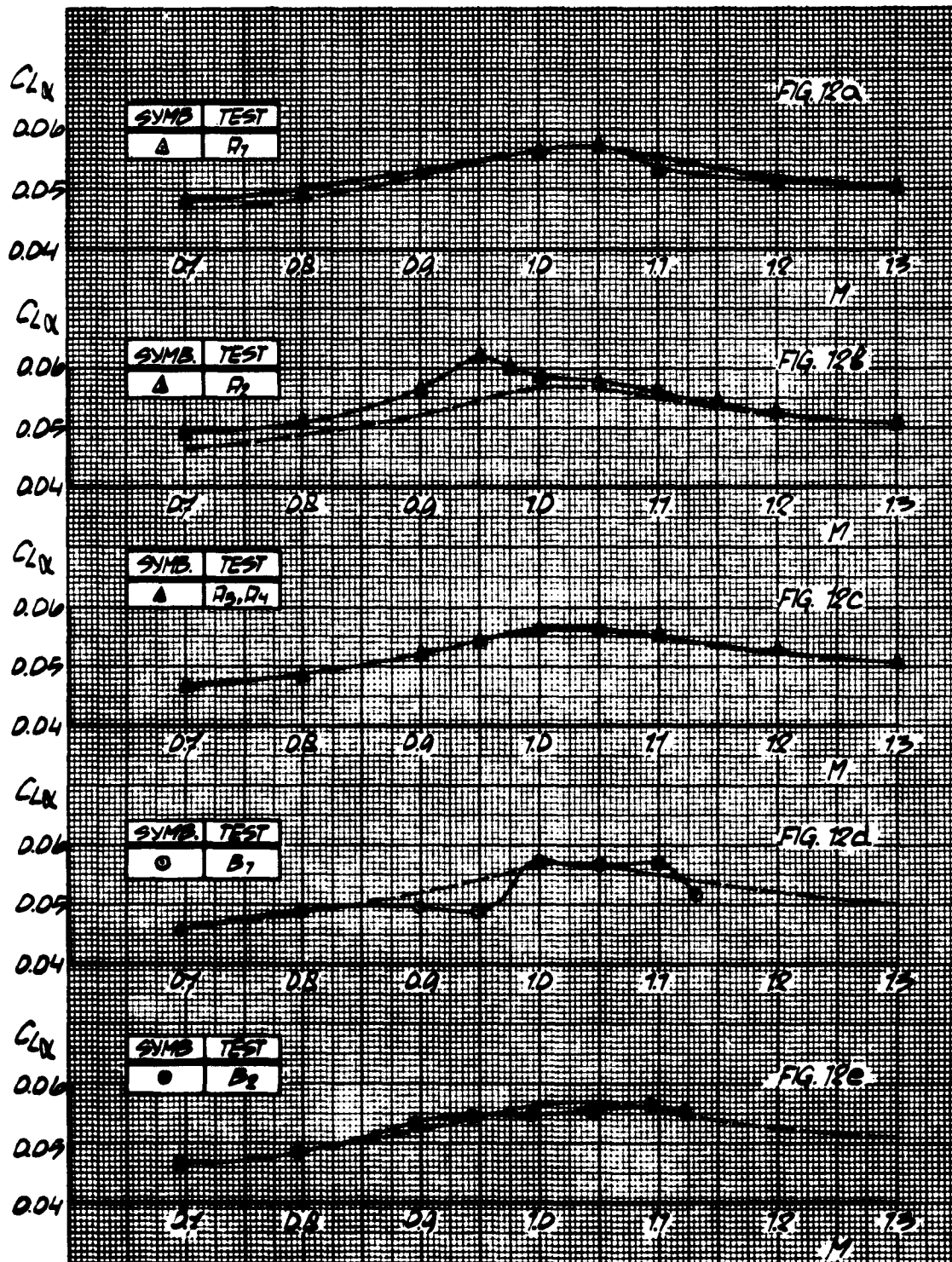


Fig.12 Comparison of data with reference curve for lift-curve slope at $C_L = 0$

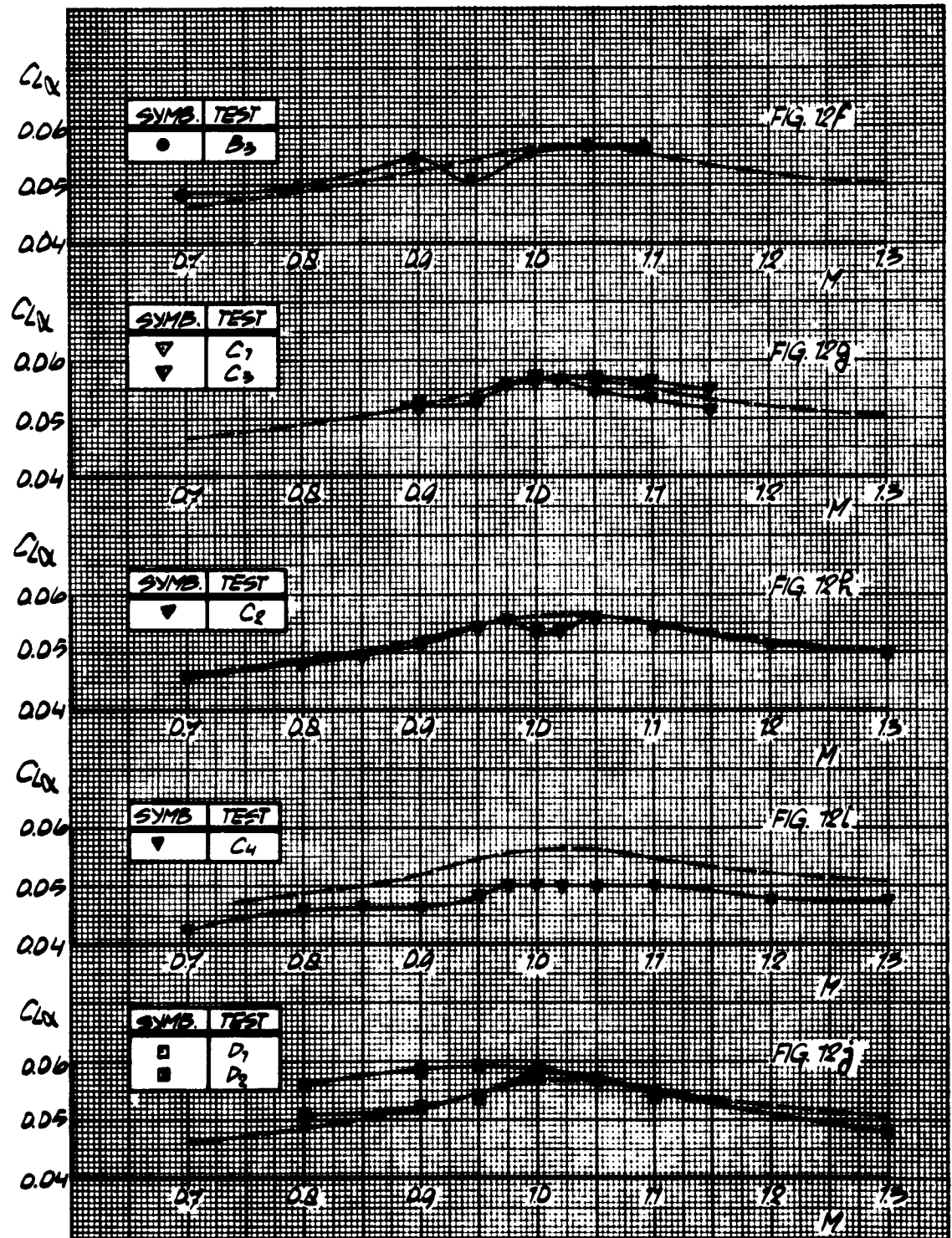


Fig.12 Comparison of data with reference curve for lift-curve slope at $C_L = 0$
(continued)

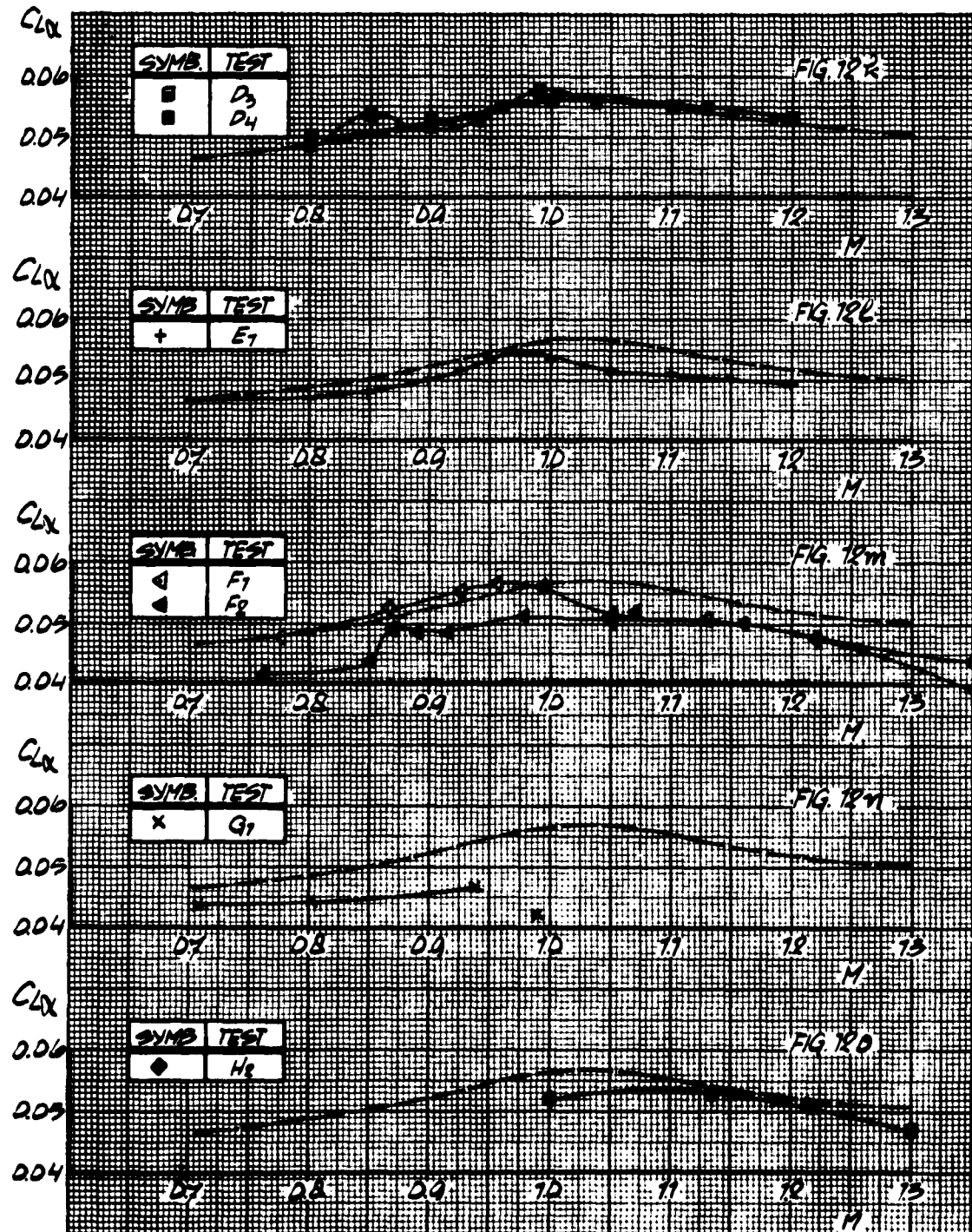


Fig.12 Comparison of data with reference curve for lift-curve slope at $C_L = 0$
(continued)

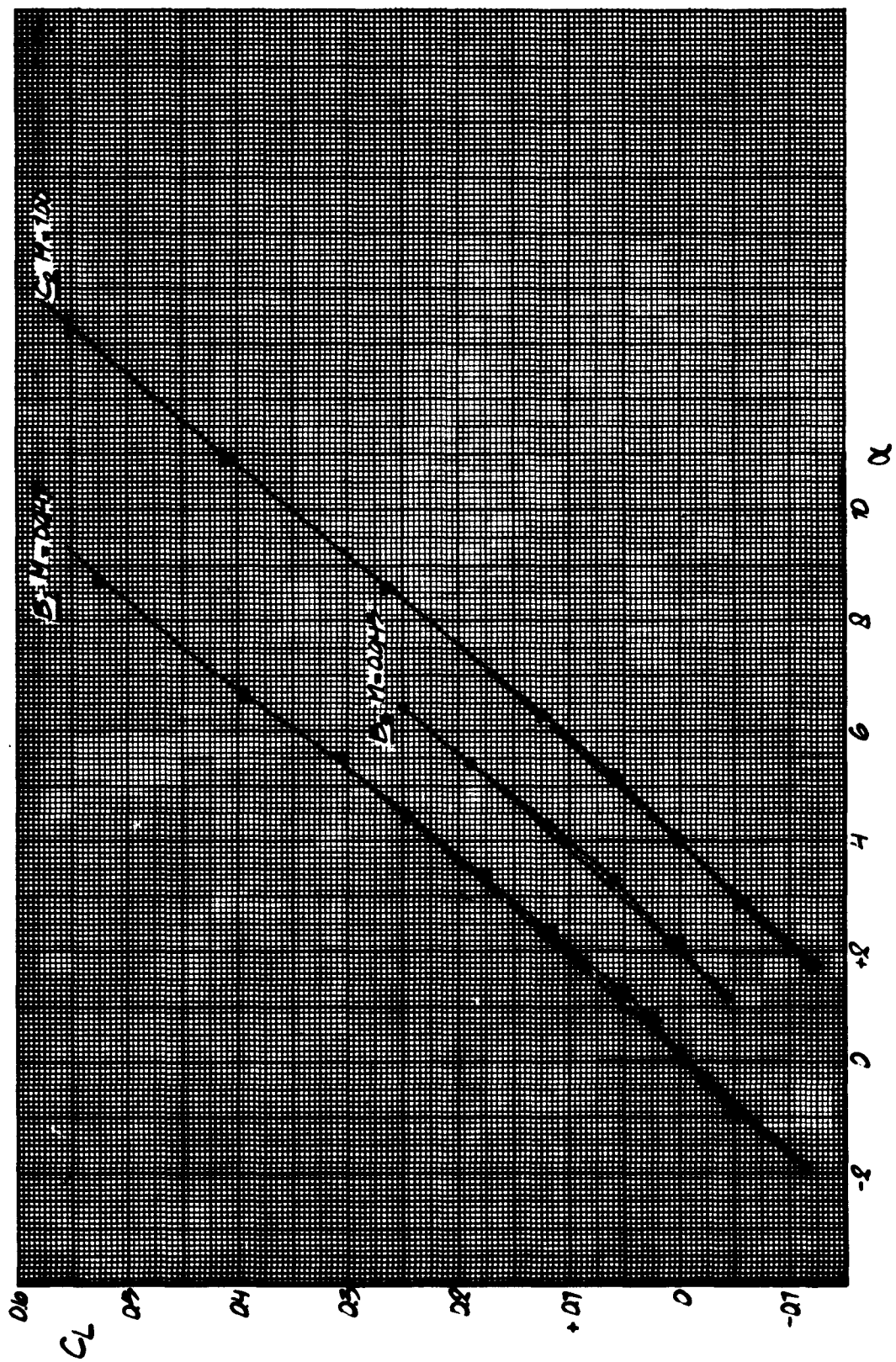


Fig. 13 Examples of lift-curve slope variation with angle of attack

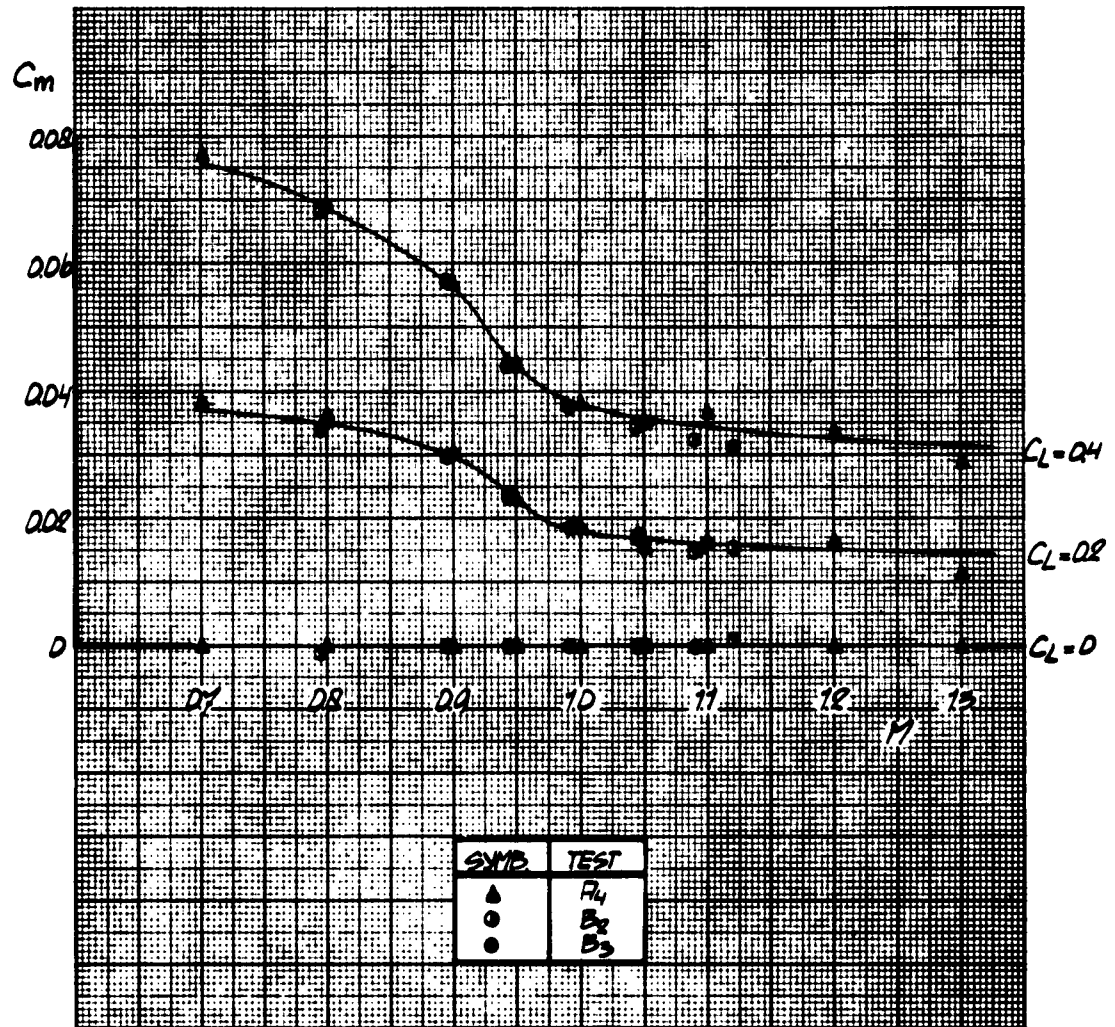


Fig.14 Reference curves for pitching moment coefficient versus Mach number

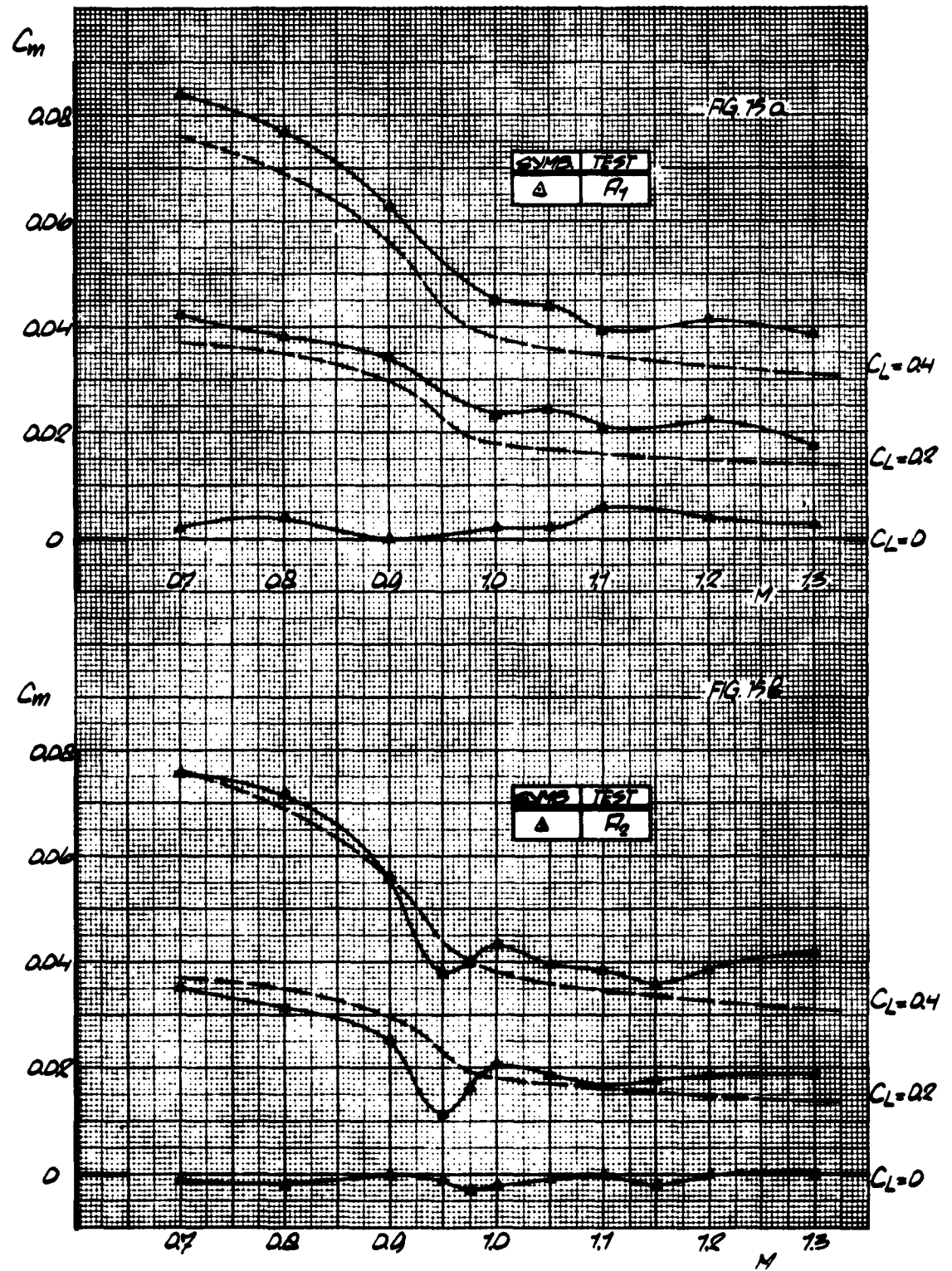


Fig.15 Comparison of data with reference curves for pitching moment

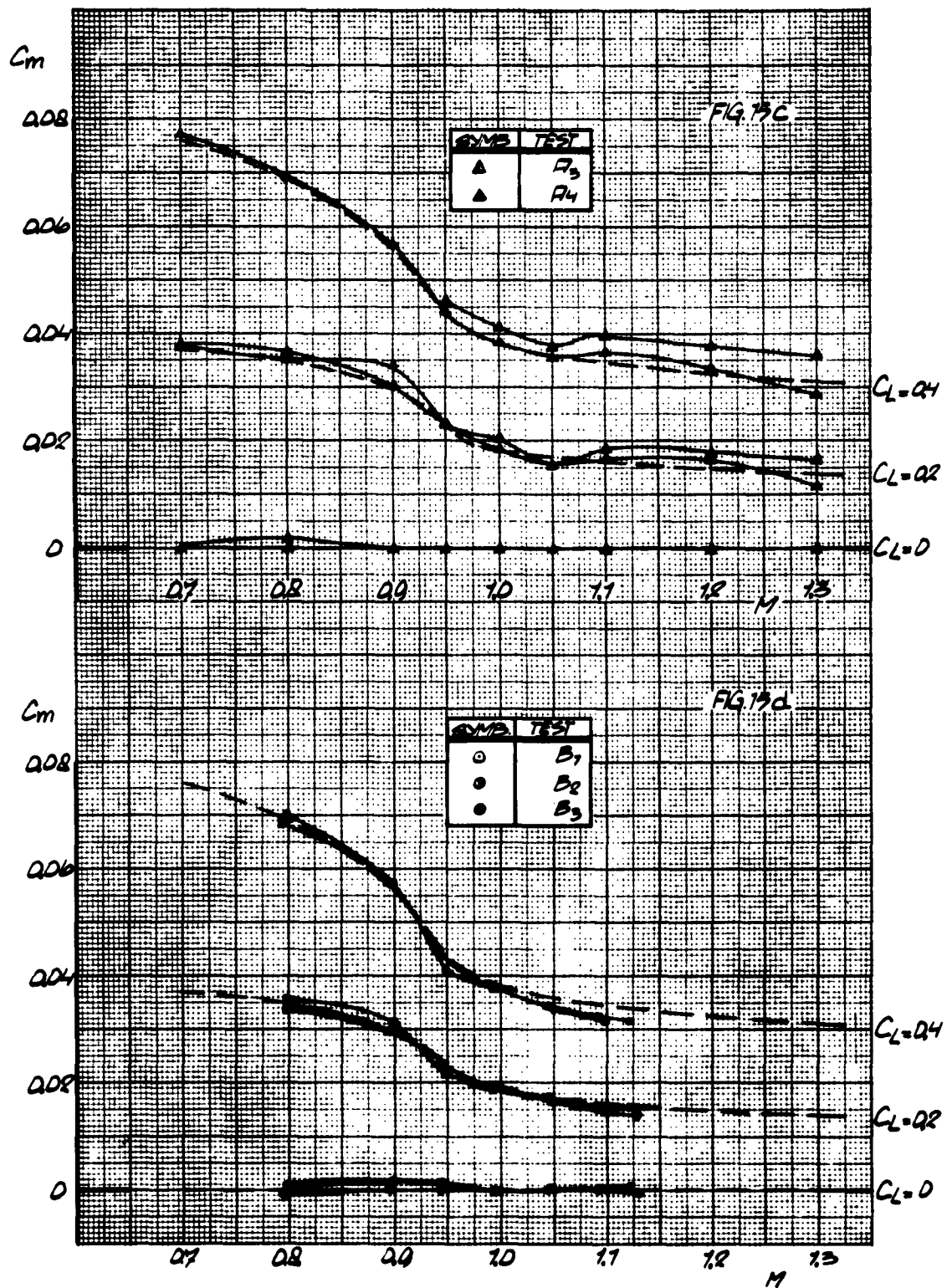


Fig. 15 Comparison of data with reference curves for pitching moment (continued)

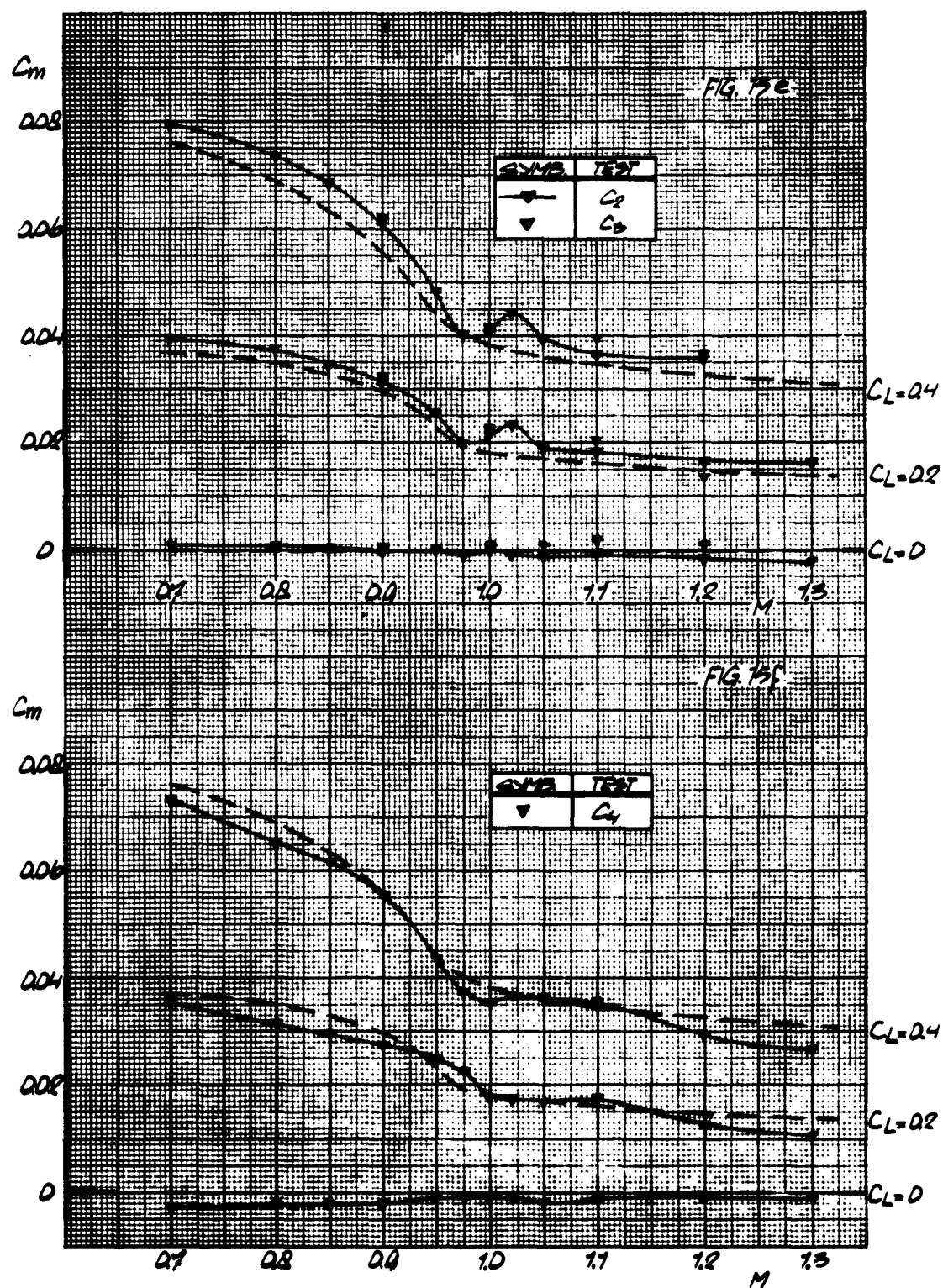


Fig. 15 Comparison of data with reference curves for pitching moment (continued)

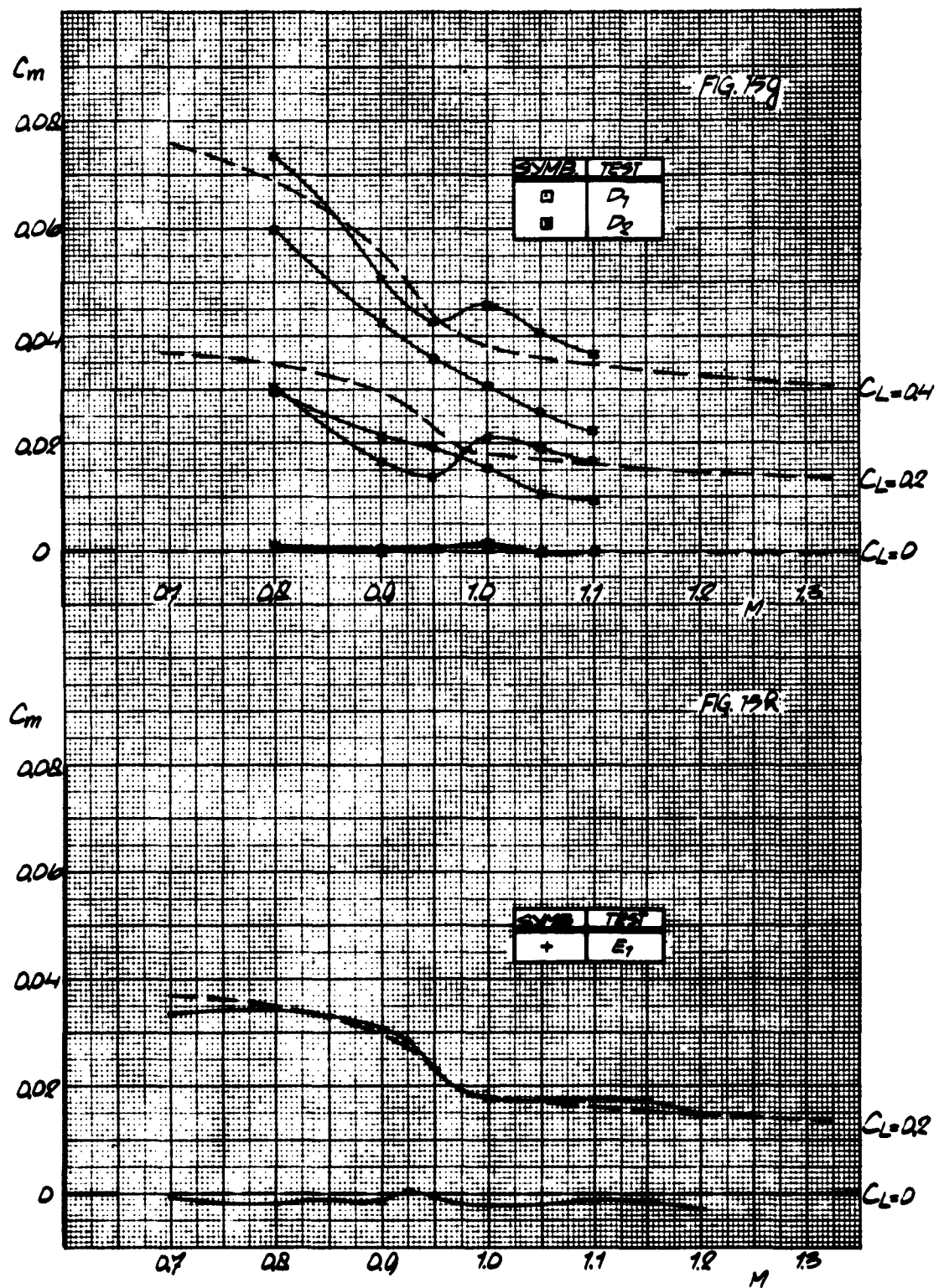


Fig.15 Comparison of data with reference curves for pitching moment (continued)

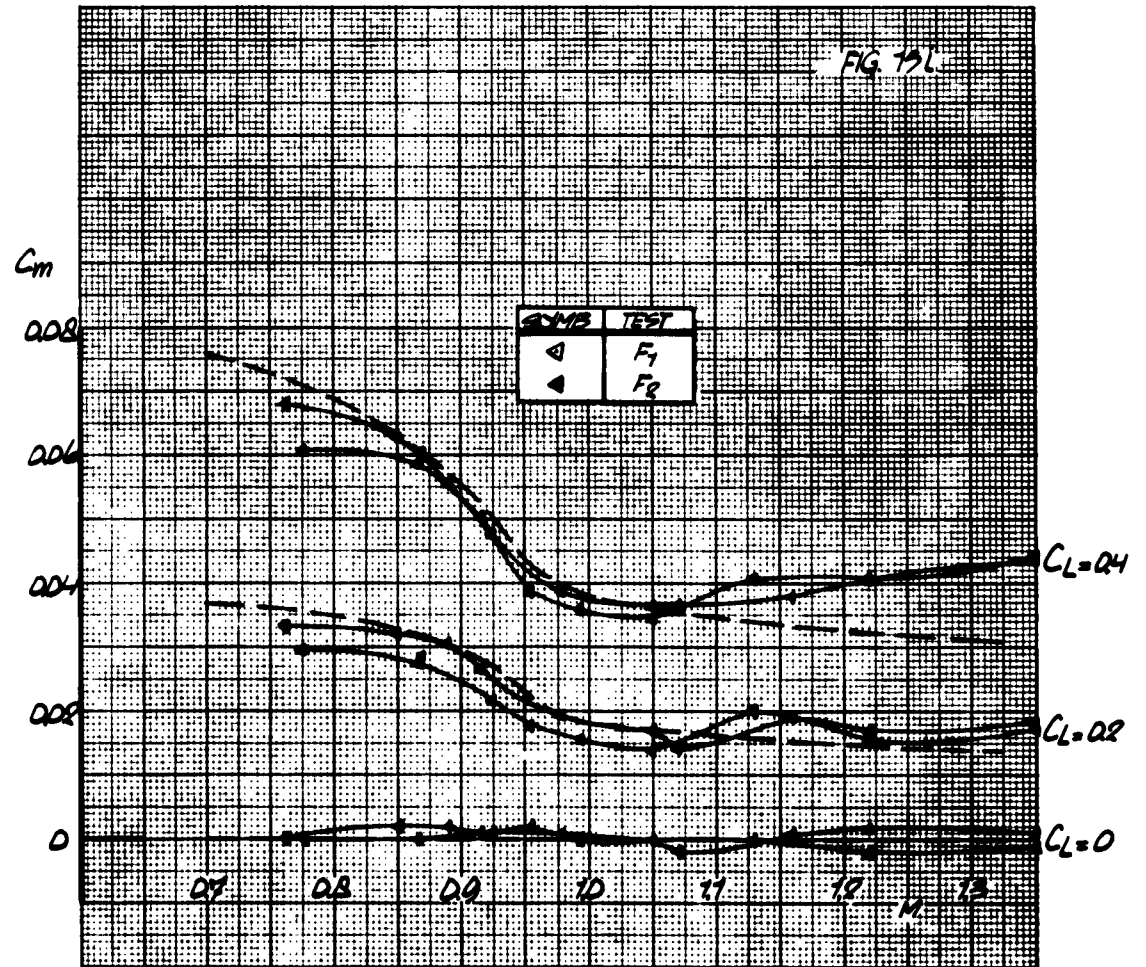


Fig.15 Comparison of data with reference curves for pitching moment (continued)

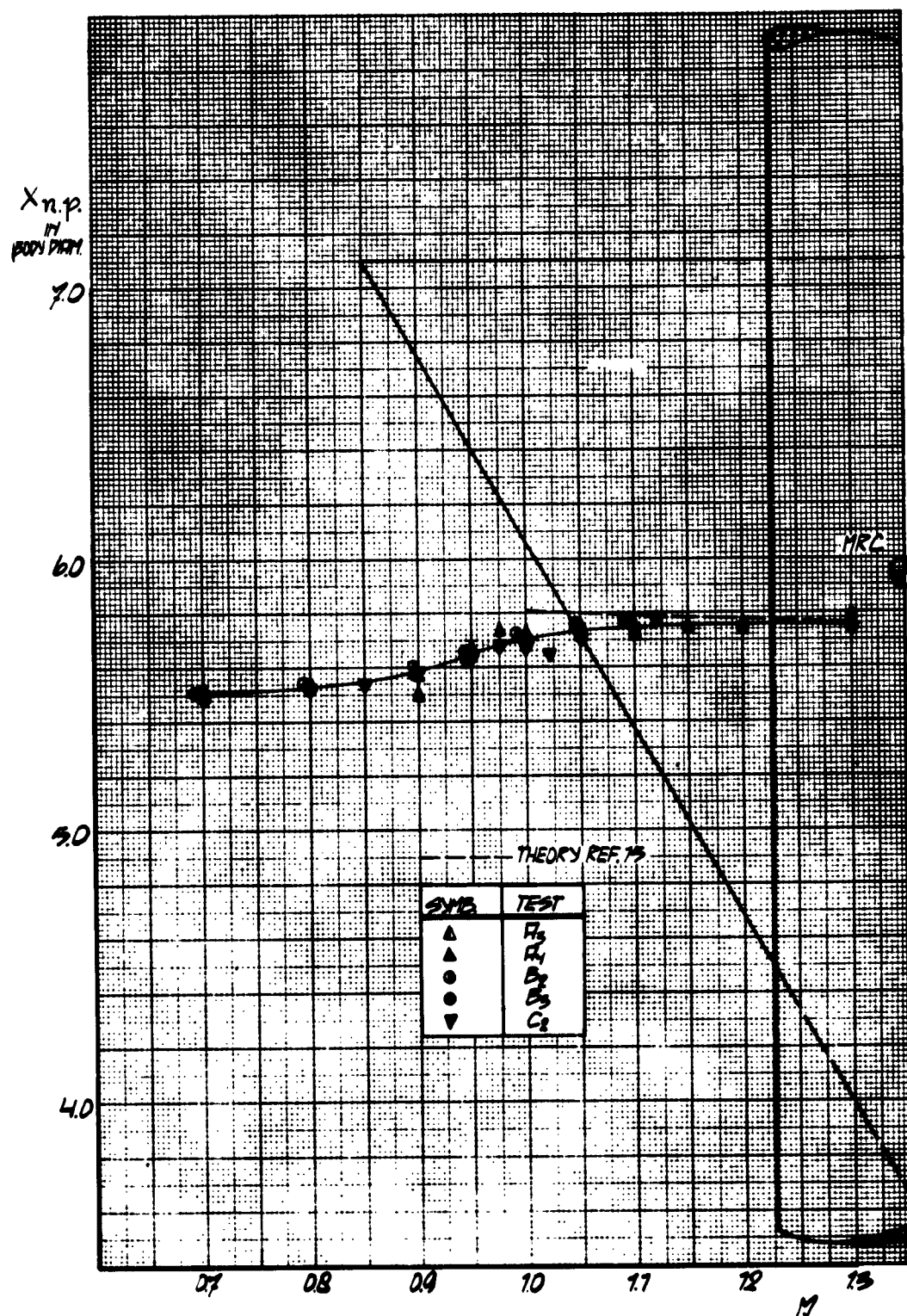


Fig. 16 Reference curve for neutral point at $C_L = 0$ versus Mach number

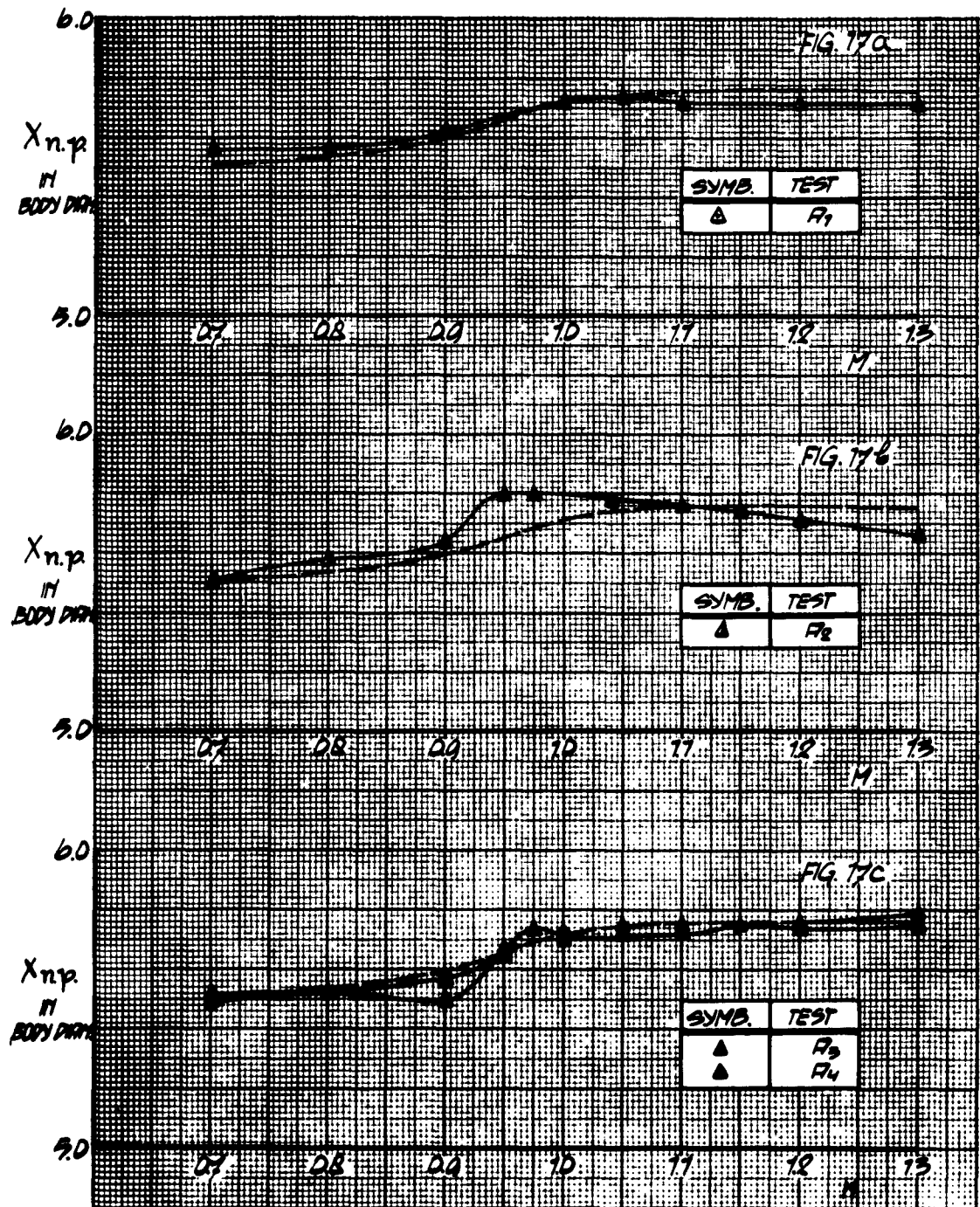


Fig.17 Comparison of data with reference curve for neutral point at $C_L = 0$

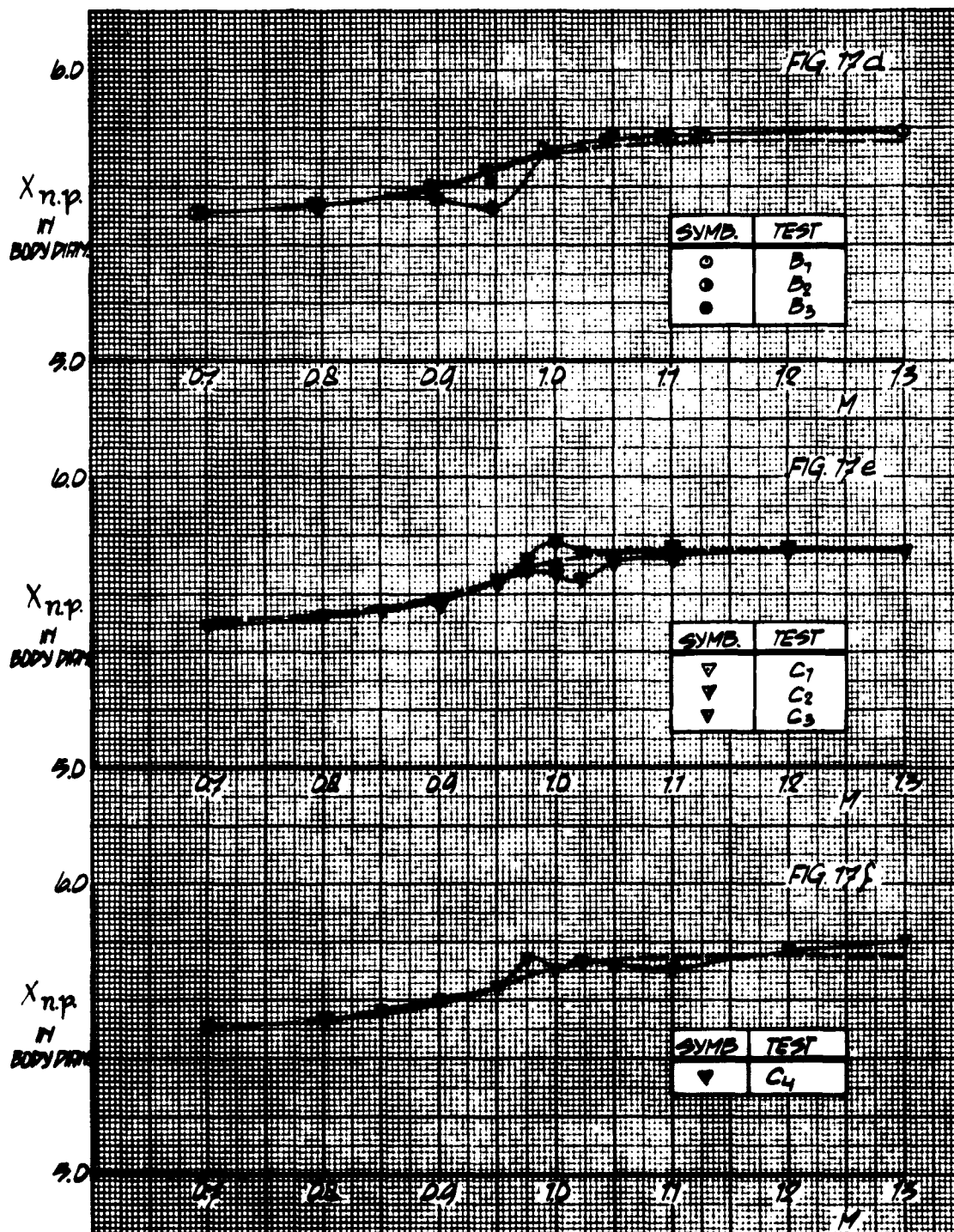


Fig. 17 Comparison of data with reference curve for neutral point at $C_L = 0$
(continued)

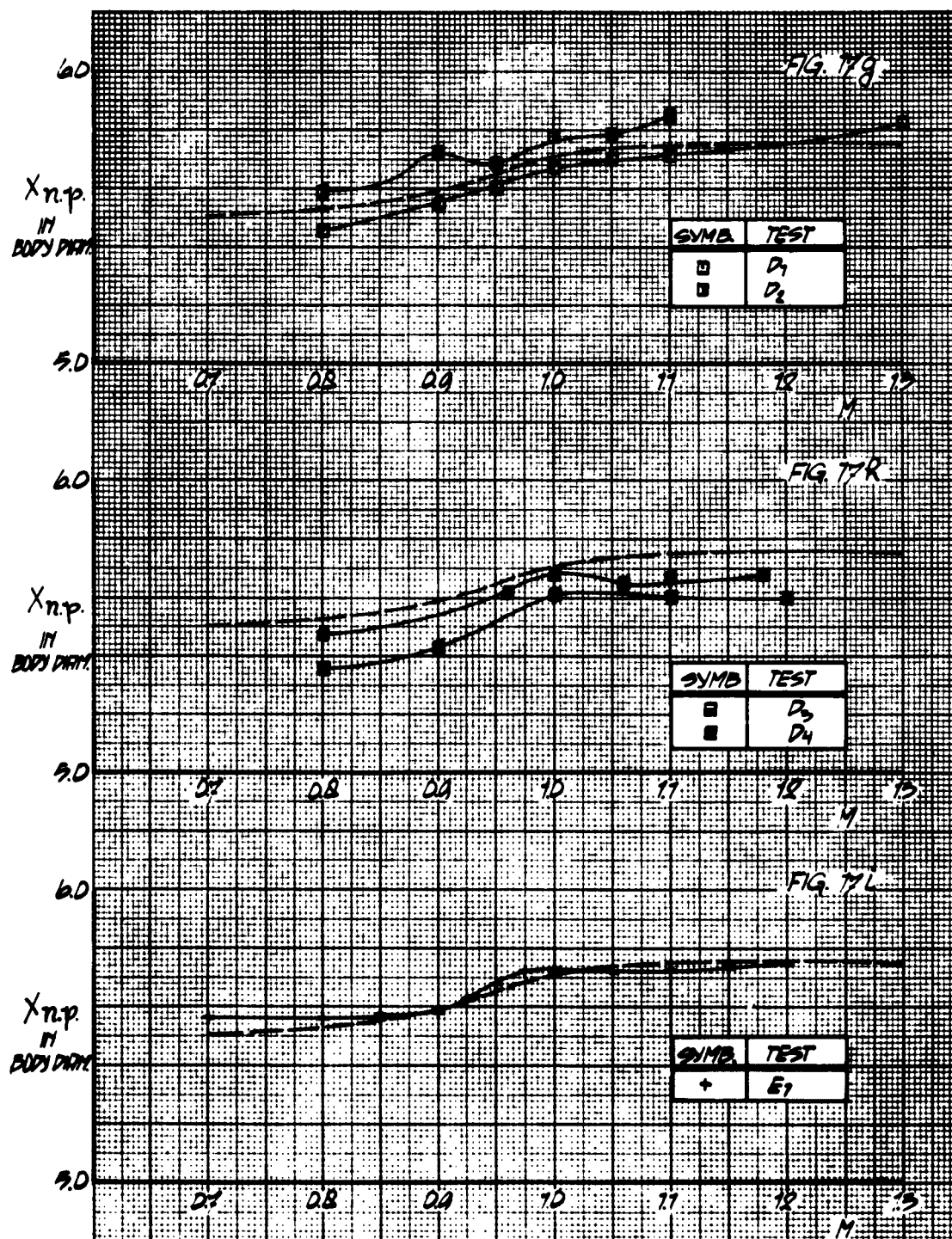


Fig.17 Comparison of data with reference curve for neutral point at $C_L = 0$
(continued)

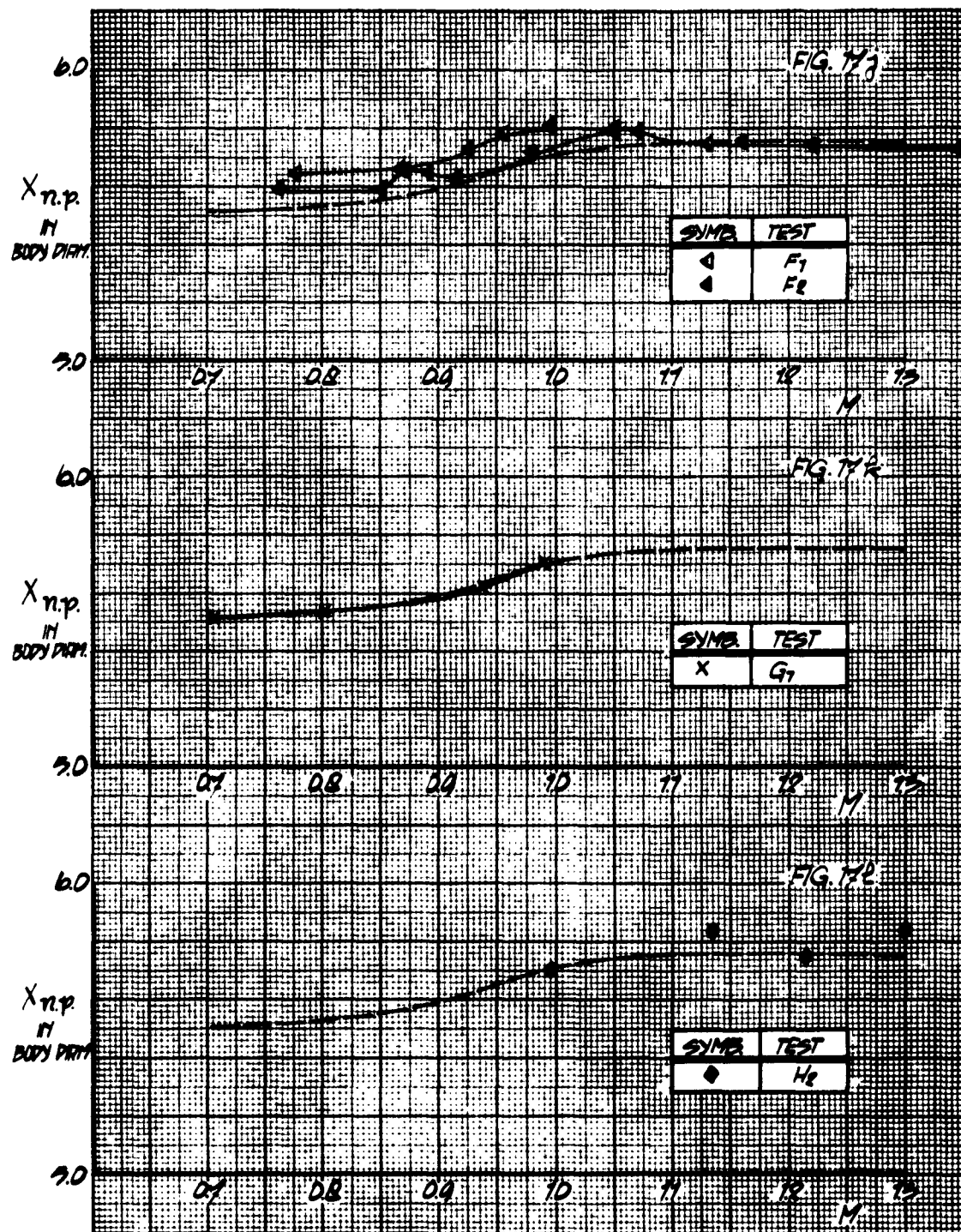


Fig. 17 Comparison of data with reference curve for neutral point at $C_L = 0$
(continued)

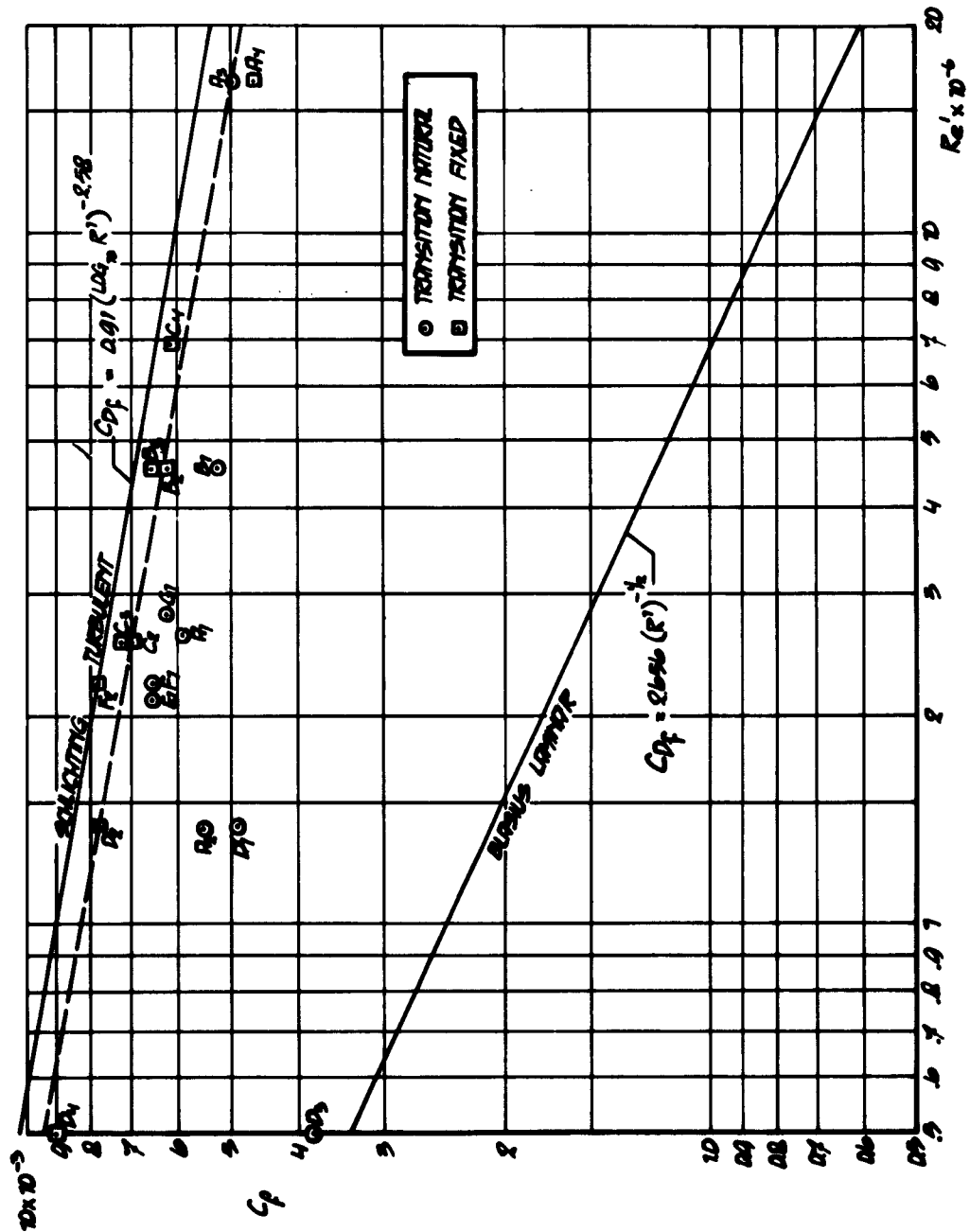


Fig. 18 Skin friction drag at $M = 0.8$ as a function of Reynolds number, based on C_{av}

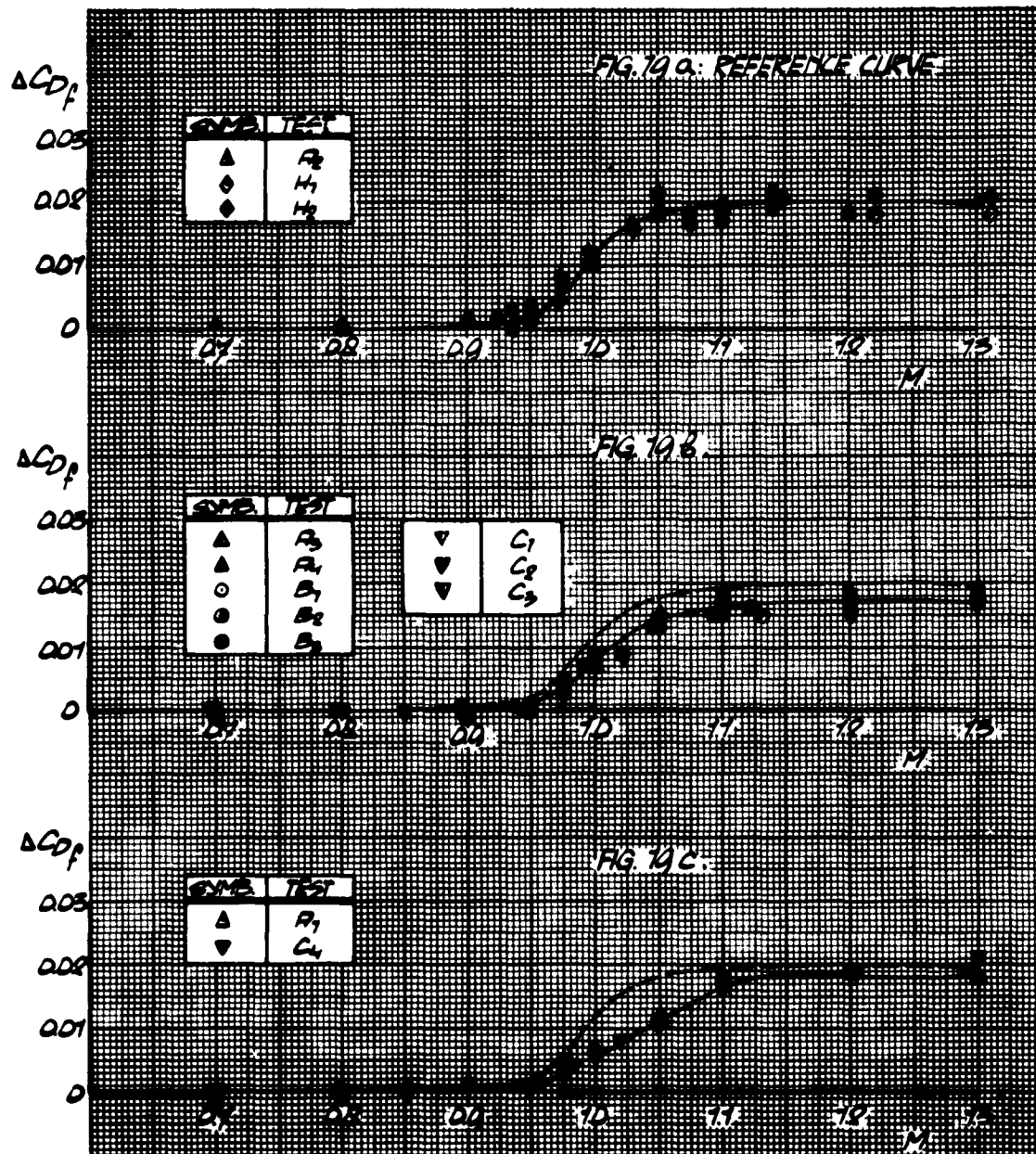


Fig.19 Reference curve for transonic drag rise at $C_L = 0$ and general comparison

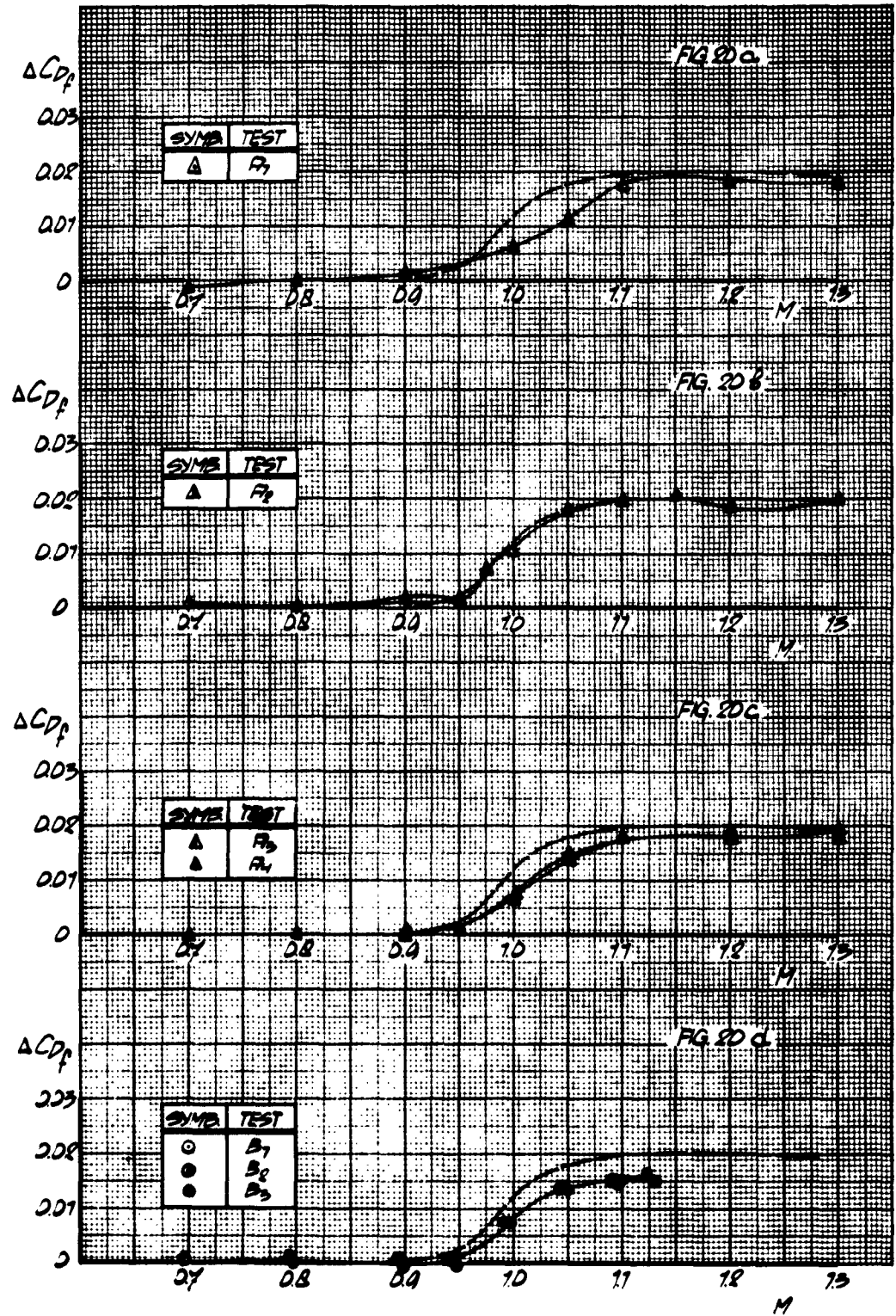


Fig.20 Comparison of data with reference curve for transonic drag rise

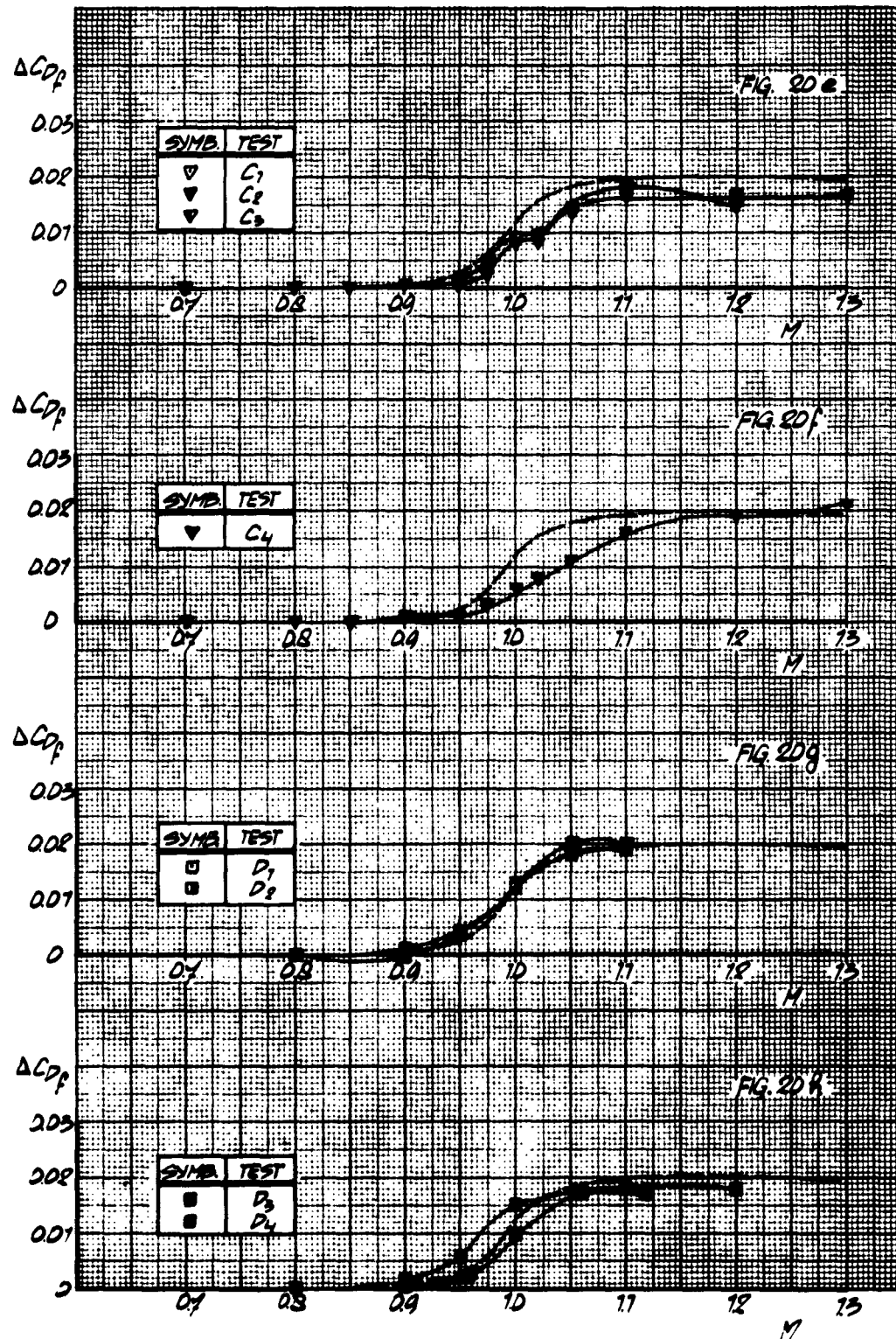


Fig. 20 Comparison of data with reference curve for transonic drag rise (continued)

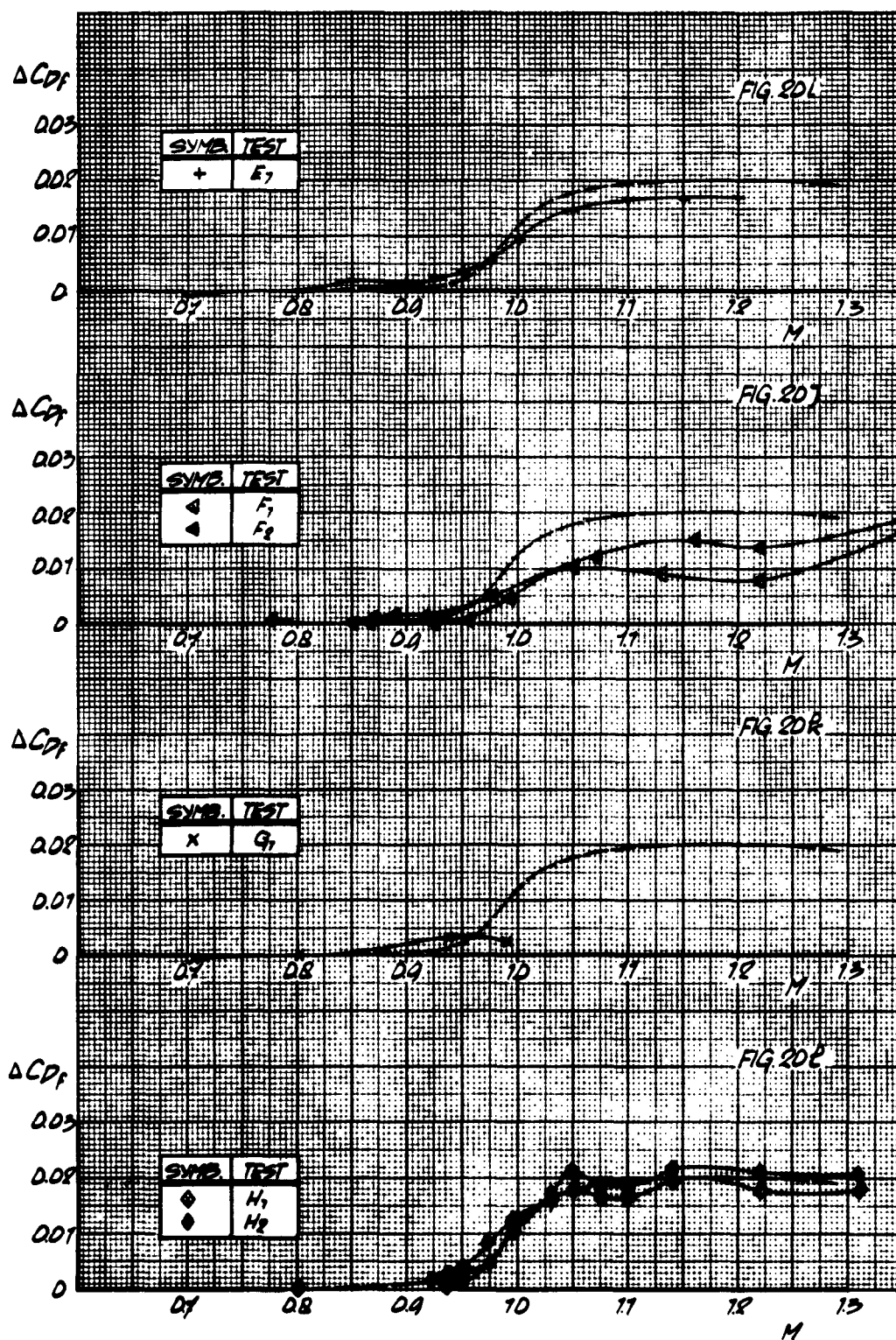


Fig. 20 Comparison of data with reference curve for transonic drag rise (continued)

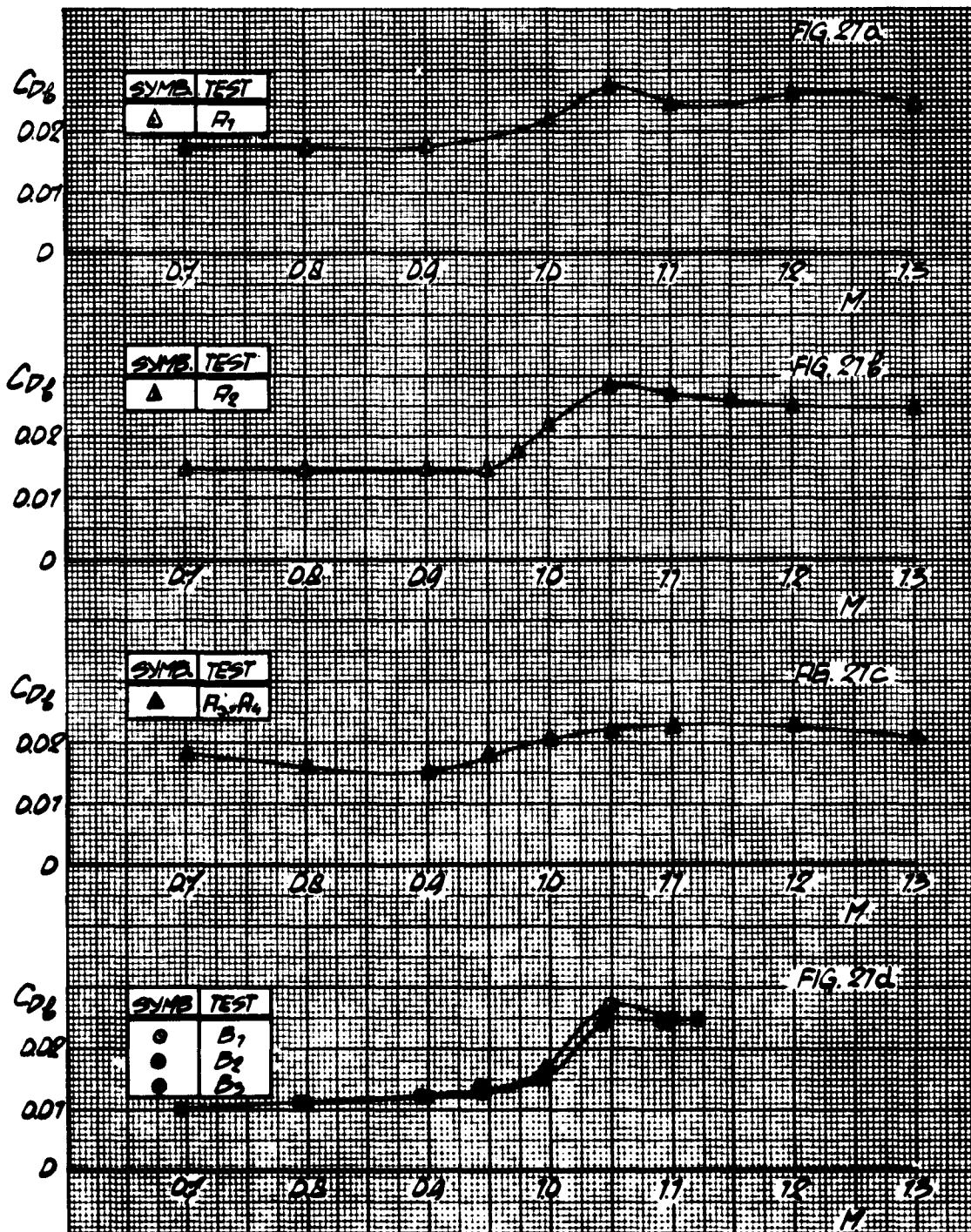


Fig. 21 Base drag coefficient at $C_L = 0$ versus Mach number

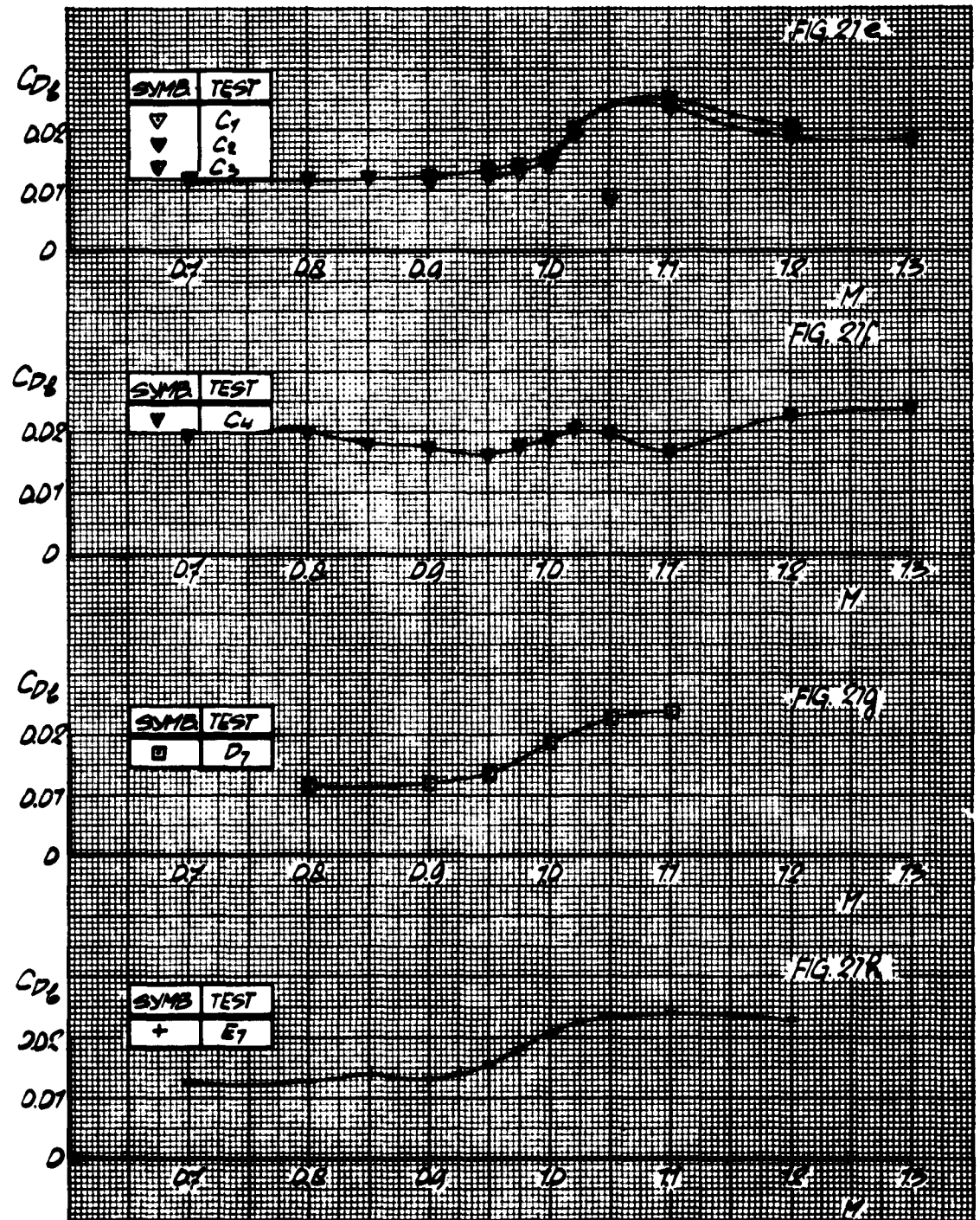


Fig.21 Base drag coefficient at $C_L = 0$ versus Mach number (continued)

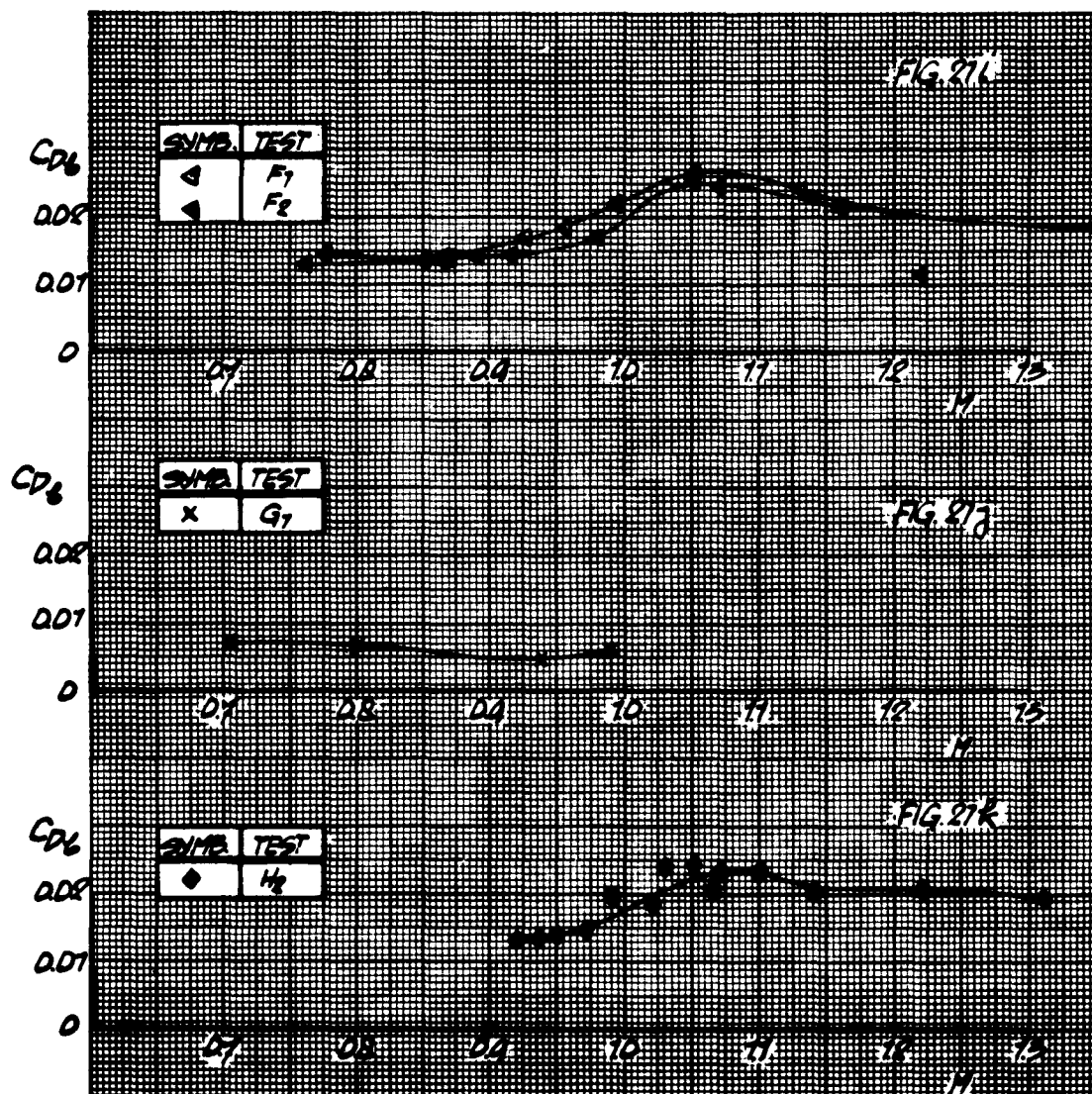


Fig. 21 - Base drag coefficient at $C_L = 0$ versus Mach number (continued)

PART III

**A REVIEW OF MEASUREMENTS ON AGARD CALIBRATION MODEL B
IN THE MACH NUMBER RANGE FROM 1.4 TO 8**

by

J.P. Hartsuiker

Nationaal Lucht- en Ruimtevaartlaboratorium, Amsterdam

•

SUMMARY

This report contains a survey and a comparison of the results from tests with AGARD Calibration Model B at Mach numbers between 1.4 and 8. The data include tests from various wind tunnels and in free flight, for a range of Reynolds numbers between 10^6 and 98×10^6 . Models with and without fixed transition of the boundary layer have been considered.

Good agreement between the various measurements of the lift, the pitching moment and the neutral point location has been found. With respect to drag many differences exist, some of which can be explained.

CONTENTS

	Page
SUMMARY	96
LIST OF TABLES	98
LIST OF FIGURES	98
NOTATION	99
1. INTRODUCTION	101
2. MODELS	101
3. RANGE OF TESTS	101
4. TEST FACILITIES	101
5. RESULTS AND DISCUSSION	102
5.1 Base Drag	102
5.2 Forebody Drag at Zero Lift	104
5.2.1 General	104
5.2.2 Forebody Drag with Natural Transition	105
5.2.3 Forebody Drag with Fixed Transition	107
5.2.4 Conclusions Relating to Forebody Drag	109
5.3 Lift	109
5.4 Pitching Moment	110
5.5 Neutral Point	111
6. CONCLUSIONS	111
REFERENCES	113
TABLES	117
FIGURES	121

LIST OF TABLES

		Page
Table I	General Data on Models and Facilities	117
Table II	Boundary Layer Trips	119
Table III	Accuracy and Repeatability of Data	120

LIST OF FIGURES

Fig.1	AGARD Calibration Model B (Ref.20)	121
Fig.2a-j	The base drag coefficient C_{Db} versus R_L , for constant M ($\alpha = 0$)	122 - 125
Fig.3	The base drag coefficient C_{Db} versus M ($R_L > 3 \times 10^6$)	126
Fig.4a-k	The forebody drag coefficient C_{Df} versus R_L ($\alpha = 0$)	127 - 131
Fig.5	The pressure drag of the body alone, as a function of M	132
Fig.6	The forebody drag coefficient versus M	132
Fig.7	C_L versus α , up to high angles of attack	133
Fig.8	Slope of lift curve $C_{L\alpha}$ versus M at $C_L = 0$	134
Fig.9	The moment coefficient versus M , for constant C_L	135
Fig.10	Neutral point location at $C_L = 0$ versus M	136

NOTATION

b	wing span
\bar{c}	mean aerodynamic chord, = 2.309 D
C_{Df}	forebody drag coefficient; drag coefficient corrected for zero base drag coefficient $(C_{Dt} - C_{Db})$, = $\frac{\text{total drag} - \text{base drag}}{qS}$
C_{Db}	base drag coefficient, = $\frac{\text{base drag}}{qS}$
C_{DB}	body pressure drag coefficient, = $\frac{\text{pressure drag}}{qS}$
C_{Dt}	total drag coefficient, = $\frac{\text{total drag}}{qS}$
C_L	lift coefficient, = lift/(qS)
C_{La}	slope of lift curve
C_m	pitching moment coefficient about a point 1/3 of the maximum wing chord ahead of the wing trailing edge, = moment/(qS \bar{c})
d	sting diameter
d'	wire diameter
D	body diameter
l	length of cylindrical part of sting
L	body length
M	Mach number
q	free stream dynamic pressure, = $\frac{1}{2}\rho V^2$
r	local body radius
R_L	Reynolds number based on body length, = $\rho VL/\mu$
R_{wire}	Reynolds number based on wire diameter, = $\rho Vd'/\mu$
S	total wing area, = 6.928 D ²
V	free stream velocity

x	distance along body axis
X_{mrc}	distance of moment reference centre aft of model nose in body diameters, = 5.943
X_{np}	distance of neutral point (at zero lift) aft of model nose in body diameters
α	angle of attack
ρ	free stream density
μ	kinematic viscosity
φ	windshield angle

A REVIEW OF MEASUREMENTS ON AGARD CALIBRATION MODEL B IN THE MACH NUMBER RANGE FROM 1.4 to 8

1. INTRODUCTION

In this report measurements with AGARD Calibration Model B from various test facilities and in free flight have been summarized. The available data of drag, lift, pitching moment and neutral point location have been compared critically.

The Mach number range considered is from $M = 1.4$ up to $M = 8$. The tests with AGARD Model B below $M = 1.4$ have been reviewed in Part II of this AGARDograph.

2. MODELS

AGARD Calibration Model B is an ogive-cylinder with a delta wing in the form of an equilateral triangle. The details of the model have been given in Reference 20; a sketch is presented in Figure 1.

A large number of model sizes has been used; the model lengths for the various tests can be found in Table I.

In Reference 20 it is recommended that a ratio of sting diameter to body diameter of 0.5 be used, in connection with a sting length of three body diameters. However, many tests were concluded before this AGARD specification was published and consequently a number of different sting dimensions have been used (see Table I).

The surface roughness of the model has only been specified for five series of tests (Table I). To induce transition it is recommended in Reference 20 that trip wires of various diameters be used on wings and body, the Reynolds number based on wire diameter varying from 500 to 10,000. In the tests reviewed here many different ways of fixing boundary layer transition have been used; a survey is given in Table II.

For free-flight tests, the models were fitted with vertical fins for lateral stabilization (half-scale exposed wings) and for one test a flow angle indicator was mounted on the nose.

3. RANGE OF TESTS

The tests reviewed here have been made in a Mach number range from 1.4 to 8.

Reynolds numbers based on body length covered the range from 10^6 to 98×10^6 .

The angle of incidence varied for the tests between -11° and $+21^\circ$ (Table I).

4. TEST FACILITIES

The results have been obtained partly from wind tunnel tests and partly from free-flight measurements.

Table I gives a survey of the test facilities used, of which a description is, in general, available in the references.

5. RESULTS AND DISCUSSION

5.1 Base Drag

The pressure on the base of a sting-supported body is, in general, a function of Mach number, Reynolds number, state of the boundary layer and mixing region, angle of attack, ratio of sting diameter to body diameter, sting length and windshield angle.

In the specification²⁰ of AGARD Model B, the following sting dimensions are recommended: $d/D = 0.5$ and $l/D = 3.0$, d being the sting diameter, l the sting length up to the windshield and D the body diameter.

However, many tests were made with different sting dimensions, partly because in an earlier specification a smaller minimum sting length was specified ($l/D = 1.5$). The ratio l/D varies in the tests reviewed here from 1.5 to 9.5, the ratio d/D from 0.296 to 0.6 (see Table I).

Several investigators have considered the problem of sting-length interference^{7,21-23}. In all cases a critical sting length was found, which means that a sting length below this critical value will influence the base pressure. The critical sting length varies with Mach number and Reynolds number. Schueler⁷ found, from measurements with an AGARD Model B, the following values for the critical sting length (for $d/D = 0.296$, windshield angle 20° and with turbulent boundary layer approaching the model base):

M	$(l/D)_{crit}$	R_L
2	2.2	$4.6 < R_L \times 10^{-6} < 13$
3	1.9	$2.3 < R_L \times 10^{-6} < 7$
4	$2.2 < (l/D)_{crit} < 3.7$	$2.3 < R_L \times 10^{-6} < 5.7$

It may be concluded therefore that, in the measurements with a sting length ratio of $l/D = 2$ (a value that borders on the critical), there will probably be sting-length interference, and that with $l/D = 1.5$ the base pressure has certainly been influenced by the sting length.

The available base drag data at zero angle of attack have been plotted in Figures 2a-2j as a function of R_L , for constant Mach number. Open symbols are used for the data with natural transition. The closed symbols stand for fixed transition and half-closed symbols give values of C_{pb} which are the same for natural and for fixed transition. Solid lines have been drawn through those measurements with natural transition where $d/D = 0.5$ and sting lengths are certainly larger than critical ($l/D \geq 3$).

Dashed lines have been drawn for the data with $d/D = 0.296$ and $l/D \geq 3$, again with natural transition.

From Figure 2 the following conclusions can be drawn for the case of natural transition:

For each Mach number C_{Db} is constant for $R_L > 3 \times 10^6$ ($d/D = 0.5$). For small Reynolds number the base drag decreases gradually with decreasing R_L . This is caused by the fact that the mixing region behind the model becomes, to an increasing extent, laminar as R_L decreases.

The data for $d/D = 0.5$ and $l/D \geq 3$ correlate well; the discrepancies can, for the greater part, be explained by the accuracies quoted ($0.0002 < |\Delta C_{Db}| < 0.0013$).

The base drag coefficient, from Reference 1, where the ratios $d/D = 0.5$ and $l/D = 2.0$ were used, correlate well with the data for longer sting length, at Mach numbers $M = 2.0, 2.5$ and 3.0 (Figs. 2d-2f). At $M = 4.0$ (Fig. 2g), however, the drag coefficients are about 15% higher than the data found with longer sting. This could be due to sting length interference. As mentioned before, Schueler⁷ found in this range of Reynolds numbers critical sting length ratios $(l/D)_{crit}$ between 2.2 and 3.7. He also found that when, at $M = 4$, the sting length is shortened below its critical value the base drag first increases, while with further decrease in l/D the base drag decreases rapidly. The data from Reference 3, however, where the same sting dimensions, $l/D = 2.0$ and $d/D = 0.5$, were used, give values of the base drag coefficient at $M = 4.0$ that compare very well with those where a longer sting was used (Fig. 2g).

The base drag data from the Boeing wind tunnel at high Reynolds numbers¹⁴ give lower values for C_{Db} at $M = 1.5$ and 2.0 if compared with other measurements. This again may be due to sting length interference ($l/D = 1.5$). Notwithstanding this low ratio, no effect is found at $M = 2.5$ and 3.0 (Figs. 2e and 2f).

The base pressure measurements on a half-model¹⁵ give values of C_{Db} that are from 20 up to 40% lower than the base drag of a complete model (Figs. 2a, 2b and 2d).

The free-flight measurements¹¹ give 5 to 10% lower values of C_{Db} than those measured in the wind tunnel (Figs. 2a, 2b and 2c). However, no direct comparison with the other data can be made because the two vertical fins were placed just in front of the base, and, of course, there is no sting present.

The measurements from O.N.E.R.A.¹⁶ give rather low values of C_{Db} at $2 \times 10^6 < R_L < 3 \times 10^6$ (Figs. 2a and 2e). This is in agreement with the trend that C_{Db} decreases when R_L becomes less than 3×10^6 . However, no direct comparison can be made with the data for $d/D = 0.5$ (solid lines), as in these tests a ratio $d/D = 0.6$ was used, and moreover the sting length is not known.

Except for the measurements at $M = 3.0$ (Fig. 2f), the tendency is that C_{Db} decreases with decreasing d/D (Figs. 2d, 2e and 2g). This is in agreement with results from sting-diameter interference tests as reported in References 23 and 24.

The tests with fixed transition (closed symbols) show the tendency that the base drag is decreased when the boundary layer is artificially tripped. This is in agreement with the theory of Crocco and Lees³¹, which predicts that the base pressure is increased with increasing ratio of boundary layer thickness to body diameter.

Finally, the base drag coefficients for $d/D = 0.5$ and $l/D \geq 3$ for $R_L > 3 \times 10^6$ (solid lines from Figs. 2a-2j) have been plotted in Figure 3 versus Mach number.

For comparison, the semi-empirical prediction for the base pressure by Love³³ has been plotted in the same figure. There appears to be good agreement, especially at high Mach numbers.

5.2 Forebody Drag at Zero Lift

5.2.1 General

In this report the drag of the body-wing combination corrected for zero-base drag has been termed forebody drag. Strictly speaking, this is not correct, but it appears to be a current expression which is conveniently short¹⁻⁸.

The forebody drag is determined by subtracting the base drag from the measured total drag. Due to the inaccuracies of their measured values no high accuracy in the forebody drag coefficient C_{Df} can be expected. Values of inaccuracies as high as $\Delta C_{Df} = \pm 0.003$ are quoted (see Table III).

The forebody drag consists of pressure drag, friction drag and (when relatively large roughnesses are applied to trip the boundary layer) 'roughness' drag. C_{Df} is a function of Mach number, Reynolds number, angle of attack, roughness size and the transition point of the boundary layer on body and wings. The transition point, in its turn, is determined by such factors as free stream turbulence, model-surface finish and ratio of wall temperature to free stream temperature.

To be able to correlate the forebody drag coefficients measured in different wind tunnels, it is necessary to know the position of the transition point on body and wings. However, no data on the location of transition are available in the various reports, except in References 7 and 19, where transition points on the body were obtained. This means that a fairly wide scatter in the values for C_{Df} can be expected, but the measured drag coefficients should lie between the values for fully turbulent and for fully laminar boundary layer, as long as the relative size of the boundary layer trip is not too large.

The forebody drag coefficients, C_{Df} at zero angle of attack, have been plotted in Figures 4a-4h, as a function of R_L , for constant Mach number.

Open symbols are used for the data with natural transition, the closed symbols denoting fixed transition.

Further, the following dashed lines have been drawn in Figure 4:

The pressure drag of the body alone. This drag has been obtained from pressure measurements on the body at Mach numbers from 1.6 to 2.4 (Ref. 16) and at $M = 8$ (Ref. 8). For Mach numbers $M = 3, 4$ and 5 the pressure drag of the body has been interpolated (see Fig. 5). For comparison a theoretical estimate is given in the same figure, which has been derived from the generalized curves of Reference 27, which were obtained by the application of similarity laws to the results of exact linearized solutions for pointed forebodies. This theoretical estimate is

appreciably lower than the experimental results. Further work is needed to examine this discrepancy.

The pressure drag of body and wings. The wing drag is determined from the theory of Reference 26.

The forebody drag of the wing-body combination with a fully laminar boundary layer. The friction drag has been determined as the drag of an equivalent flat plate with

$$\text{chord} = \frac{\text{wetted model surface}}{2(b - D) + D}$$

This method was used also for the comparison of the measurements with AGARD Model B in the transonic speed range²⁹. It appeared that only very small differences exist between the results obtained with this method and those obtained with a method where wing and body are considered separately. Skin-friction drag coefficients for compressible flow with zero heat transfer have been used, following Reference 27.

The forebody drag of the wing-body combination with a fully turbulent boundary layer. The friction drag was determined as the drag of an equivalent flat plate, in the same way as for the laminar boundary layer.

It should be stressed here that the estimated curves for the forebody drag coefficient, as determined in this way, give only the trend of variation with Reynolds number, the actual values not being very accurate.

5.2.2 Forebody Drag with Natural Transition

Solid lines have been drawn in Figures 4d-4k through those points where the Reynolds number was varied sufficiently during the tests to give a drag-Reynolds number curve for the model-tunnel combination considered.

Figure 4f is an example ($M = 2.5$). Two solid lines have been drawn in this figure, giving the variation of C_{Df} with R_L for two series of tests, made with different models and in different wind tunnels at A.E.D.C.^{7,19}. It is clear from the figure that the two combinations have different transition Reynolds numbers, which is also shown in Reference 19.

It can be concluded that, in order to be able to correlate the data of the forebody drag coefficient from various wind tunnels, it is necessary to know the transition location in the boundary layer. However, as already mentioned, no such data are provided in the various sources, except in References 7 and 19.

In the Mach number range considered here, most of the values of C_{Df} lie somewhere between the estimated laminar-drag curve and a line that is somewhat lower than the turbulent-drag curve. This could be explained, of course, by the fact that the boundary layer is always partly laminar.

No explanation can be given here for the rather low value for C_{Df} at $M = 1.6$ and $R_L = 4 \times 10^6$ (Fig.4c, Ref.14), nor for the low value of C_{Df} at $M = 2.5$ and $R_L = 2.6 \times 10^7$ (Fig.4f, Ref.14); this last value is even lower than the estimated pressure drag of the model.

It appeared, however, that the model used for the tests in the Boeing wind tunnel has a nose profile that does not conform to the AGARD specification (see Table I, Ref.14). Because of this error the drag data of Reference 14 (Figs.2b, 2d, 2e and 2f) must be considered doubtful.

The available data on forebody drag at $M = 4$ are presented in Figure 4h. Nearly all the data are from tests in Tunnels E-1 and A at A.E.D.C. Two solid lines have been drawn in the figure, one for the tests in Tunnel A, as reported in Reference 19, the other for the tests in Tunnel E-1 (Ref.3). It appears that, in the Reynolds number range between 1.5×10^6 and 5×10^6 , there is a difference between the two series of tests of approximately 15% in the forebody drag coefficient.

Other data from Tunnel E-1 (Ref.1) give values of C_{Df} for three Reynolds numbers (see Fig.4h). The measurements in this case were performed with the same model as in Reference 3. It is interesting to note that only the value of C_{Df} at $R_L = 5 \times 10^6$ agrees with the measurements of Reference 3, while the other measured forebody drag coefficients are on the same level as the data¹⁹ from Tunnel A.

In general, however, it appears that the repeat tests³ at $M = 4$ with the same model and in the same Tunnel E-1 gave higher values than the drag results presented in Reference 1.

Although repeat tests were not made at $M = 5$, the forebody drag coefficients also appear to be consistently high (Fig.4i, Ref.3).

Between the tests of References 1 and 3 some changes to the tunnel were made; a heater was installed, together with a mixing chamber with baffles and screens. Moreover the settling-chamber temperature level was changed from between -40° and 60°F to between 170 and 220°F .

This change in the tunnel and in the test conditions could well account for the discrepancies noted. According to unpublished AEDC data the installation of the mixing chamber resulted in a reduction of the transition Reynolds number from 3.5×10^6 to 3×10^6 for a 5° half-angle cone at $M = 4.5$ and a settling-chamber temperature of 100°F .

Another factor that could cause the higher drag results is the fact that during the repeat tests the body surface roughness was somewhat higher¹³.

Of particular interest in correlating the forebody drag results is the correlation obtained with models of near identical scale which were tested in the same facility at identical test conditions. An AEDC model ($L = 16.63$ in.) was loaned to the Jet Propulsion Laboratory for their test program which also included tests of a JPL model ($L = 17.03$ in.).

It appears, from Figures 4c and 4e-4i (Ref. 12), that the drag levels obtained with the AEDC model are consistently high and that they correspond closely with the values obtained when transition was fixed on the JPL model.

The same AEDC 16.63 in. model was tested⁶ in the AEDC 40 in. supersonic Tunnel A. Comparison of these results with those¹⁹ on a 49.3 in. model in the same Tunnel A shows again that the data obtained on the 16.62 in. model are consistently high (see Figs. 4g-4i).

Examination of the model details reveals that in the first place the ratios of radius (diameter D) of the nose and leading edge of the wings are largest for the 16.63 in. model; secondly, the local profile thickness of the wings forward of the maximum thickness is larger for the 16.63 in. model than for the 17.03 in. model and, thirdly, of all three models considered the average surface roughness is largest for the 16.63 in. model (5μ in. compared with 4 and 3μ in. for the other models).

It is possible that these differences in model details are responsible for the high drag levels measured on the AEDC 16.63 in. model.

The free-flight tests¹¹ were made with a model equipped with two vertical fins for stabilization, with a pressure probe and a flow angle indicator mounted on the nose. The dimensions of the fins are half those of the wings. The forebody drag of a model without probes and fins will be somewhat lower than the values plotted in Figures 4a-4d. This means that, for the body-wing combination only, a value for the forebody drag coefficient is found which is approximately equal to the estimated value with a completely laminar boundary layer. This could have been caused by the stabilizing effect on the boundary layer due to the thermal lag of a model in free flight²⁵.

5.2.3 Forebody Drag with Fixed Transition

The boundary layer trips that are used in the present tests can be divided into three classes; wires, carborundum and strips. A survey of the trips used in the various tests is given in Table II.

(a) Wires

It is recommended in the AGARD specification²⁰ that tests be done with wires of various diameters. These diameters are defined by the values 500, 1000, 2000, 5000 and 10,000 of the Reynolds number based on wire diameter (R_{wire}).

The increase in drag due to the use of a wire is caused in the first place by the forward movement of the transition point and, with larger wire diameters, also by the drag of the wire itself. However, as long as the actual location of transition is not known, nothing can be said about the increase in drag that may be expected. An illustration of the effect of wire size on drag is given by the half-model tests reported in Reference 15 at $M = 1.6$ (Fig. 4c). Here the Reynolds number based on wire diameter varied between $R_{wire} = 3000$ and $R_{wire} = 7600$. The ratio of wire diameter to local profile thickness at the wing root varied from 0.08 to 0.20. With increasing wire size the drag coefficient becomes larger, the largest wire diameter giving a C_{Df} somewhat higher than the estimated value with fully turbulent boundary layer.

From the figures it may be concluded, in general, that all measurements with transition induced by wires ($1500 < R_{wire} < 9000$) give data for C_{Df} that lie somewhere within the expected range, between the value of C_{Df} without wires and the value for a completely turbulent boundary layer.

(b) *Carborundum*

The use of carborundum as a boundary layer trip results in an increased drag, in the first place due to the forward movement of the transition point and in the second place (when relatively large particles are used) due to the roughness drag. Therefore the drag could be dependent on such parameters as Reynolds number based on particle diameter, the form and the place of the carborundum strip, the distribution of particles and the ratio of particle size to a characteristic model dimension. No attempt has been made to compare the various tests with carborundum, as no systematic measurements are available.

The influence of carborundum as a boundary layer trip on the forebody drag is illustrated by the tests of Reference 13, where different roughness sizes were used (see Fig.4c at $M = 1.6$ and Fig.4f at $M = 2.5$).

At $M = 2.5$ the measured value for C_{Df} with natural transition is near the estimated laminar value. Four tests were made with carborundum on the body only and with grit numbers varying from 120 to 24. (The grit number denotes the approximate number of meshes per inch of the sieves used to select the different sized particles). With increasing roughness, C_{Df} increases from 110 to 130% of its value without a boundary layer trip. Other tests were performed with carborundum also on the wings in a band 0.15 in. wide, 2 in. from the leading edge, the carborundum on the body being kept the same.

Here the forebody drag varies with increasing roughness from 115% to as much as 150% of the C_{Df} value with no roughness added on the wings.

It is evident from Figure 4f that this rapid rise in forebody drag coefficient cannot be caused by the forward movement of the transition point on the wing only, but that the roughness drag plays an important part. This must be due to the large particle sizes compared with wing dimensions. Indeed, at the lowest grit number, the particles that are pasted on the upper and lower surface of the wings are of the same dimensions as the local profile thickness at the wing root.

The other tests that have been done with carborundum as a boundary layer trip¹ give consistently higher values for C_{Df} than the estimated value for the model with a completely turbulent boundary layer (Figs.4d-4f). Here again, the size of the applied roughness on both surfaces of the wings is of the same order as the local wing thickness at the root. Therefore it is reasonable to assume that the high drag found in this case is also due to the large amount of roughness drag.

The tests of Reference 5 at $M = 1.4$ and 1.5 show a slightly smaller forebody drag with fixed transition than in the case where no artificial transition was used. In these tests a band of carborundum was used on the wings only (see also Table II).

The change of the wing drag is caused in the first place by the forward movement of the transition point, but in the second place by the change in displacement

thickness of the boundary layer, resulting in a different pressure distribution over the wing. Young²⁸ has shown that, in certain circumstances, a decrease in drag of a biconvex profile may be observed, which is due to this change in effective displacement of the surface. It is possible that the decrease in drag found in the tests mentioned is caused by such a phenomenon.

(c) Strips

In one series of tests¹⁰ a transition strip, 3/16 in. wide and 2/100 in. high, was used on body and wings. The strips on the wings were placed 1/4 in. behind the leading edge (wing root chord 2 in.).

The drag coefficients found here are up to 30% higher than the estimated values with fully turbulent boundary layer (see Figs. 4c, 4e and 4f). This again may be due to the rather large thickness of the transition strip compared with the wing dimensions. In this case the thickness of the strip is 57% of the local thickness of the wing at the root.

5.2.4 Conclusions Relating to Forebody Drag

The following conclusions can be drawn:

There exists a large scatter in the various measurements of the forebody drag coefficient. This scatter appears to be due to such factors as Reynolds number effects, model imperfections and differences in wind tunnel installations and test conditions. The ranges of measured C_{Df} have been plotted versus M in Figure 6.

It is difficult to compare the available data on forebody drag. In the first place because, in many of the tests, the Reynolds number was not varied systematically. Secondly, because there is, in general, no information about the actual position of the transition point and thirdly, because of the relatively large boundary layer trips that have been used in many cases.

It is desirable to know the transition point location in all cases.

When artificial roughness is used to induce transition, the size of the roughness should not be much larger than the minimum roughness dimension necessary to fix transition at the desired position.

5.3 Lift

The lift of AGARD Model B has been determined over a wide range of Reynolds numbers. The lift could be dependent on Reynolds number, because of the effect of this parameter on the separation of the boundary layer. However, no effect of Reynolds number variation on the lift coefficient could be traced.

Further, the lift coefficient appears to be a linear function of the angle of attack, up to about 8° . At higher angles there is a slight deviation from the straight line relationship. The relatively few measurements that are available in this range of angles of attack are compared in Figure 7. The agreement between the various measurements appears to be good.

In Figure 8 the slope of lift curve $C_{L\alpha}$ at zero angle of attack has been plotted versus Mach number. The agreement between the numerous measurements is good, with the following exceptions:

$C_{L\alpha}$ at $M = 1.5$, as measured in the transonic wind tunnels at A.E.D.C. (Refs. 2 and 4), appears to be about 6% higher than the other data. Examination of the basic plot of C_L versus α from which these slopes were taken indicated that the curves are slightly non-linear near the origin, the local slope being approximately 5% lower than the mean slope. The higher slopes are reproduced in Figure 8. The reason for this non-linearity is not known, but it may be significant that these two sets of data were obtained with the same model and balance.

The half-model measurements¹⁵ give values of $C_{L\alpha}$ at $M = 1.46$ and 1.57 that are about 5% lower. For this series of tests $C_{L\alpha}$ was too low for the whole transonic range, as compared with other measurements²⁹.

The free-flight measurements¹¹ give data for $C_{L\alpha}$ that are 5% under the average value. The same was found in Reference 29 at $M = 1.3$.

5.4 Pitching Moment

The available data on pitching-moment coefficient C_m have been plotted in Figure 9 as a function of Mach number for constant lift coefficient.

The centre of moments has been taken (as specified in Ref. 20) at a point 1.155 D ahead of the trailing edge of the wing. This means that the data from References 2, 4, 5, 13 and 15, where a different reference point was chosen, have been converted. Undoubtedly this has had some unfavourable influence on the accuracy of these data.

Further, it has been found that in a number of cases the moment is not zero for zero lift. These measurements (Refs. 2, 4, 5, 10 and 14) have been corrected by a parallel shift of the C_m curve in such a way that $C_m = 0$ at zero lift.

No data from the free-flight tests of Reference 11 have been included, as the C_m data could not be read accurately enough in that report. Due to the scatter in the data of the moment coefficient with fixed transition in References 13 and 15, no data from these reports have been included.

The following conclusions can be drawn from Figure 9:

With the exception of References 10 and 15, the scatter of data with natural transition lies within the maximum quoted inaccuracy of the measurements ($\Delta C_m = \pm 0.005$). In view of this the agreement in moment coefficient appears to be good for the various measurements; no effect of Reynolds number can be traced.

Except for $M = 1.6$, the data of Reference 10 give consistently too high values of the moment coefficient. The cause of this discrepancy is not clear. No explanation can be given either for the behaviour of C_m as a function of M for the half-model tests of Reference 15.

With regard to artificial transition, the following points may be noted:

No influence on moment coefficient is found when wires are used to trip the boundary layer¹².

Depending on Mach number, angle of attack and particle size, the data with carborundum on body and wings¹ give values of C_m that are up to 10% higher than the moment coefficient found without the use of artificial transition. No influence of carborundum on the wings only has been found⁵.

In the tests of Reference 10 a rather large strip (compared with model dimensions, see Table II) has been used to trip the boundary layer. Compared with the data without artificial transition, differences up to 20% in moment coefficient have been measured in this case. It seems fair to attribute this large difference to the relatively large size of the trip used.

5.5 Neutral Point

For zero lift, the distance of the neutral point, in body diameters aft of the model nose, has been plotted in Figure 10 as a function of Mach number.

The position of the neutral point is determined by

$$x_{np} = x_{mc} - \left(\frac{dC_m}{dC_L} \right)_{C_L=0} \left(\frac{\bar{c}}{d} \right)$$

It appears from Figure 10 that there exists a fair agreement in the results for the neutral point, the position of which appears to be independent of Reynolds number. This could be expected, as this parameter could only be significant in the case of separation of the boundary layer, that is at higher angles of attack. For the same reason, no effect of the fixing of the transition point of the boundary layer has been found.

6. CONCLUSIONS

Tests with AGARD Calibration Model B in various wind tunnels and in free flight have been critically compared in the Mach number range from 1.4 to 8. Many discrepancies between the results of these tests can be explained.

The following conclusions can be drawn:

There exists a wide scatter in the measured values of the total drag of the model at zero lift. The total drag has been divided into two parts, the forebody drag and the base drag.

Most of the discrepancies in the base drag coefficient would be explained by the influence of the parameters that affect the base pressure, such as Mach number, Reynolds number, and ratios of sting diameter and of sting length to body diameter.

The forebody drag coefficient is a function of Mach number, Reynolds number and the transition point of the boundary layer.

The transition point is determined by such factors as Reynolds number, free-stream turbulence, model surface finish and ratio of wall temperature to free-stream temperature. Nearly all values of measured forebody drag coefficient with natural transition lie between the estimated values for fully laminar and fully turbulent boundary layer; however, no better correlation could be found as nothing is known about the actual transition point of the boundary layer on the models in the different wind tunnels or in free flight.

In general the forebody-drag coefficient of the models with transition fixed by wires ($1500 < R_{\text{wire}} < 9000$) lies somewhere in the expected range, i.e. between the measured value of the drag of the model without wires and the estimated value for a fully turbulent boundary layer.

Transition induced by carborundum on body and wings results, in several cases, in rather high values of the forebody drag coefficient. This might be attributed to the relatively large particles that were used.

Good agreement has been found in the results of the measurements of lift, pitching moment and neutral point position of the model.

With regard to the model specification²⁰ the following points may be noted:

- (a) The radii of the nose and wing leading edges have been given in Reference 20 as $D/500$. Obviously, this radius cannot be constant all along the wing leading edge. For most of the tests reviewed here it is not known how the models were made in this respect. As the leading edge radii may be the cause of some differences in the measurements (see Section 5.2.2) it is recommended for future investigations that the wing leading edges are made in the same way as in References 8 and 19, where the theoretical root chord was made with the specified radius of $D/500$ but the remainder of the wing had leading edge radii of a constant percentage of the local chord.
- (b) Sting support dimensions of $d/D = 0.5$ and $l/D = 3$ were recommended in the specifications²⁰, but it was not noted that these criteria should apply only to the case of turbulent flow approaching the base. Future investigations at low Reynolds numbers and at high Mach numbers, where long runs of laminar flow are encountered, will require a re-examination of these criteria (see Ref.7).

REFERENCES

1. Schueler, C.J.
Strike, W.T. *An Investigation of the Lift, Drag and Pitching Moment Characteristics of AGARD Calibration Models A and B.* Arnold Engineering Development Center, AEDC-TN-55-34, February 1956.
2. Milillo, J.R.
Chevalier, H.L. *Test Results of the AGARD Calibration Model B and a Modified AGARD Model C in the AEDC Transonic Model Tunnel.* Arnold Engineering Development Center, AEDC-TN-57-6, May 1957.
3. Schueler, C.J. *Lift, Drag and Pitching Moment Characteristics of AGARD Calibration Models A and B at Mach Numbers 3.98 and 4.98.* Arnold Engineering Development Center, AEDC-TN-57-9, May 1957.
4. Milillo, J.R. *Transonic Tests of an AGARD Model B and a Modified Model C at 0.01 percent Blockage.* Arnold Engineering Development Center, AEDC-TN-58-48, August 1958.
5. Dick, R.S. *Tests in the PWT 16 ft Transonic Circuit of an AGARD Model B and a Modified Model C at 1.15 percent Blockage.* Arnold Engineering Development Center, AEDC-TN-59-32, April 1959.
6. Schueler, C.J.
Strike, W.T. *Calibration of a 40 in. Continuous Flow Tunnel at Mach Numbers 1.5 to 6.* Arnold Engineering Development Center, AEDC-TN-59-136, November 1959.
7. Schueler, C.J. *An Investigation of Support Interference on AGARD Calibration Model B.* Arnold Engineering Development Center, AEDC-TN-60-35, February 1960.
8. Kayser, L.D.
Fitch, C.R. *Force and Pressure Tests of an AGARD Calibration Model B at a Mach Number of 8.* Arnold Engineering Development Center, AEDC-TN-60-34, July 1960.
9. Piland, R.O. *The Zero-Lift Drag of a 60° Delta-Wing-Body Combination (AGARD Model 2) Obtained from Free-Flight Tests Between Mach Numbers of 0.8 and 1.7.* NACA TN 3081, April 1954.
10. Bromm, A.F., Jr. *Investigation of Lift, Drag and Pitching Moment of a 60° Delta-Wing-Body Combination (AGARD Calibration Model B) in the Langley 9 in. Supersonic Tunnel.* NACA TN 3300, September 1954.
11. Mitchell, J.L. *Rocket Model Investigation of the AGARD Model B Configuration by the NACA Langley Laboratory.* NACA Memorandum, February 7, 1957.

12. Douglas, D.W.
Martin, R.E. *An Investigation of the Lift, Drag and Pitching Moment Characteristics of the AGARD Calibration Model B at Mach Numbers 1.65 to 5.00 in the 20 in. Supersonic Wind Tunnel (Preliminary). Jet Propulsion Laboratory, SWT 20-C28, February 1959.*
13. North American
Aviation *Supersonic Wind Tunnel Test of the AGARD Calibration Models to Obtain Comparative Force Data. North American Aviation, MD 58-37 SAL 147, November 1957.*
14. Schreiber, B. *A Compilation of Data from Tests of AGARD Models B and C in the Boeing Wind Tunnels. Boeing, Seattle, Document D2-5360.*
15. Laberge, J.G. *Half-Model Measurements of Longitudinal Force and Moment Characteristics of AGARD Model B at Subsonic and Supersonic Speeds. National Research Council of Canada, LR-267, December 1959.*
16. La Direction
Aérodynamique de
l'O.N.E.R.A. *Premiers Resultats d'Essais sur Maquettes Etalons AGARD. AGARD 6ème session du Comité Souffleries, Novembre 1954.*
17. O.N.E.R.A. *Caractéristiques Supersoniques de la Maquette AGARD B. Fiche Documentaire Provisoire No.206, ONERA, Octobre 1959.*
18. Hills, R. *Measurements from Aircraft Research Association Supersonic Wind Tunnel; Unpublished data, June 1960.*
19. Coats, J.D. *Force Tests of an AGARD Calibration Model B at $M = 2.5$ to 6.0 . Arnold Engineering Development Center, AEDC-TN-60-182, October 1960.*
20. A. G. A. R. D. *Wind Tunnel Calibration Models. AGARD Specification 2, September 1958.*
21. Love, E.S. *A Summary of Information on Support Interference at Transonic and Supersonic Speeds. NACA RM L53K12, August 1955.*
22. Reller, J.O., Jr.
Hamaker, F.M. *An Experimental Investigation of the Base Pressure Characteristics of Non-Lifting Bodies of Revolution at Mach Numbers from 2.73 to 4.98. NACA TN 3393, March 1955.*
23. Whitfield, J.D. *Support Interference at Supersonic Speeds (AEDC). Preprint of a paper presented at the AGARD Specialists' Meeting on Wind Tunnel Corrections and Interference Effects, Rhode-St.Genève, Belgium, March 1959.*

24. Sivier, K.R.
Bogdonoff, S.M. *The Effect of Support Interference on the Base Pressure of a Body of Revolution at High Reynolds Numbers.* Princeton University Report 332, October 1955.
25. Schueler, C.J. *AGARD Tests Comparison of Wind Tunnel and Free Flight Results (AEDC).* Presented at the 7th Semi-Annual Meeting of the Supersonic Tunnel Association. Redstone Arsenal, Huntsville, Alabama, April 1957.
26. Beane, B. *The Characteristics of Supersonic Wings Having Biconvex Sections.* Journal of the Aeronautical Sciences, Vol.18, No.1, 1951.
27. Royal Aeronautical Society *Aerodynamics Data Sheets.* Royal Aeronautical Society Volumes 1 and 2.
28. Young, A.D.
Kirkby, S. *The Profile Drag of Biconvex and Double Wedge Wing Sections at Supersonic Speeds.* Proceedings of a symposium 'Boundary Layer Effects in Aerodynamics', held at the National Physical Laboratory on 31st March and 1st April 1955.
29. Valk, H.
van der Zwaan, J.H. Part II of this AGARDograph
30. Perry, R.W.
MacDermott, W.N. *Development of the Spark-Heated, Hypervelocity, Blowdown Tunnel Hotshot.* Arnold Engineering Development Center, AEDC-TR-58-6, June 1958.
31. Crocco, L.
Lees, L. *A Mixing Theory for the Interaction Between Dissipative Flows and Nearly Isentropic Streams.* Journal of the Aeronautical Sciences, Vol.19, No.10, 1952.
32. Fitch, C.R.
et alii *Air Liquefaction Effects on the Aerodynamic Characteristics of the AGARD Calibration Model B at Mach Numbers 5 and 8.* Arnold Engineering Development Center, AEDC-TN-61-24, February 1961.
33. Love, E.S. *Base Pressure at Supersonic Speeds on Two-Dimensional Airfoils and on Bodies of Revolution With and Without Fins Having Turbulent Boundary Layers.* NACA TN 3819, January 1957.

Ref.	Symbol	Facility	Model			
			L (in.)	l/D	d/D	Surface roughness (μ in.)
1	○	A.E.D.C. supersonic tunnel E-1 12 in. x 12 in.	11.474	2.0	0.5	2 to 10
2	△	A.E.D.C. transonic tunnel 12 in. x 12 in.	16.63	3.0	0.488	-
3	▽	A.E.D.C. supersonic tunnel E-1 12 in. x 12 in.	11.474	2.0	0.5	2 to 9
4	□	A.E.D.C. transonic tunnel 16 ft x 16 ft	16.63	3.0	0.488	-
5	◇	A.E.D.C. transonic tunnel 16 ft x 16 ft	183.60	3.08	0.5	-
6	▵	A.E.D.C. supersonic tunnel A 40 in. x 40 in.	16.626	9.46	0.5	-
7	▴	A.E.D.C. supersonic tunnel E-1 12 in. x 12 in.	11.474	various	0.296	-
8	▽	A.E.D.C. hypersonic tunnel 50 in. diameter	49.300	2.0	0.5	-
9	▽	Free flight	10.625	-	-	-
10	▷	Langley supersonic tunnel 9 in. x 9 in.	6.8	2.0/ 3.0	0.5/ 0.375	-
11	◁	Free flight	59.50	-	-	-
12	▾	J.P.L. supersonic tunnel 20 in.	17.027/ 16.63	3.06	0.5	3(rms)
13	▵	N.A.A. supersonic tunnel 16 in. x 16 in.	10.625	> 4.3	0.4	-
14	▴	Boeing supersonic tunnel 4 ft x 4 ft	38.751	1.5	0.5	-
15	▽	N.A.E. tunnel 30 ft x 16 ft	15.3	-	-	6-8(rms)
16	✧	La Courneuve tunnel	6.7	-	0.6	-
17	▴	Vernon tunnel	13.4	-	-	-
18	◐	A.R.A. supersonic tunnel	17.0	-	0.5	-
19	⊙	A.E.D.C. supersonic tunnel A 40 in. x 40 in.	49.312	3.0	0.5	4-15(rms)
30	-	A.E.D.C. hypersonic tunnel 16 in. diameter	-	-	-	-
32	⊙	A.E.D.C. supersonic tunnel A 40 in. x 40 in. and A.E.D.C. hypersonic tunnel B 50 in. diameter	49.3	3.0/ 2.0	0.5	-

TABLE I

General Data on Models and Facilities

Model			M	$R_L \times 10^{-6}$	α (degrees)	Ref.	Remarks
d/D	Surface roughness (μ in.)	Boundary layer trip					
0.5	2 to 10	carborundum	1.70-2.01-2.47-3.02-4.02	2.6 to 22.0-3.1 to 18.7 3.8 to 16.2-3 to 13.0 3.1 to 7.6	-4.5 to +8	1	
0.488	-	-	1.40-1.50	7.2-6.9	-2 to +10	2	
0.5	2 to 9	-	3.98-4.98	1.6 to 4.3-1.1 to 2.5	-4 to +8	3	
0.488	-	-	1.50	3.7	-4 to +10	4	
0.5	-	carborundum	1.40-1.50-1.60	29.4-28.7-28.0	-4 to +9	5	
0.5	-	-	1.5-2.0-3.0-4.0-5.1	8	-	6	
0.296	-	-	2.0-3.0-4.0	varies from 1.1 to 13.2	0	7	l/D varied from 1.21 to 5.19
0.5	-	-	8	varies from 0.8 to 11.0	-5 to +15	8	
-	-	-	1.4 to 1.74	7.1 to 11.7	0	9	vertical fins, total drag only for base pressure tests
0.5/ 0.375	-	strip	1.62-1.94-2.41	3.0	-6 to +6	10	l/D = 3.6 and d/D = 0.375
-	-	-	1.4 to 1.74	9.6 to 16.0	-2 to +3	11	vertical fins
0.5	3(rms)	wires	1.65-2.01-2.47-3.01-3.98-5.00	varies from 4.3 to 8.5	-11 to +21	12	2 models (JPL and AEDC)
0.4	-	carborundum	1.56-1.88-2.47-3.24	4.0-3.6-2.8-2.0	-2.4 to +2.1	13	
0.5	-	-	1.5-2.0-2.5-3.0-3.5	24.7-24.9-27.9-31.9-37.9	-4 to 6.2	14	nose profile different, curve is circle with radius 9.2740
-	6-8(rms)	wires	1.46-1.57-1.78-2.03	5.8-5.7-5.1-4.6	-2 to +14	15	half model
0.6	-	wire	1.44-1.61-1.80-2.04-2.47	3.3-3.2-3.0-2.8-2.3	-	16	
-	-	-	2.14-3.20-4.26	7.5	-	17	
0.5	-	-	1.4-1.7-2.0-2.5-3.0	4.5-5.2-5.1-4.5-3.3	-5 to +20	18	
0.5	4-15(rms)	-	2.5-3-4-5-6	3.4 to 17-2.9 to 19-1.9 to 22-1.8 to 26-4 to 15.5	-4 to +10	19	
-	-	-	15.0 to 16.0	0.2	-	30	not included as the tests were of a very preliminary nature
0.5	-	-	5 and 8	12 and 22-6.5 and 11	-4 to +8 at M = 5 -5 to +15 at M = 8	32	

2

TABLE II
Boundary Layer Trips

Ref.	Body		Wing																			
	Type	Placed at	Type	Placed at																		
1	Carborundum No.80: strip 3/16 in. wide	15% length	Carborundum No.80: strip 3/16 in. wide	15% chord																		
5	-	-	Carborundum No.60: strip 1% chord width	15% chord																		
10	Strips 3/16 in. x 2/100 in.	7.35% length	Strips 3/16 in. x 2/100 in.	¼ in. from leading edge																		
12	Wires	11% length	-	-																		
	<table><tr><th>M</th><th>d'(in.)</th><th>R_{wire}</th></tr><tr><td>1.65</td><td>0.003</td><td>1500</td></tr><tr><td>2.01</td><td>0.003</td><td>1500</td></tr><tr><td>3.01</td><td>0.015</td><td>5500</td></tr><tr><td>3.98</td><td>0.025</td><td>9000</td></tr><tr><td>5.00</td><td>0.025</td><td>6300</td></tr></table>	M	d'(in.)	R _{wire}	1.65	0.003	1500	2.01	0.003	1500	3.01	0.015	5500	3.98	0.025	9000	5.00	0.025	6300			
M	d'(in.)	R _{wire}																				
1.65	0.003	1500																				
2.01	0.003	1500																				
3.01	0.015	5500																				
3.98	0.025	9000																				
5.00	0.025	6300																				
13	Carborundum 0.3 in. wide (various grits)	6.6% length	Carborundum 0.15 in. wide (various grits)	2 in. from leading edge																		
15	Wires: 0.008 in. < d' < 0.020 in., 3000 < R _{wire} < 7600	15% length	Wires: 0.008 in. < d' < 0.020 in., 3000 < R _{wire} < 7600	15% chord																		
16	Wires: d' = 0.005 in., 1600 < R _{wire} < 2500	15% length	Wires: d' = 0.005 in., 1600 < R _{wire} < 2500	15% chord																		

TABLE III

Accuracy and Repeatability of Data

Ref.	ΔM	$\Delta \alpha$	ΔC_L	ΔC_{Dt}	ΔC_{Df}	ΔC_{Db}	ΔC_m	ΔX_{np}
1	± 0.04	$\pm 0.02^\circ$	± 0.0029	± 0.0004	± 0.0006	± 0.0002	± 0.0029	± 0.005
2	± 0.006	$\pm 0.1^\circ$	± 0.010	-	± 0.002	± 0.0002	± 0.003	-
3	± 0.01	$\pm 0.01^\circ$	± 0.0014	± 0.0002	± 0.0008	± 0.0005	± 0.0016	± 0.05
4	± 0.004	$\pm 0.3^\circ$	± 0.010	-	± 0.003	± 0.001	± 0.003	-
5	± 0.010	$\pm 0.05^\circ$	± 0.004	-	± 0.003	± 0.0003	± 0.002	-
6	± 0.030	$\pm 0.06^\circ$	± 0.0005	± 0.0008	± 0.0005	± 0.0013	± 0.0005	± 0.05
7	± 0.001	-	-	-	-	$\Delta P_b/p = \pm 0.05$	-	-
8	± 0.082	-	-	-	-		-	-
9	± 0.005	$\pm 0.3^\circ$	-	± 0.001	-		-	-
10	± 0.001	$\pm 0.01^\circ$	± 0.0004	± 0.001	-	± 0.002	± 0.0004	-
11	-	$\pm 0.4^\circ$	-	-	-	-	-	-
12	-	-	± 0.0030	± 0.0022	-	-	± 0.0030	-
15	± 0.03	$\pm 0.02^\circ$	± 0.005	± 0.002	-	± 0.0002	± 0.005	-
19	-	$\pm 0.1^\circ$	± 0.004	-	± 0.002	-	± 0.004	-
32	± 0.08	-	± 0.0020	± 0.0027	-	-	± 0.0017	-

Remarks

The values for ΔM represent the flow uniformity in the test section for wind tunnel measurements (Refs.1, 2, 3, 4, 5, 6, 7, 8, 15 and 32).

For the free-flight tests (Refs.9 and 10) the uncertainty in the measurement of M is given.

In this table only the maximum quoted inaccuracies are presented.

- Refs.13 and 12 : in terms of data repeatability, the uncertainty of the data being determined from a frequency distribution of the scatter in all the repeat data.
- Ref.2 : errors in balance read-out system, base pressure and stream parameters have been combined, based on a 95% confidence level and a normal error distribution.
- Ref.10 : estimated errors combined by a method based on the theory of least squares.
- Refs.6, 16 and 19 : maximum uncertainties of the computed parameters.
- Refs.4, 5, 9 and 15 : method unknown.
- Refs.13, 14, 16, 17 and 18 : no data available.

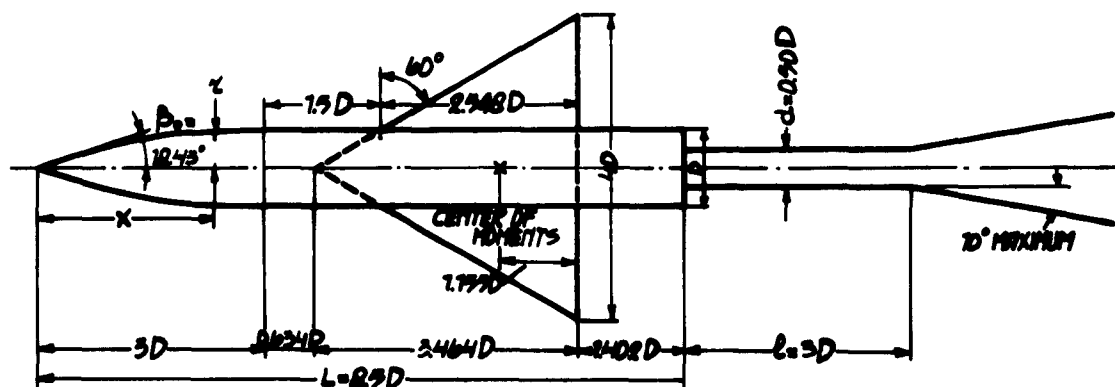


Fig.1 AGARD Calibration Model B
(Ref. 20)

Wing profile : symmetrical circular arc section. Thickness ratio = 0.04

Nose profile : length $3D$. Equation of curve: $r = \frac{x}{3} \left[1 - \frac{1}{9} \left(\frac{x}{D} \right)^2 + \frac{1}{54} \left(\frac{x}{D} \right)^3 \right]$

Radii of nose and wing leading edges should be $D/500$.

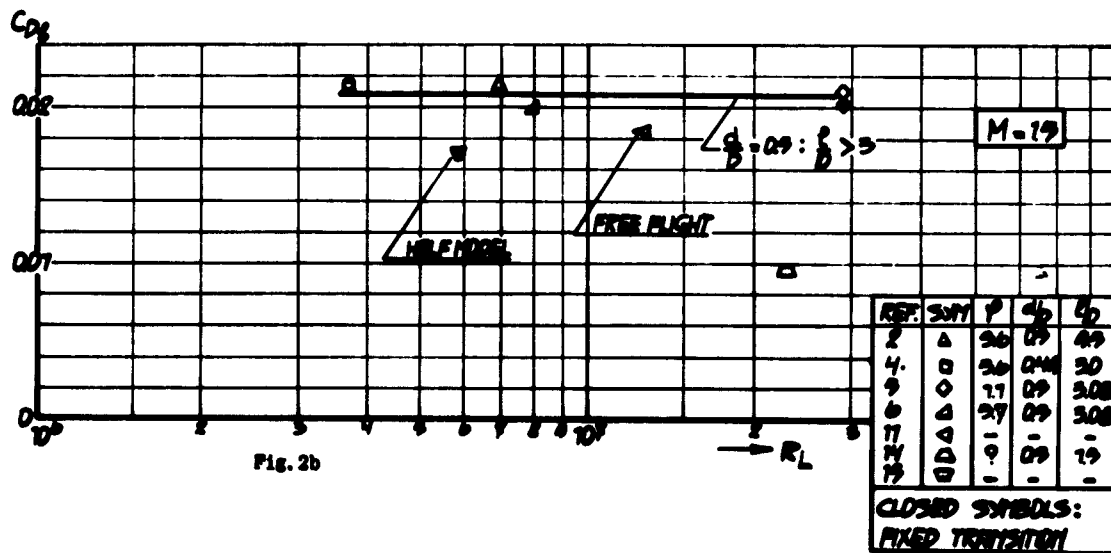
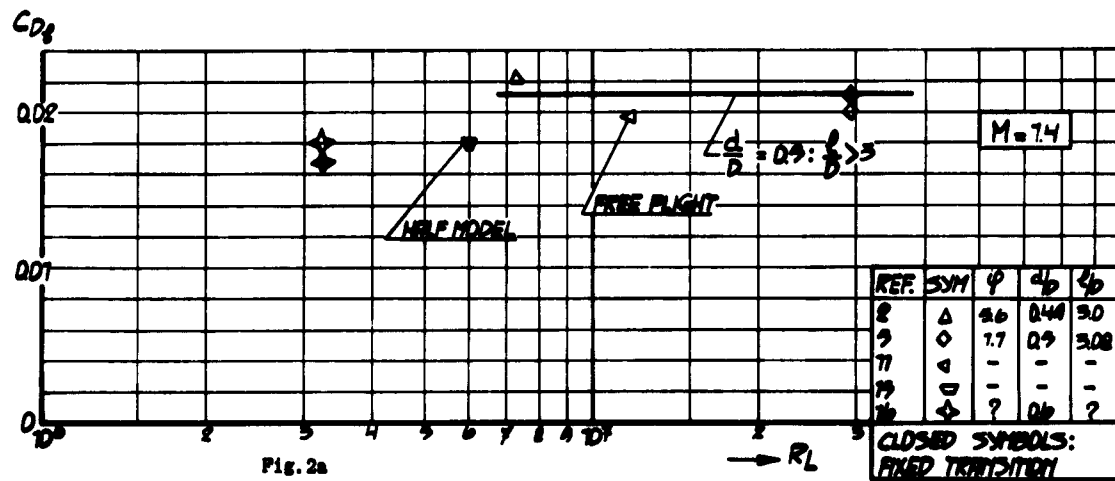


Fig. 2 The base drag coefficient C_{Db} versus R_L , for constant M ($\alpha = 0$)

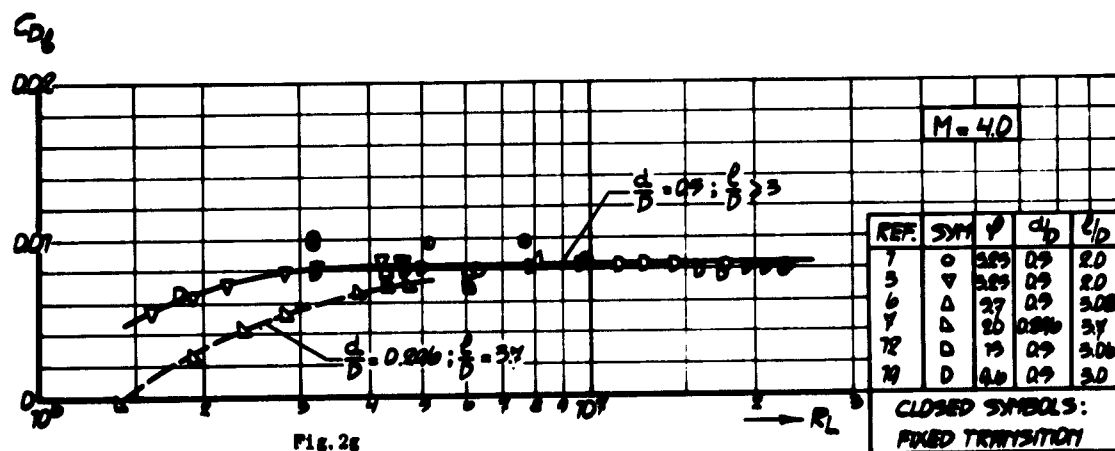
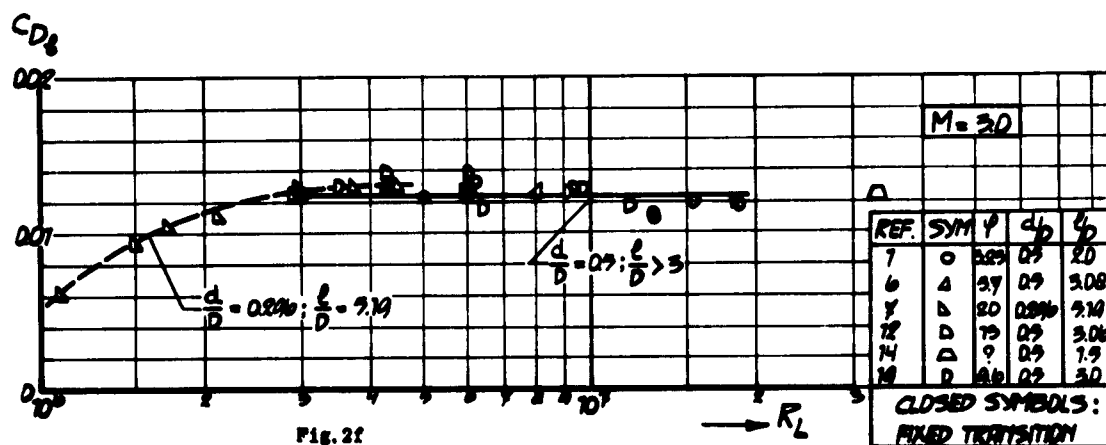
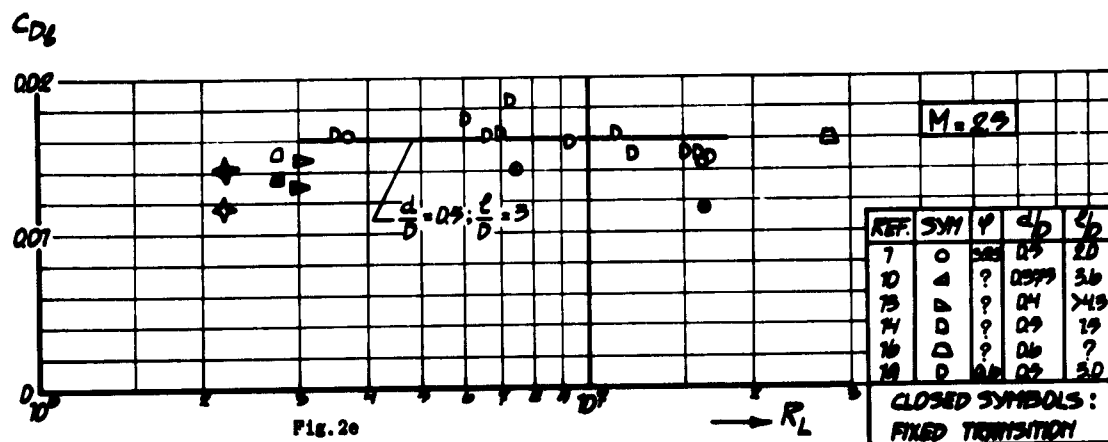


Fig. 2 The base drag coefficient C_{D_b} versus R_L , for constant M ($\alpha = 0$)
(continued)

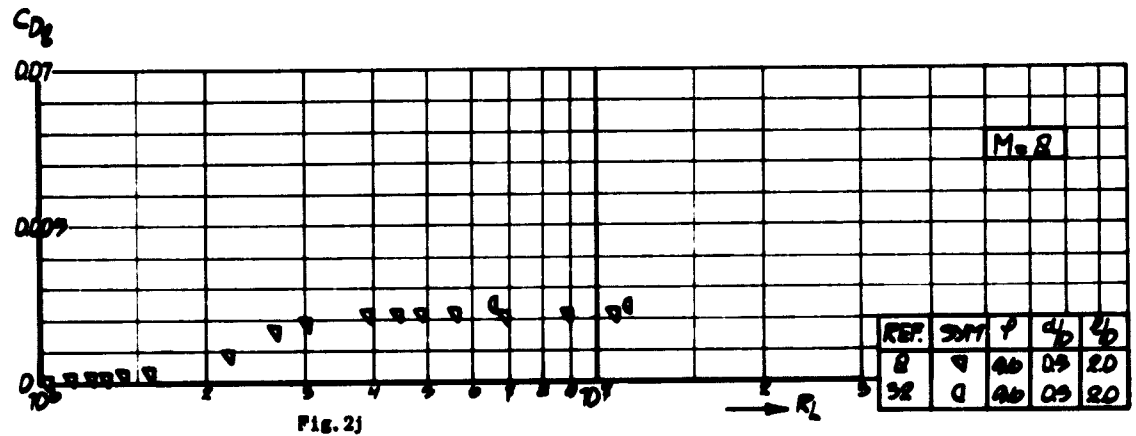
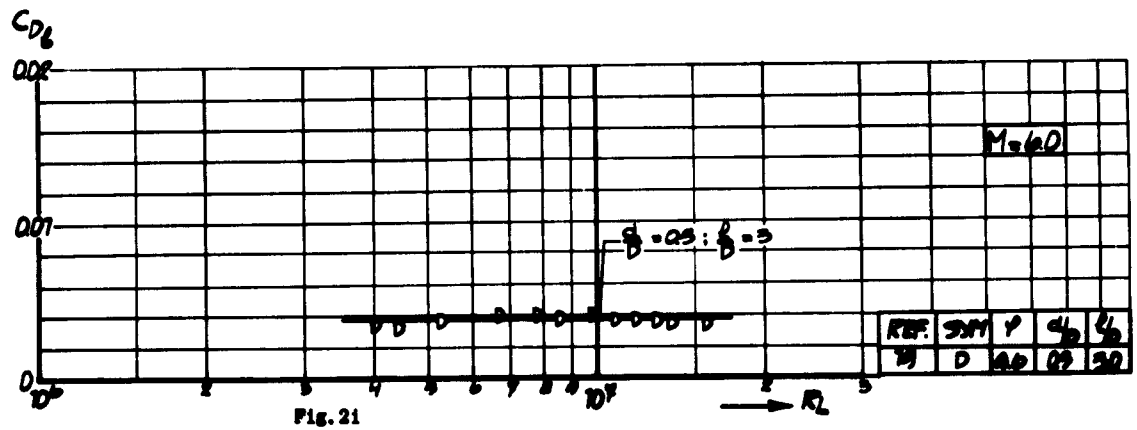
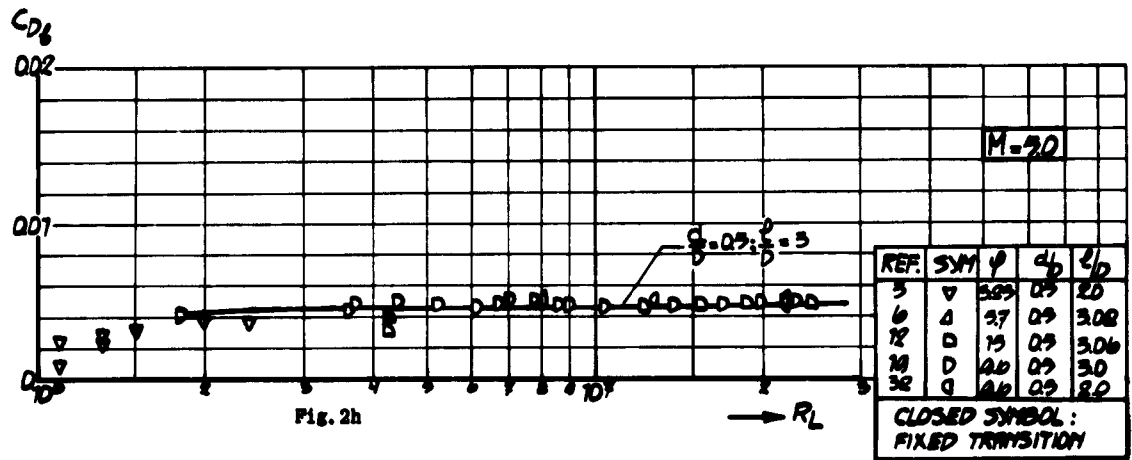
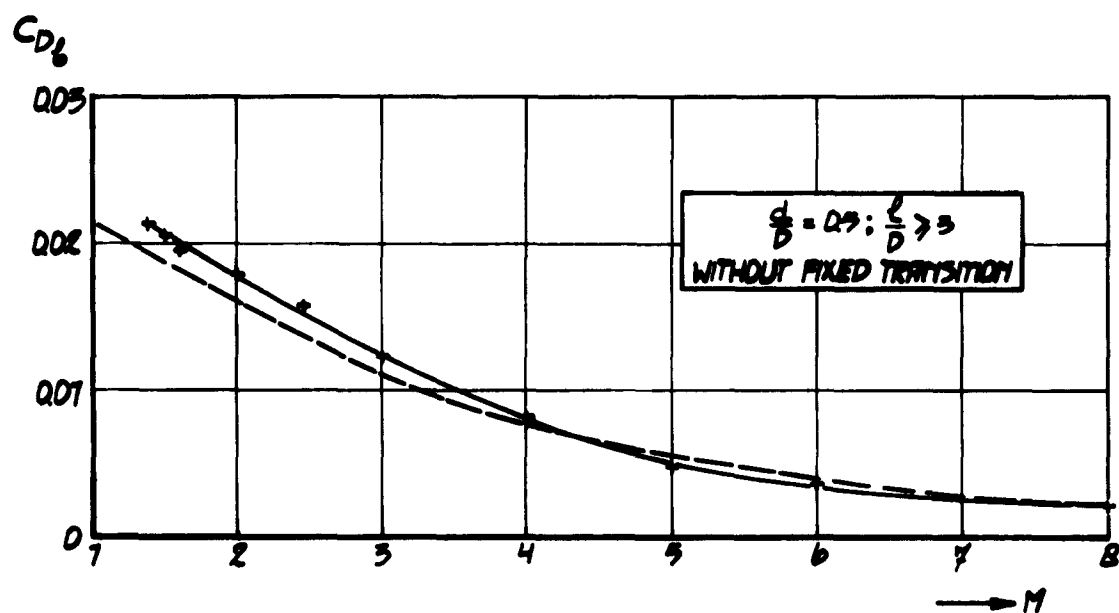


Fig. 2 The base drag coefficient C_{Db} versus R_L , for constant M ($\alpha = 0$)
(continued)



----- SEMEMPirical PREDICTION OF LOVE (REF. 33)
FOR TURBULENT BOUNDARY LAYERS, NO STING.

Fig.3 The base drag coefficient C_{Db} versus M ($R_L > 3 \times 10^6$)

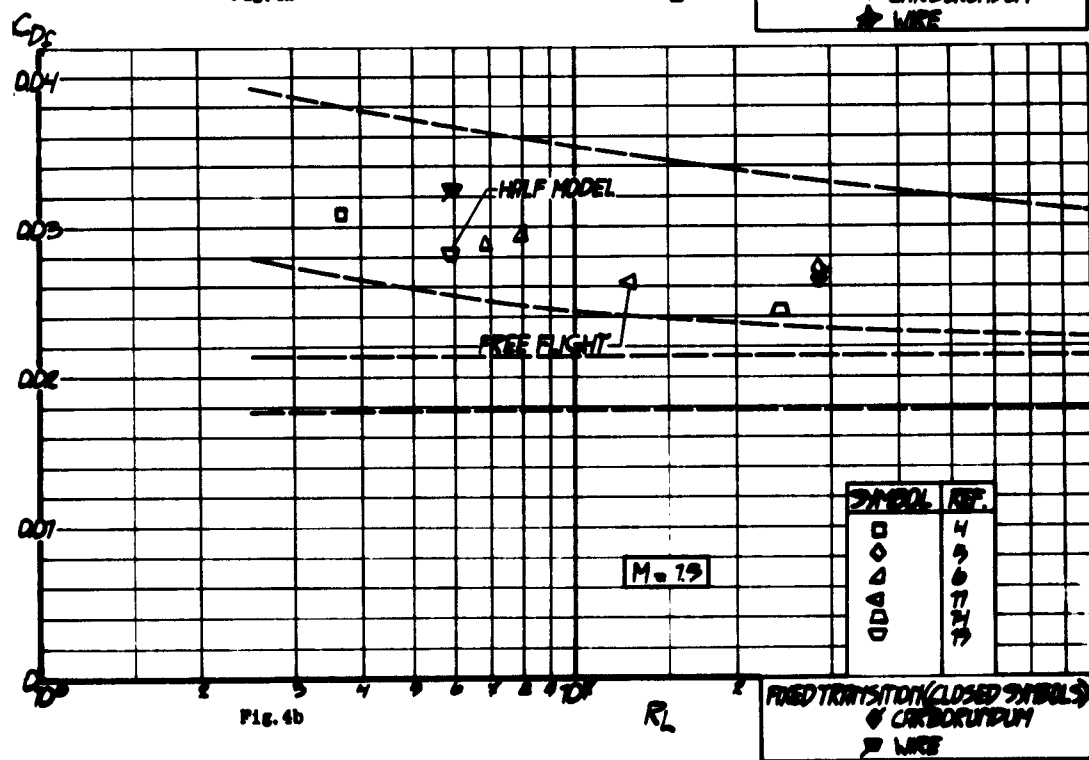
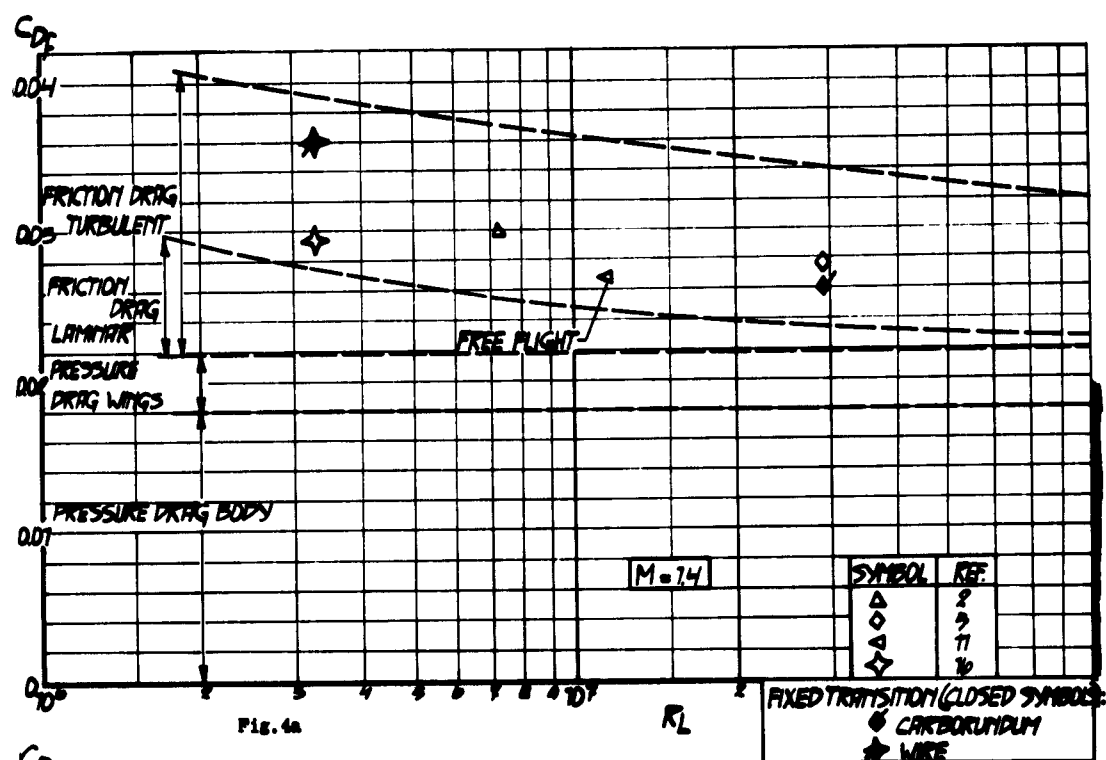


Fig. 4 The forebody drag coefficient C_{Df} versus R_L ($\alpha = 0$)

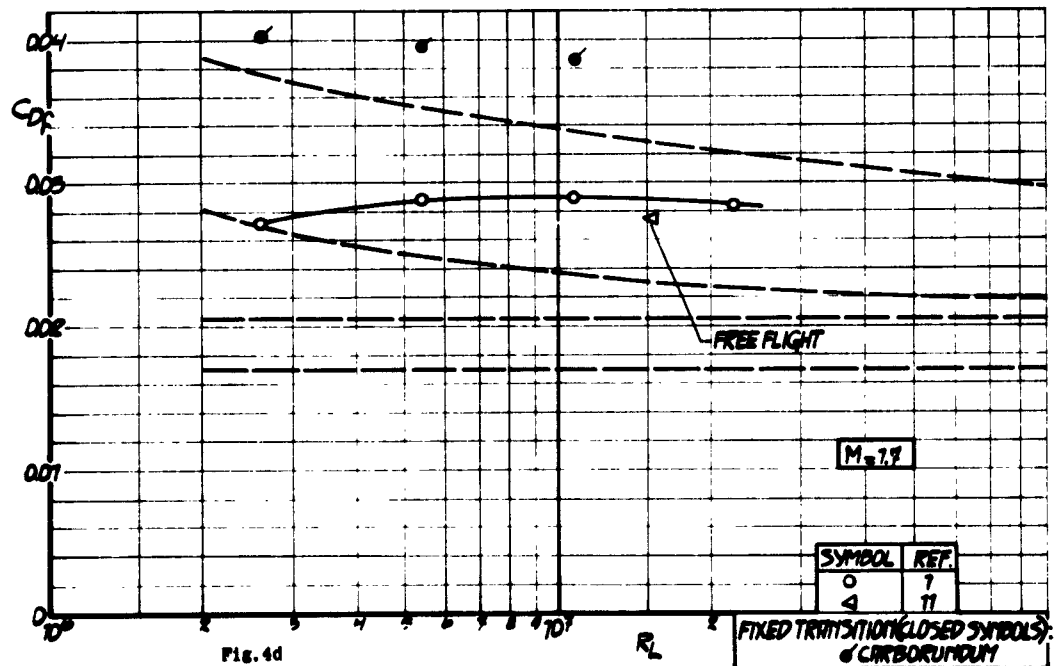
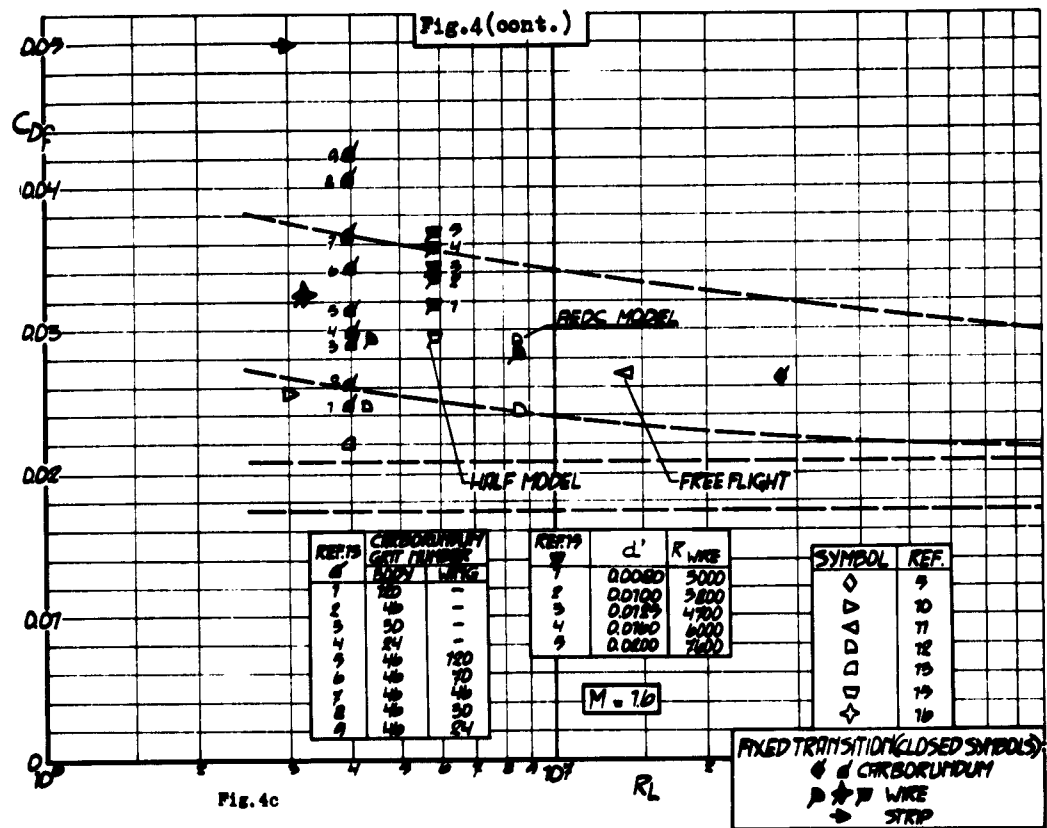


Fig.4 The forebody drag coefficient C_{Df} versus R_L ($\alpha = 0$) (continued)

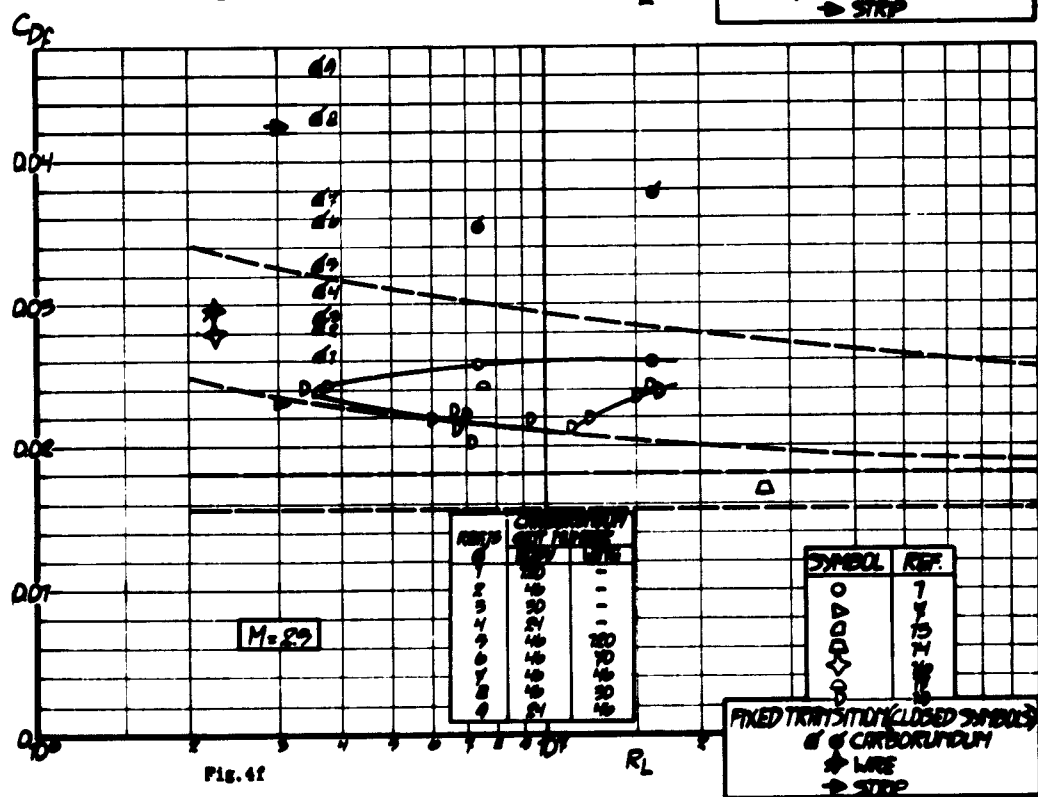
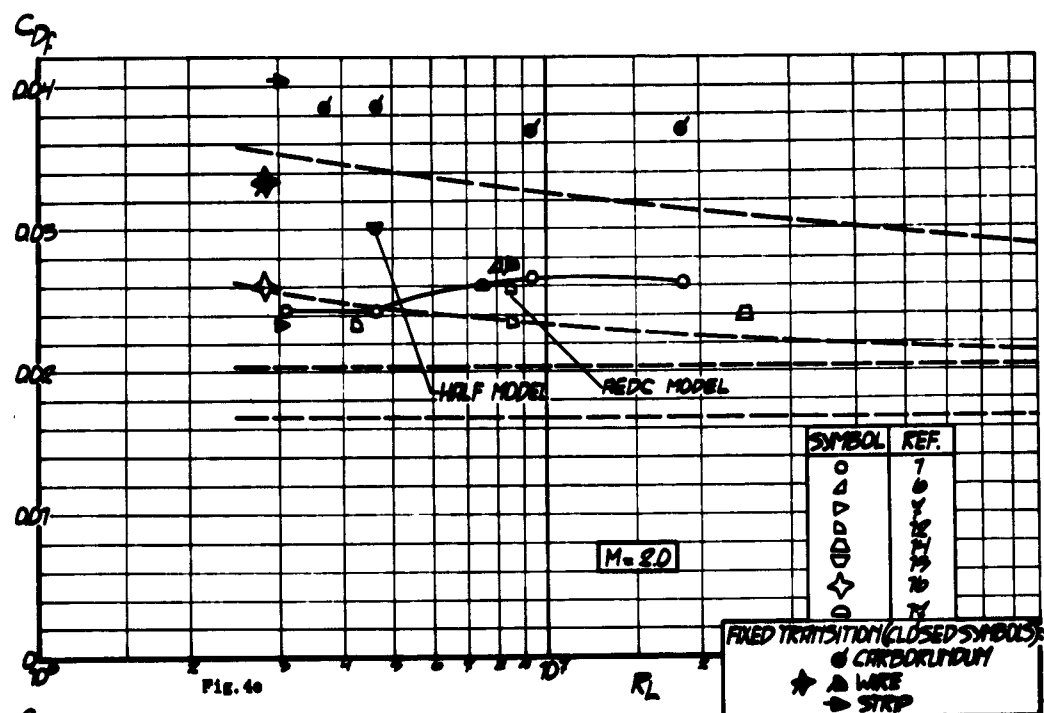


Fig. 4 The forebody drag coefficient C_{Df} versus R_L ($\alpha = 0$) (continued)

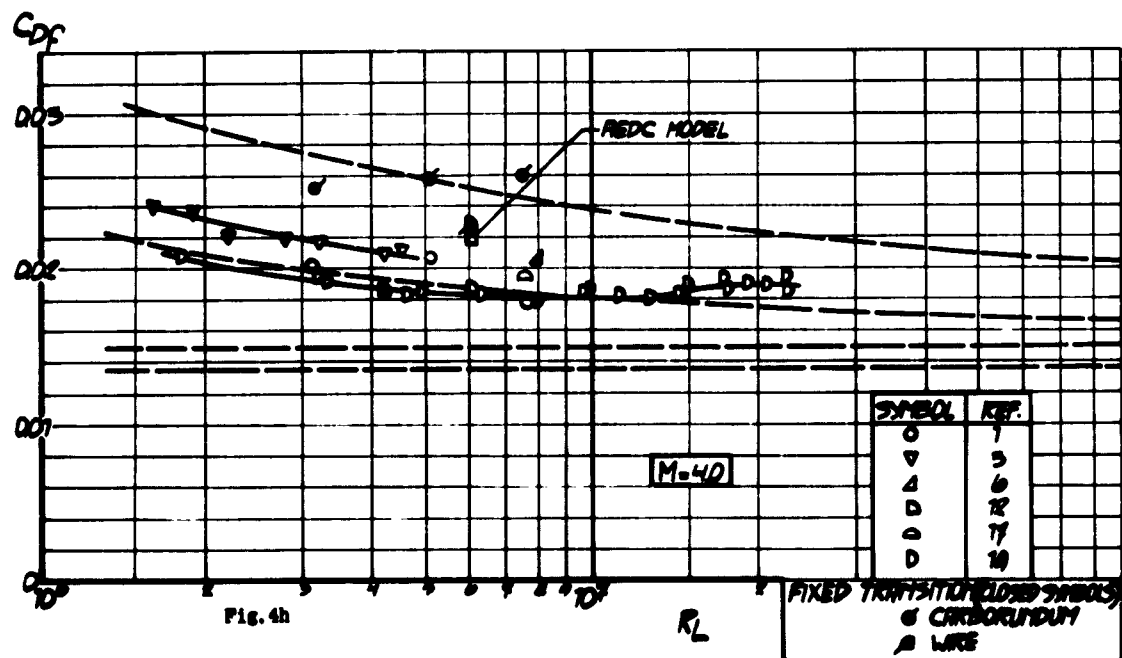
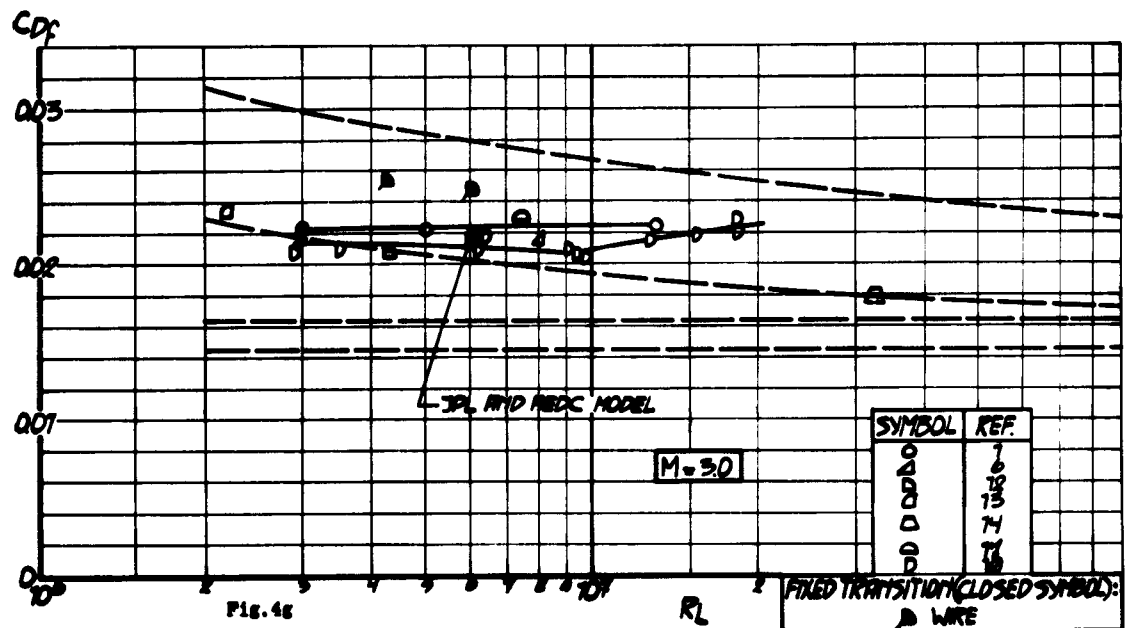


Fig. 4 The forebody drag coefficient C_{Df} versus R_L ($\alpha = 0$) (continued)

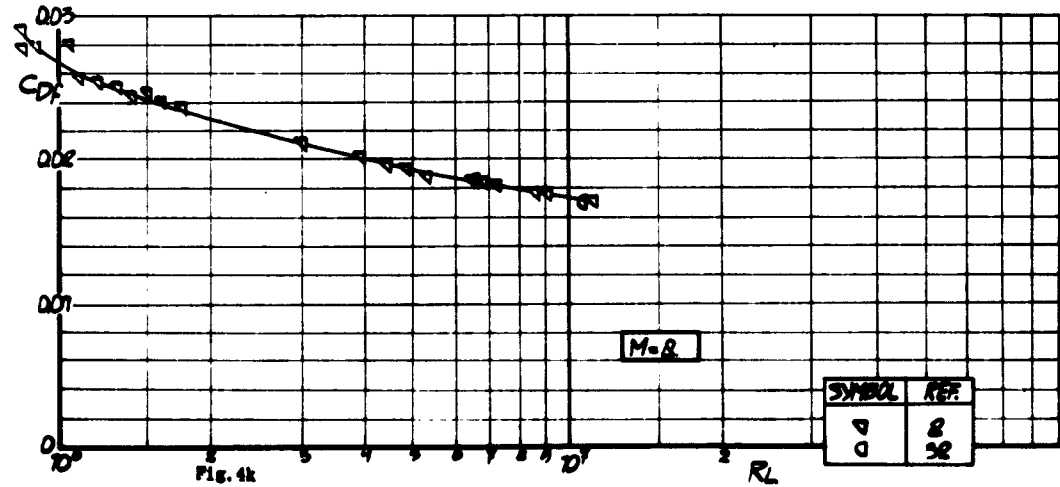
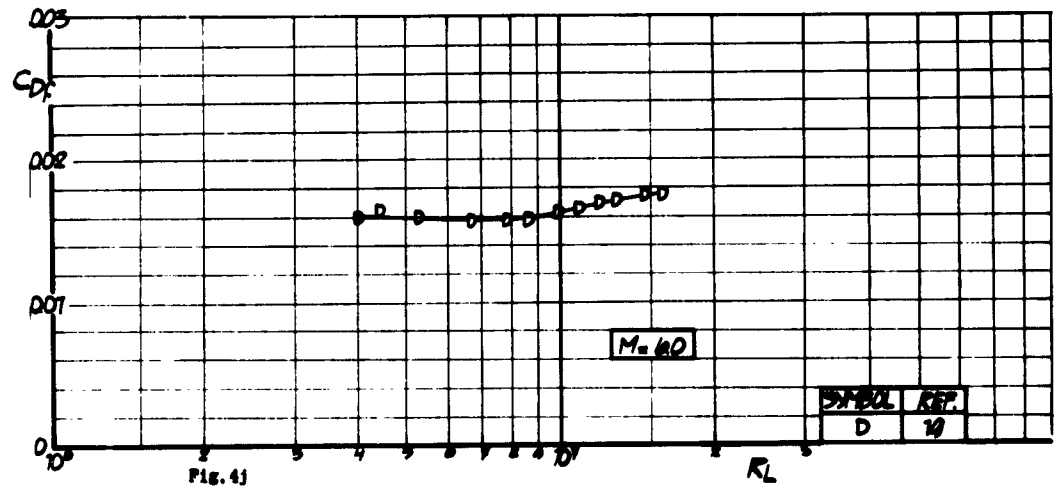
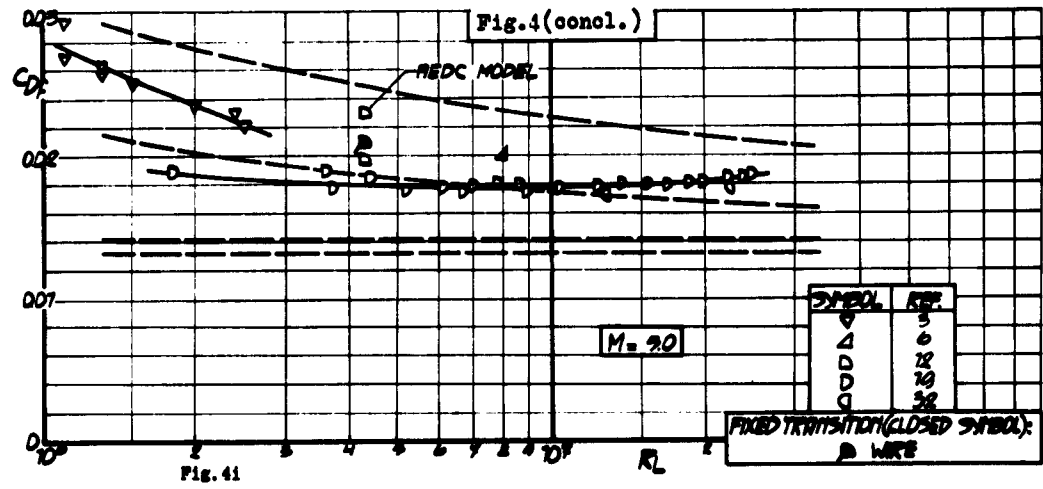


Fig. 4 The forebody drag coefficient C_{Df} versus R_L ($\alpha = 0$) (continued)

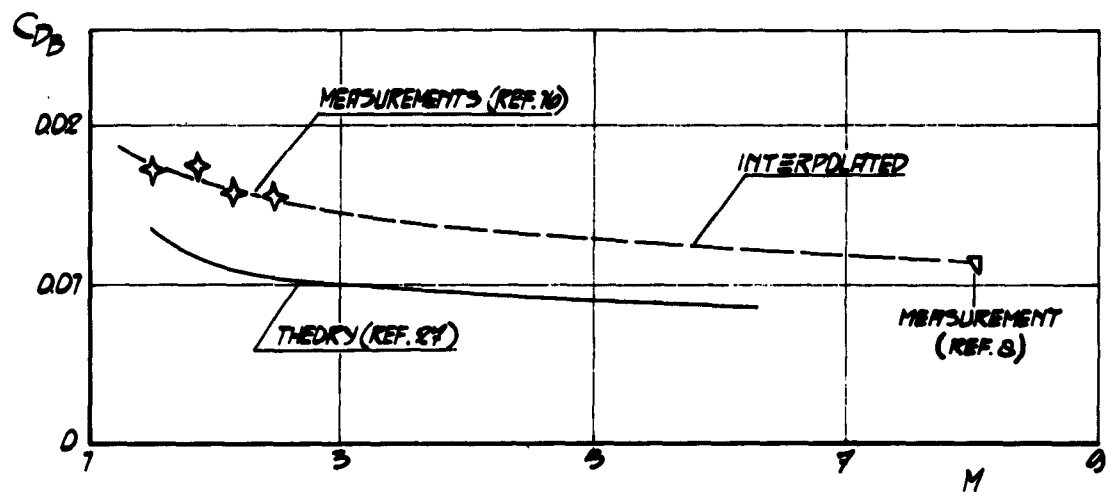


Fig. 5 The pressure drag of the body alone, as a function of M

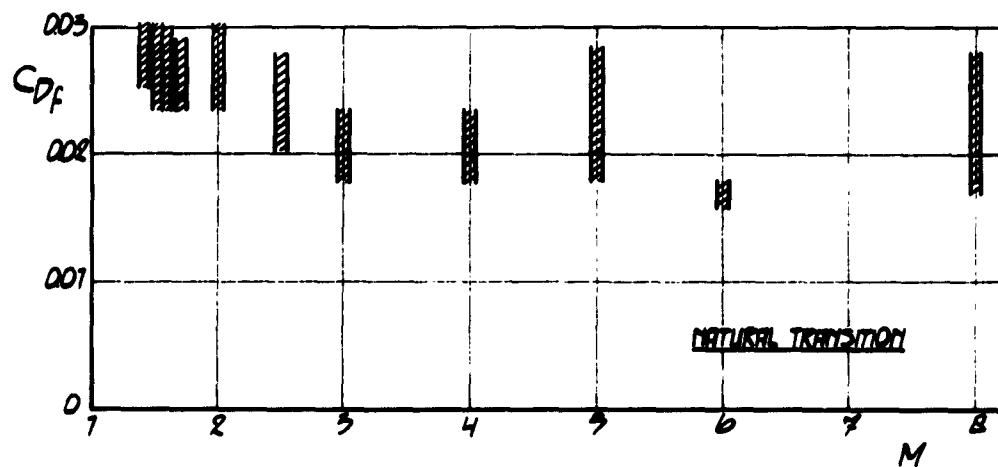


Fig. 6 The forebody drag coefficient versus M

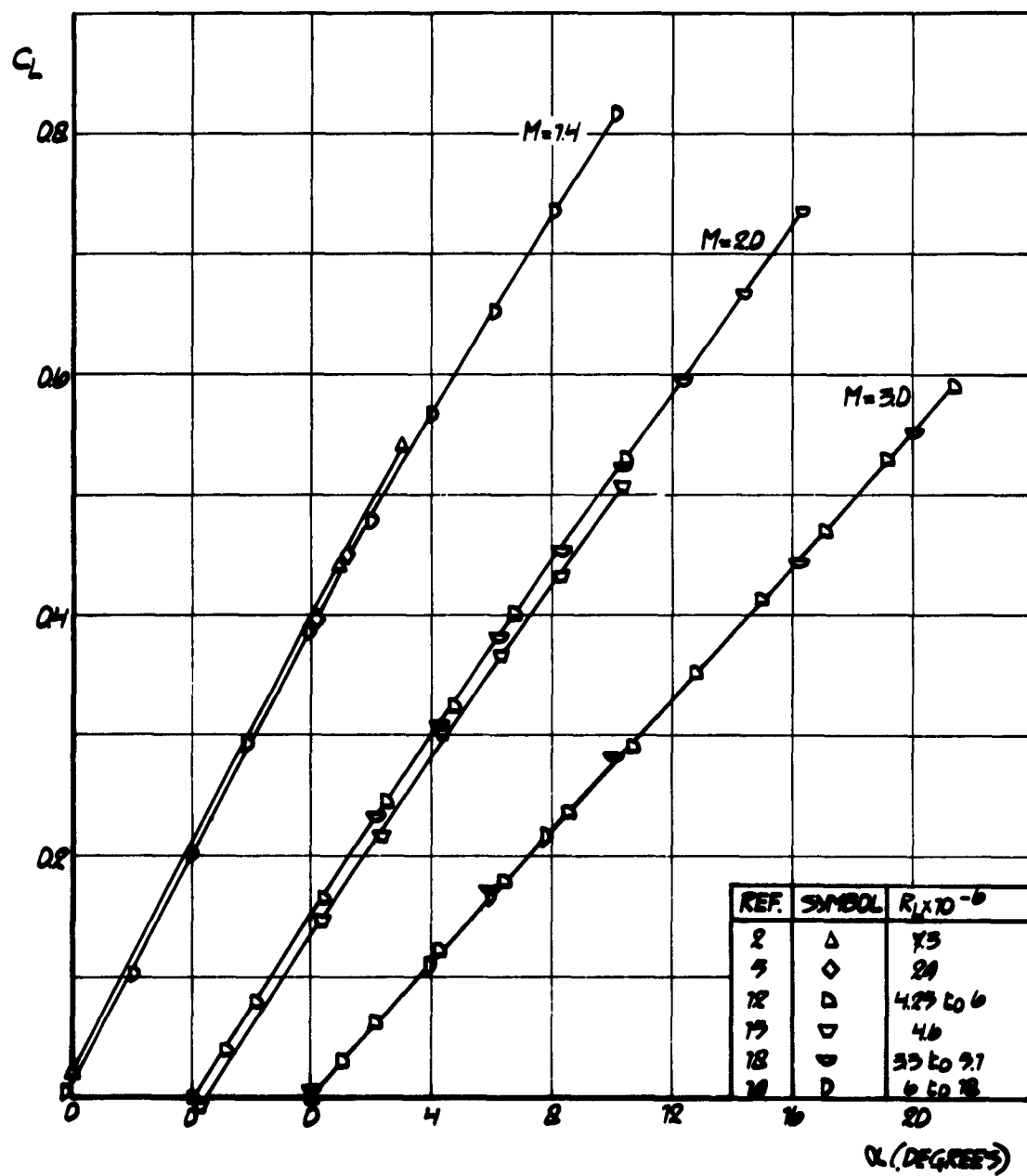
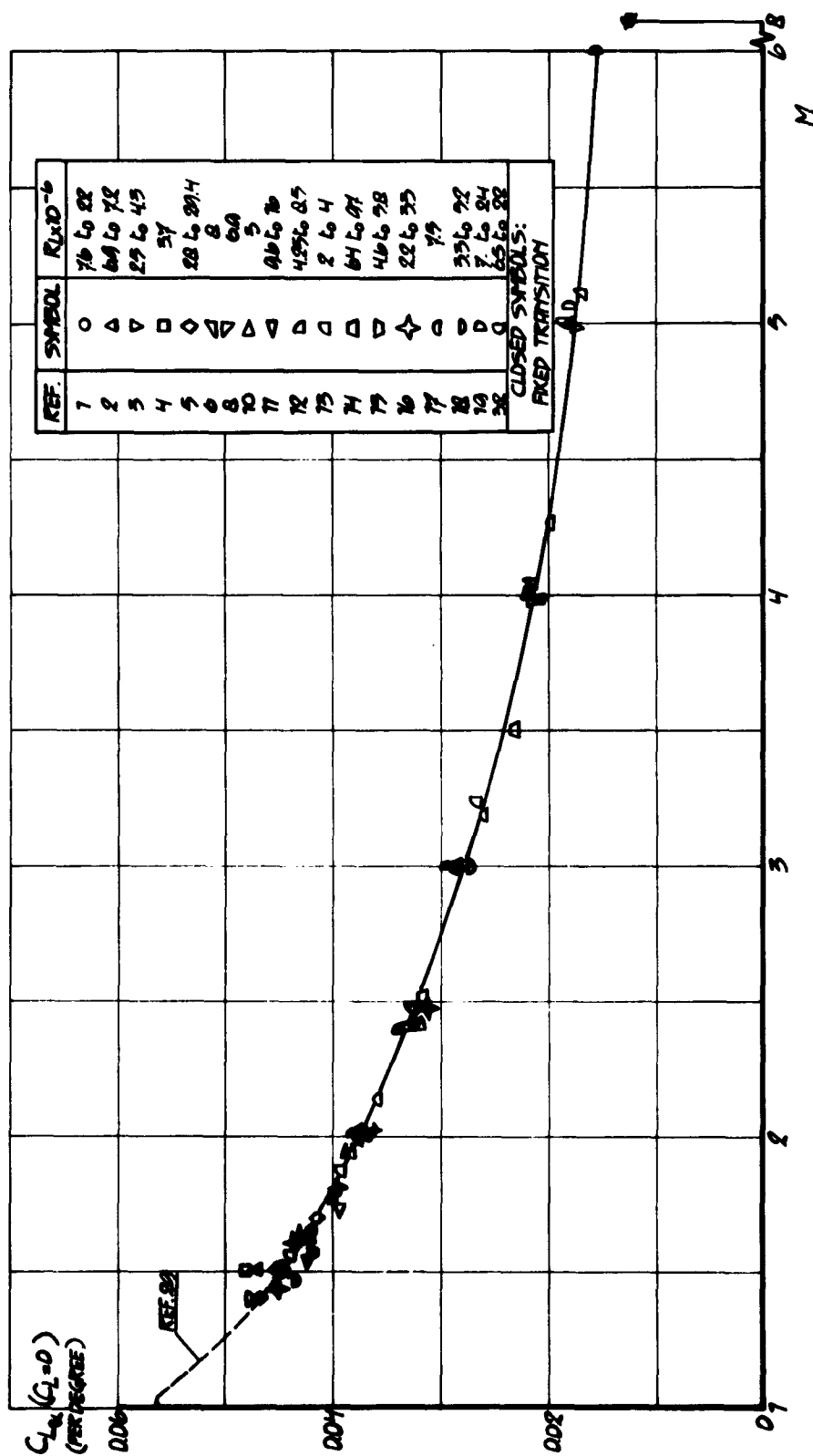


Fig. 7 C_L versus α , up to high angles of attack

Fig. 8 Slope of lift curve $C_{L\alpha}$ versus M at $C_L = 0$

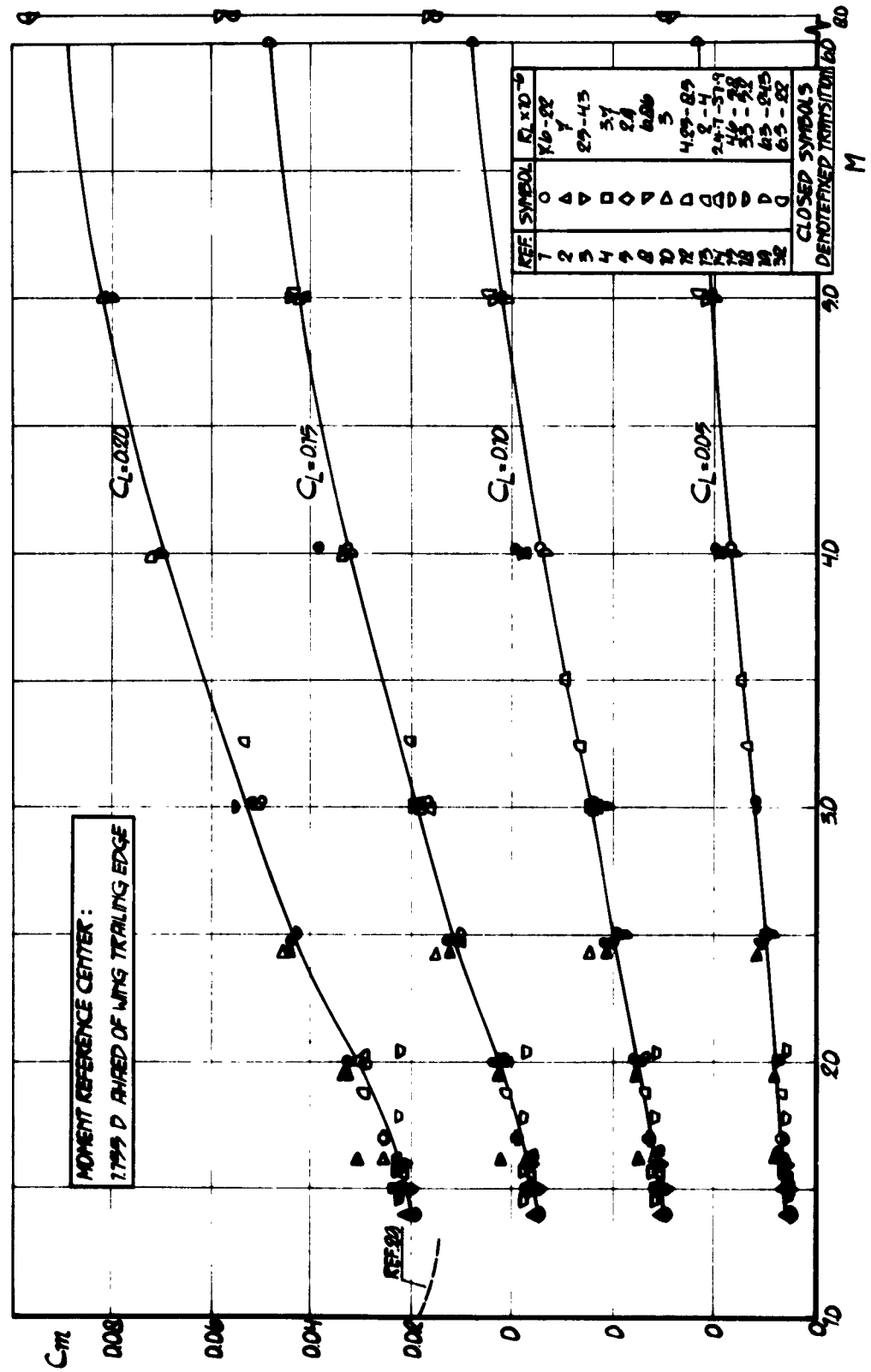
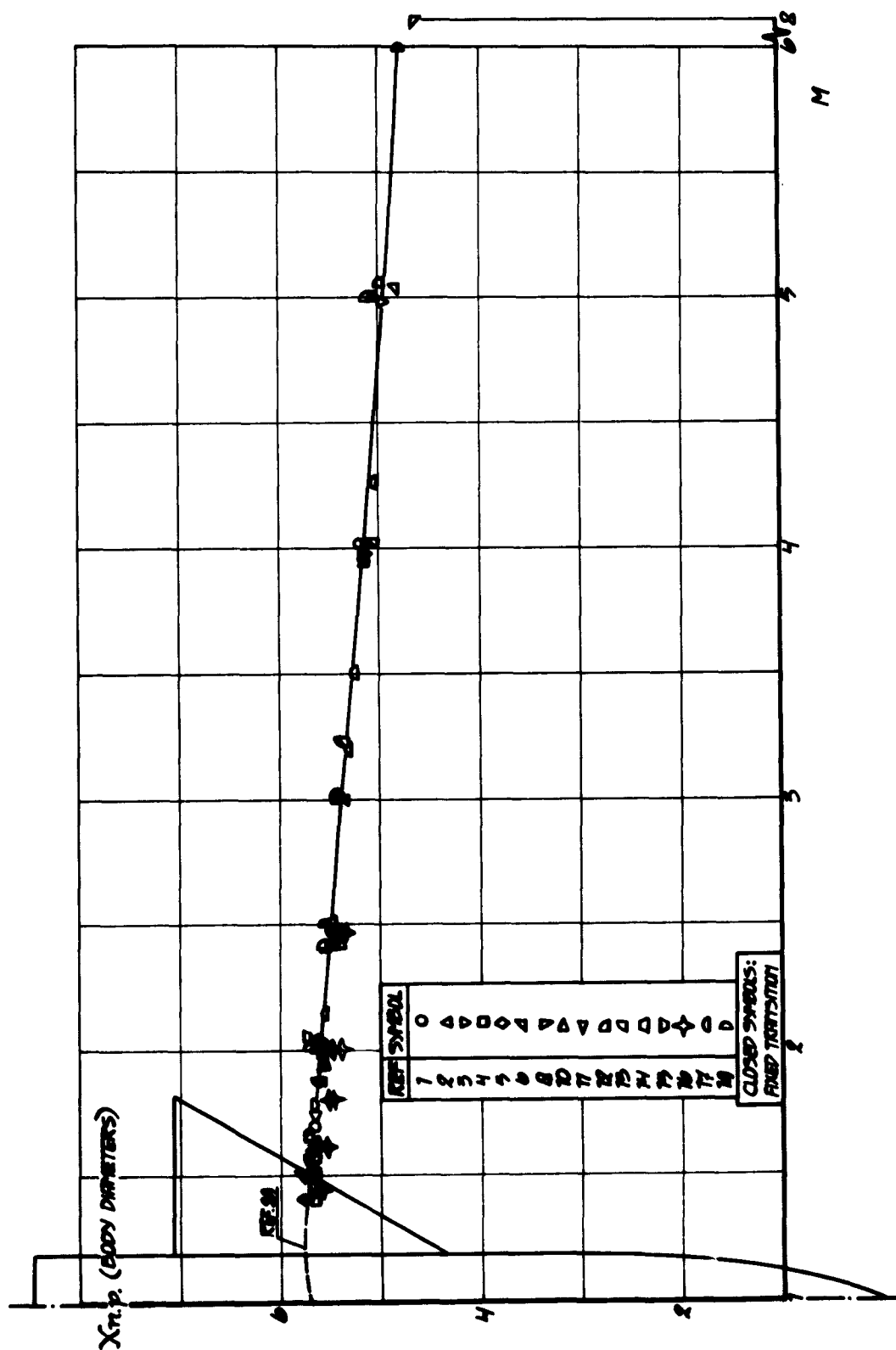


Fig. 9 The moment coefficient versus M , for constant C_L

Fig.10 Neutral point location at $C_L = 0$ versus M

PART IV

**A REVIEW OF MEASUREMENTS ON AGARD CALIBRATION MODEL C
IN THE TRANSONIC SPEED RANGE**

by

H. Valk

Nationaal Lucht- en Ruimtevaartlaboratorium, Amsterdam

SUMMARY

This report contains a survey and a comparison of the results from tests with AGARD Calibration Model C at Mach numbers between 0.7 and 1.3. The available data include tests in different wind tunnels, at different Reynolds numbers and blockage percentages, on models with and without fixed transition of the boundary layer.

The correspondence between the results of the various tests is not very satisfactory. There are many differences and the pitching moment, especially, shows large discrepancies in value and in trend. Some indications are given of the probable origins of the discrepancies. More tests seem to be desirable to achieve better agreement.

CONTENTS

	Page
SUMMARY	138
LIST OF TABLES	140
LIST OF FIGURES	140
NOTATION	142
1. INTRODUCTION	145
2. APPARATUS	145
2.1 Test Facilities	145
2.2 Models	145
2.3 Model Supports	145
3. RESULTS AND DISCUSSION	146
3.1 General	146
3.2 Base Drag	147
3.3 Forebody Drag	149
3.4 Pitching Moment	150
3.4.1 General	150
3.4.2 Influence of Base Pressure (Excluding Effects Due to Shock Wave Interaction)	152
3.4.3 Influence of Downwash Distribution	153
3.4.4 Influence of Shock Wave Interactions	154
3.4.5 Concluding Remarks	155
3.5 Neutral Point	156
3.6 Lift	157
3.7 Lift-Curve Slope	158
4. CONCLUSIONS	158
REFERENCES	160
TABLES	163
FIGURES	167

LIST OF TABLES

		Page
Table I	General Data on Models and Facilities	163
Table II	Boundary Layer Trips	165
Table III	Deviations of Model Configurations	165
Table IV	Accuracy and Repeatability of the Measurements, as Stated in the References	166

LIST OF FIGURES

Fig. 1	AGARD Calibration Model C	167
Fig. 2	Reynolds number (based on mean aerodynamic chord) versus Mach number	168
Fig. 3a-b	Base drag coefficient versus Mach number	169
Fig. 4a-b	Forebody drag coefficient versus Mach number	170
Fig. 5a	Moment coefficient versus Mach number. Tests A1-J2 ($C_L = 0, 0.2$ and 0.4)	171 - 172
Fig. 5b	Moment coefficient versus Mach number. Tests K1-K15	173
Fig. 6a	Neutral point at $C_L = 0$ versus Mach number. Tests A1-J2	174
Fig. 6b	Neutral point at $C_L = 0$ versus Mach number. Tests K7-K15	175
Fig. 7a	Lift coefficient versus Mach number. Tests A1-J2	176
Fig. 7b	Lift coefficient versus Mach number. Tests K1-K15	177
Fig. 8a	Lift curve slope at $C_L = 0$ versus Mach number. Tests A1-J2	178
Fig. 8b	Lift curve slope at $C_L = 0$ versus Mach number. Tests K1-K15	179
Fig. 9a-b	Base drag coefficient versus Mach number at different Reynolds numbers	180

		Page
Fig. 10	Base drag coefficient versus Mach number for different sting configurations	181
Fig. 11	Base drag coefficient versus Mach number for different model sizes	181
Fig. 12	Base drag results of 'interference free' models	181
Fig. 13a-d	Presentation of base drag data	182
Fig. 14a	Skin friction drag at $M = 0.8$ as a function of Reynolds number, based on c_{av} . Tests A1-J2	183
Fig. 14b	Skin friction drag at $M = 0.8$ as a function of Reynolds number, based on c_{av} . Tests K1-K15	184
Fig. 15a-b	Transonic drag rise versus Mach number	185
Fig. 16a-k	Presentation of transonic drag rise data	186 - 188
Fig. 17	Moment coefficient versus Mach number for two different sting configurations	189
Fig. 18	Moment coefficient versus Mach number for different model sizes (transition fixed)	190
Fig. 19a	Moment coefficient versus Mach number at different Reynolds numbers (transition natural)	191
Fig. 19b	Moment coefficient versus Mach number at different Reynolds numbers (transition fixed)	192
Fig. 20a-f	Presentation of moment data	193 - 198
Fig. 21a-d	Neutral point at $C_L = 0$ versus Mach number at different Reynolds numbers	199
Fig. 22	Comparison of neutral point data of tests B1, D2, D4 and J1 and reference curve for K1-K15	200
Fig. 23a-f	Presentation of neutral point data	201
Fig. 24a-j	Presentation of lift data	202 - 208
Fig. 25a-k	Presentation of lift-curve slope data	209 - 211

NOTATION

A_b	body base area, $= (\pi/4)D^2$
b	wing span, $= 4D$
b'	horizontal tail span, $= 1.63D$
B	test section width
\bar{c}	mean aerodynamic chord, $= 2.309D$
c_{av}	average geometric chord of wing-body-tail combination, $= \frac{\text{wetted area of wing-body-tail combination}}{2(b - D) + \pi D + 2b' + 2h} = 1.25 \bar{c}$
C_{Db}	base drag coefficient, $= - (A_b/S)C_{pb}$
C_{Df}	forebody drag coefficient, $= \frac{\text{forebody drag}}{qS} = C_{Dt} - C_{Db}$
ΔC_{Df}	transonic drag rise coefficient, $= C_{Df} - (C_{Df})_{M=0.8}$
C_{Dt}	total drag coefficient, $= \frac{\text{total drag}}{qS}$
C_f	skin friction drag coefficient, $= \frac{\text{skin-friction drag}}{q \times \text{half wetted area}}$
C_L	lift coefficient, $= \text{lift}/(qS)$
$C_{L\alpha}$	lift curve slope, $= dC_L/d\alpha$ (per degree)
C_m	pitching moment coefficient about 50% of mean aerodynamic chord (mrc), $= \text{moment}/(qS\bar{c})$
C_{pb}	base pressure coefficient relative to free stream static pressure, $= (p_b - p)/q$
d	sting diameter
D	body diameter
h	height of vertical tail, $= 0.92D$
H	test section height
l	length of cylindrical portion of sting

l_H	distance between the points at 50% of the mean aerodynamic chords of wing and horizontal tail, = $2.204 \bar{c}$
L	length of model, = $11.494 D$
M	Mach number
mrc	moment reference centre, 50% of mean aerodynamic chord of wing
p	free stream static pressure
p_b	base pressure
q	free stream dynamic pressure, = $\frac{1}{2} \rho V^2$
r	local body radius
Re	Reynolds number based on \bar{c}
Re'	Reynolds number based on c_{av}
S	total wing area, = $6.928 D^2$
V	free stream velocity
x	distance along body axis
X_{mrc}	distance of moment reference centre aft of model nose in body diameters, = 5.943
X_{np}	distance of neutral point at $C_L = 0$ aft of model nose in body diameters, = $X_{mrc} - (\bar{c}/D)(dC_m/dC_L)_{C_L=0}$
α	angle of attack
θ	cone angle of sting
ρ	free stream density

A REVIEW OF MEASUREMENTS ON AGARD CALIBRATION MODEL C IN THE TRANSONIC SPEED RANGE

1. INTRODUCTION

AGARD Calibration Model C has been designed primarily for testing and calibration in the transonic speed range. It is identical to AGARD Calibration Model B, except that the body is extended aft over 1.5 body diameters and vertical and horizontal tail surfaces have been added. The addition of a horizontal tail may make it easier to detect reflected shock waves from anomalies in the pitching moment curves.

This report contains a comparison of the results of tests at Mach numbers between 0.7 and 1.3. The available data were taken from References 1-8. The data were obtained from tests in several wind tunnels, as shown in Table I.

2. APPARATUS

2.1 Test Facilities

The most significant details of the test sections, such as size, wall shape and open percentage, are shown in Table I. Further details of the test facilities are given in References 1-9 and will not be repeated here.

2.2 Models

The AGARD Calibration Model C is shown in Figure 1 (see also Ref.10). The model sizes for the various tests in relation to the test section sizes are given in Table I.

In some tests the transition of the boundary layer was fixed by wires or carborundum strips at 1.5 body diameters aft of the model nose and on both sides of the wing, the horizontal tail and the vertical tail at 15% of the local chord. A survey of the transition methods used is given in Table II.

The model configuration for some tests deviated from the prescribed form given in Reference 10. The deviations are listed in Table III.

2.3 Model Supports

The ultimate specification of the sting dimensions, given in Reference 10, was published after the completion of many tests, and a number of different sting configurations was used. The sting dimensions for the various tests are given in Table I.

3. RESULTS AND DISCUSSION

3.1 General

In this report the analysis of the data is confined to a Mach number range of 0.7 to 1.3. This range covers the greater part of the available measurements*. The Reynolds numbers of the various tests are shown in Figure 2 and in Table I.

Base drag, forebody drag, pitching moment, neutral point, lift and lift-curve slope are compared. The coefficients have been plotted against Mach number.

The available data are gathered in Figures 3-8. Since the number of tests performed in the transonic wind tunnel of the N.L.R. (Ref.8) clearly exceeds the number of tests performed in the other wind tunnels, for each component the results of Reference 8 and the other references are presented in two separate figures, in order to obtain a better overall picture. With the exception of Figure 4, reference curves in both figures facilitate comparison†.

Obviously, there is considerable scatter in the results.

The factors which, in general, affect the data come under the following headings:

- (i) instrument errors,
- (ii) model imperfections,
- (iii) general imperfections of the tunnel flow (tunnel wall interference and sting interference excepted),
- (iv) tunnel-wall interference,
- (v) sting interference,
- (vi) Reynolds number and methods of fixing boundary layer transition.

Very little is known about the first three factors. The available information about accuracy and repeatability of the measurements is shown in Table IV. Model imperfections are not known, with the exception of the deviations given in Table III. Unless stated otherwise, in this report an attempt will be made to explain the differences caused by the last three factors.

The procedure followed in Reference 11 (the analysis report on AGARD Model B in the transonic speed range) was to try to take into account the foregoing factors in the form of suitable parameters and thus to select corresponding results. Where this procedure succeeded, so-called 'reference curves' were established and the other data

* Only a few tests were performed at higher Mach numbers (in Reference 1 up to 1.4; in Reference 3 up to 1.6).

† The choice of the reference curves will be explained in the following sections.

were compared with these curves. For AGARD Model C, however, this procedure failed, because of the poor agreement between the various test results for this model.

Since Models B and C were tested in several wind tunnels under the same conditions, some of the results for both models could be compared. In view of the correspondence between the two models it may be expected that the lift and drag forces will be of the same order. The moment for AGARD Model C is strongly influenced by the flow conditions around the horizontal tail and will therefore differ significantly from the moment obtained for AGARD Model B.

Since the results of Reference 8 (tests K1-K15) all come from one wind tunnel (NLR transonic wind tunnel HST) it was possible to explain some of the effects in these results. More information can be expected from this source when N.L.R. have completed a more extensive analysis, which is still in hand.

In view of these circumstances this report should, in the first place, be considered as a collection of the available results. The discussions should be regarded as tentative only, with the object of detecting the more obvious effects. Much remains unexplained that nevertheless deserves explanation.

3.2 Base Drag

In Figure 3 a survey is given of all the available base drag data for $C_L = 0$. In general the important parameters for the base drag are:

Reynolds number and methods, if any, of fixing boundary layer transition,
sting configuration*,
imperfections, if any, in the tunnel flow downstream of the base
shock waves and shock wave reflections.

The effect of Reynolds number may be large if the transition occurs in the mixing region or just upstream of it. For the tests under consideration it may be expected that transition already occurs on the body. Furthermore, the base drag is generally slightly influenced by the thickness of the boundary layer. A small Reynolds number influence is shown in Figure 9a, where the results of tests on the same model, but at different Reynolds numbers, are compared (tests K1, K2, K3 and K4). With transition fixed no marked differences are apparent (Fig. 9b, tests K5, K6, K7 and K8).

The effect of the length of the cylindrical portion of the sting is demonstrated in Figure 10, where the corresponding tests K7 and K15 for the same model, but with different sting configurations, are compared. The effect of a shorter cylindrical portion of the sting (1.5 instead of 3D), shown in this figure, does not seem large. The influence of the sting configuration disappears at supersonic Mach numbers.

* The sting is defined here as that part of the model support which is specified in the AGARD specification¹⁰.

In some tests the sting did not have the specified diameter, but it did not seem possible to draw positive conclusions about the effect of sting diameter.

Test section calibration tests¹² at A.E.D.C. have shown that flow irregularities in the aft part of the test section, in particular due to the model support, may affect the base pressure, even if the base is located at a position where the flow in the empty test section (no model support system installed) is undisturbed. In this case disturbances are propagated upstream through the (subsonic) wake. It is obvious that the position of the base in the test section in such cases may be an important parameter.

Care should be given to a possible correlation between model size and position of the base in the test section. Such a correlation may lead to an (indirect) influence of model size on base pressure. This seems to be the main explanation of the differences in Figure 11 (tests K7, K12, K13 and K14), with the exception, however, of the Mach number range between 1.0 and 1.1. For these tests the boundary layer transition was fixed and - except for test K14 - the same sting configuration was used. In the subsonic and in the supersonic region above $M = 1.1$ the more downstream position of the base (larger model) resulted in a lower base drag (higher base pressure). The largest model (test K14) was placed in an unusually rearward position. This explanation has been confirmed in a recent test at N.L.R. (results unpublished), where test K7 was repeated with a more upstream position of the model, in such a way that the model base coincided with the position of the model base in test K12. The base drag results of this test and test K12 show better agreement (outside the region $1.0 < M < 1.1$).

The last factor which remains to be discussed is the interaction between shock waves and reflected shock waves and the mixing region. This type of influence is held responsible for the irregularities in the curves for the K-tests of Figure 11 in the Mach number range between 1.0 and 1.1, though a detailed explanation of the phenomena is lacking. In general, shock waves may falsify the results in three ways:

shocks belonging to the model (e.g. bow wave, leading-edge shock) may reflect at the tunnel walls and hit the rear of the body,

the position of shocks belonging to the model (e.g. tail shock system, body shock) may be influenced by the vicinity of the tunnel walls,

the bow wave of the model support may interfere with the model base.

Clarification of these effects demands schlieren photographs and measurements with very small intervals between the successive Mach numbers.

In view of this discussion, it may be expected that, of the NLR results, the results obtained with the smallest model are the most reliable. The results of the tests K9 and K12 (blockage ratio 0.016%) are therefore used for the reference curve in Figure 3, which is represented by the dotted line. It is interesting to see in Figure 12 the agreement between the base drag results of test A2 (blockage ratio 0.01%) and the tests K9 and K12.

In Figure 13 the available results of the tests, with the exception of the NLR results already presented, are given. No further comment about these results is available at present.

3.3 Forebody Drag

The forebody drag is obtained by subtracting the drag due to the base from the total drag. In this report the forebody drag is observed only at $C_L = 0$; the results are presented in Figure 4.

Because the aft end of the body is entirely cylindrical, and because the drag arising from interference between the base and the tail surfaces can be considered negligible, the forebody drag may be expected, to a large extent, to be independent of the phenomena downstream of the model.

The forebody drag consists of pressure drag and friction drag. As in Reference 11, it is assumed that at a Mach number of 0.8 the forebody drag is almost completely caused by friction forces. The friction drag coefficient is dependent on the Reynolds number and is only slightly influenced by the Mach number in this Mach number range. To separate, to a certain extent, the Reynolds number effect from other effects, the drag at $M = 0.8$ was subtracted from the forebody drag. The remaining drag was termed the transonic drag rise.

To obtain some idea of the value of the friction drag, a comparison was made between the friction drag and the drag of a flat plate at a Mach number of 0.8. For this purpose the friction coefficient C_f has been converted to a flat-plate value by using half of the total wetted area of the model as a reference surface instead of the wing area. The problem arose as to what reference length to use for the Reynolds number in order to compare the wing-tail-body combination with a simple rectangular flat plate. An average geometric chord for the complete wing-tail-body combination c_{av} was chosen. The choice of about $1.25 \bar{c}$ is somewhat arbitrary, but is acceptable as a basis for comparison.

In Figure 14 the skin friction values are plotted against Reynolds number. Since the influence of compressibility on the skin friction is small at subsonic Mach numbers, no correction is made for this effect. A tendency of Reynolds number influence on the results obtained with natural transition is not clearly detectable. The 'transition fixed' results are lower than, and run nearly parallel to, the turbulent value of the flat plate friction drag. The somewhat high value for test K12 is due to a relatively thick wire. The relatively low value for test K5 is due to the transition wires being not fully effective at the low Reynolds number at which the model was tested.

The transonic drag rise results are presented together in Figure 15 and more individually in Figure 16.

The reference curve for the K-tests (dotted line) in Figure 15 represents the results of the tests with a small model, which is assumed to be interference free, (blockage ratio 0.016%), namely test K9 (natural transition) and K12 (fixed transition).

The results of the tests K10 and K13 (Figs. 16i and 16j) - the 'transition natural' and 'transition fixed' results for a model also having a relatively small blockage ratio (0.05%) - agree fairly well with this reference curve.

The transonic drag rise results of the tests K1-K4 (natural transition) in Figure 16g and K5-K8 (fixed transition) in Figure 16h - all tests performed with the same model (blockage ratio 0.16%) but at different Reynolds numbers - show good agreement. Reynolds number and artificial transition have no marked influence on the behaviour of the transonic drag rise. The transonic drag rise of this model is somewhat higher than the transonic drag rise of the reference curve. No explanation for this phenomenon can be offered.

Test K11 (natural transition, blockage ratio 0.32%) in Figure 16i shows good agreement with the tests K1-K8; however, the 'transition fixed' results for the same model (test K14) in Figure 16j show a lower transonic drag rise, but the cause of this is not known.

The sting configuration was expected to have no marked effect, which is confirmed by the comparison of the tests K7 and K15 in Figure 16k.

At several establishments the AGARD Models B and C were tested under the same conditions, which makes it interesting to see how the data for both models correspond.

In Figure 16a, test A2 (blockage ratio 0.01%) shows a smaller transonic drag rise than the corresponding test on AGARD Model B. The transonic drag rise for this relatively small model agrees fairly well with the reference curve of the K-tests.

The transonic drag rise curves for the tests A1 and A3 in Figure 16a (blockage ratio 2.5% and 1.15%), B1 in Figure 16b (blockage ratio 0.17%) and to a smaller extent E1 in Figure 16e (blockage ratio 1.12%) are similar to the curves for the corresponding tests on AGARD Model B up to a Mach number of about 1.05. The maximum in the transonic drag rise for these tests is somewhat higher than was obtained for AGARD Model B. This type of agreement does not exist for the tests D1 and D2 in Figure 16c (blockage ratio 0.5%) and D3 and D4 in Figure 16d (blockage ratio 0.7%). The results of test A3 are in good agreement with the results of the tests K1-K8.

For Model B it was found that a higher blockage ratio tends to give a flatter transonic drag rise. For the Model C it does not yet seem possible to draw any conclusions about the effect of blockage ratio, nor about other effects on the transonic drag rise.

3.4 Pitching Moment

3.4.1 General

For all tests the moment coefficient was plotted against Mach number for three values of C_L (0, 0.2 and 0.4). At higher lift insufficient data are available.

Figure 5 shows the available moment data. There is a considerable scatter, appreciably greater than the scatter in the moment results for AGARD Model B. Obviously a substantial part of the scatter is due to the horizontal tail.

The study of the pitching moment proved to be the most difficult part of the task in analysing the Model C results. It was felt that this was, in particular, due to the fact that the principal factors mentioned in Section 3.1 do not have a direct influence on the pitching moment, but work through the intermediary of certain other factors. Of those other factors the base pressure and the downwash appear to be important. With these factors, the effects of Reynolds number, fixation of transition, sting configuration, flow irregularities and model imperfections are interrelated. Only the effect of shock wave interaction has been considered directly. Therefore this section has been subdivided as follows:

Effect of base pressure (excluding effects due to shock wave interaction).

Effect of downwash distribution of the wing.

Effect of shock wave interaction.

Concluding remarks.

The relation between this new classification and the more fundamental one of Section 3.1 is provided by the following scheme. This scheme (though, with the data available, it could not be confirmed in every respect) serves as a basis for the discussion of the pitching-moment data.

- (i) Imperfection of tunnel flow in the aft part of the test section (as mentioned in Section 3.2).
Influence through: base pressure.
- (ii) Sting interference.
Influence through: base pressure.
- (iii) Reynolds number or methods of fixing boundary layer transition.
Influence through:
base pressure
downwash distribution
pressure distribution on wing and horizontal tail.
- (iv) Tunnel wall interference, in particular shock wave interaction.
- (v) Model imperfections, in particular wing nose radius.
Influence through: downwash distribution.

Tunnel wall interference, apart from shock wave interaction, could not be traced. A rough estimate showed that lift interference on the moment must be extremely small, because of the relatively small wing area, and blockage effects on the moment are not to be expected.

As far as the Reynolds number effect on the moment, through the pressure distribution of wing and horizontal tail, is concerned, it is very likely that there is an effect, also in view of the AGARD Model B results¹¹. However, it did not seem possible to separate this effect from other Reynolds number effects, so this point is not considered in the following discussions.

3.4.2 Influence of Base Pressure (Excluding Effects Due to Shock Wave Interaction)

Figure 5 shows that the moment for $C_L = 0$ is not zero, but has a definite value. This is because the horizontal tail is located in the expansion region of the base*. The effect of the expansion is a relative decrease of the pressure at the lower side of the horizontal tail, which results in a positive moment. A low base pressure is associated with a strong expansion and causes a high positive moment and a high base drag. Consequently there is a relationship between the results for the moment and for the base drag. A significant example of this effect will be found in the comparison between Figure 18 (C_m at $C_L = 0$) and Figure 11 (C_{Db}) with regard to tests K7, K12, K13 and K14. To be excluded from this comparison is the Mach number region between 1.0 and 1.1 (for the largest model (test K14) also $M = 1.15$), because in this region shock wave interactions may overshadow the base pressure effect, as pointed out in more detail in Section 3.4.4. For the other data points the correspondance between C_m at $C_L = 0$ and C_{Db} is marked. A rough estimate of the relation to be expected between differences in moment and base drag confirms that the experimental differences are of about the right order of magnitude.

The other available comparisons between C_m at $C_L = 0$ and C_{Db} are given in the table below.

Test	C_m at $C_L = 0$	C_{Db}	Other Factors	Comment
A1, 2, 3	Fig. 20a	Fig. 13a	Reynolds number, fixing of transition	less convincing
K1, 2, 3, 4	Fig. 19a	Fig. 9a	natural transition	some agreement (not for K4)
K5, 6, 7, 8	Fig. 19b	Fig. 9b	-	not conclusive (differences negligible)
K7, 15	Fig. 17	Fig. 10	effect of sting bow wave (see below)	agreement for $M < 1.0$
K9, 10, 11	Fig. 20f	Fig. 13d	natural transition	reasonable agreement

It may be concluded that the assumed relationship between C_m and C_{Db} exists. Therefore the conclusions of Section 3.2 about base drag are relevant here.

* The contribution of the drag of the tail surfaces to the moment may be neglected.

*Sting configuration**

An example of sting interference is given in Figure 17. For the tests K7 and K15 the same model with trip wires was used, but for test K15 the model was supported by a sting with a shorter cylindrical portion (1.5 instead of 3 body diameters). The moment for test K15 is lower than for K7. The base drag results for both models (Fig.10) show a similar difference at subsonic Mach numbers, but at supersonic Mach numbers there was no difference. At these Mach numbers, shock wave interference between the horizontal tail and the mixing region has been established by schlieren pictures (unpublished). Possibly the sting configuration affects this interference and thus causes a difference in moment.

Flow irregularities in the aft part of the test sections

In Section 3.2 it was mentioned that flow irregularities in the aft part of the test section, in particular due to the model support, affect the base pressure even if the base is located in the 'undisturbed' flow region. The position of the base is then an important parameter.

This effect is illustrated in the tests K7, K12, K13 and K14 (Fig.18), as already discussed in Section 3.2 and at the beginning of this section. It is interesting to note that the repetition of K7 (already mentioned in Section 3.2) with a more upstream position of the model gave results (unpublished) which correspond very satisfactorily with the results of test K12.

Reynolds number and fixing of transition

To establish the Reynolds number effect, the same model was tested at different stagnation pressures in the transonic wind tunnel of the N.L.R. (Fig.19a: tests K1, K2, K3 and K4). These tests were repeated with fixed transition of the boundary layer (Fig.19b: tests K5, K6, K7 and K8). It appears from the figures that the data obtained with natural transition show marked differences, while the data obtained with fixed transition agree much better. In the supersonic region the differences in the results of both series of tests are of the same order.

The effect of the Reynolds number on the moment was partly due to the base pressure. The differences in the subsonic region of the base drag for the tests K1, K2 and K3 in Figure 9a are in proportion to the differences of the moment for these tests at $C_L = 0$ in Figure 19a†. The rather low value of the moment in test K5 in Figure 19b is possibly due to the fact that the transition wire was not fully effective at the low Reynolds number at which the test was performed.

3.4.3 Influence of Downwash Distribution

The moment at higher lift coefficients can be subdivided into a contribution from the wing and from the horizontal tail. Subtracting from the measured values the

* The sting is here defined as that part of the model support which is specified in the AGARD specification¹⁰.

† However, test K4 does not agree with this tendency.

contribution of the wing, which can be estimated from Reference 11, and the contribution of the horizontal tail for $C_L = 0$, there remains only the increment of the moment due to the incidence of the horizontal tail. From a simple calculation it appears that there must be an appreciable downwash near the tail, which is only a little smaller than the angle of attack of the model. This phenomenon was confirmed during recent tests (results unpublished) at the N.L.R., where the boundary layer flow was visualized. At low angles of attack, up to about $2-3^\circ$, the streamlines on the upper wing and tail surfaces were in the same direction as the free stream. At an angle of attack of about 4° a change occurred in the flow pattern on the wing. A vortex, caused by leading-edge separation, swept the boundary layer from the inner part of the wing towards the leading edge. At higher angles of attack the vortex moved more inside. The boundary layer flow pattern on the horizontal tail, however, did not change, even at the highest angles of attack in the test (up to 12°). Thus the effective incidence of the horizontal tail did not exceed about $2-3^\circ$. This magnitude of downwash is in agreement with the results of other tests on delta wings, as mentioned in Reference 13.

The downwash is caused mainly by the vortex which leaves the wing at the trailing edge. The lateral distance between the vortex core and the tail is relatively small, especially at high incidences, when the vortex moves more inboard. It is obvious that small variations in the spanwise location of the vortex will produce a considerable change in downwash at the tail and consequently a difference in pitching moment. The importance of the influence of variations in downwash near the tail can be understood from the fact that a difference in effective incidence of $+0.1^\circ$ will produce a difference in moment of about $\Delta C_m = -0.002$.

From Reference 14 it is known that the leading-edge nose radius is an important parameter for the spanwise position of the vortex. An increase of the nose radius is equivalent to a more outboard position of the vortex. Consequently the downwash near the tail decreases, which causes a lower moment.

In Section 3.4.2 a certain agreement was found between the Reynolds number effect on the base drag and on the moment at $C_L = 0$ in Figures 9a and 19a. At angle of attack this agreement is no longer apparent. It is assumed that the effect of Reynolds number at angle of attack also occurs by virtue of the downwash distribution.

3.4.4 Influence of Shock Wave Interactions

Reflected shock waves may have large effects on the pitching moment, if they are acting on or upstream of the horizontal tail. In this case they influence the pressure distribution over the horizontal tail, which leads to an increase or decrease of the moment. On the other hand the position of shock waves belonging to the model (especially the body) may be influenced by the vicinity of the walls. It is very difficult to trace these effects from the moment results, because the effects of the factors mentioned in Sections 3.4.2 and 3.4.3 already result in an irregular moment curve. Moreover, the intervals between the Mach numbers at which the models are tested are not usually sufficiently small.

If the reflection of the bow wave has passed the model, no effects of shock wave reflection need be expected. For each test the Mach number at which the reflected bow wave has passed the model has been roughly determined. The results are given in the table on the next page.

<i>Test</i>	<i>Mach Number</i>	<i>Test</i>	<i>Mach number</i>
A1	3	J1	1.40
A2	1.01	J2	1.02
A3	2	K1-K8, K12	1.15
B1	1.10	K9, K12	1.02
D1, D2	1.35	K10, K13	1.05
D3, D4	1.75	K11, K14	1.30
E1	1.90		

Up to the Mach number quoted, the influence of shock wave reflections may be expected. At very low supersonic Mach numbers the influence can generally be neglected.

At a further stage of the testing of this model it might be as well to study the detailed behaviour of the shock waves around the model, on the one hand by taking measurements at very small intervals of Mach number, and on the other hand by taking schlieren pictures and pressure measurements.

3.4.5 Concluding Remarks

Resuming general discussion of the pitching-moment results, it can be said that the AGARD Model C is very sensitive in so far as the moment is concerned, the influence both of the base pressure and of the downwash of the wing. Consequently the model is very sensitive to those factors that influence the base pressure and the downwash of the wing, which have already been mentioned in Section 3.4.1. In a certain Mach number range - depending on model size - shock wave position and shock wave reflection may have a large influence.

The model, however, is not very sensitive to lift and blockage interference.

With the present model, testing can only be considered to be of value if:

the Reynolds number is sufficiently high or the transition of the boundary layer is fixed,

the same sting configuration is used (in accordance with the specification in Reference 10).

Another conclusion which can be drawn is that, of the tests K1-K15, the test K12 should give the most reliable pitching moment results, this test having been executed on a small model with fixed boundary layer transition. The results of test K12 were therefore used for the establishment of the reference curve in Figure 5.

Figure 20 presents separately the pitching-moment results of all the tests, with the exception of the NLR results already presented in earlier figures. Further explanations cannot be given, but a few general remarks are offered.

Figure 20a gives the curves of tests A1, A2 and A3. The models used for these tests had a tail configuration which deviated as described in Table III. This

elongated the distance between the horizontal tail and the moment reference centre by about 2%. This should correspond with about 2% increase of the C_m -value at $C_L = 0$. Moreover, the position of the tail with respect to the base has been changed. The effect of this on the moment is unknown, but it can be assumed that the rearward shift of the tail brings a larger part of the horizontal tail into the expansion region of the base. In this case there will be a further increase in moment. According to A.E.D.C. (unpublished information) the data of test A2 are not considered to be highly accurate. The model was subjected to 'flow angle oscillations'². A.E.D.C. considered the model for test A1 too large for reliable lift and moment, the blockage ratio being 2.5% (unpublished information).

Figure 20c presents the results of tests D1 and D2. According to Reference 5, the horizontal tail span is smaller than was prescribed (see Table III). The contribution of the horizontal tail to the moment should therefore be about 20% too small.

The differences in Figure 20f (tests K9-K11) are due to a superposition of the effects mentioned in Sections 3.4.2, 3.4.3 and 3.4.4.

3.5 Neutral Point

For $C_L = 0$ the distance of the neutral point, in body diameters aft of the model nose, has been plotted in Figure 6.

The position of the neutral point is defined by

$$X_{np} = X_{nrc} - \left(\frac{dC_m}{dC_L} \right)_{C_L=0} \frac{\bar{c}}{D}$$

so there is a linear relation between the neutral point and dC_m/dC_L at zero lift. Since the general agreement for the lift data is much better than for the moment data (compare Sections 3.4 and 3.6), differences between the various results for the neutral point must be attributed in the first place to differences in the moment results.

In Figure 21 the results of tests K1-K15 are presented in four groups. Figures 21a and 21b show the results of tests on the same model, but at varying Reynolds numbers, with natural and fixed transition of the boundary layer respectively. Figures 21c and 21d refer to tests on four models of different sizes, also at varying Reynolds numbers and with natural and fixed transition. It appears that the results for fixed transition show fair agreement, independent of the model size and the Reynolds number. In Figure 21d there are marked differences only between the Mach numbers 1.0 and 1.1, which are apparently correlated with the large differences in base drag in that region (Fig.11). Tests with a different sting configuration - K14 in Figure 21d and K15 in Figure 21b - also show the same agreement. Thus Reynolds number (including the fixing of boundary layer transition) has the main effect on the neutral point, which means that, around zero angle of attack, the effect of the other factors on the moment does not generally change with angle of attack.

In Figures 21a and 21c a tendency to a downstream shift of the neutral point with decreasing Reynolds number is apparent. In Section 3.4 it has been mentioned that

the effect of the Reynolds number can be seen as an influence on the base pressure, on the downwash distribution, and - possibly - on the pressure distribution over the wing and the horizontal tail. Variations in base pressure appeared to be of minor importance for the neutral point (compare Figs. 21d and 11). The effect of the pressure distribution is not known, but it is not thought that this will explain the differences between the neutral point data. The variation of downwash with angle of attack is directly related to the position of the neutral point, so it can be assumed that the effect of Reynolds number can mostly be traced as the effect of the downwash. Furthermore, the results of the tests K4 and K11 with a relatively high Reynolds number (above 2×10^6) agree fairly well with the transition fixed results.

As for the moment results, the results of test K12 are taken as the reference curve for the tests K1-K15. The curve agrees rather well with the 'transition fixed' results of the tests K1-K15. The reference curve is shown in Figure 6 as a dotted line.

Figure 23 presents the neutral point data of all the tests, with the exception of the N.L.R. data already presented. Figure 22 compares those that are in fair agreement with each other. This refers to tests with fixed transition (D2 and D4) or tests with a Reynolds number greater than 2×10^6 (B1 and J1). These results come close to the reference curve for the N.L.R. tests. No comment can be made on the other results.

3.6 Lift

For all the tests the lift coefficient was plotted against Mach number in Figure 7 for three different values of angle of attack, 0° , 4° and 8° . At higher angles of attack not enough data are available.

The scatter in Figure 7a is of the same order as the scatter in the tests¹¹ on AGARD Model B.

The reference curves for the NLR tests were established by taking the mean value of tests K1-K15 and are shown in Figure 7 as dotted lines.

The negative lift at zero angle of attack is caused by the lift contribution of the horizontal tail. The horizontal tail contributions to the lift and to the moment are related by $\Delta C_m = l_H/\bar{c} \Delta C_L$, where $l_H/\bar{c} = 2.204$. So the large differences in moment should be seen, to a small extent, in the lift results, which means that the agreement for the lift on wing alone is better than for total lift.

In Figure 24 the results of Figure 7 are given individually. A comparison with the results of corresponding tests¹¹ on AGARD Model B shows that there is a fair agreement between the results for both models in the tests A1, A2 and A3 (Fig. 24a), B1 (Fig. 24b) and E1 (Fig. 24d).

As for AGARD Model B, large effects of tunnel-wall interference on lift for this model are not likely, because the wing area is relatively small. An exception should be made for test A1, the blockage ratio for this test being extreme (2.5%). Tunnels designed to provide the least interference over a wide range of transonic Mach numbers behave somewhat like open jet tunnels at Mach numbers near one. Therefore the

indicated Mach number should be corrected (decreased) as a function of model size*.

3.7 Lift-Curve Slope

The lift-curve slope is taken at $C_L = 0$. The results of all the tests are presented in Figure 8 and are shown individually in Figure 25.

From Reference 8 it appeared that the results of the NLR tests obtained with natural transition of the boundary layer (K1, K2, K3 and K4 in Fig.25g and K9, K10 and K11 in Fig.25i) show, near $M = 1$, the same irregularity in lift-curve slope in the region of zero angle of attack as appeared in several tests on AGARD Model B. A definite trend with Reynolds number is apparent: compare K1 and K9 ($Re = 0.6 \times 10^6$) with K2 and K10 ($Re = 1 \times 10^6$), with K3 ($Re = 1.8 \times 10^6$) and with K4 and K11 ($Re = 1.5 \times 10^6$). The C_L - α curves for fixed transition have more the character of a straight line, although a short change in lift-curve slope is apparent. The dotted line in Figure 8 represents the mean value of the 'transition fixed' results of the tests K1-K15.

Several other tests also show this irregularity in the C_L - α curves, but in most cases in the references a smooth line was drawn through the measured points because the discrepancies were considered to be within the accuracy of the measurements.

On the results available, it does not seem possible to give a further explanation of the singularities mentioned.

4. CONCLUSIONS

The present analysis gives a presentation of the results of tests on AGARD Calibration Model C in various wind tunnels. It is apparent that the correspondence between the results of the various tests is much worse than would normally be expected - or hoped for. In particular, the comparison of the moment shows great differences in values and in trends.

Detailed explanations of the differences could not be given; consequently the analysis had to be confined to the presentation of the results with some tentative conclusions, arising mainly from the tests K1-K15.

Base Drag

- (i) The base drag is only slightly affected by the Reynolds number.
- (ii) The effect of the sting configuration is small, but:
- (iii) Flow irregularities, if any, in the aft part of the test section may have a large influence.
- (iv) The influence of shock wave interaction is important in a certain Mach number range.

* Taken from correspondence with A.E.D.C.

Forebody Drag

- (i) Differences in the subsonic values of the forebody drag are, in general, due to the effect of the Reynolds number or of the methods of fixing the transition of the boundary layer.
- (ii) An effect of the blockage ratio on the transonic drag rise may exist, but a definite trend could not be found.

Pitching Moment

- (i) The pitching moment is very sensitive, both to the base pressure and to the downwash distribution.
- (ii) Within a definite supersonic Mach number range, depending on the relative model size, shock wave interaction generally has an appreciable effect.
- (iii) No direct evidence is present of Reynolds number effect due to the pressure distribution over wing and horizontal tail.
- (iv) Tunnel-wall (lift and blockage) interference could not be traced.

Neutral Point

- (i) The neutral point is especially sensitive to Reynolds number, through the effect of the Reynolds number on the downwash distribution.
- (ii) Other factors appear to have only a small effect.
- (iii) Results obtained from tests with 'fixed transition', or with a sufficiently high Reynolds number, show fair agreement.

Lift

- (i) The agreement between the lift results is about the same as for AGARD Model B.
- (ii) Tunnel-wall interference could not be traced; an exception may be test A1 (blockage ratio 2.5%).

Lift-Curve Slope

- (i) In the region around $C_L = 0$ similar irregularities in the lift-curve slope are found as for AGARD Model B.

Taking these conclusions together, the essential point seems to be that AGARD Model C is not sensitive to tunnel blockage and lift interference but, on the other hand, it is very sensitive to several other factors, largely depending on the location of the boundary layer transition point and the shape of the model.

The fixing of the boundary layer transition has a favourable effect on the agreement of the results, which especially applies to the NLR results in this report.

Important features of the model shape are the relatively large base area and the location of the horizontal tail with respect to the base. Therefore the large differences found are not fully representative of the agreement in general between the results of measurements in different transonic wind tunnels*.

The author is fully aware that the analysis presented here is far from complete. At this stage only an initial approach could be made, but, even in the present form, the results may prove to be useful for certain purposes.

REFERENCES

1. Milillo, J.R.
Chevalier, H.L. *Test Results of the AGARD Calibration Model B and a Modified AGARD Model C in the AEDC Transonic Tunnel.* Arnold Engineering Development Center, AEDC-TN-57-6, May 1957.
2. Milillo, J.R. *Transonic Tests of an AGARD Model B and a Modified Model C at 0.01 percent Blockage.* Arnold Engineering Development Center, AEDC-TN-58-48, April 1959.
3. Dick, R.S. *Tests in the PWT 16 ft Transonic Circuit of an AGARD Model B and a Modified Model C at 1.5 percent Blockage.* Arnold Engineering Development Center, AEDC-TN-59-32, April 1959.
4. Schreiber, B. *A Compilation of Data from Tests of AGARD Models B and C in the Boeing Wind Tunnels.* Boeing, Seattle, Document D 2 - 5360.
5. O.N.E.R.A. *Caractéristiques Transsoniques des Maquettes AGARD B and C - Essais de l'ONERA.* ONERA Fiche Doc. 176.
6. Wijker, R.C.
Fisher, R.A. *An Investigation of the Lift, Drag and Pitching Moment Characteristics of AGARD Calibration Models B and C at the Ohio State University Transonic Wind Tunnel.* North American Aviation Report 57 H-618, 1957.
7. Dickie, D., Jr. *Preliminary Presentation of Wind Tunnel Test Data Obtained With an AGARD C Calibration Model.* United Aircraft Corporation Report.
8. Valk, H. *Results of Tests on the AGARD Calibration Model C in the Transonic Wind Tunnel HST.* Period July 1959 - October 1960. NLR-TM T.36, July 1962.

* In some cases, where the N.L.R. were able to compare results from tests in different wind tunnels on models of actual aircraft, much better agreement existed. In these cases the transition of the boundary layer was fixed.

9. Wykes, R.C. *Test and Model Information for Transonic and Supersonic Wind Tunnel Tests of Sting-Mounted, AGARD Calibration Models B and C at the Ohio State University 12 in. x 12 in. Wind Tunnel and at the North American Aviation, Inc., Supersonic Aerodynamic Laboratory (SAL) 16 in. x 16 in. Wind Tunnel.* North American Aviation Report 56H-274, June 26, 1956.
10. A.G.A.R.D. *Wind Tunnel Calibration Models.* AGARD Specification 2, September 1958.
11. Valk, H.
van der Zwaan, J.H. *A Review of Measurements on AGARD Calibration Model B in the Transonic Speed Range.* Part II of this AGARDograph.
12. Chevalier, H.L. *Calibration of the PWT 16-foot Transonic Circuit with a Modified Model Support System and Test Section.* Arnold Engineering Development Center, AEDC-TN-60-164, August 1960.
13. Neely, R.H.
Griner, R.F. *Summary and Analysis of Horizontal-Tail Contribution to Longitudinal Stability of Swept-Wing Airplanes at Low Speeds.* NASA TR T-49, 1959.
14. Oenberg, T. *A Note on the Flow Around Delta Wings.* KTH, Sweden, Aero TN 38, February 20, 1954.

Test	Ref.	Symbol	Institute	Wind Tunnel		
				Name	Test Section	
					Size	Wall
A1	1	○	A.E.D.C.	Transonic Model Tunnel	1 x 1 ft ²	4 per
A2	2	⊙	A.E.D.C.	PWT Transonic Circuit	16 x 16 ft ²	4 per
A3	3	●	A.E.D.C.	PWT Transonic Circuit	16 x 16 ft ²	4 per
B1	4	X	Boeing	Transonic Wind Tunnel	8 x 12 ft ²	4 slot
D1	5	◻	O.N.E.R.A.	Soufflerie Courneuve	0.28 x 0.28 m ²	4 per
D2	5	◼	O.N.E.R.A.	Soufflerie Courneuve	0.28 x 0.28 m ²	4 per
D3	5	◻	O.N.E.R.A.	Soufflerie S5 Chalais	0.2 x 0.3 m ²	2 slot
D4	5	◼	O.N.E.R.A.	Soufflerie S5 Chalais	0.2 x 0.3 m ²	2 slot
E1	6	+	O.S.U.	Transonic Wind Tunnel	12 in. x 12 in.	4 per
J1	7	✧	U.A.C.	Transonic Wind Tunnel	17 in. x 17 in.	4 per
J2	7	◆	U.A.C.	Subsonic Wind Tunnel	8 x 8 ft ²	solid
K1	8	▽	N.L.R.	Transonic Wind Tunnel HST	1.6 x 2.0 m ²	2 slot
K2	8	▼	N.L.R.	Transonic Wind Tunnel HST	1.6 x 2.0 m ²	2 slot
K3	8	▼	N.L.R.	Transonic Wind Tunnel HST	1.6 x 2.0 m ²	2 slot
K4	8	▼	N.L.R.	Transonic Wind Tunnel HST	1.6 x 2.0 m ²	2 slot
K5	8	△	N.L.R.	Transonic Wind Tunnel HST	1.6 x 2.0 m ²	2 slot
K6	8	▲	N.L.R.	Transonic Wind Tunnel HST	1.6 x 2.0 m ²	2 slot
K7	8	▲	N.L.R.	Transonic Wind Tunnel HST	1.6 x 2.0 m ²	2 slot
K8	8	▲	N.L.R.	Transonic Wind Tunnel HST	1.6 x 2.0 m ²	2 slot
K9	8	◇	N.L.R.	Transonic Wind Tunnel HST	1.6 x 2.0 m ²	2 slot
K10	8	◆	N.L.R.	Transonic Wind Tunnel HST	1.6 x 2.0 m ²	2 slot
K11	8	◆	N.L.R.	Transonic Wind Tunnel HST	1.6 x 2.0 m ²	2 slot
K12	8	◻	N.L.R.	Transonic Wind Tunnel HST	1.6 x 2.0 m ²	2 slot
K13	8	◼	N.L.R.	Transonic Wind Tunnel HST	1.6 x 2.0 m ²	2 slot
K14	8	◼	N.L.R.	Transonic Wind Tunnel HST	1.6 x 2.0 m ²	2 slot
K15	8	◼	N.L.R.	Transonic Wind Tunnel HST	1.6 x 2.0 m ²	2 slot

1

H : test section height
 B : test section width
 L : model length
 b : wing span

D : bo
 d : st
 l : le
 θ : cor

TABLE I

General Data on Models and Facilities

Tunnel			Model					Sting			Reynolds Number Range ($\times 10^{-6}$)	Remarks (see also Table III)
Test Section			D	L/H	b/B	Blockage %	Transition (see Table II)	d/D	l/D	$\theta/2$		
Size	Walls	Open %										
$\times 1 \text{ ft}^2$	4 perf.*	6	1.956 in.	1.9	0.65	2.5	natural	0.488	1.5	5.6°	1.6-2	Different tail configuration
$\times 16 \text{ ft}^2$	4 perf.*	6	1.956 in.	0.12	0.04	0.01	natural	0.488	1.5	5.6°	0.7-1.2	
$\times 16 \text{ ft}^2$	4 perf.*	6	21.6 in.	1.3	0.45	1.15	carborundum	0.50	1.58	1.11°	8.5-1.2	
$\times 12 \text{ ft}^2$	4 slotted	11	4.559 in.	0.55	0.13	0.17	natural	0.483	1.48	2.94°	2.9-3.4	Slightly different model nose
$\times 0.28 \text{ m}^2$	4 perf.	8	20 mm	0.8	0.29	0.5	natural	0.60	-	4°	0.92	Different tail configuration
$\times 0.28 \text{ m}^2$	4 perf.	8	20 mm	0.8	0.29	0.5	wire	0.60	-	4°	0.92	
$\times 0.3 \text{ m}^2$	2 slotted	-	20 mm	1.15	0.27	0.7	natural	0.60	-	4°	0.33	
$\times 0.3 \text{ m}^2$	2 slotted	-	20 mm	1.15	0.27	0.7	wire	0.60	-	4°	0.33	
1. $\times 12 \text{ in.}$	4 perf.	-	1.25 in.	1.2	0.42	1.12	natural	0.40	3.5	-	1.3-1.9	
1. $\times 17 \text{ in.}$	4 perf.	-	1.25 in.	0.85	0.30	0.55	natural	0.765	2.8	11.2°	1.8-3.3	
$\times 8 \text{ ft}^2$	solid	0	1.25 in.	0.15	0.05	0.02	natural	0.765	2.8	11.2°	1.0-1.1	
$\times 2.0 \text{ m}^2$	2 slotted	7	70 mm	0.50	0.14	0.16	natural	0.50	3.0	5°	0.5-0.8	
$\times 2.0 \text{ m}^2$	2 slotted	7	70 mm	0.50	0.14	0.16	natural	0.50	3.0	5°	0.8-1.1	
$\times 2.0 \text{ m}^2$	2 slotted	7	70 mm	0.50	0.14	0.16	natural	0.50	3.0	5°	1.5-2.1	
$\times 2.0 \text{ m}^2$	2 slotted	7	70 mm	0.50	0.14	0.16	natural	0.50	3.0	5°	2.3-2.9	
$\times 2.0 \text{ m}^2$	2 slotted	7	70 mm	0.50	0.14	0.16	wire	0.50	3.0	5°	0.5-0.8	
$\times 2.0 \text{ m}^2$	2 slotted	7	70 mm	0.50	0.14	0.16	wire	0.50	3.0	5°	0.8-1.1	
$\times 2.0 \text{ m}^2$	2 slotted	7	70 mm	0.50	0.14	0.16	wire	0.50	3.0	5°	1.5-2.1	
$\times 2.0 \text{ m}^2$	2 slotted	7	70 mm	0.50	0.14	0.16	wire	0.50	3.0	5°	2.3-2.9	
$\times 2.0 \text{ m}^2$	2 slotted	7	22 mm	0.16	0.04	0.016	natural	0.50	3.0	5°	0.5-0.7	
$\times 2.0 \text{ m}^2$	2 slotted	7	40 mm	0.29	0.08	0.05	natural	0.50	3.0	5°	0.9-1.2	
$\times 2.0 \text{ m}^2$	2 slotted	7	100 mm	0.72	0.20	0.32	natural	0.50	1.5	5°	2.0-2.8	
$\times 2.0 \text{ m}^2$	2 slotted	7	22 mm	0.16	0.04	0.016	wire	0.50	3.0	5°	0.5-0.7	
$\times 2.0 \text{ m}^2$	2 slotted	7	40 mm	0.29	0.08	0.05	wire	0.50	3.0	5°	0.9-1.2	
$\times 2.0 \text{ m}^2$	2 slotted	7	100 mm	0.72	0.20	0.32	wire	0.50	1.5	5°	2.0-2.8	
$\times 2.0 \text{ m}^2$	2 slotted	7	70 mm	0.50	0.14	0.16	wire	0.50	1.5	5°	1.5-2.1	

D : body diameter

d : sting diameter

l : length of cylindrical portion of sting

 θ : cone angle of sting

- no data available

* inclined holes

TABLE II

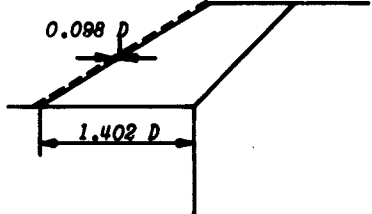
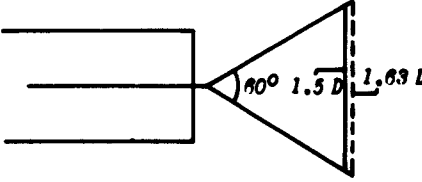
Boundary Layer Trips

<i>Test</i>	<i>Method</i>	<i>Relative Thickness*</i>	<i>Remarks</i>
A3	Carborundum No. 60, height 0.025 in., width 1% chord	0.02	no trip on body
D2	wire, $d = 0.07$ mm	0.07	
D4	wire, $d = 0.07$ mm	0.07	
K5, K6, K7, K8, K15	wire, $d = 0.25$ mm	0.07	
K12	wire, $d = 0.15$ mm	0.13	
K13	wire, $d = 0.20$ mm	0.09	
K14	wire, $d = 0.25$ mm	0.05	

* Relative thickness = trip height divided by wing root thickness at 15% chord

TABLE III

Deviations of Model Configurations

<i>Test</i>	<i>Description of Deviations</i>	
A1, A2, A3	Horizontal tail and leading edge of vertical tail displaced downstream over $0.098 D$. Vertical tail root chord is $1.402 D$ instead of $1.5 D$ (according to References 1, 2 and 3)	
B1	Model nose slightly different* (according to Reference 4)	
D1, D2 (probably also D3, D4)	Horizontal tail span is $1.5 D$ instead of $1.63 D$ (according to Reference 5)	

* The difference is quite small, so that no influence on the measurements is to be expected

TABLE IV

Accuracy and Repeatability of the Measurements, as Stated in the References

Test	M	α	C_L	C_m	C_{Df}	C_{Db}	Remarks
A1	± 0.002	$\pm 0.10^0$	± 0.0140	± 0.0020	± 0.0040	± 0.0005	$0.70 \leq M \leq 1.15$
A1	± 0.006	$\pm 0.10^0$	± 0.0100	± 0.0010	± 0.0020	± 0.0002	$1.20 \leq M \leq 1.50$
A2	± 0.003	$\pm 0.30^0$	± 0.0150	± 0.0050	± 0.0060	± 0.0020	$0.70 \leq M \leq 1.15$
A2	± 0.006	$\pm 0.30^0$	± 0.0100	± 0.0020	± 0.0030	± 0.0010	$1.20 \leq M \leq 1.50$
A3	± 0.003	$\pm 0.05^0$	± 0.0040	± 0.0020	± 0.0030	± 0.0003	$0.70 \leq M \leq 1.10$
A3	± 0.006	$\pm 0.05^0$	± 0.0040	± 0.0020	± 0.0030	± 0.0003	$1.20 \leq M \leq 1.60$
B1	-	-	-	-	-	-	
D1, D2	-	-	-	-	-	-	
D3, D4	-	-	-	-	-	-	
E1	-	-	-	-	-	-	
J1, J2	-	-	-	-	-	-	
K1, K5	-	-	0.0022	0.0012	0.0013	0.0003	
K2, K6	-	-	0.0016	0.0008	0.0004	0.0002	
K3, K7, K15	-	-	0.0013	0.0007	0.0007	0.0002	
K4, K8	-	-	0.0013	0.0006	0.0003	0.0001	
K9, K12	-	-	0.0032	0.0006	0.0008	0.0002	
K10, K13	-	-	0.0019	0.0014	0.0007	0.0002	
K11, K14	-	-	0.0020	0.0007	0.0004	0.0002	

- no data available

Notes, taken from the references:

1. The accuracy of the data of tests A1, A2 and A3 has been determined by combining the errors in the balance read-out system, base pressure and stream parameters by a method based on a 95% level and a normal error distribution.
2. For K1-K15 the testing procedure resulted in the repetition of some model attitudes at each Mach number. The coefficient repeatability is defined as the average of the absolute values of the differences between two corresponding data points.

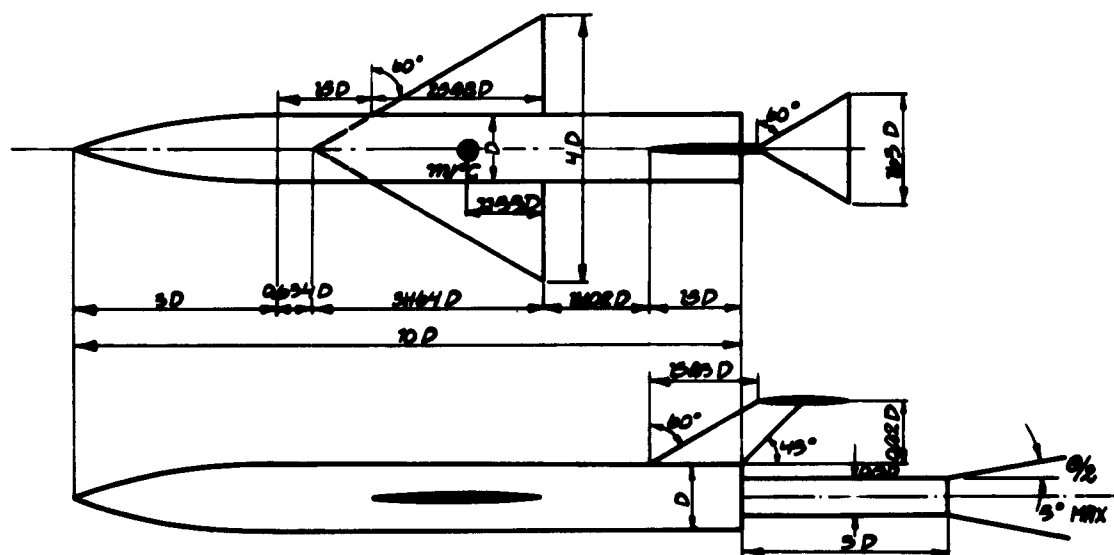


Fig.1 AGARD Calibration Model C

Wing and tail profile: symmetrical circular arc section thickness ratio = 0.04.

Nose profile: length $3D$. Equation of curve $r = \frac{x}{3} \left[1 - \frac{1}{9} \left(\frac{x}{D} \right)^2 + \frac{1}{54} \left(\frac{x}{D} \right)^3 \right]$.

Radius of nose and wing leading edges should be $D/500$.

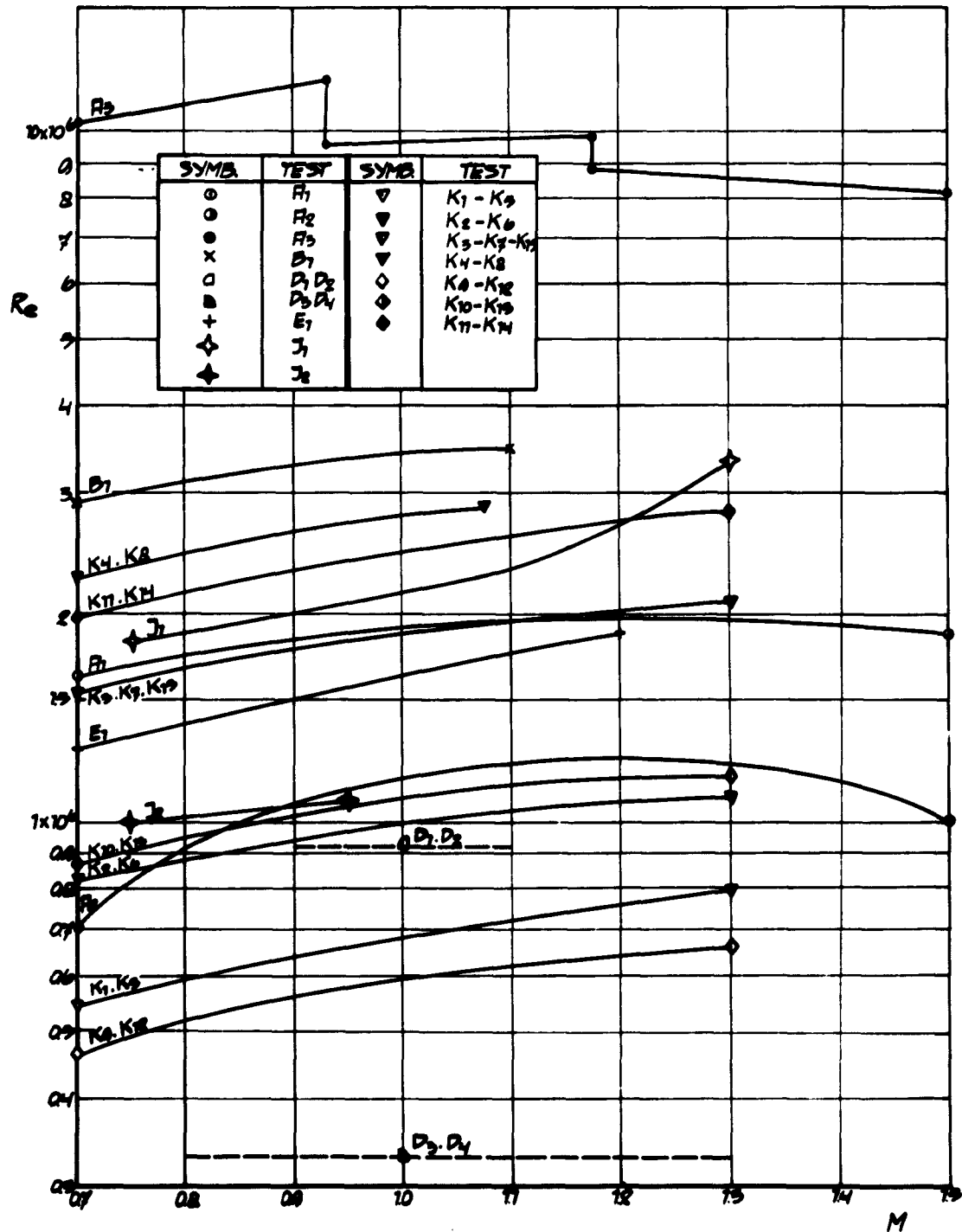


Fig. 2 Reynolds number (based on mean aerodynamic chord) versus Mach number

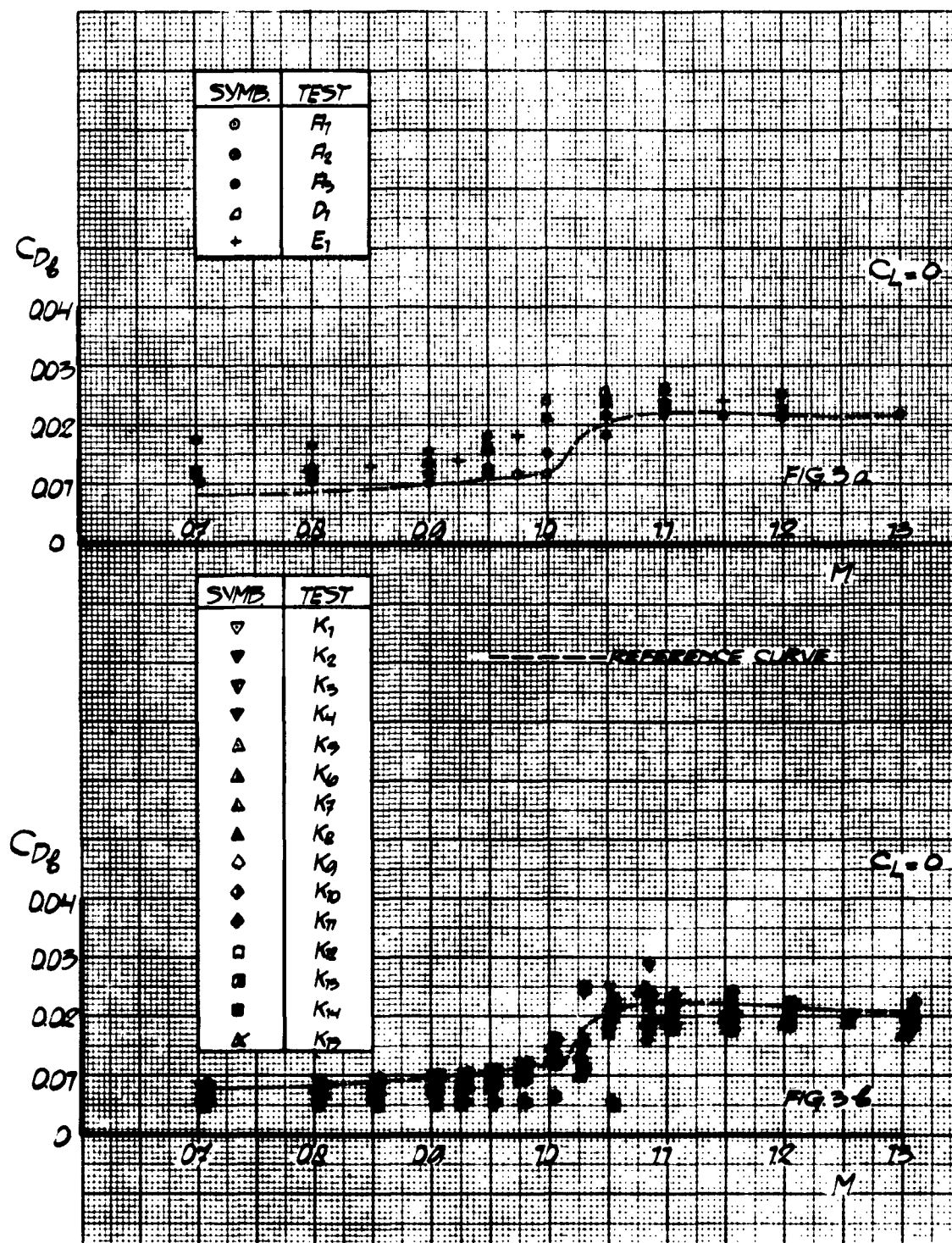


Fig.3 Base drag coefficient versus Mach number

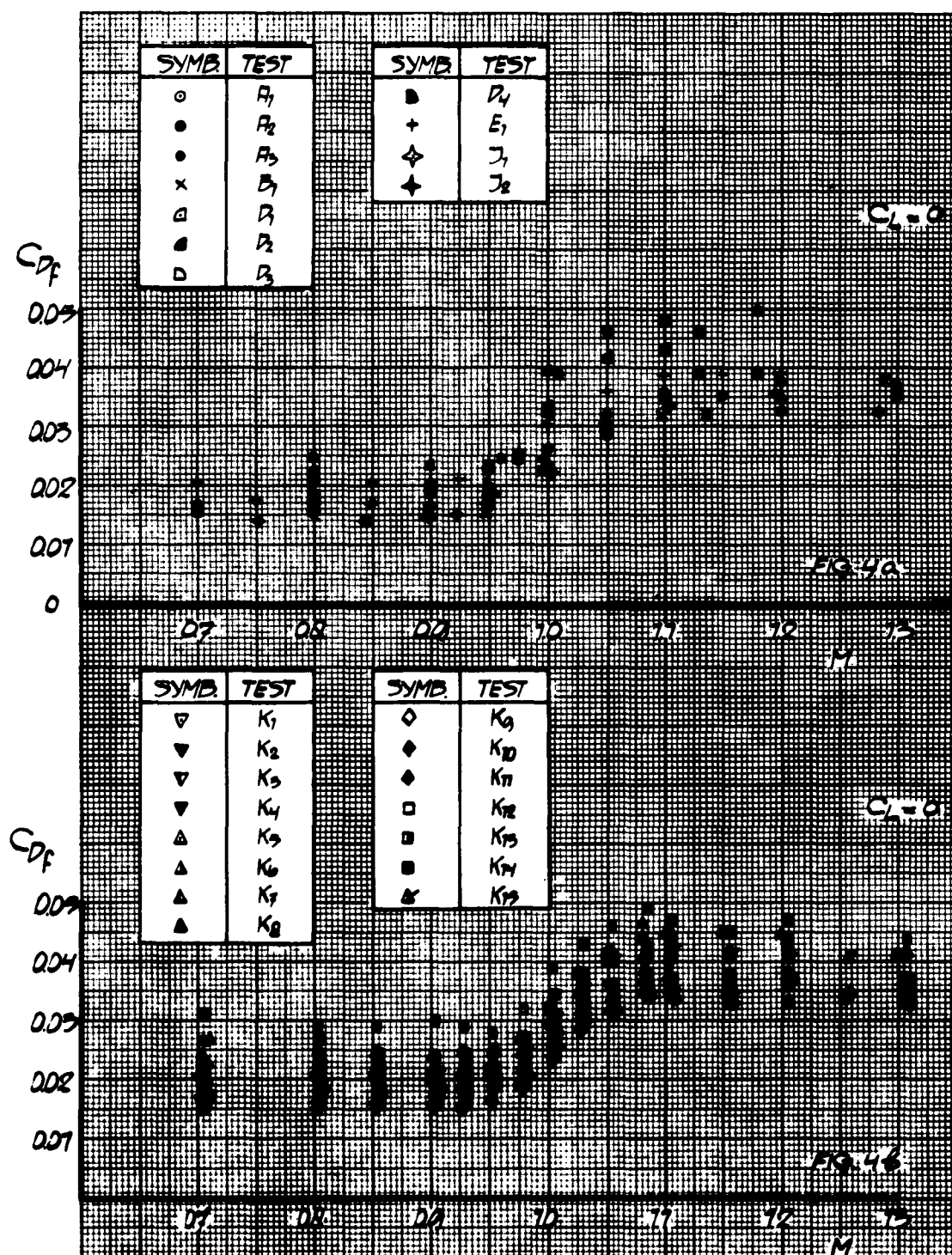


Fig. 4 Forebody drag coefficient versus Mach number

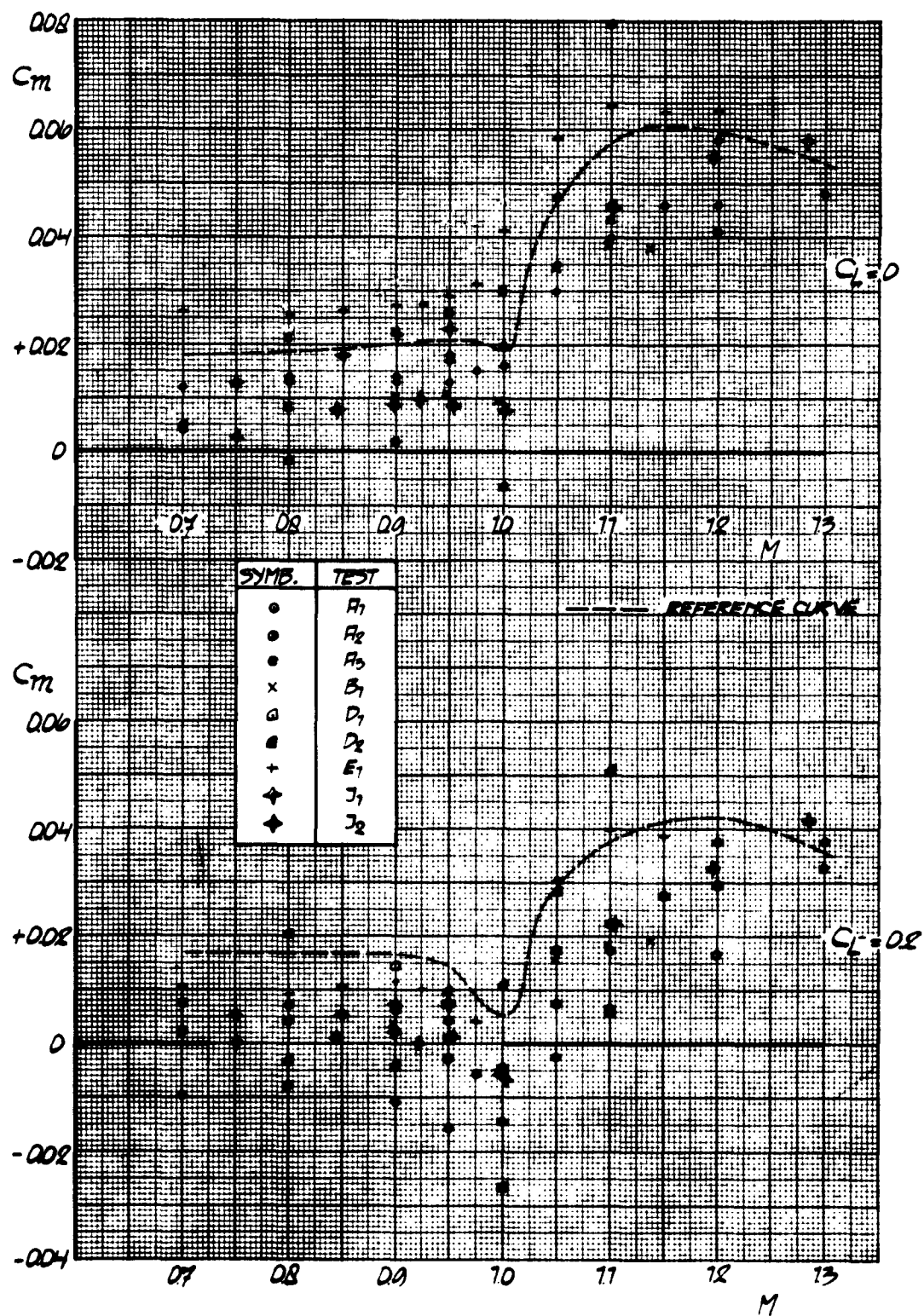


Fig. 5a Moment coefficient versus Mach number. Tests A1-J2 ($C_L = 0$ and 0.2)

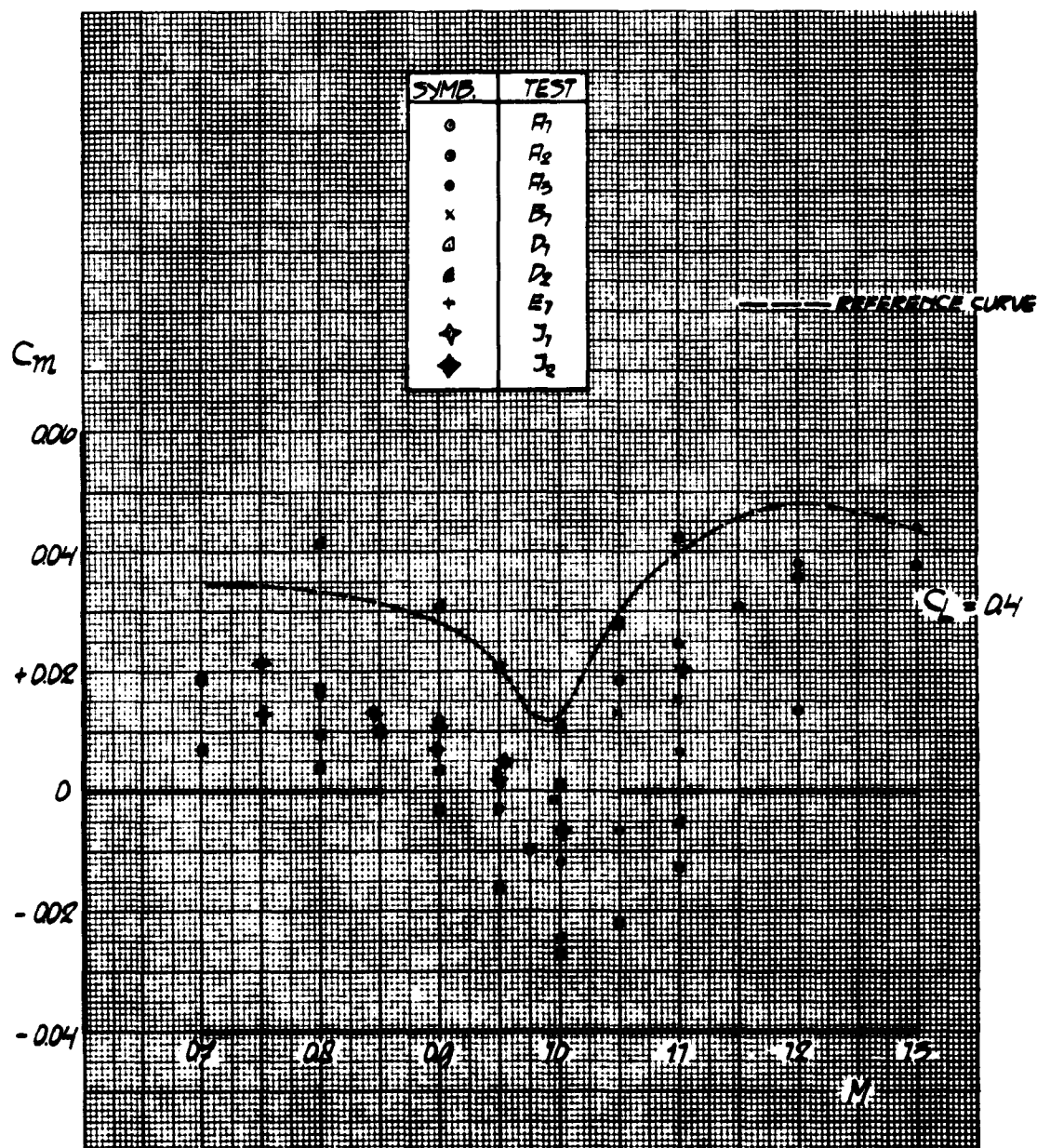


Fig. 5a Moment coefficient versus Mach number. Tests A1-J2 ($C_L = 0.4$) (continued)

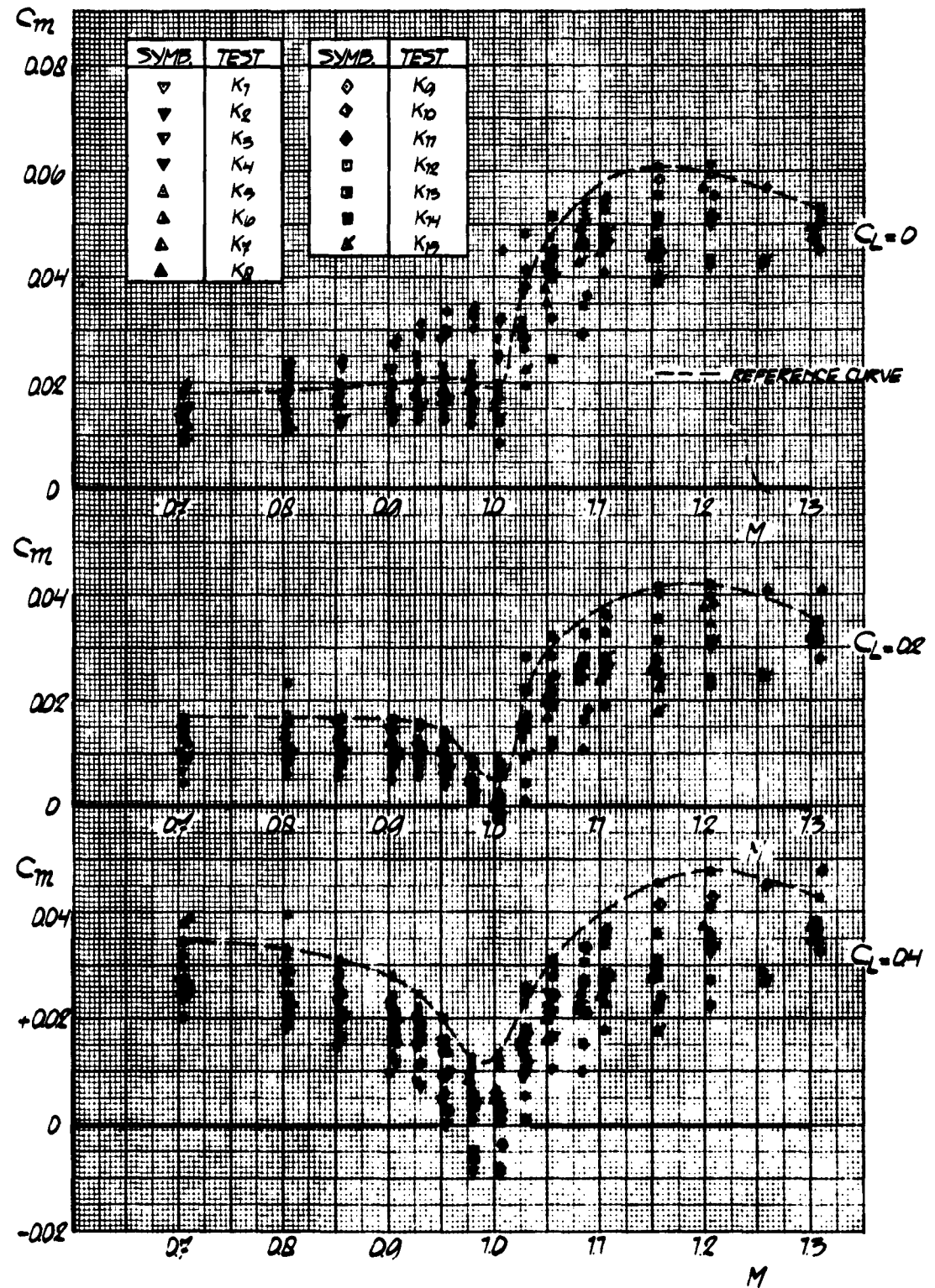


Fig. 5b Moment coefficient versus Mach number. Tests K1-K15

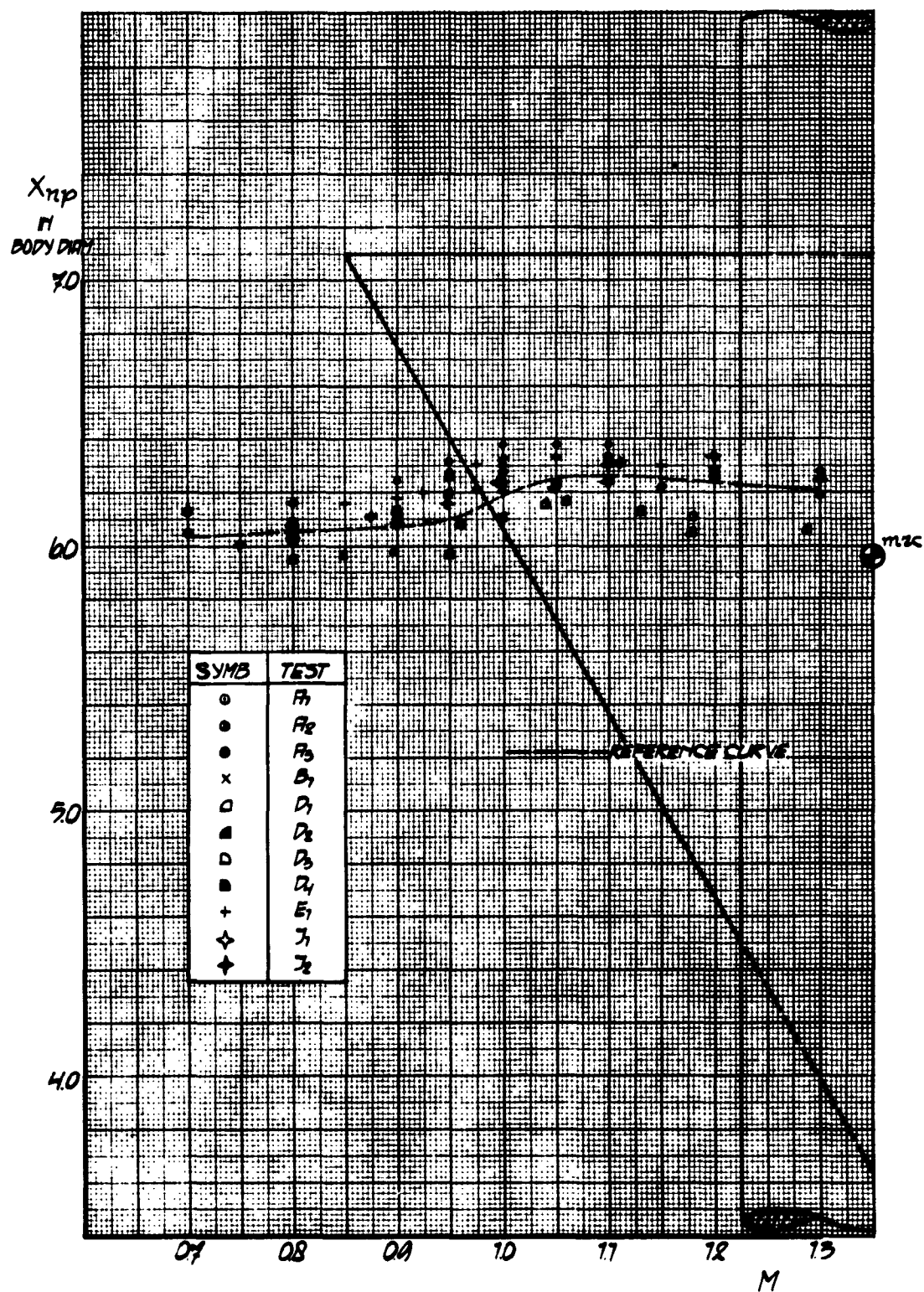


Fig. 6a Neutral point at $C_L = 0$ versus Mach number. Tests A1-J2

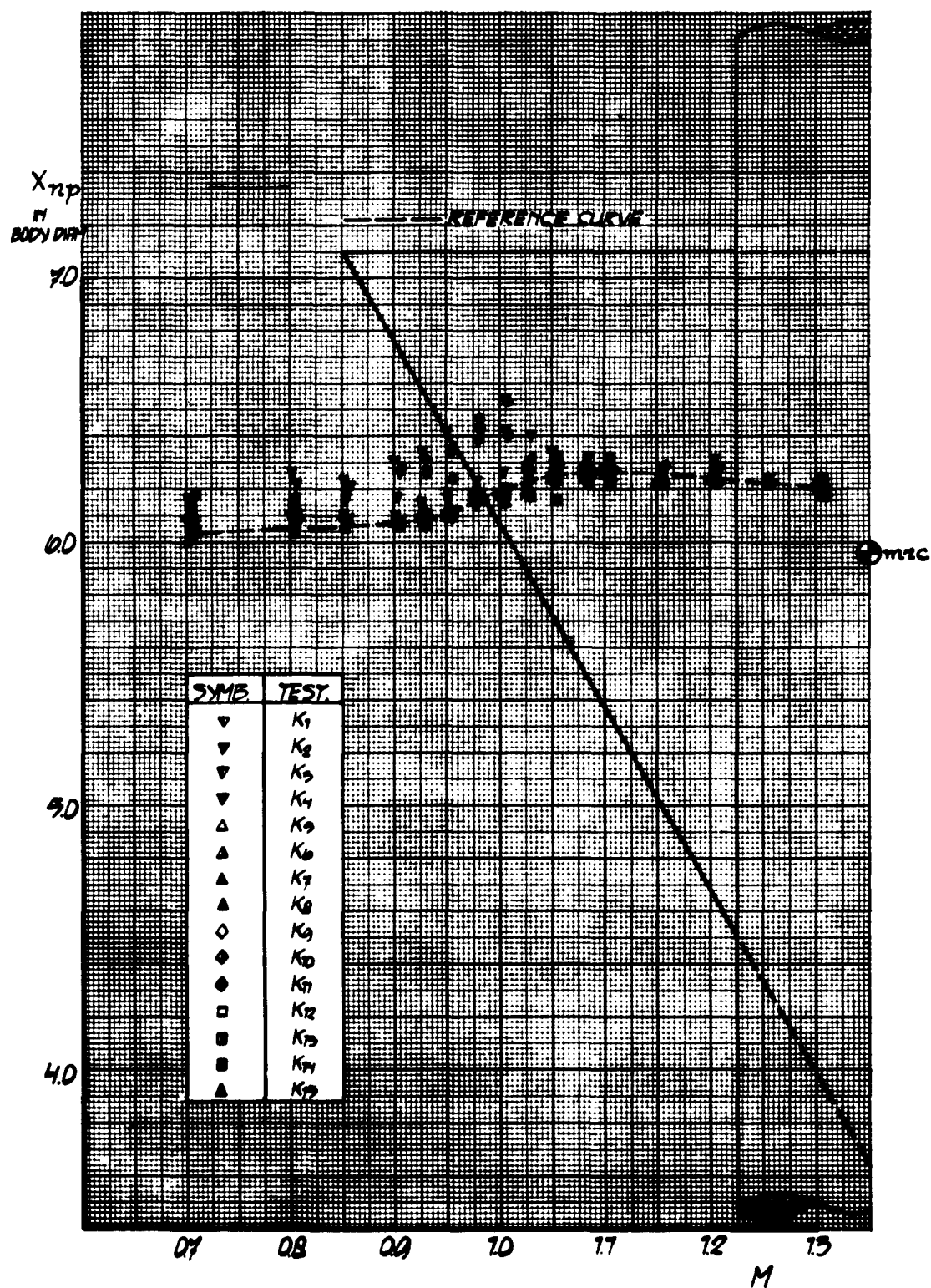


Fig. 6b Neutral point at $C_L = 0$ versus Mach number. Tests K7-K15

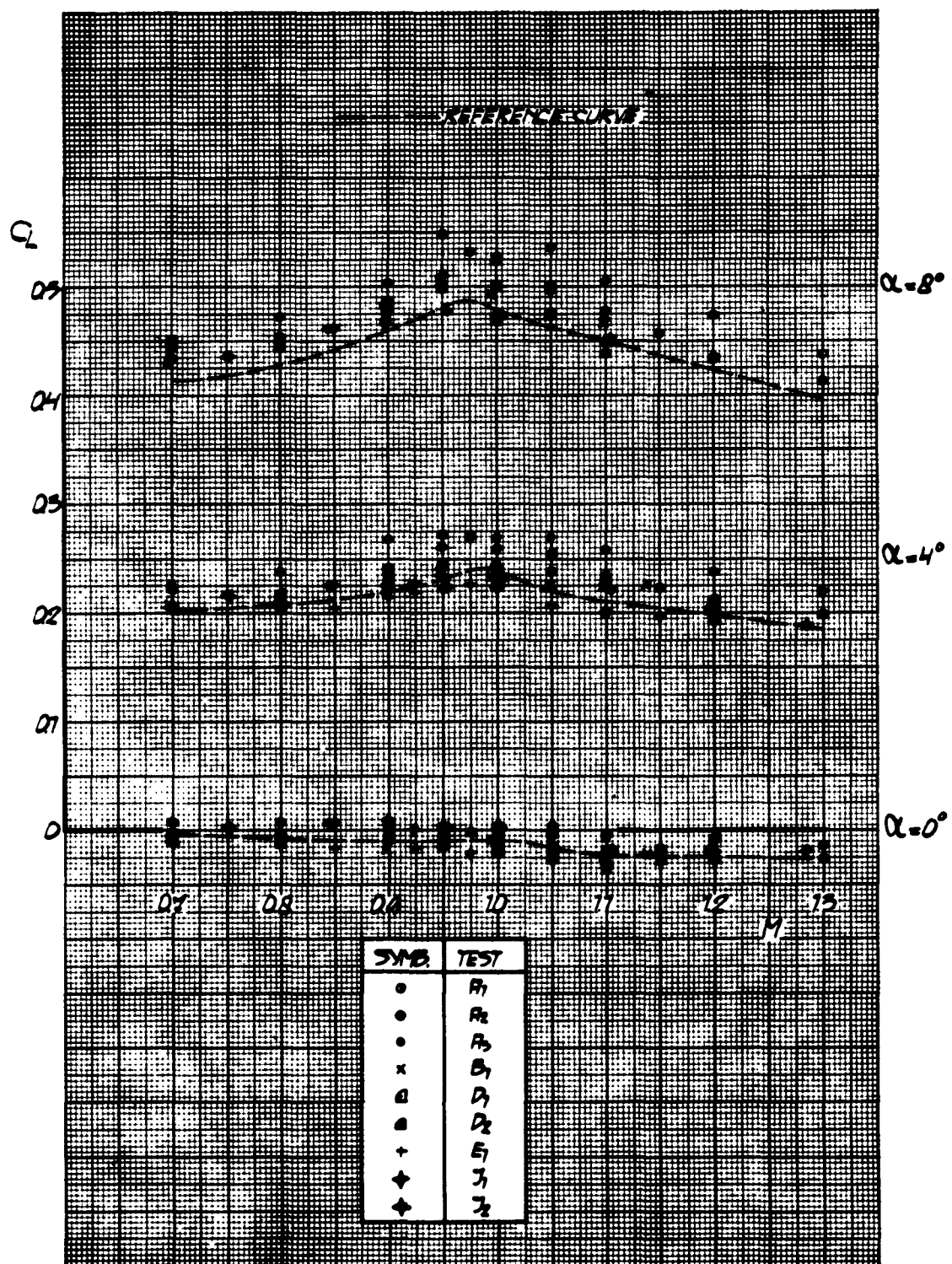


Fig. 7a Lift coefficient versus Mach number. Tests A1-J2

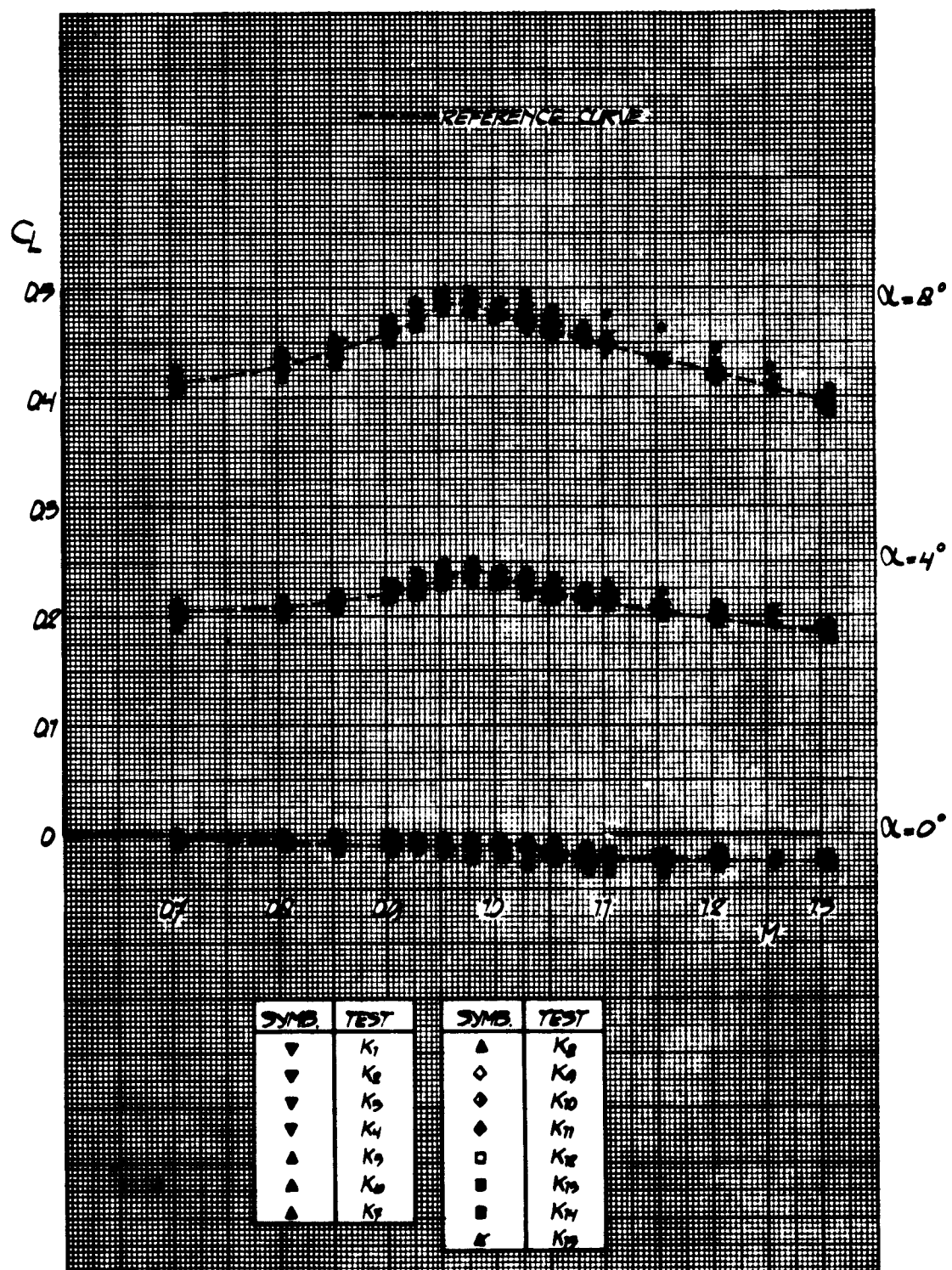


Fig. 7b Lift coefficient versus Mach number. Tests K1-K15

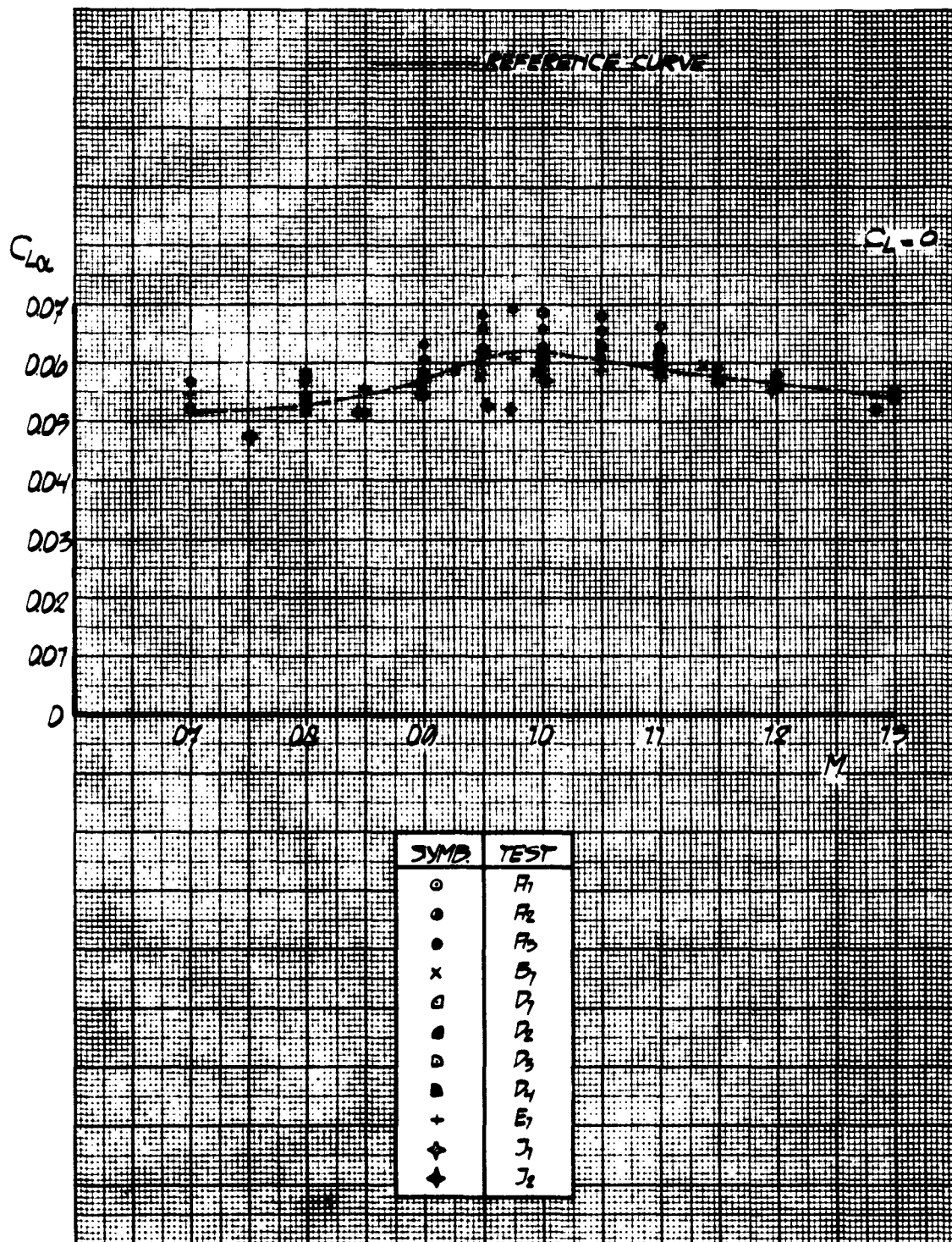


Fig. 8a Lift curve slope at $C_L = 0$ versus Mach number. Tests A1-J2

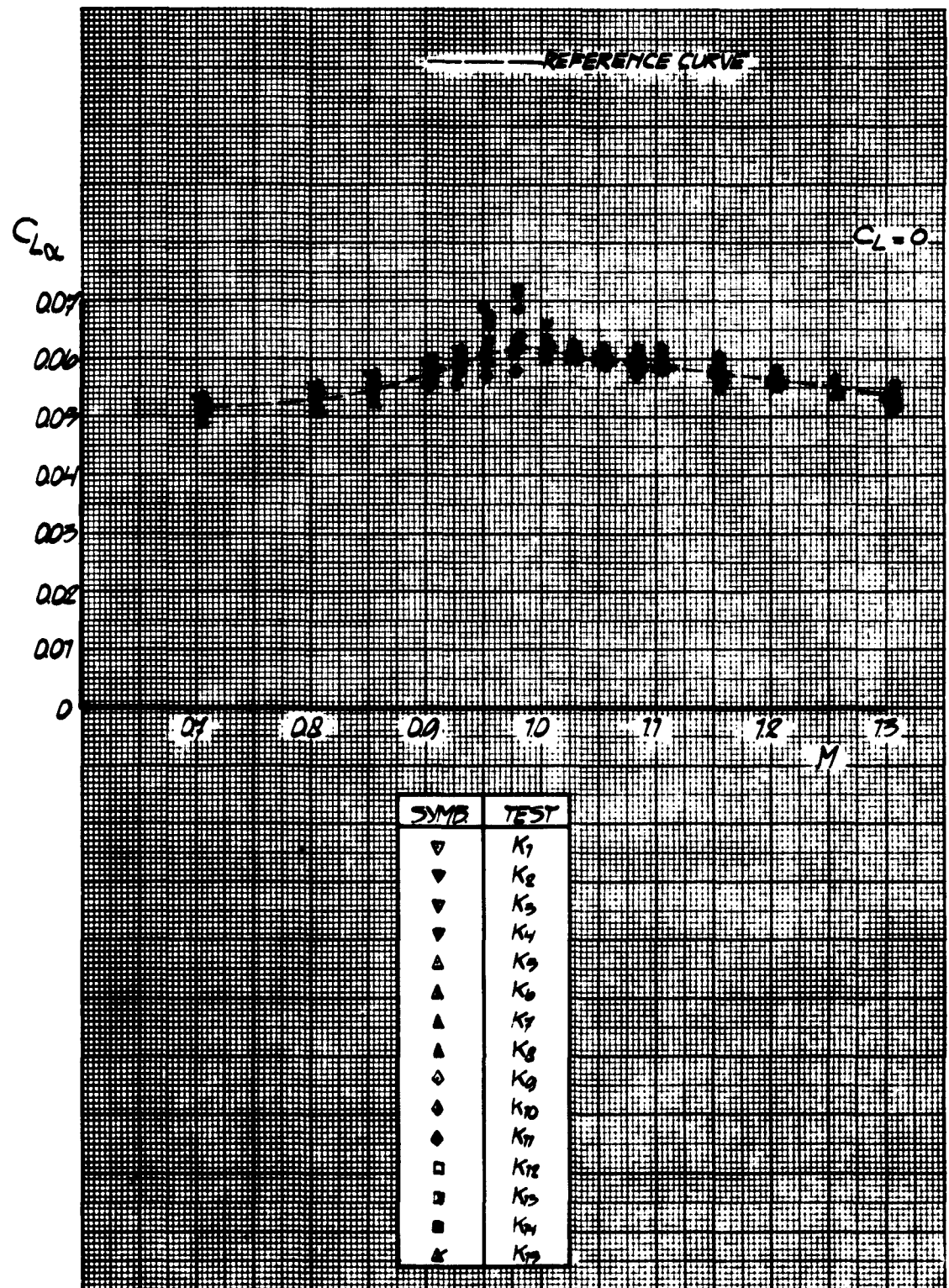


Fig. 8b Lift curve slope at $C_L = 0$ versus Mach number. Tests K1-K15

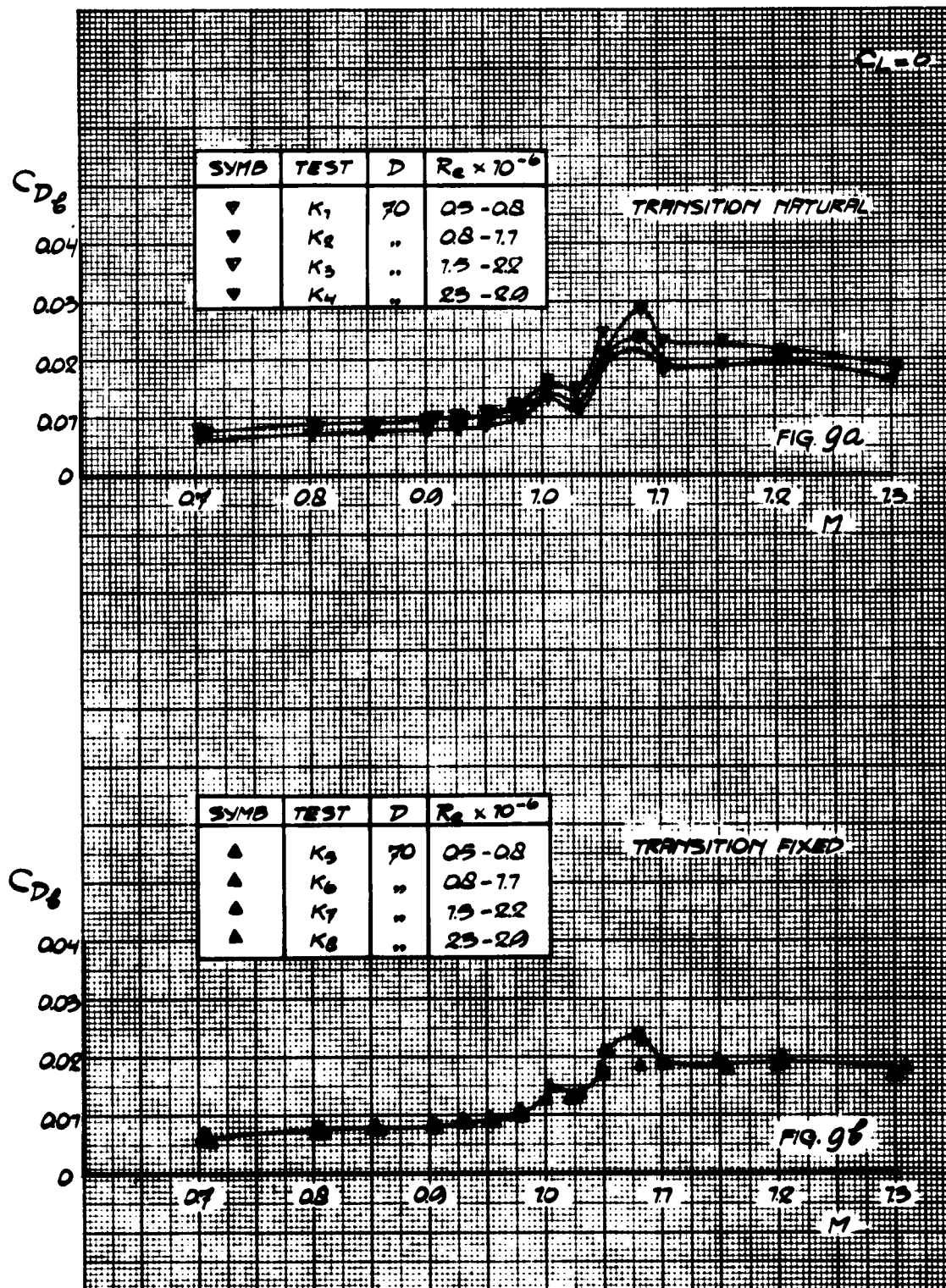


Fig. 9 Base drag coefficient versus Mach number at different Reynolds numbers

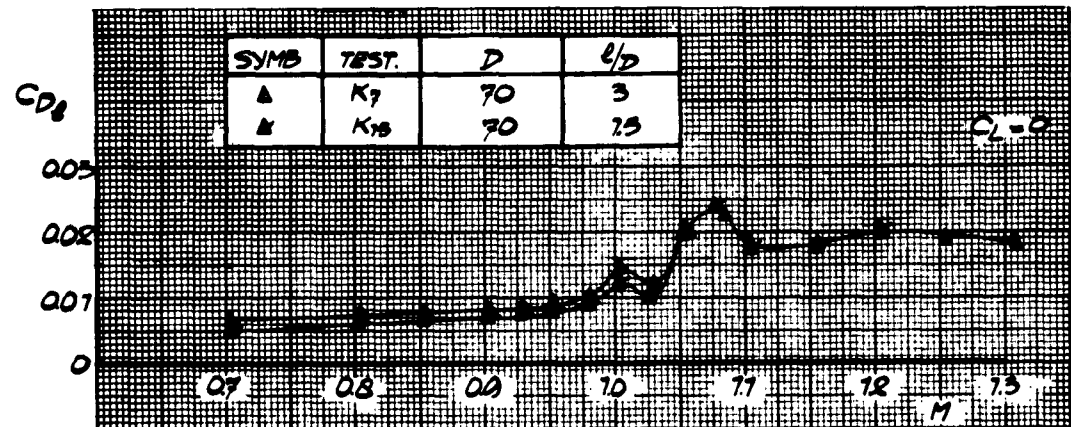


Fig.10 Base drag coefficient versus Mach number for different sting configurations

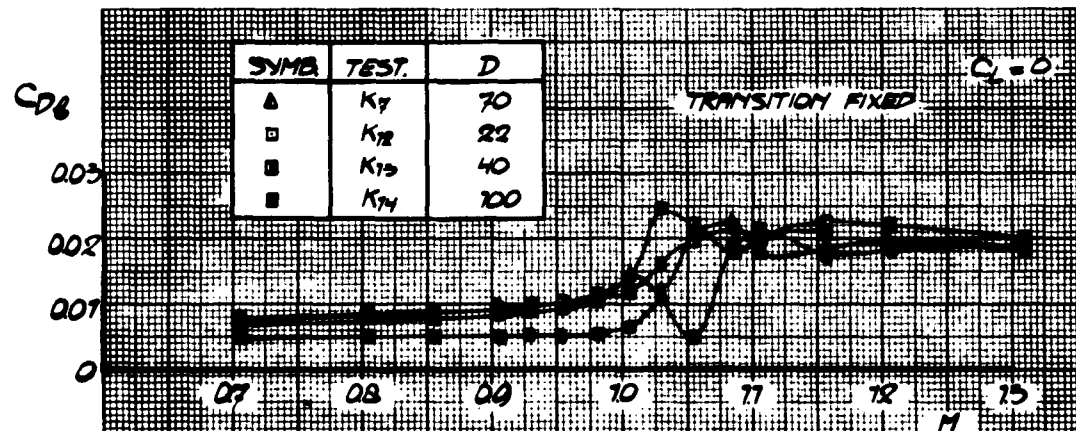


Fig.11 Base drag coefficient versus Mach number for different model sizes

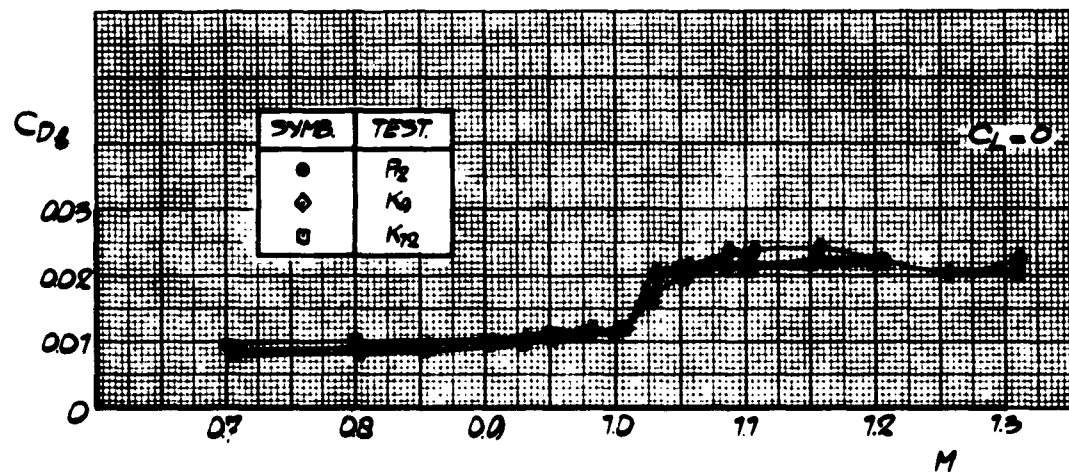


Fig.12 Base drag results of 'interference free' models

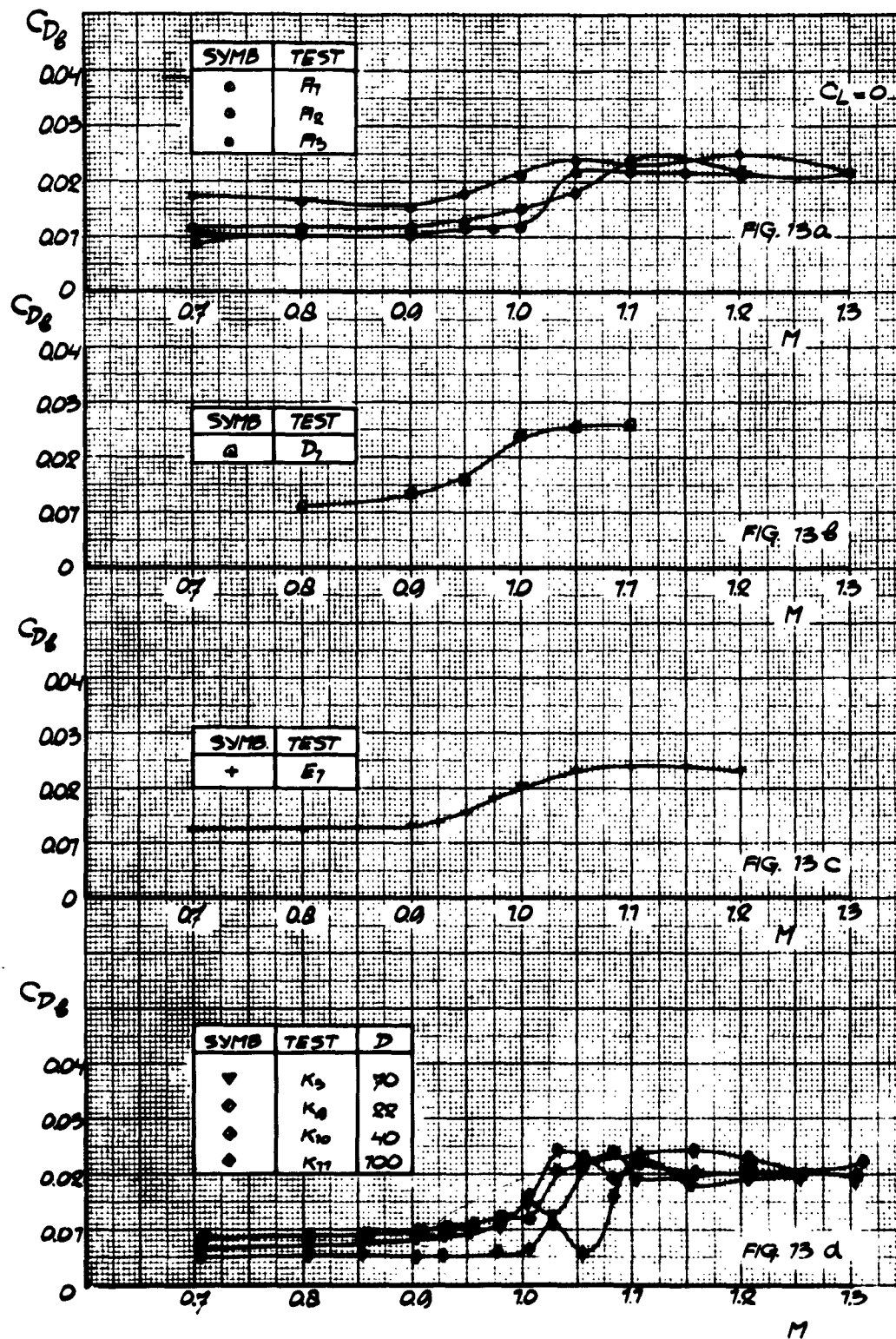


Fig.13 Presentation of base drag data

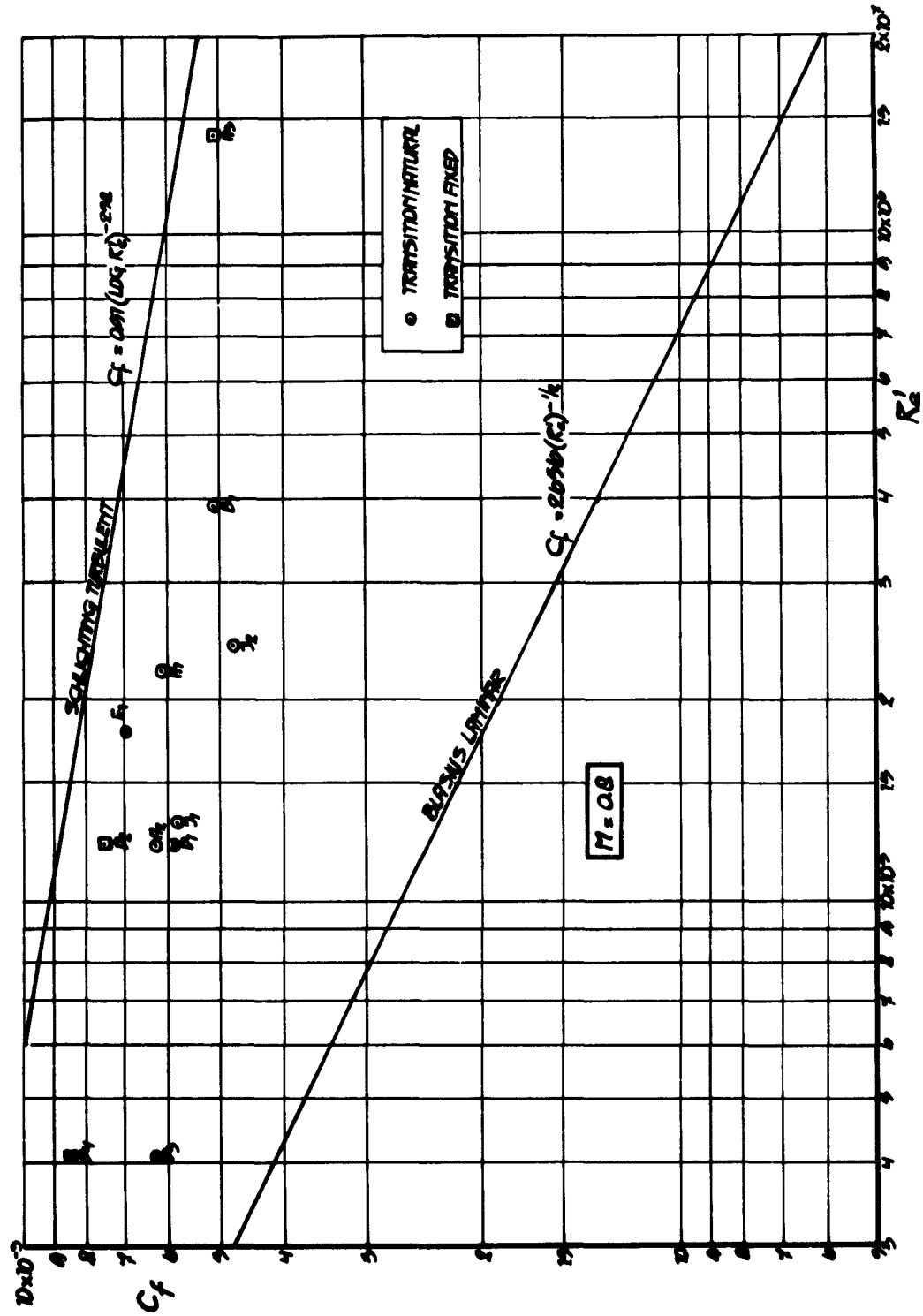


Fig. 14a Skin friction drag at $M = 0.8$ as a function of Reynolds number, based on c_{av} . Tests A1-J2

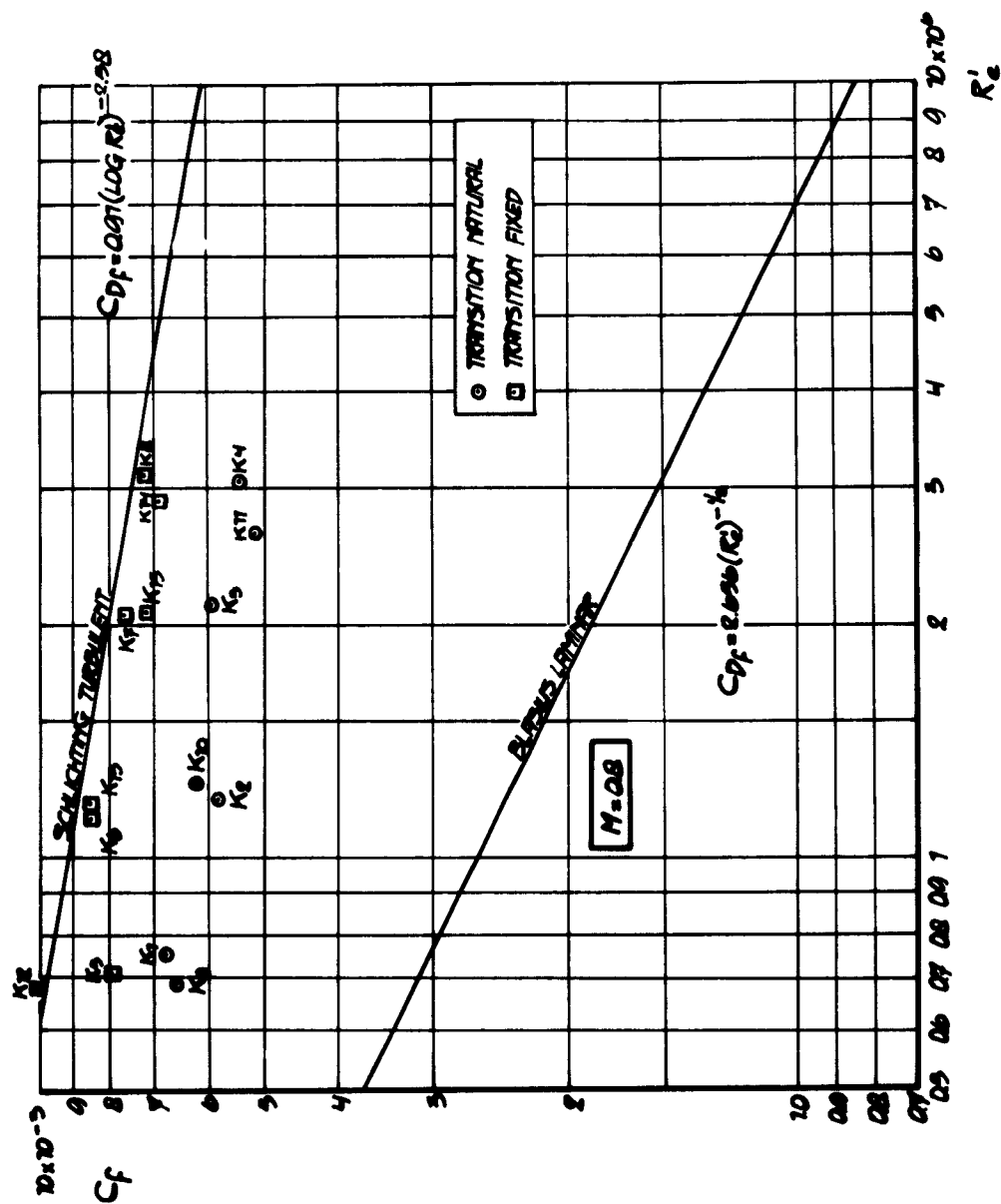


Fig. 14b Skin friction drag at $M = 0.8$ as a function of Reynolds number, based on C_{av} . Tests K1-K15

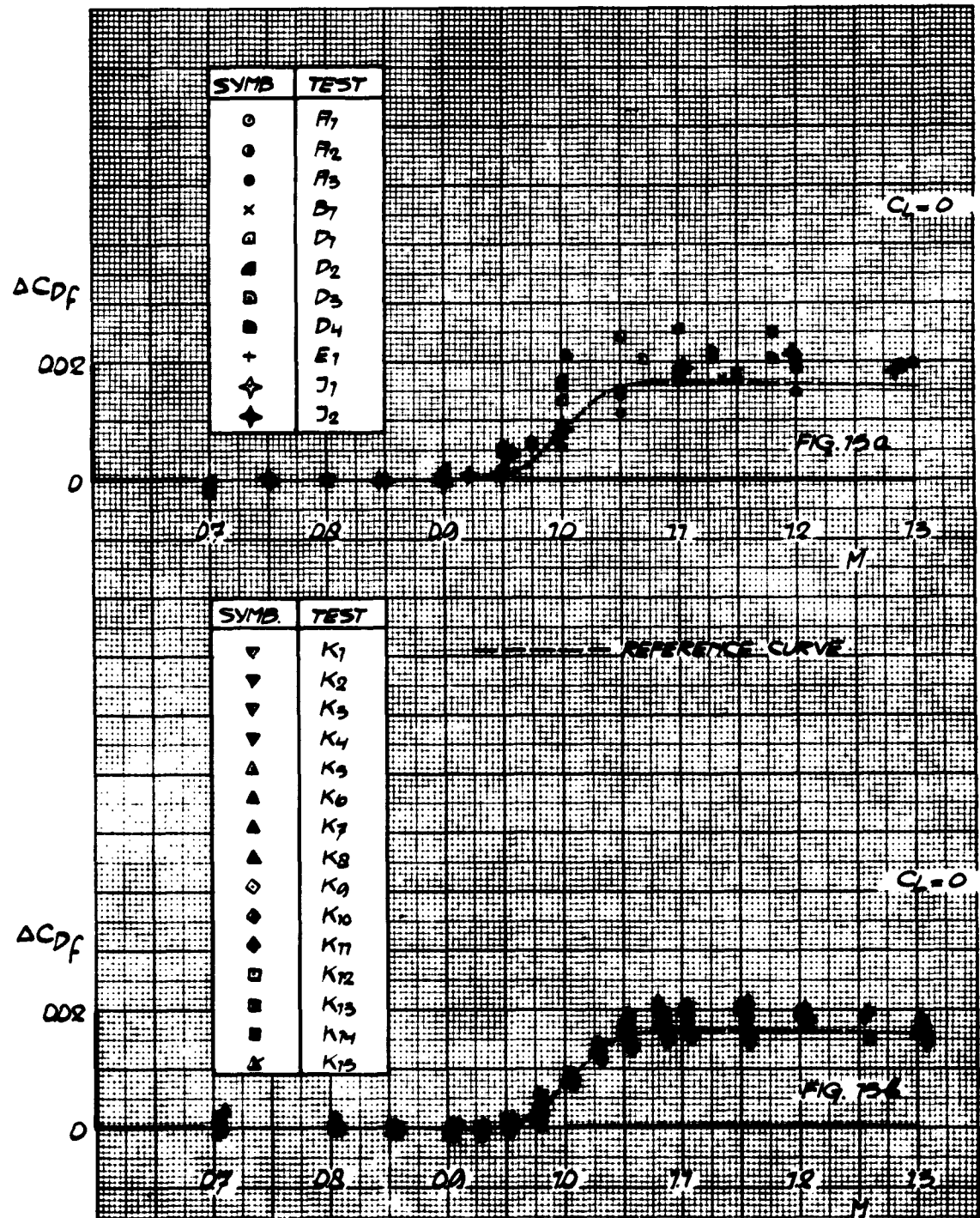


Fig.15 Transonic drag rise versus Mach number

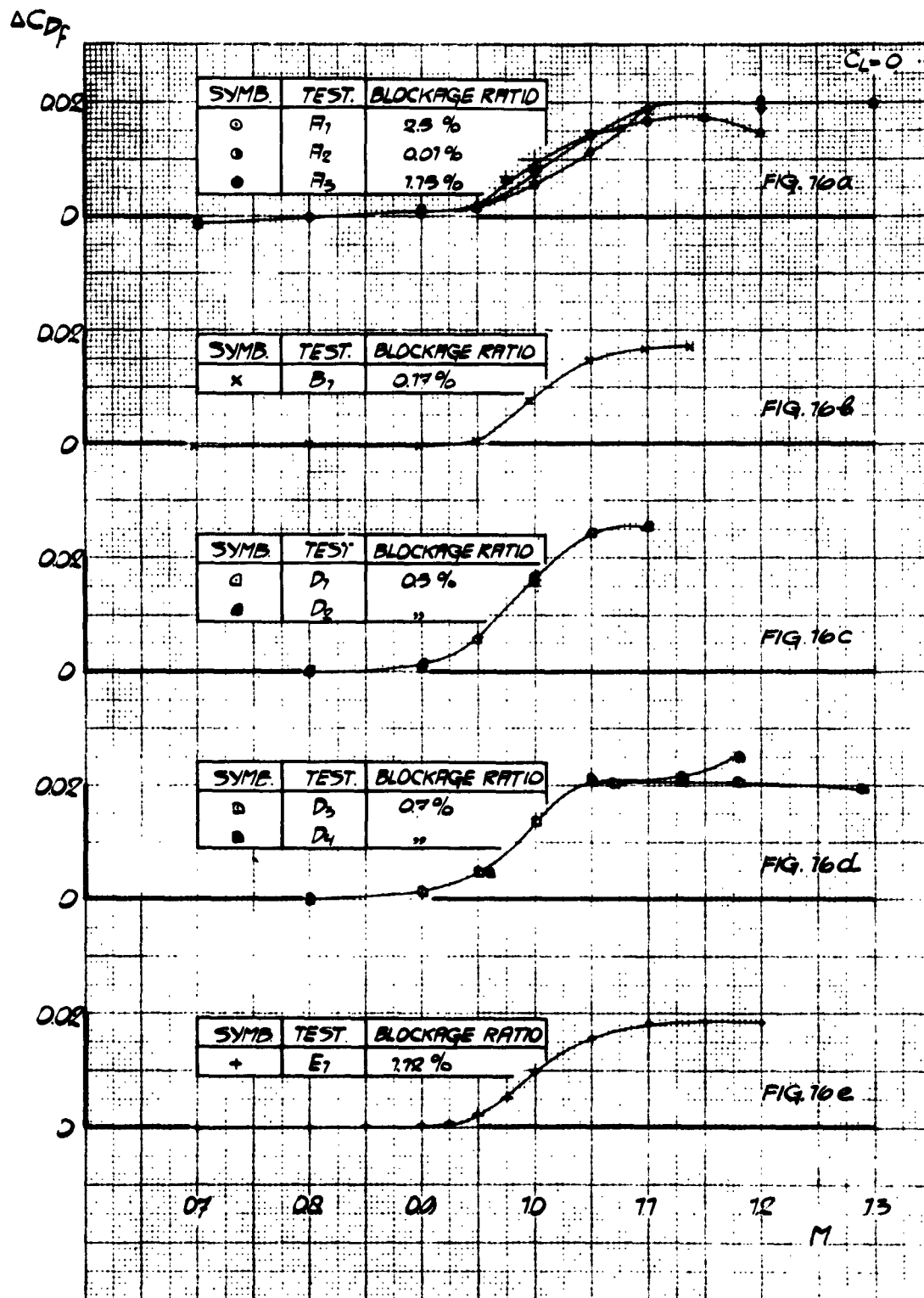


Fig.16 Presentation of transonic drag rise data

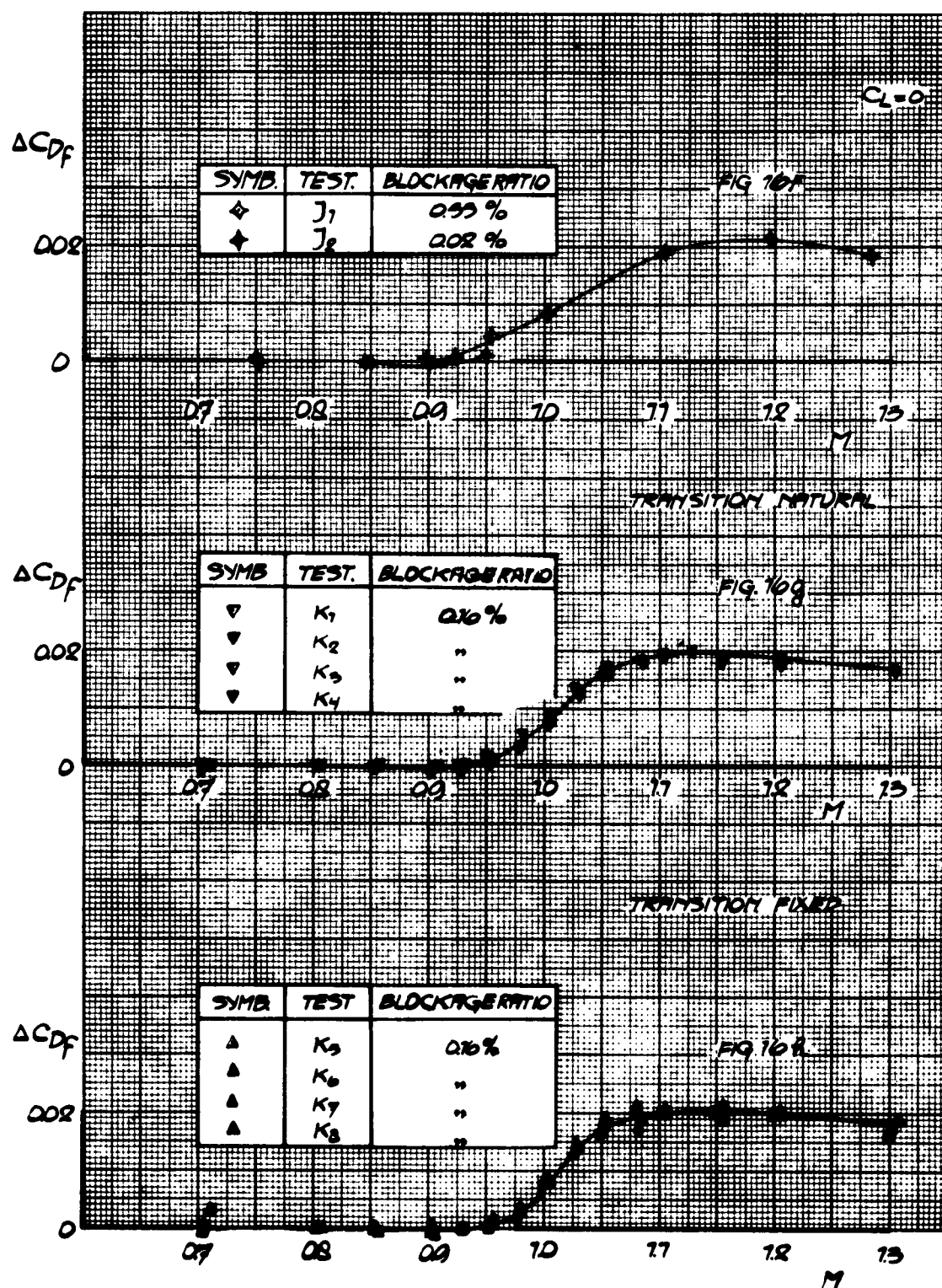


Fig.16 Presentation of transonic drag rise data (continued)

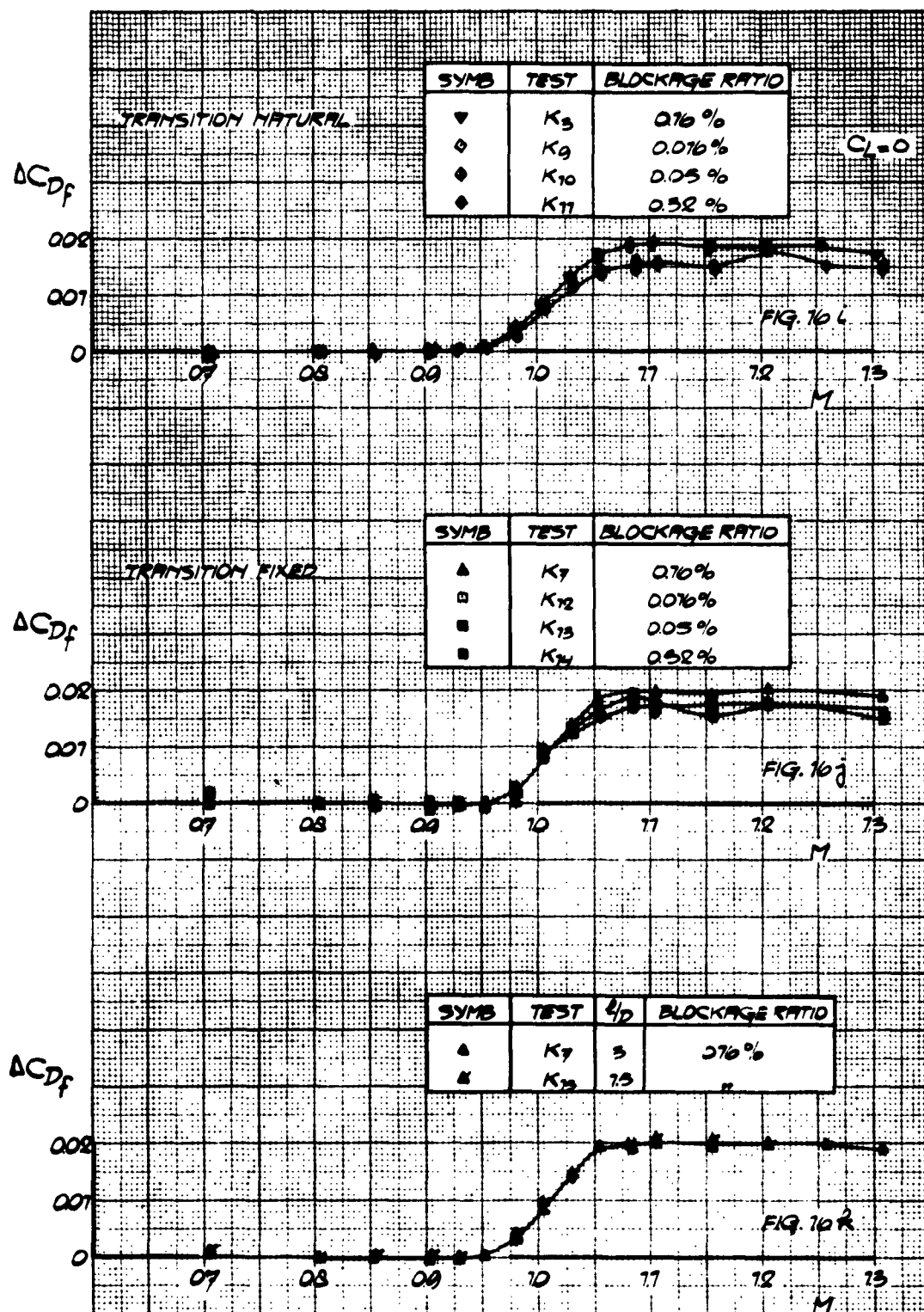


Fig.16 Presentation of transonic drag rise data (continued)

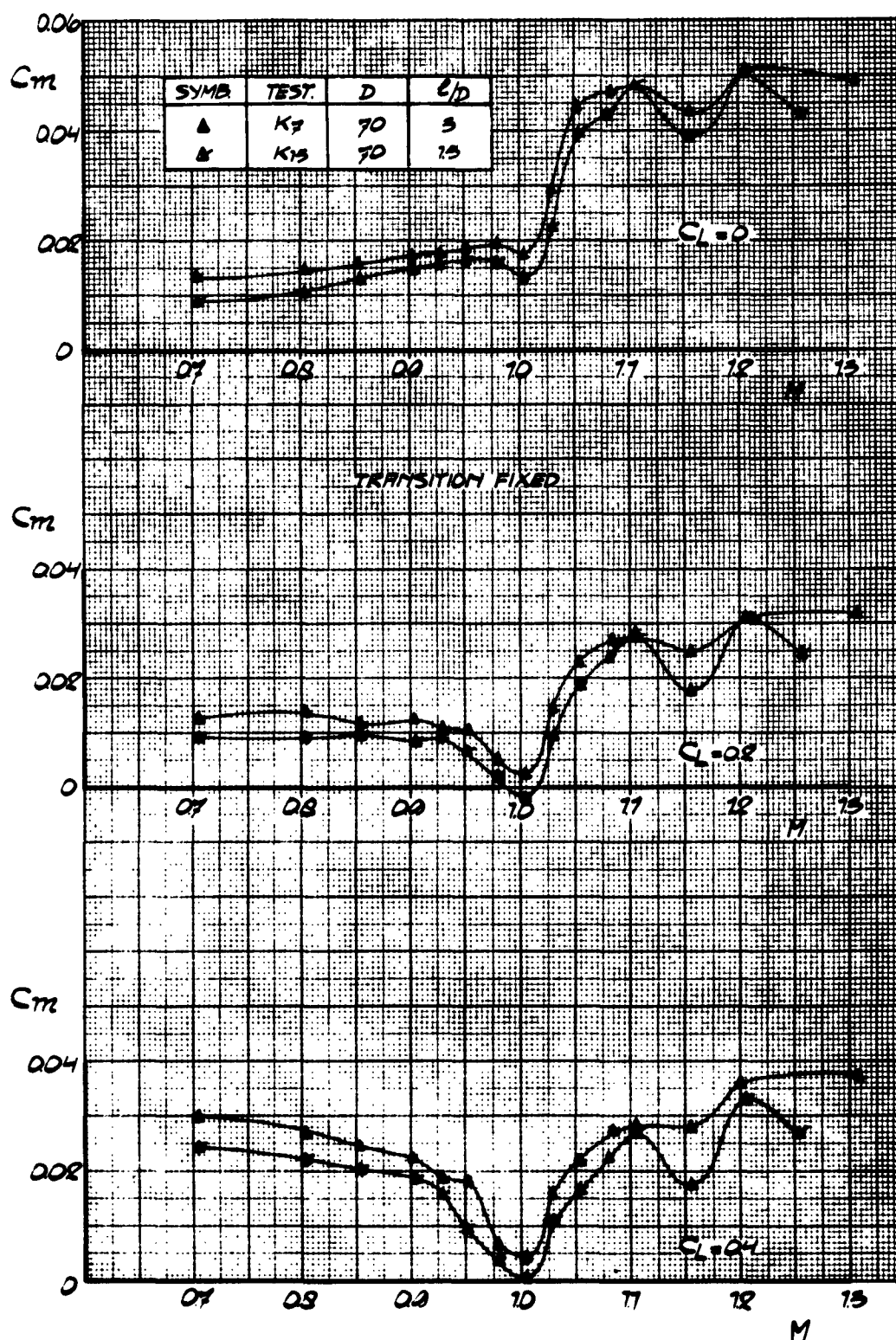


Fig.17 Moment coefficient versus Mach number for two different sting configurations

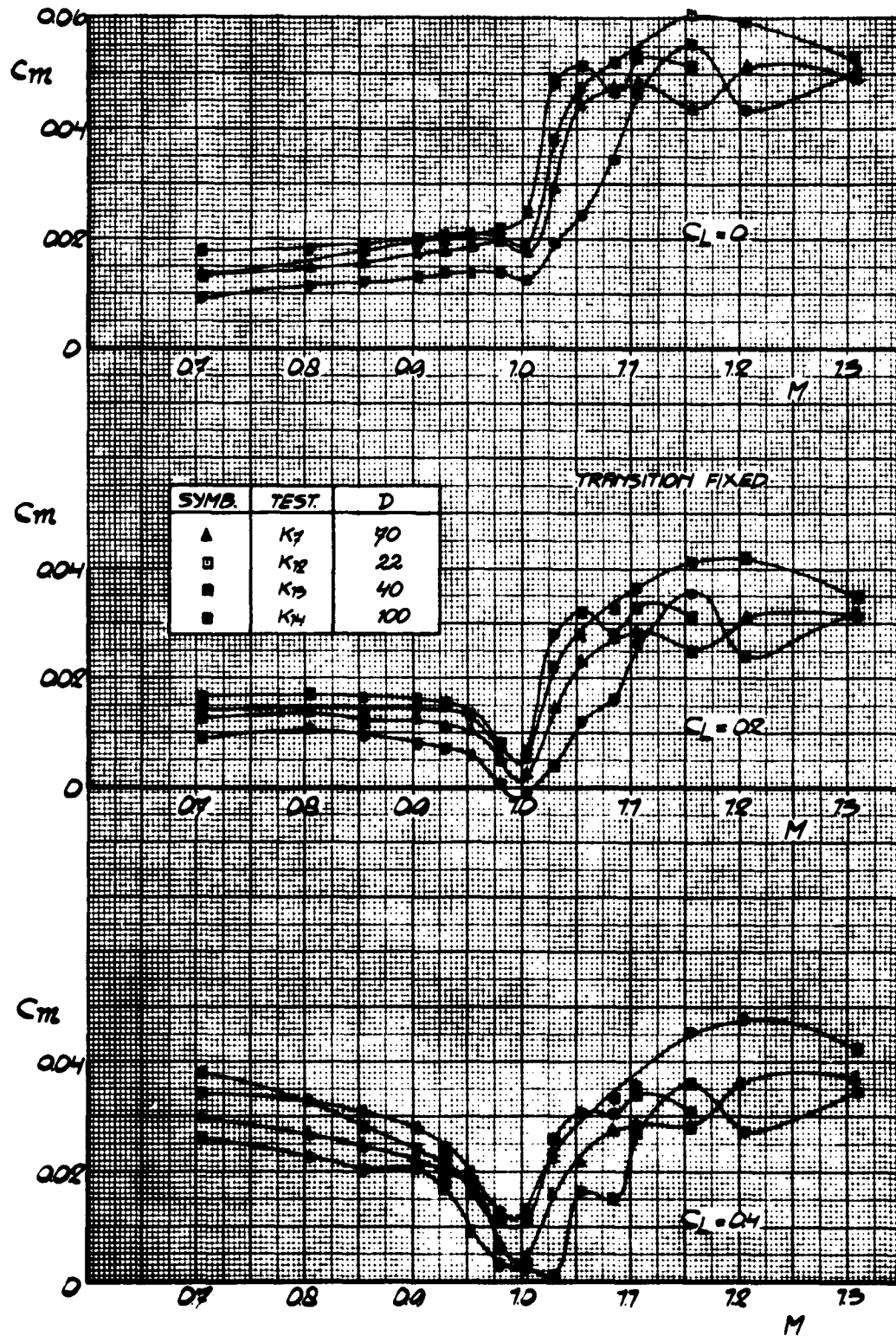


Fig.18 Moment coefficient versus Mach number for different model sizes (transition fixed)

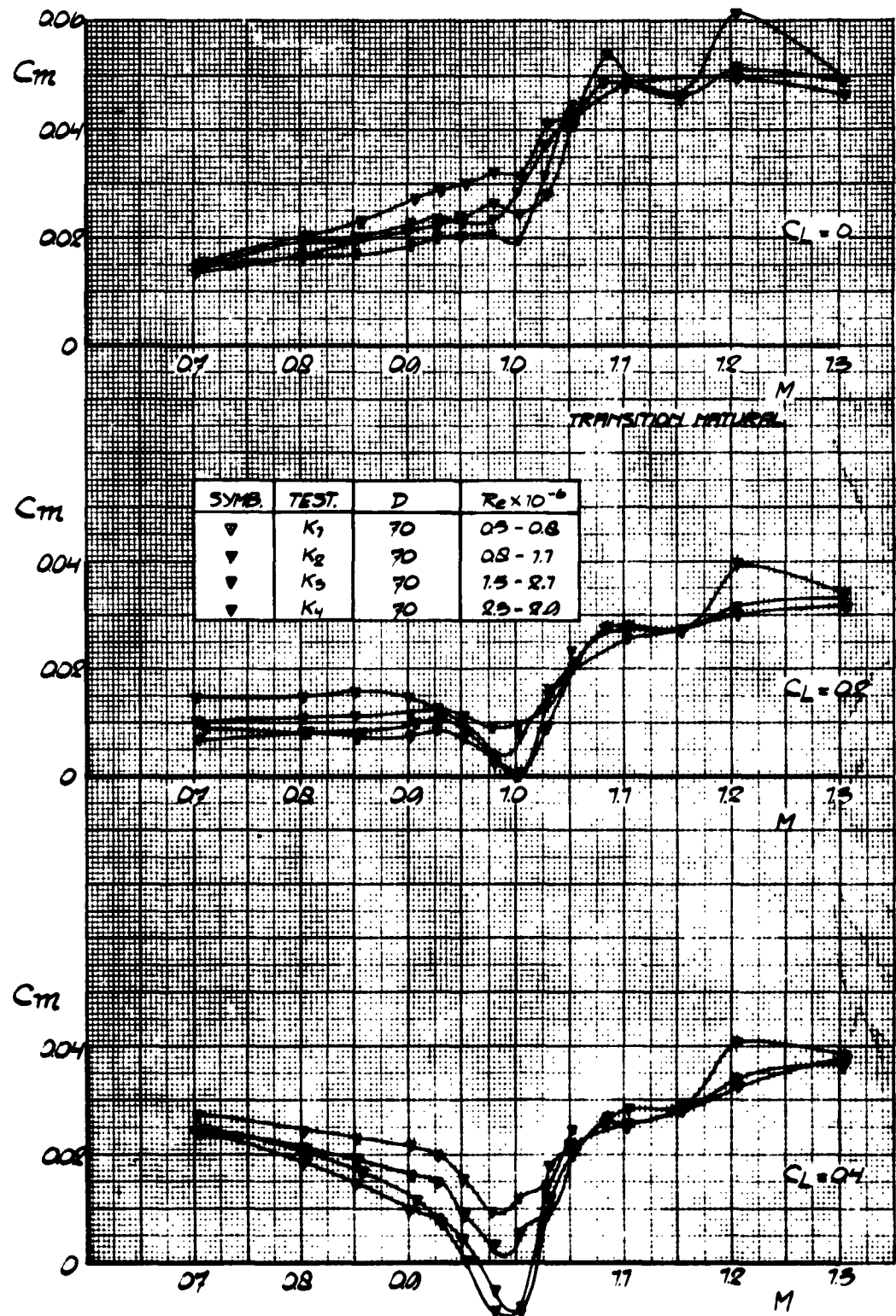


Fig. 19a Moment coefficient versus Mach number at different Reynolds numbers (transition natural)

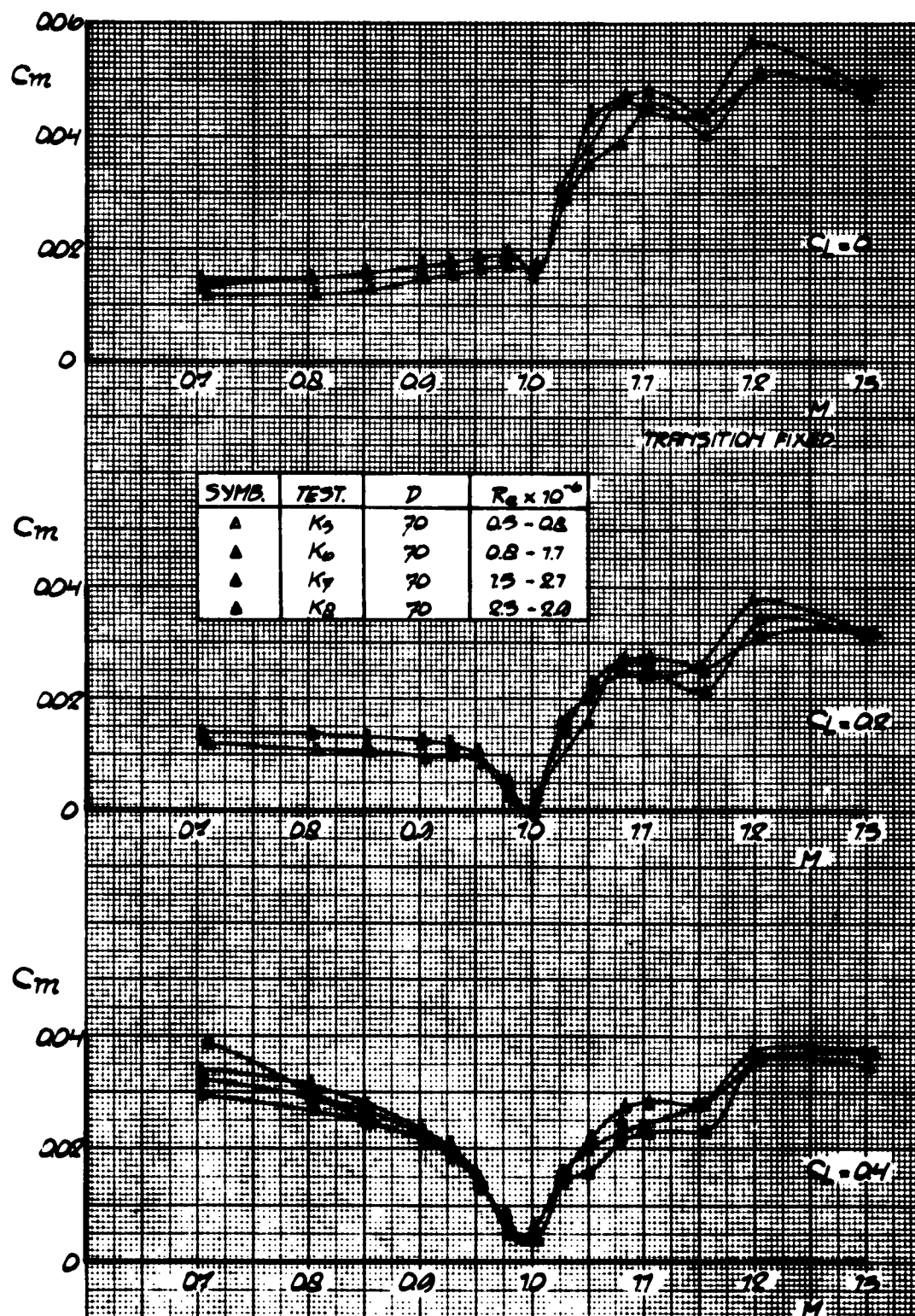


Fig. 19b Moment coefficient versus Mach number at different Reynolds numbers (transition fixed)

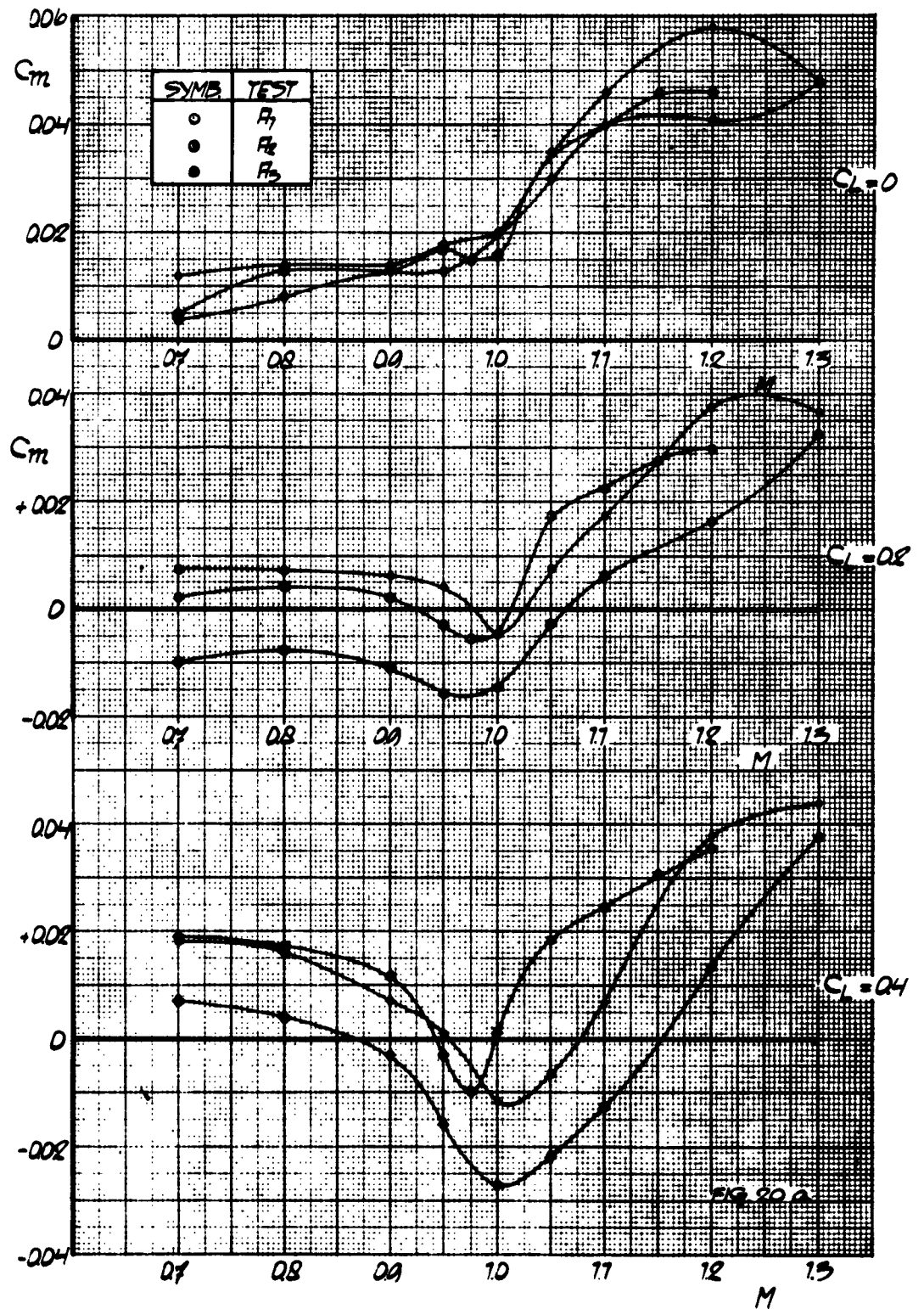


Fig. 20a Presentation of moment data

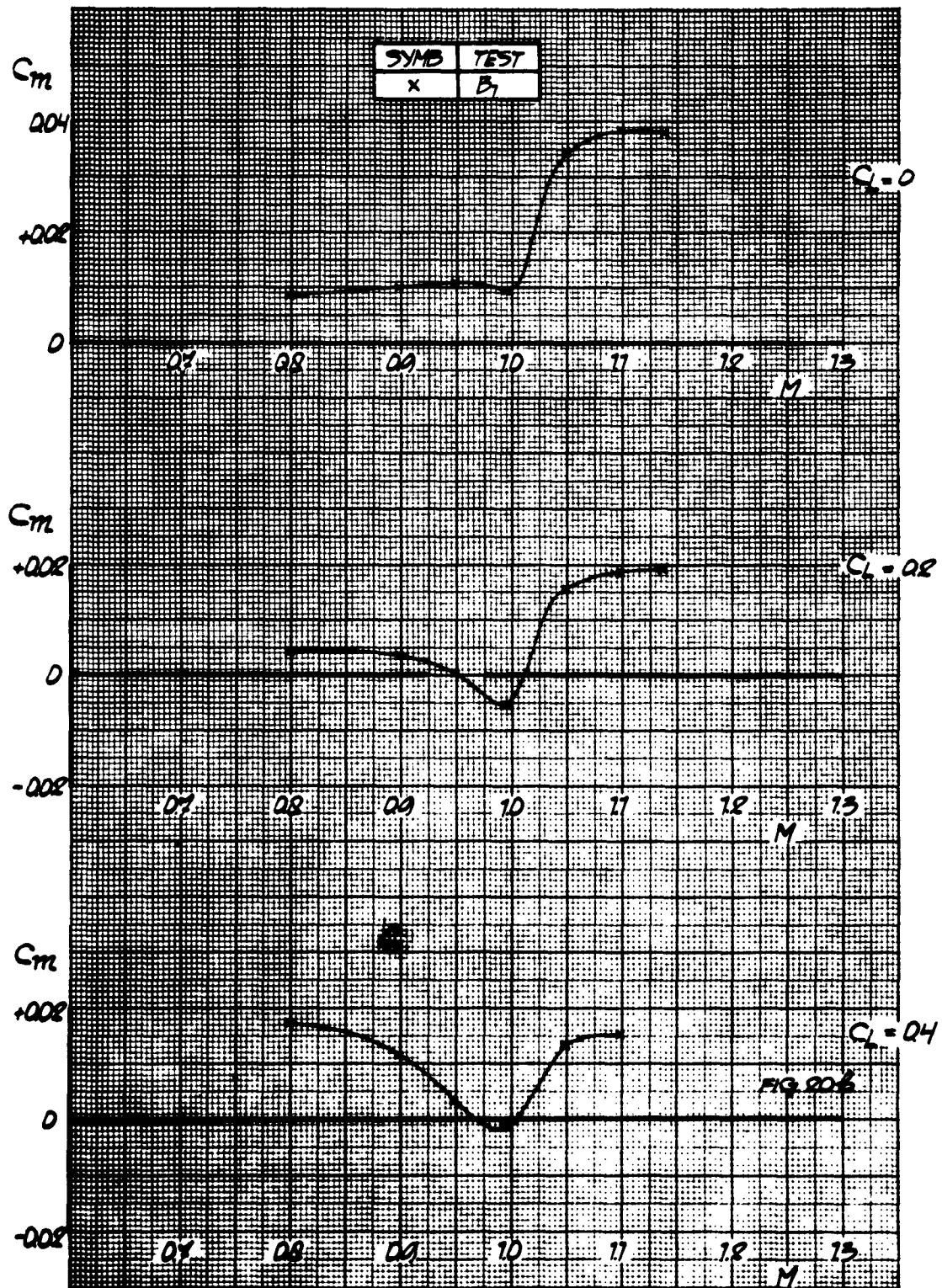


Fig.20b Presentation of moment data (continued)

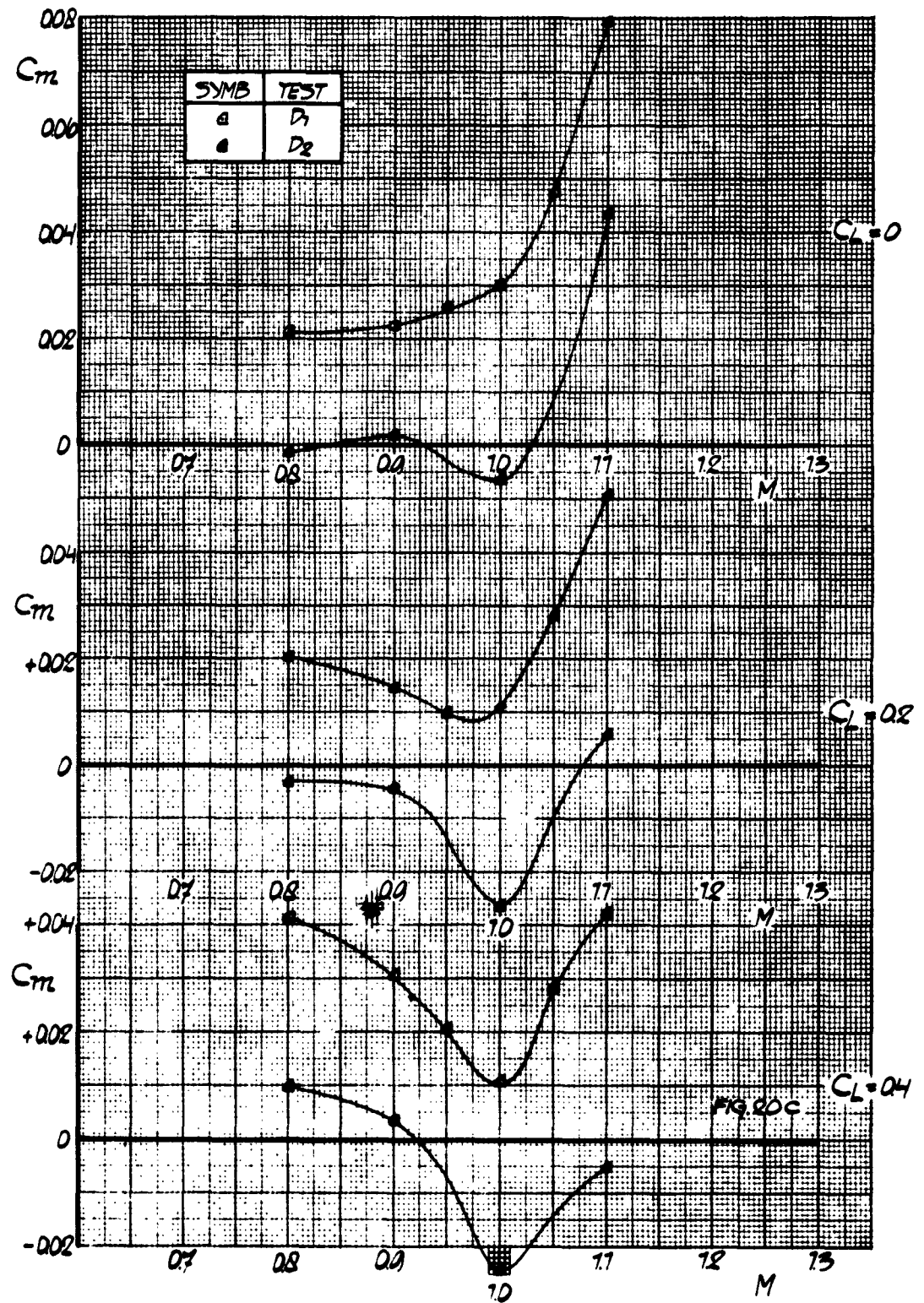


Fig. 20c Presentation of moment data (continued)

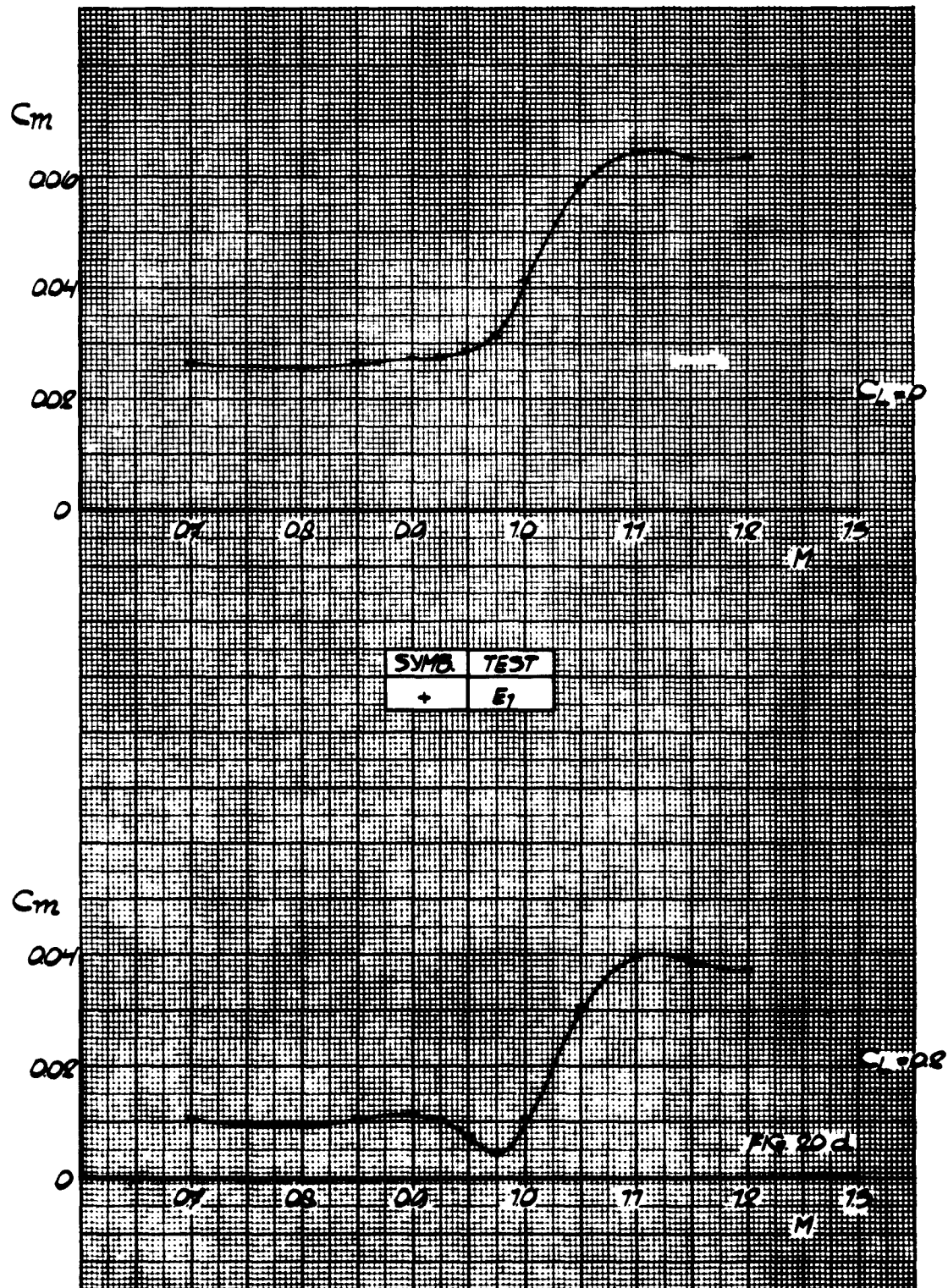


Fig. 20d Presentation of moment data (continued)

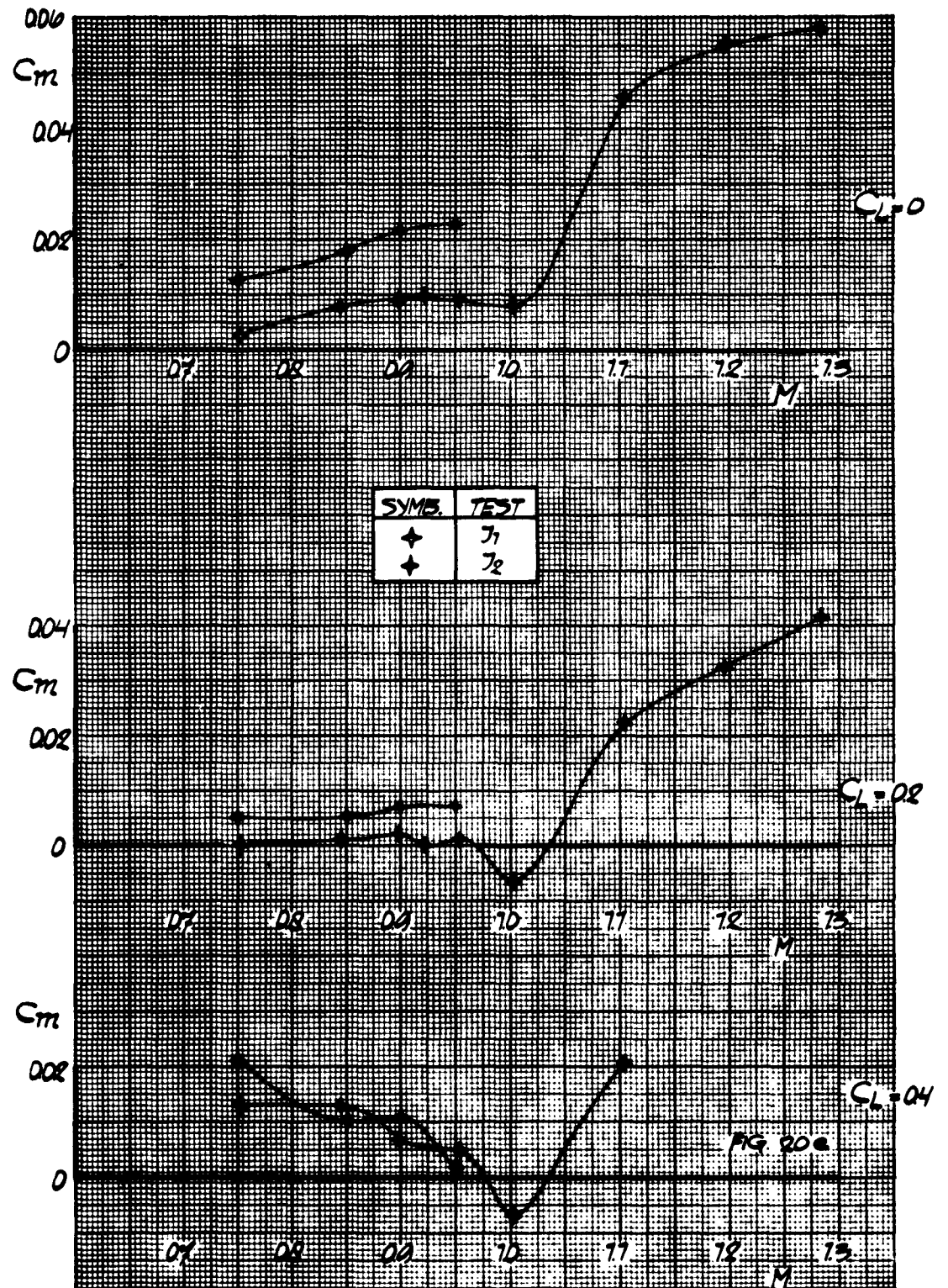


Fig. 20e Presentation of moment data (continued)

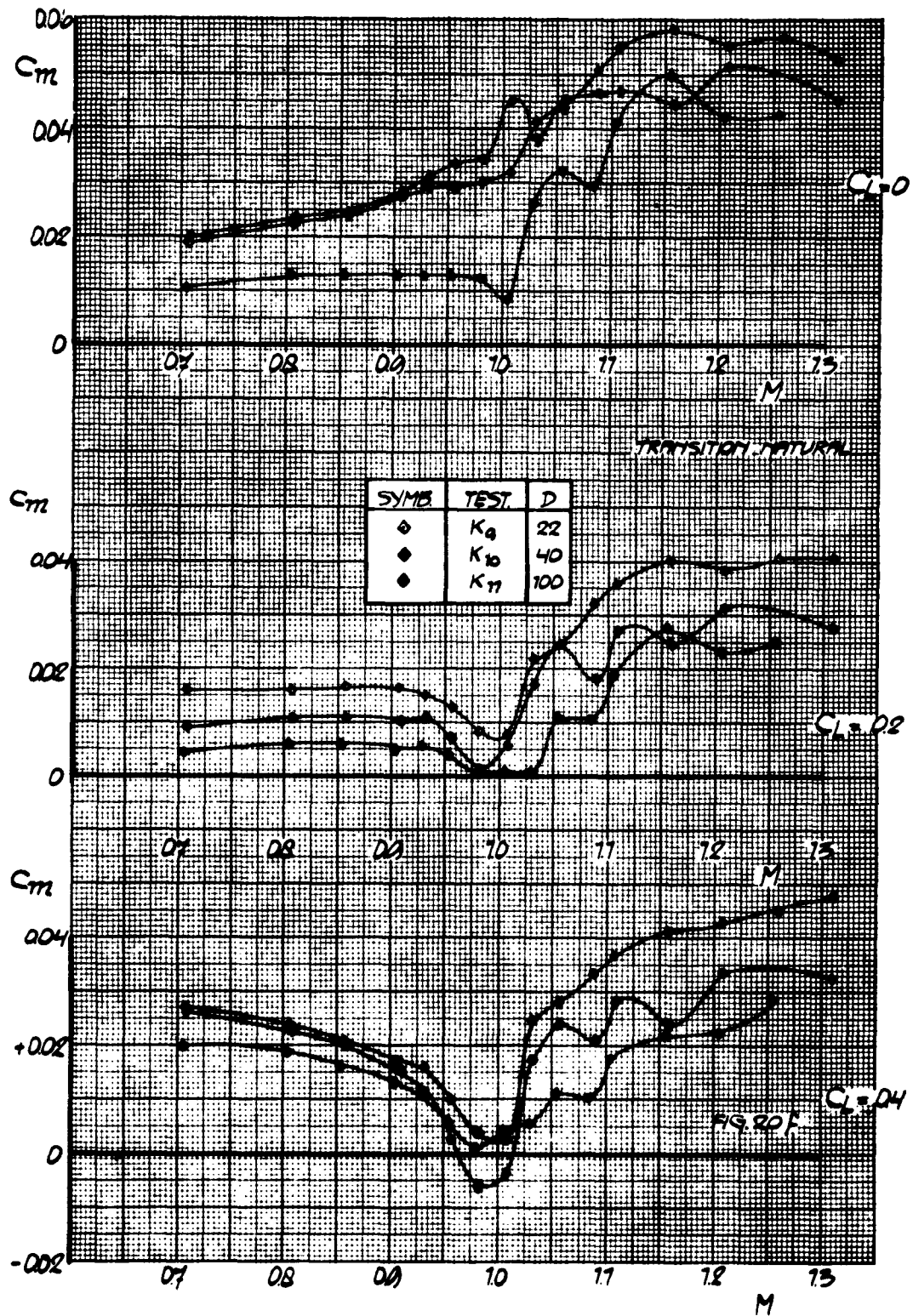


Fig. 20f Presentation of moment data (continued)

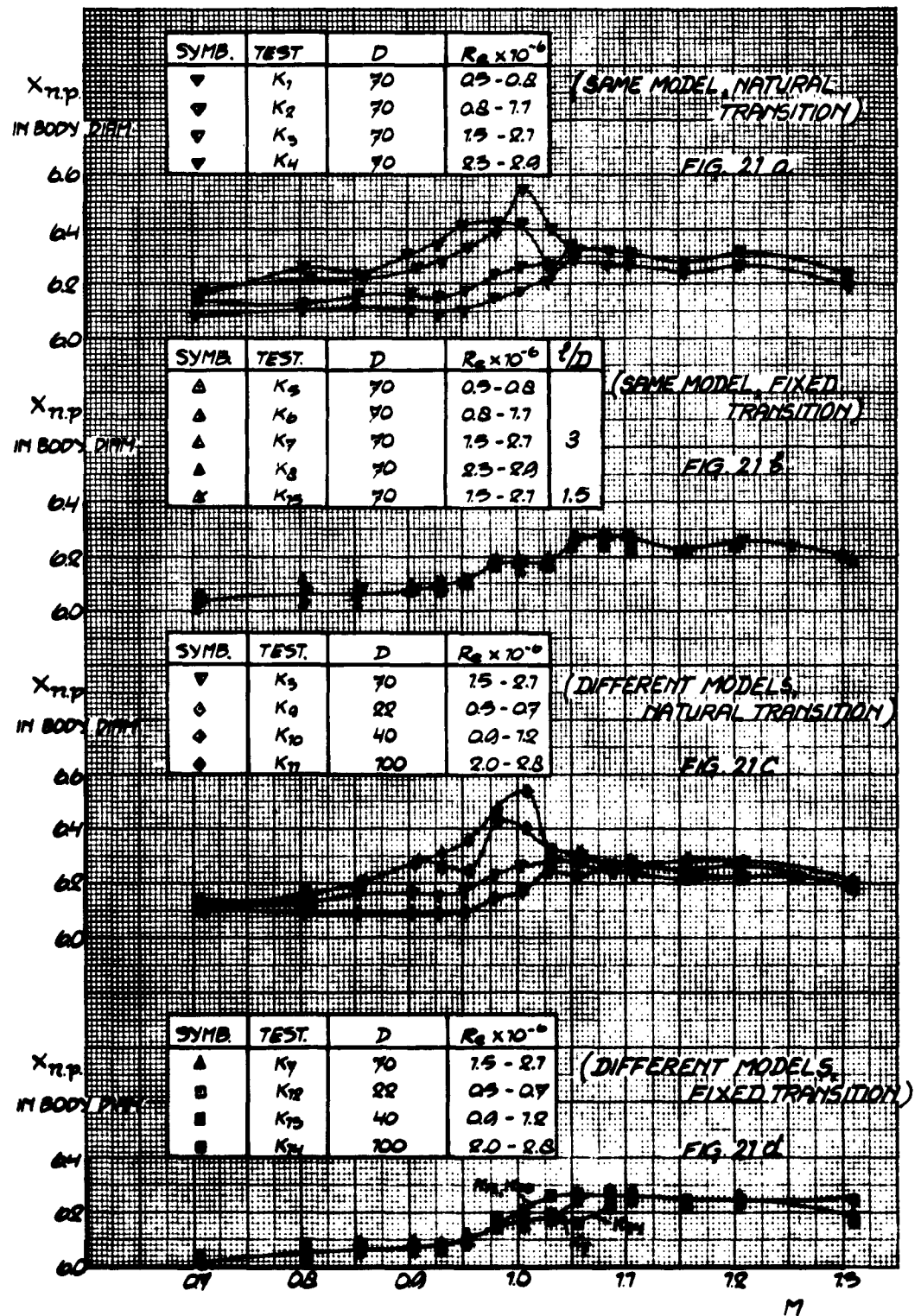


Fig. 21 Neutral point at $C_L = 0$ versus Mach number at different Reynolds numbers

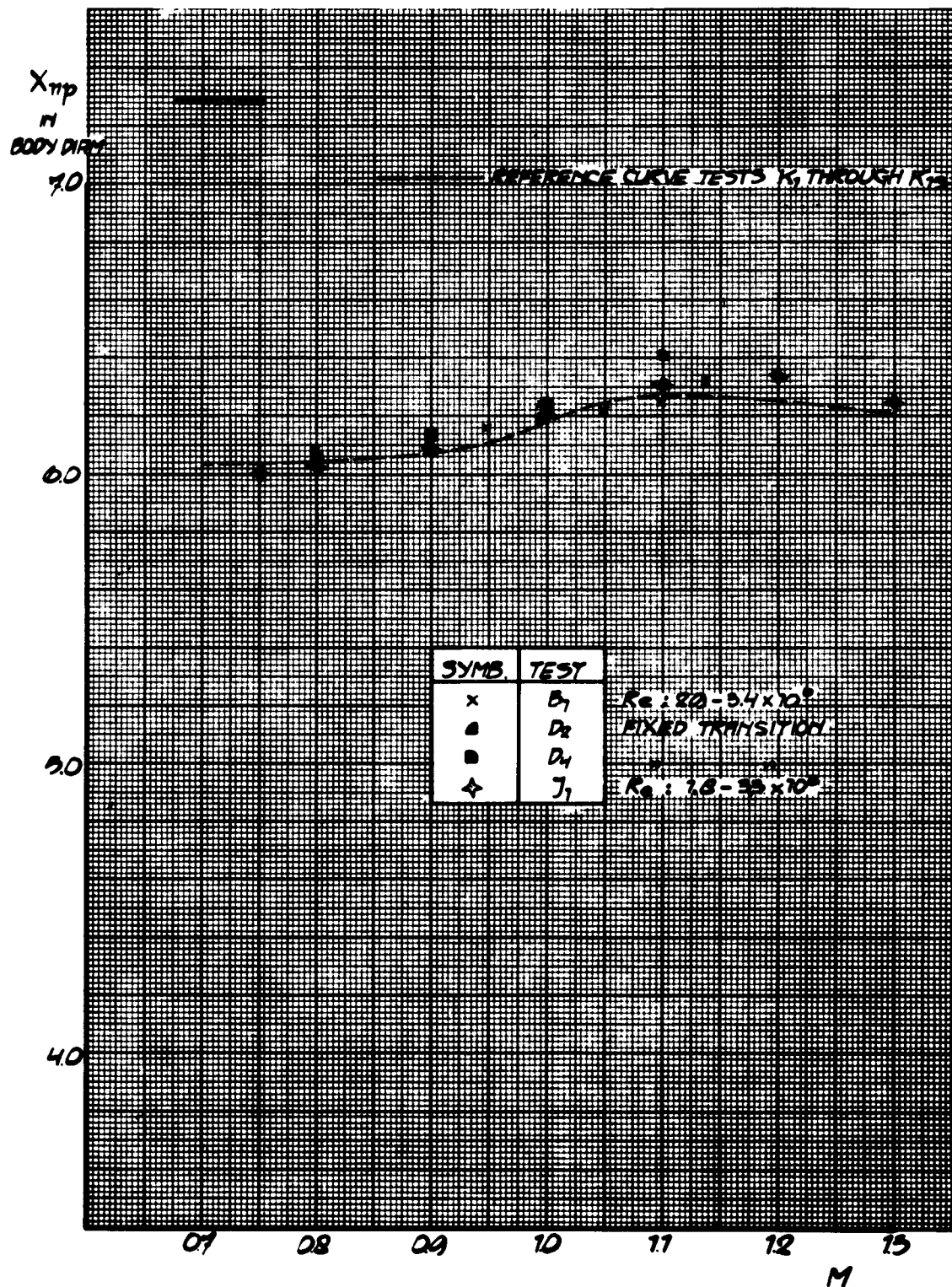


Fig. 22 Comparison of neutral point data of tests B1, D2, D4 and J1 and reference curve for K1-K15

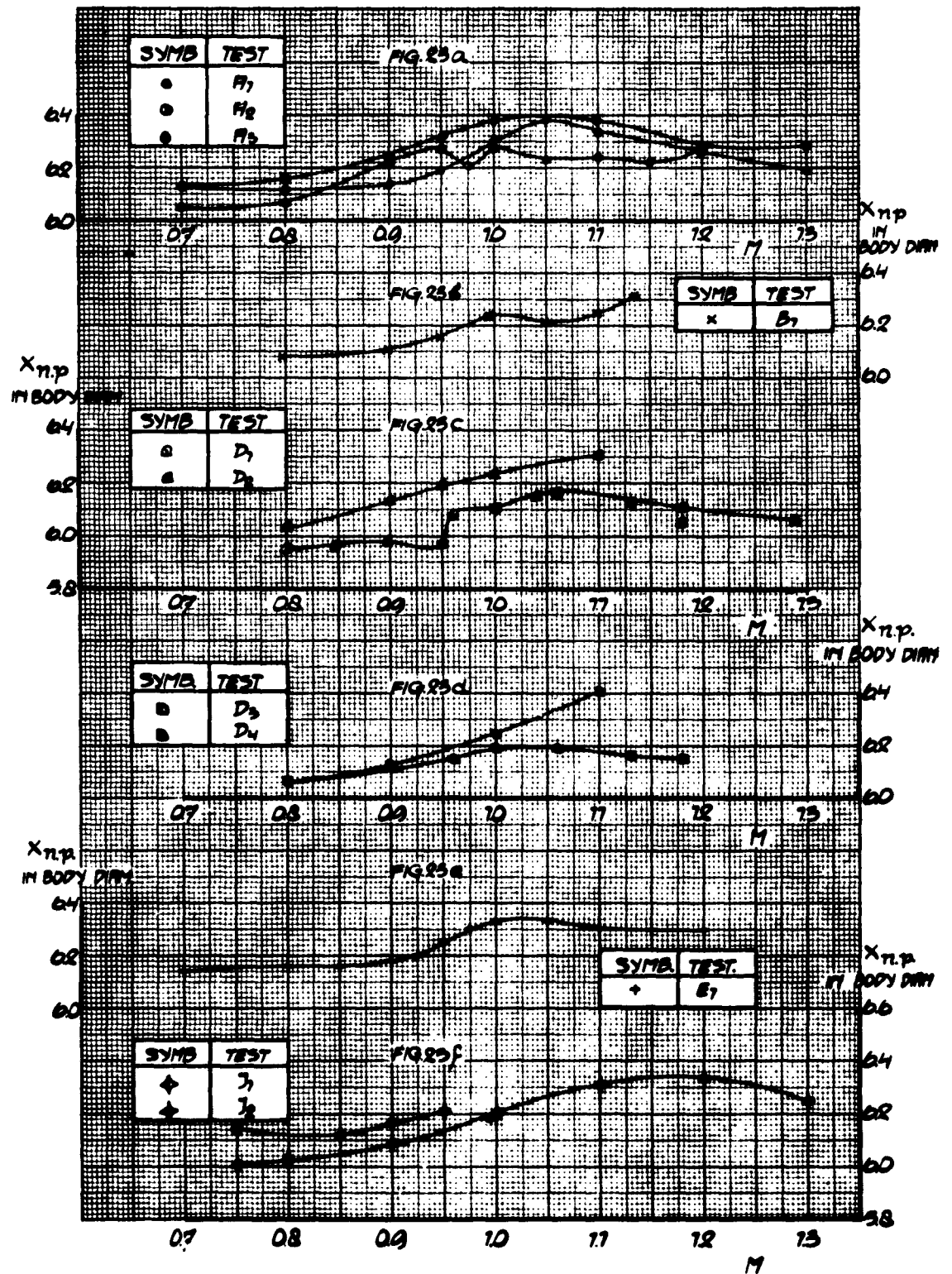


Fig.23 Presentation of neutral point data

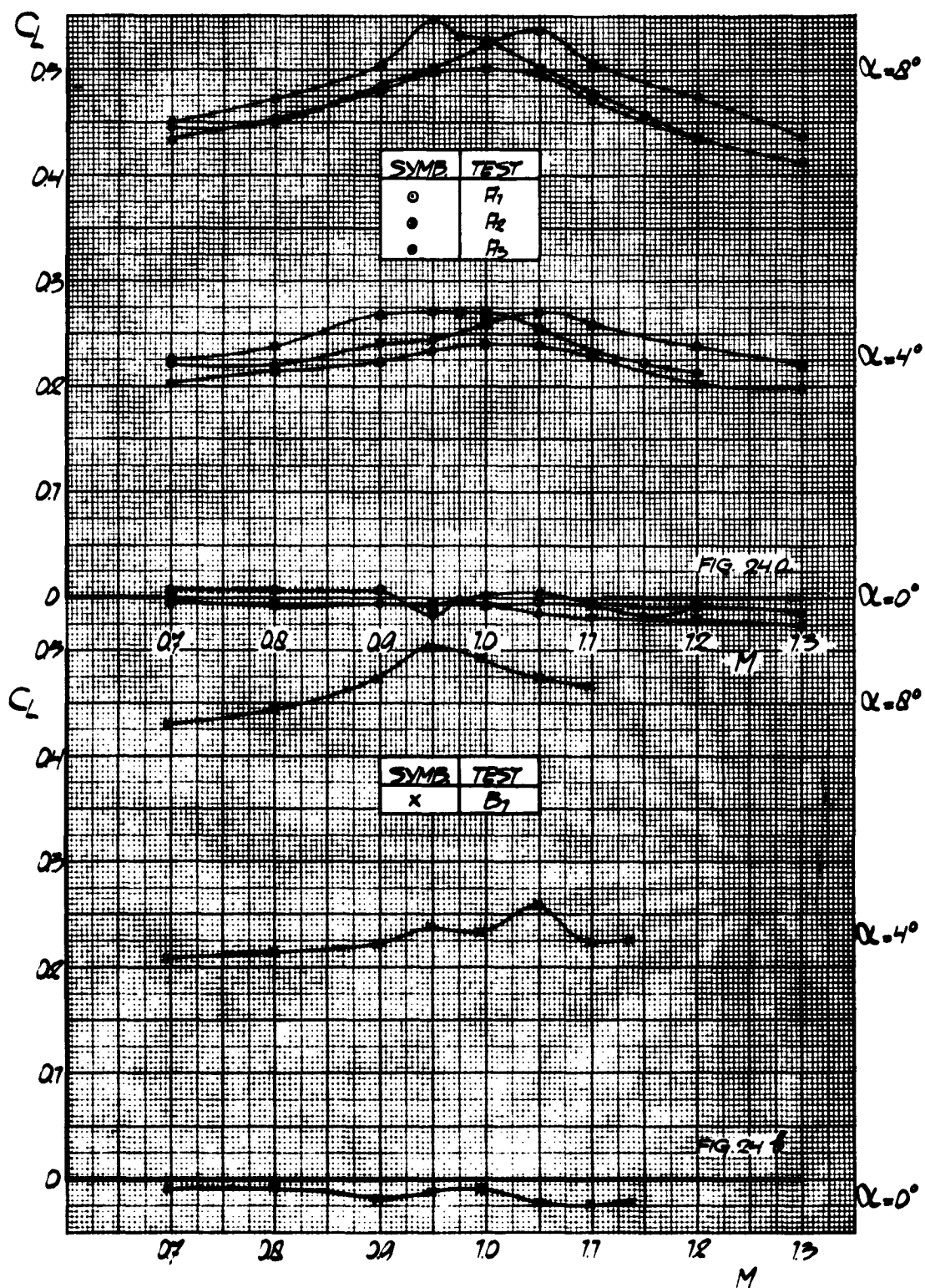


Fig. 24 Presentation of lift data

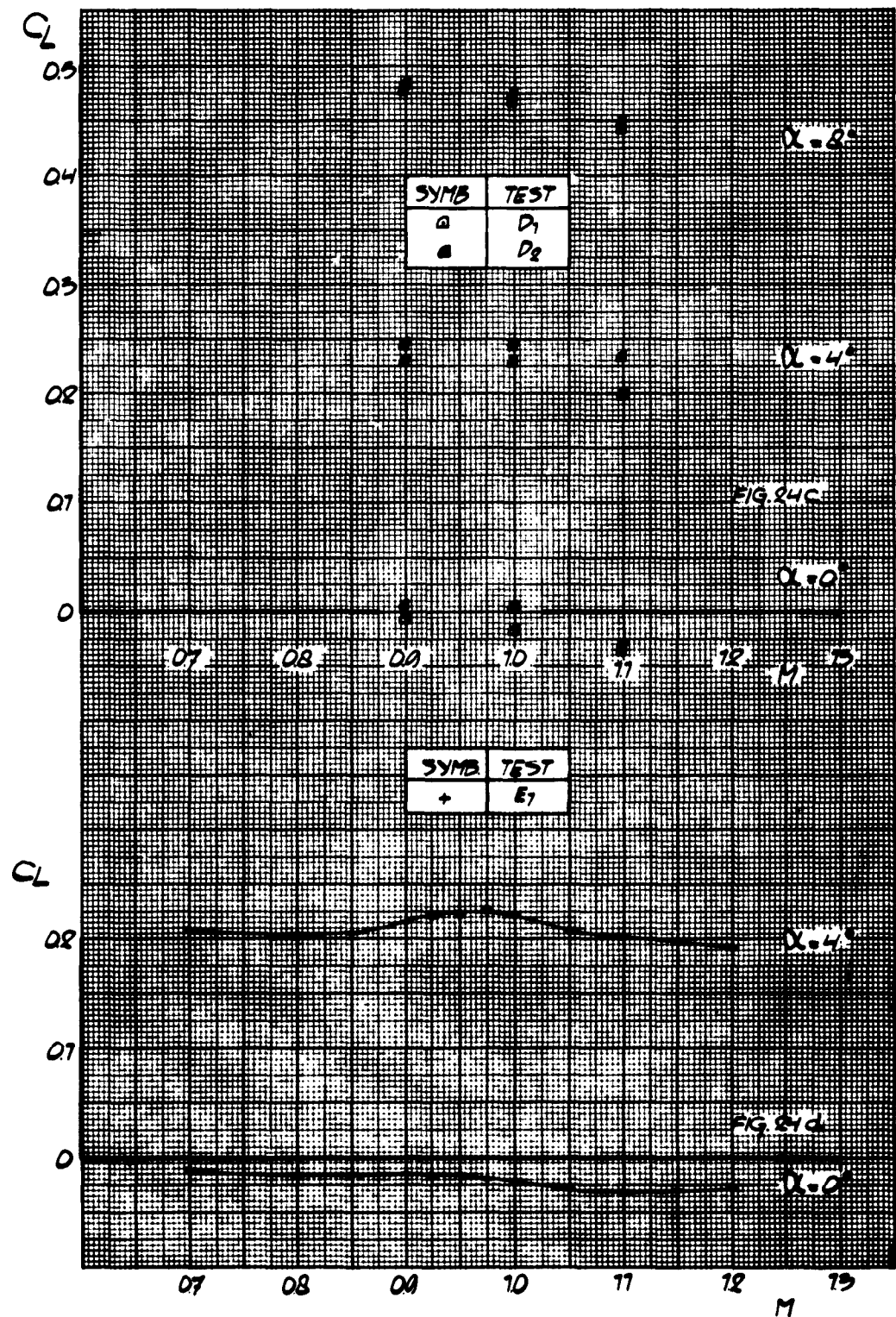


Fig.24 Presentation of lift data (continued)

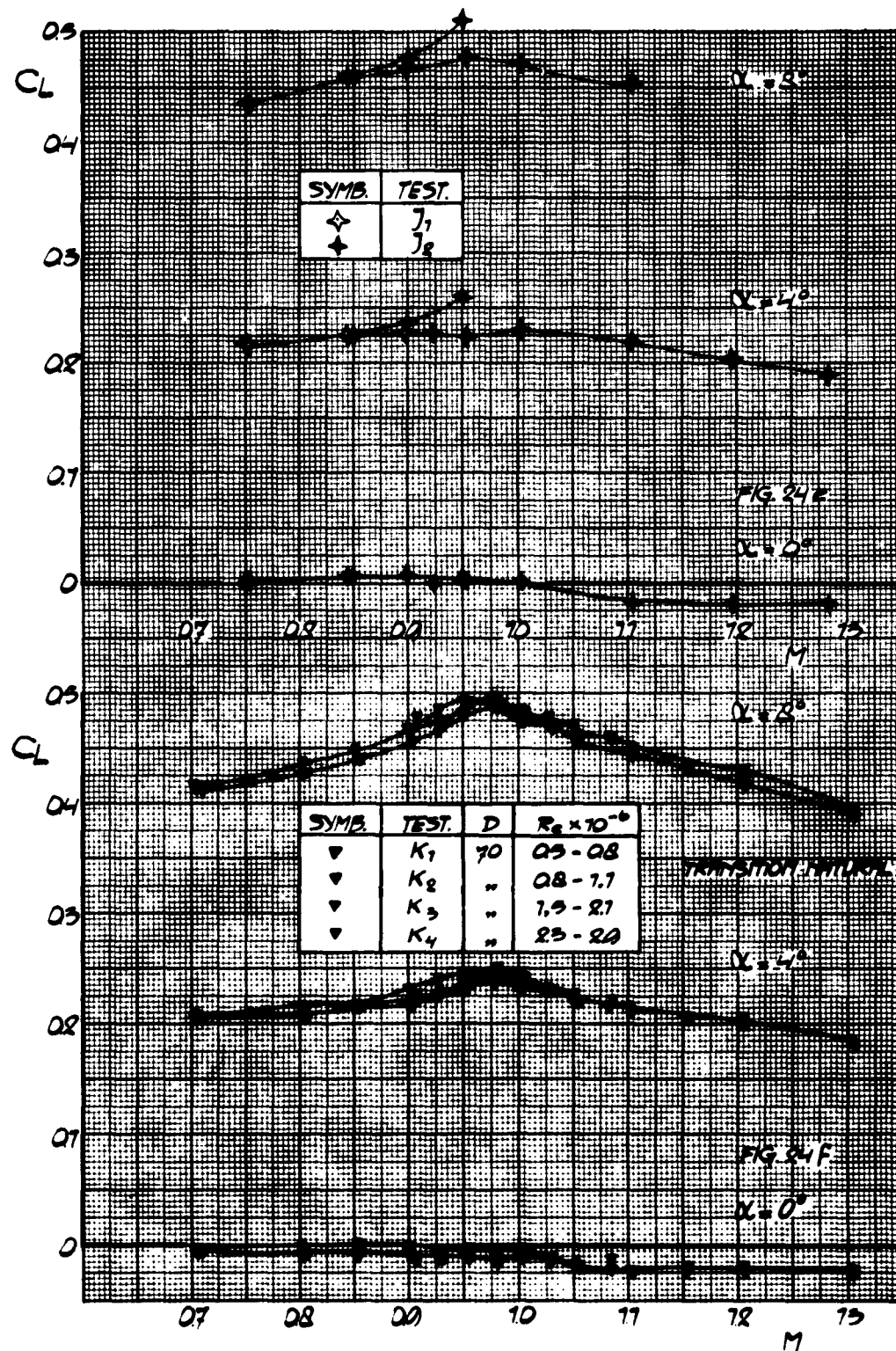


Fig 24 Presentation of lift data (continued)

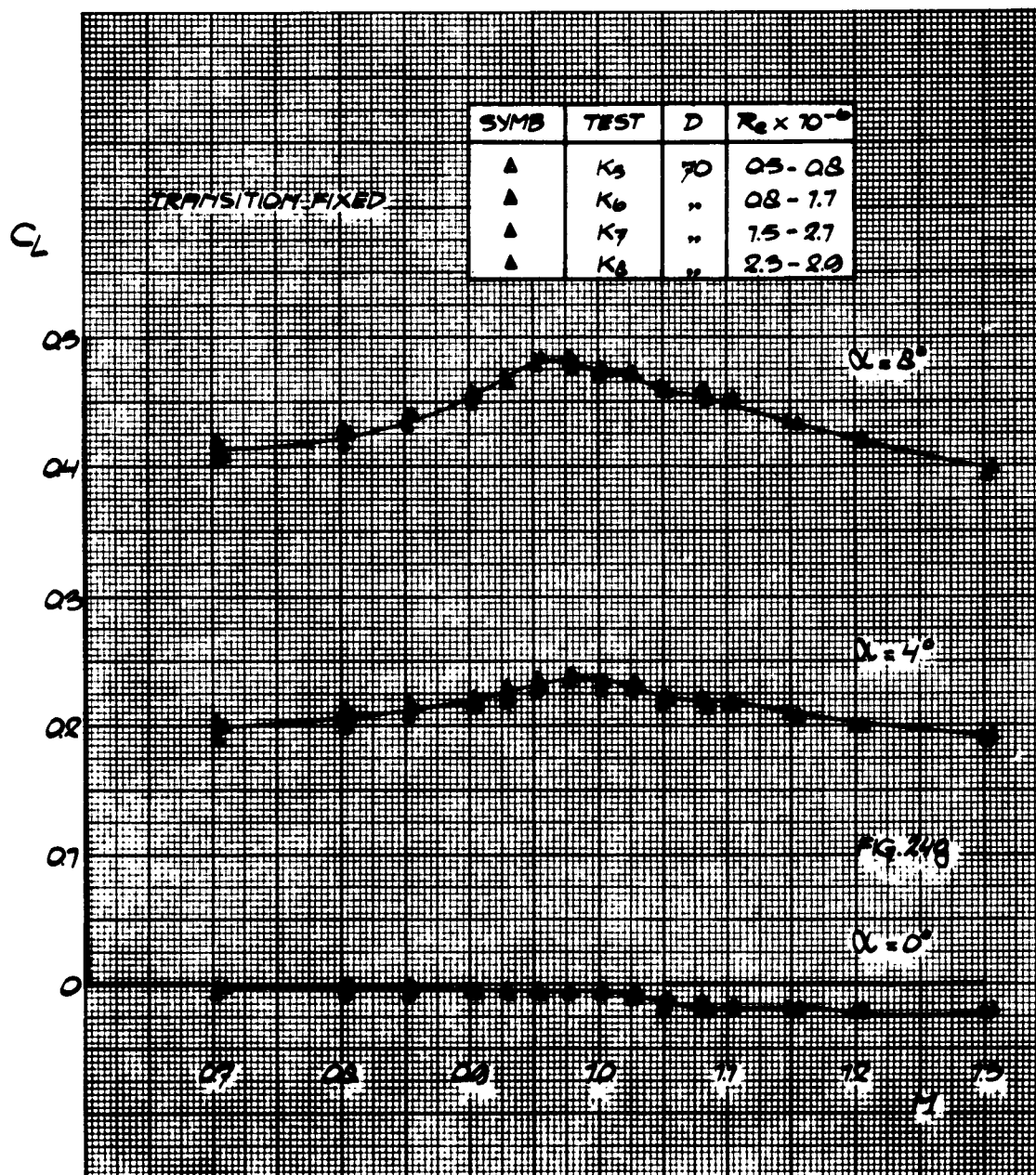


Fig. 24 Presentation of lift data (continued)

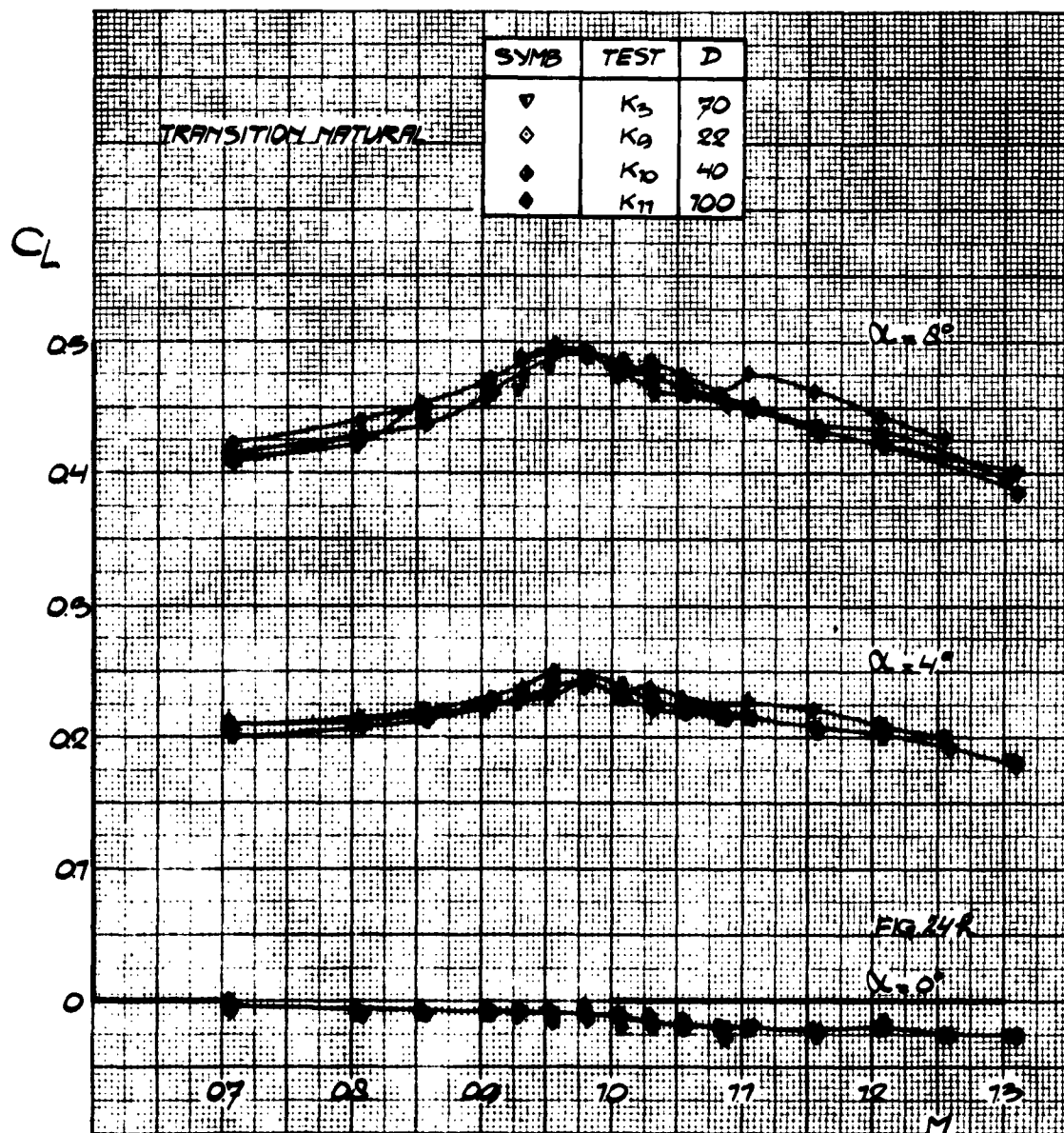


Fig.24 Presentation of lift data (continued)

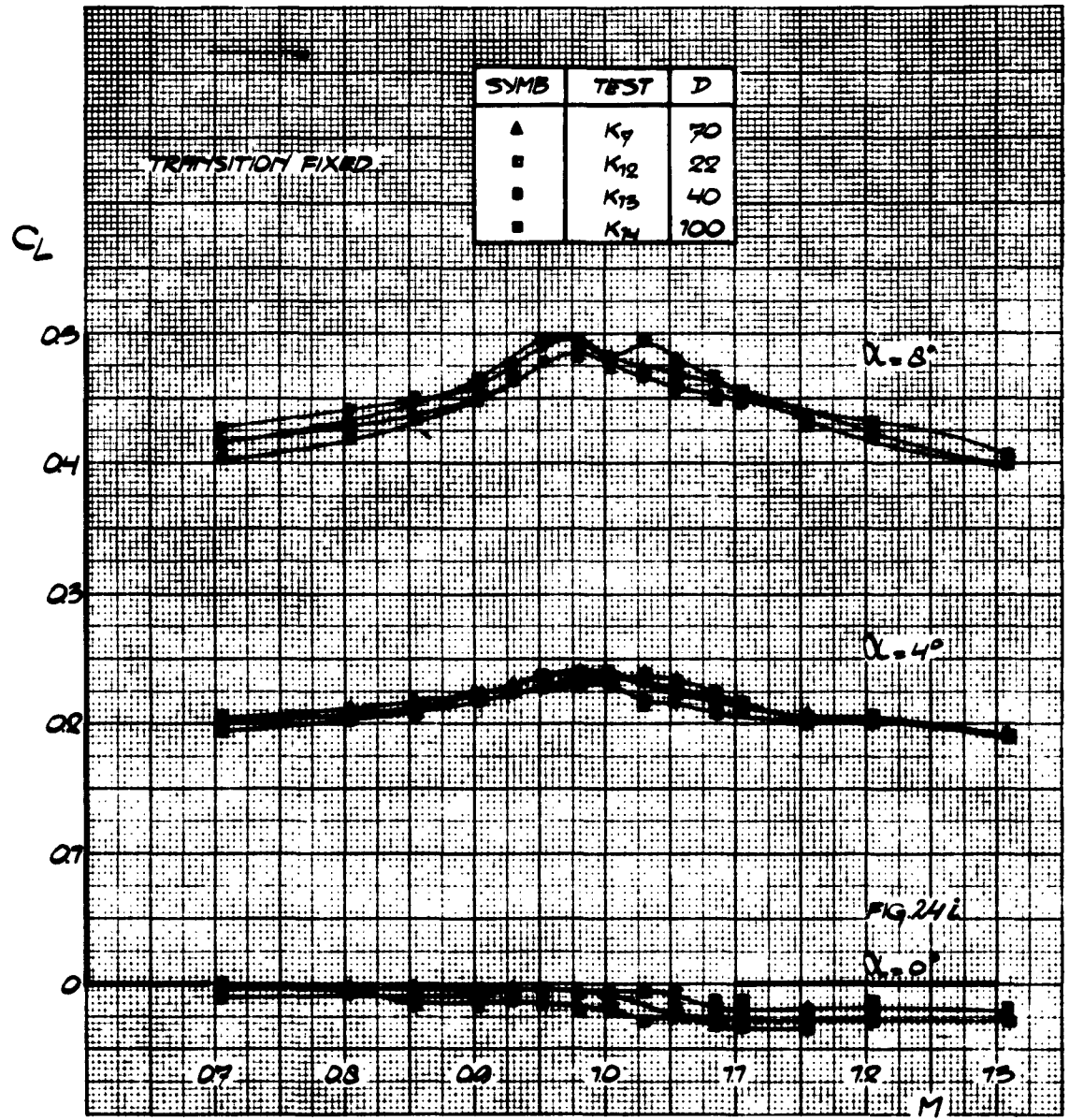


Fig.24 Presentation of lift data (continued)

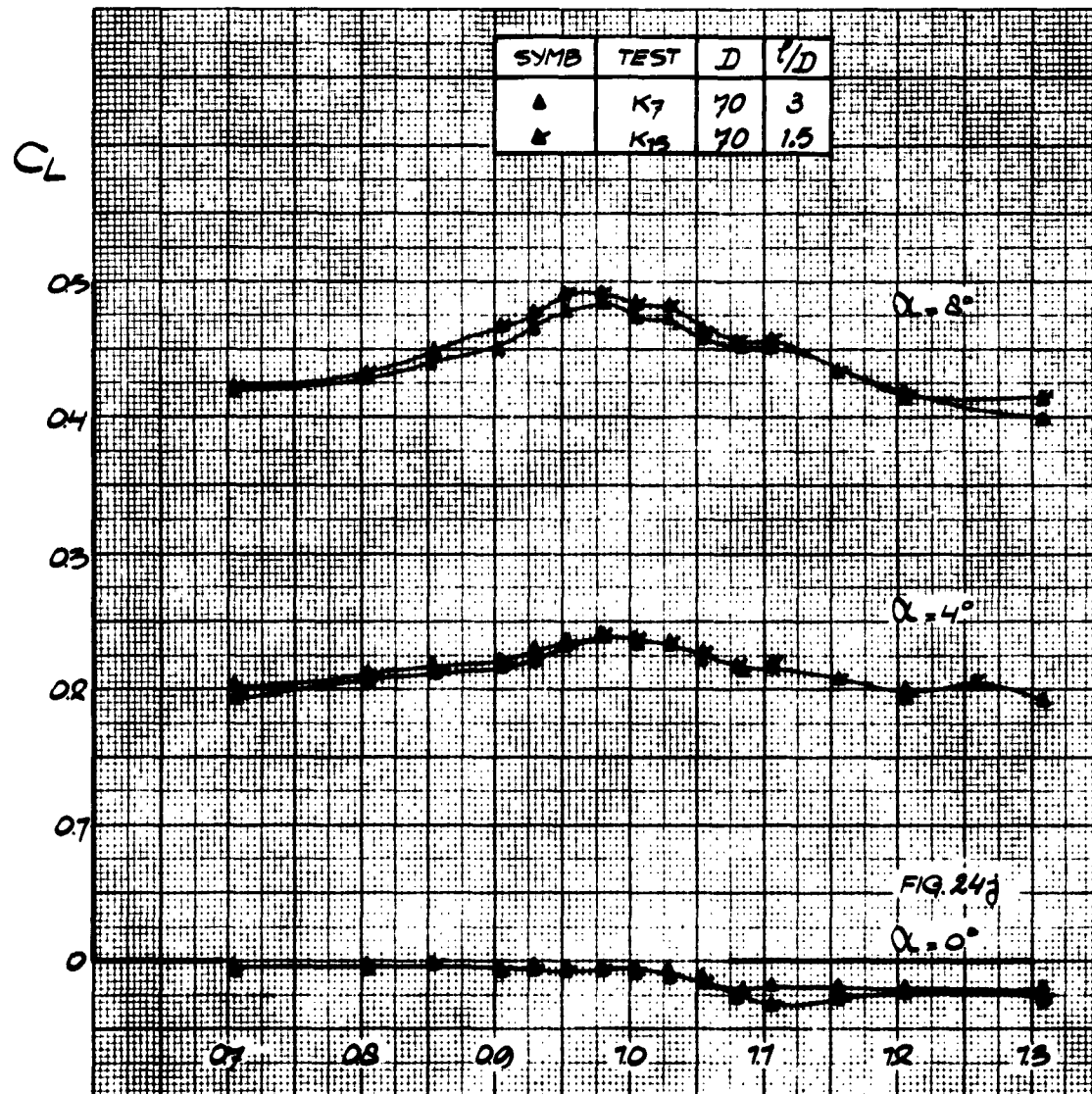


Fig.24 Presentation of lift data (continued)

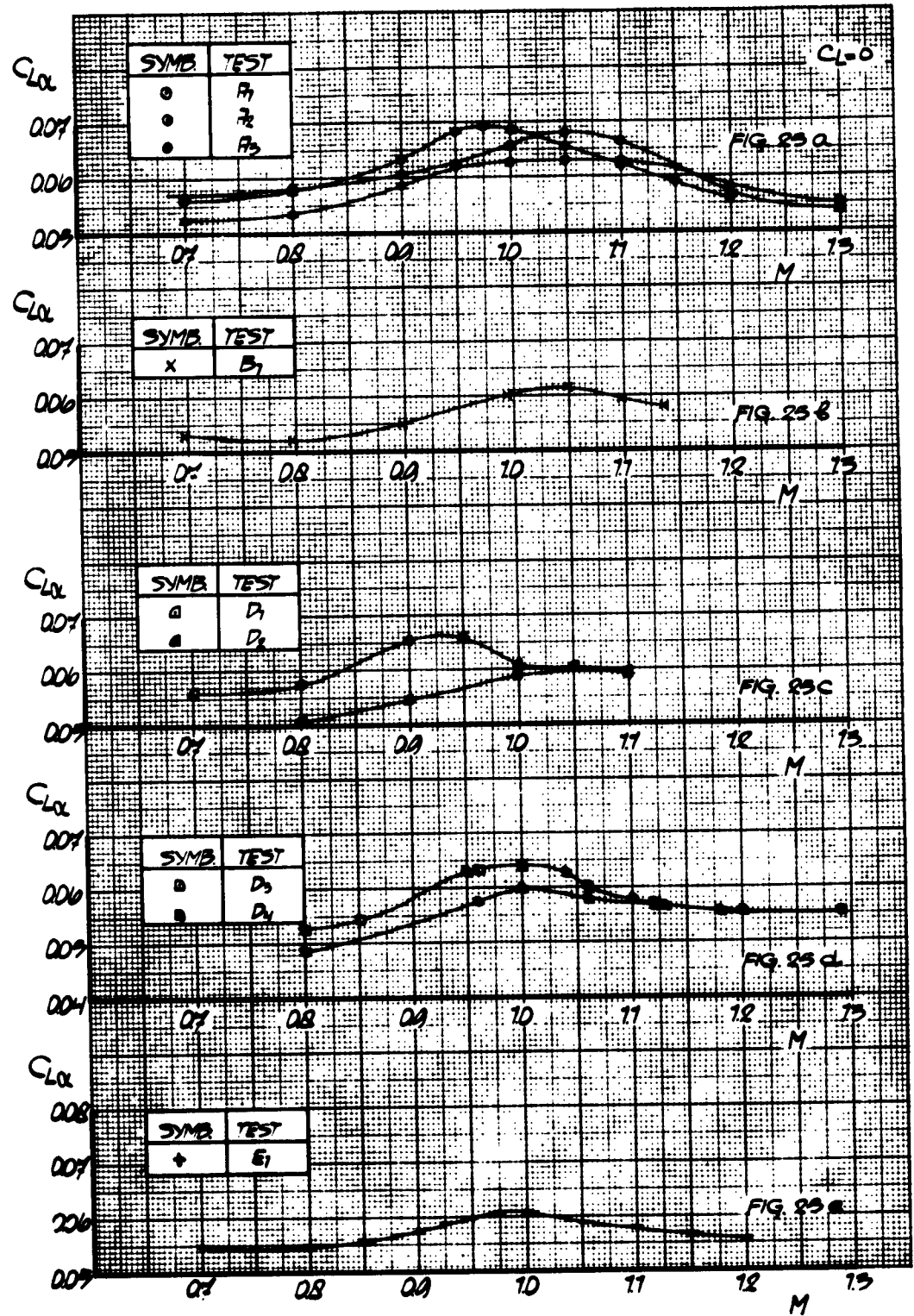


Fig. 25 Presentation of lift-curve slope data

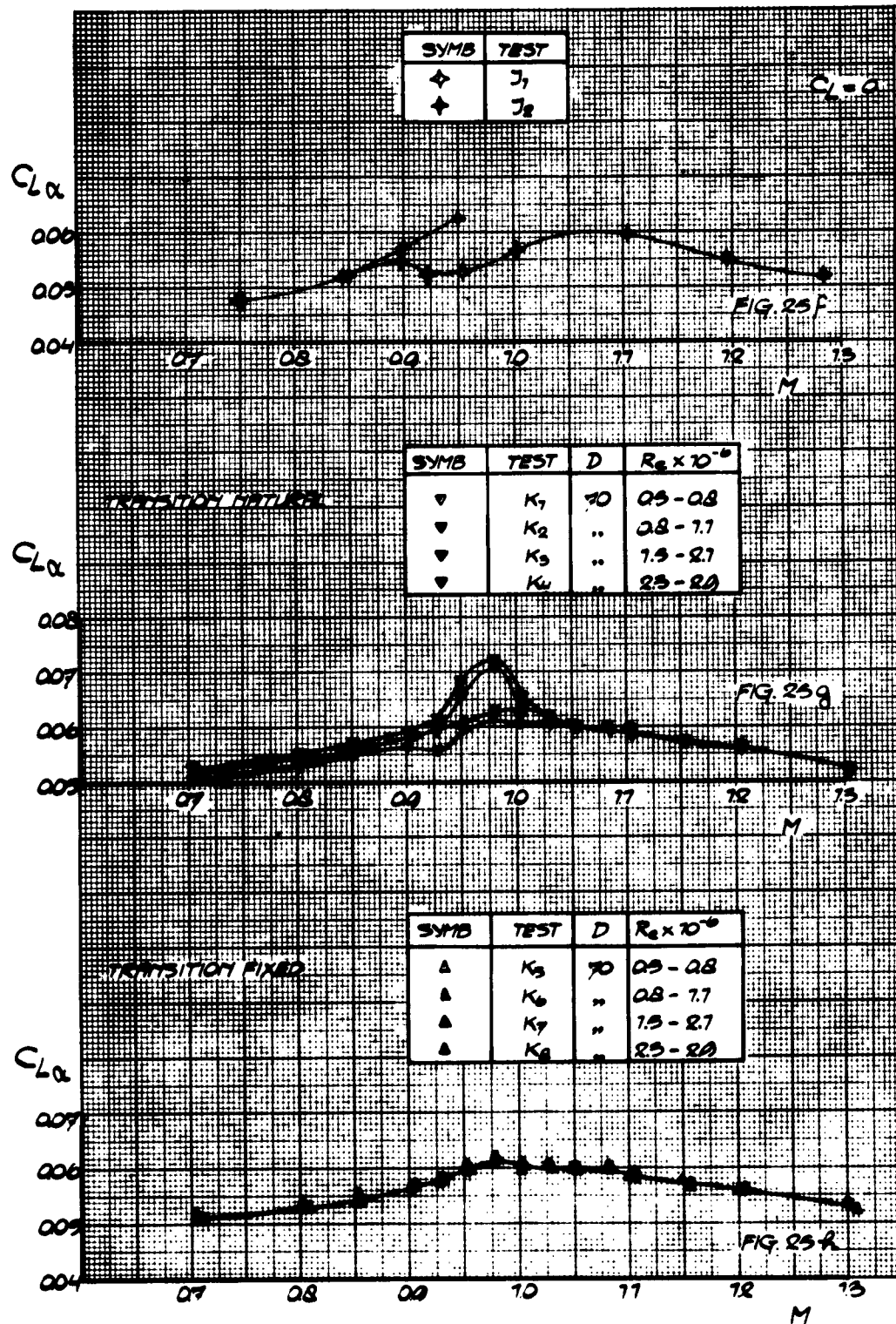


Fig.25 Presentation of lift-curve slope data (continued)

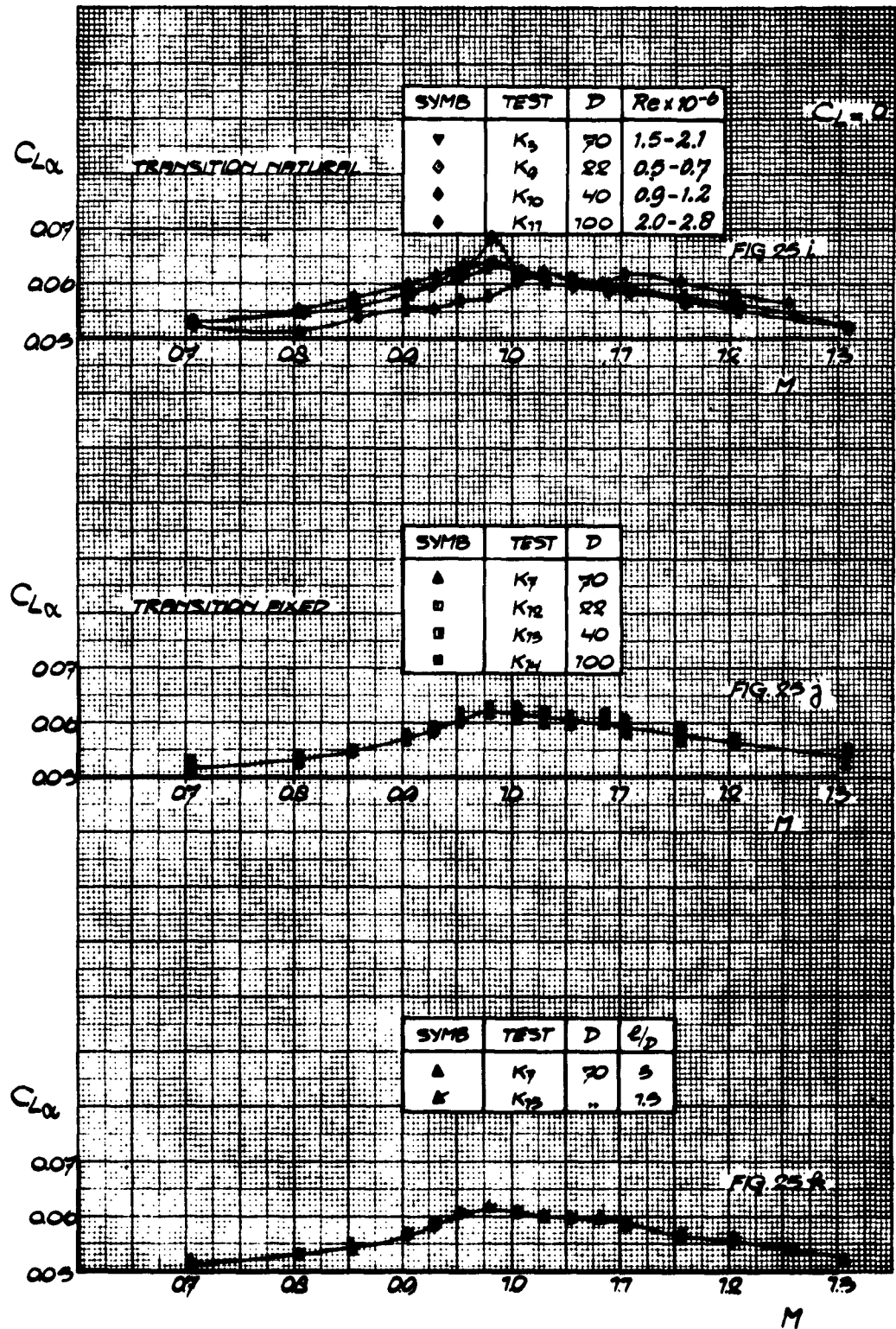


Fig. 25 Presentation of lift-curve slope data (continued)

PART V

TESTS ON AGARD MODEL D

by

R. Hills

Aircraft Research Association, Bedford, England

SUMMARY

Measurements of damping derivatives made in four different low speed tunnels on an unswept tapered wing are compared. All the tunnels used a forced oscillation technique, but had different methods of taking the measurements. The results show reasonable agreement, though there is a considerable scatter in any one set of measurements.

CONTENTS

	Page
SUMMARY	214
LIST OF TABLES	216
LIST OF FIGURES	216
NOTATION	217
1. INTRODUCTION	219
2. DETAILS OF TESTS	219
2.1 ONERA Tests	219
2.2 NLL Tests	219
2.3 NACA Tests	219
2.4 INFM Tests	220
3. DETAILS OF MODELS AND TUNNELS	220
4. RESULTS AND DISCUSSIONS	221
5. CONCLUSIONS	222
REFERENCES	222
FIGURES	223

LIST OF TABLES

	Page
Table I AGARD Model D	220

LIST OF FIGURES

Fig.1	General configuration of AGARD Model D	223
Fig.2	AGARD Model D. Pitching moment derivatives due to pitch	224
Fig.3	AGARD Model D. Lift and pitching moment derivatives with and without body	225
Fig.4	AGARD Model D. Rolling derivatives due to pitch and rate of pitch	226
Fig.5	AGARD Model D. Rolling and yawing moment derivatives due to rate of roll	227

NOTATION

b	overall span
c	centre line chord
f	frequency of oscillation (c/s)
k	radius frequency parameter, $= \frac{\omega b}{2V}$ or $\frac{\omega c}{2V}$
L	lift
l	rolling moment
m	pitching moment
n	yawing moment
p	angular velocity in roll
q	angular velocity in pitch
r	angular velocity in yaw
S	wing area
V	free-stream velocity
α	angle of incidence
β	angle of sideslip
ρ	mass density of air
ω	circular frequency of oscillation, $= 2\pi f$ (rad/sec)

Coefficients

$$C_L = \frac{L}{\frac{1}{2}\rho V^2 S}$$

$$C_{L\alpha} = \frac{\partial C_L}{\partial \alpha}$$

$$C_{Lq} = \frac{\partial C_L}{\partial \frac{qc}{2V}}$$

$$C_l = \frac{l}{\frac{1}{2}\rho V^2 b}$$

$$C_{l\alpha} = \frac{\partial C_l}{\partial \alpha}$$

$$C_{lq} = \frac{\partial C_l}{\partial \frac{qc}{2V}}$$

$$C_n = \frac{n}{\frac{1}{2} \rho V^2 c}$$

$$C_{n\alpha} = \frac{\partial C_n}{\partial \alpha}$$

$$C_{n\dot{\alpha}} = \frac{\partial C_n}{\partial \frac{d\alpha}{dt}}$$

$$C_n = \frac{n}{\frac{1}{2} \rho V^2 b}$$

$$C_{np} = \frac{\partial C_n}{\partial \frac{pb}{2V}}$$

$$C_{lp} = \frac{\partial C_l}{\partial \frac{pb}{2V}}$$

$$C_{nq} = \frac{\partial C_n}{\partial \frac{qc}{2V}}$$

$$C_{n\dot{q}} = \frac{\partial C_n}{\partial \frac{dq}{dt}}$$

$$C_{np} = \frac{\partial C_n}{\partial \frac{pb^2}{4V^2}}$$

$$C_{lp} = \frac{\partial C_l}{\partial \frac{pb^2}{4V^2}}$$

TESTS ON AGARD MODEL D

1. INTRODUCTION

AGARD Model D is a wing with a rectangular centre section and tapered tips. It was designed for checking measurements of damping derivatives in low-speed wind tunnels. The wing is supported by a sting (Fig.1) and a body shape is given, suitable for enclosing any measuring mechanism or supports at the rear of the sting. Tests were suggested with the model symmetrically mounted on the sting and alternatively with the sting attachment along axis XX' (Fig.1).

Tests have been made on this model in four different low speed tunnels and the results are compared here. There are differences in the non-dimensional coefficients used to quote the results, and here the NACA system has been used (see Notation). A summary of the tunnel conditions in the various tunnels is included in Section 2. All the measurements were made at zero wing incidence.

2. DETAILS OF TESTS

2.1 ONERA Tests

These tests¹ were made in the Alger tunnel of O.N.E.R.A. Measurements were made on a stability balance of normal force, pitching, rolling and yawing moments. The model was oscillated about the roll axis (horizontal along the sting) and about a vertical axis OZ (Fig.1). With the wing span vertical, the oscillation about axis OZ gave the derivatives due to pitch, and with the wing span horizontal the derivatives due to yaw. Some tests were included with the wing span vertical and the sting in the unsymmetrical position fixed along axis XX' (Fig.1). For most of the tests the forces on the body were included in the measurements but a few results are given where the body was present but the forces on it not included in the measured values.

2.2 NLL Tests

The NLL tests² were made on the same model as used in the ONERA tests but no body was present, the sting being bent round at right-angles at the point O in Figure 1 and taken through a fixed fairing to the oscillating mechanism under the floor of the tunnel. In these tests the model oscillations were forced through a spring. The motion of the model and the driving motion were both recorded by converting them to voltages by means of potentiometers. The amplitudes of the driving and model motions were measured when there was a 90° phase difference between the two motions.

Measurements were made of pitching moments due to a pitching oscillation with the model symmetrically fixed on the sting. Corrections were made to the results for sting bending.

2.3 NACA Tests

These tests³ were made in the Langley Field stability tunnel. The model was supported by the sting connected to a strain-gauge balance in the body. The model

was oscillated in roll and pitch and was only tested in the symmetrically supported condition. The measurements were taken by feeding the strain gauges with a voltage obtained from a sine-cosine resolver driven by the oscillating mechanism. This gave strain gauge output signals proportional to the forces in phase and out of phase with the model.

The results given in Reference 3 have not been corrected for deflections of the model under load. Estimates have now been made of these effects by N.A.C.A. and the results quoted here have been corrected for these estimated deflections.

2.4 IMFM Tests

These tests⁴ were made in an open jet tunnel. The model was oscillated in pitch and some tests were included with the wing unsymmetrically mounted on the sting. Measurements were also made with the model rolled at a continuous rate. The model was supported by the strain-gauge balance mounted in the body and the measurements were obtained from strain gauges in a similar manner to the NACA tests. The method used is described in detail in Reference 5.

3. DETAILS OF MODELS AND TUNNELS

Details of the models and of the tunnels in which they were tested are contained in Table I, which follows.

TABLE I

AGARD Model D

<i>Tunnel</i>	Model c(ft)	V (ft/sec)	$R \times 10^6$	Axis	f (c/s)	Amp.	Ref.
O.N.E.R.A.	0.656	65 - 130	0.26 - 0.52	p, q	1.3	-	1
N.L.L. 6' x 9'	0.656	100 - 180	0.4 - 0.76	q	1.4 - 2.4	-	2
N.A.C.A. 6' x 6'	0.656	85	0.33	q p	1 - 1.5 1 - 3	$\pm 4^\circ$ $\pm 4^\circ$	3
I.M.F.M.	0.656	42 - 130	0.17 - 0.52	q p	0.92 -*	$\pm 2.7^\circ$	4

* Continuous at 10.25 radians per second

4. RESULTS AND DISCUSSIONS

In the pitching moment tests the combined derivatives which were measured are $C_{mq} + C_{m\dot{a}}$, the damping term, and $C_{ma} - k^2 C_{m\dot{q}}$, the stiffness term. Figure 2 shows the comparison of the various tests and the theoretical estimates. Though there is a large scatter in the results, the NACA measurements of the damping derivative appear to be high. This error could be associated with inaccuracies in the large correction for deflection. The measurements at I.M.F.M. of the stiffness term also appear to be rather higher than the mean of the other experimental results.

Figure 3 shows the measurements made by O.N.E.R.A. where forces on the body were investigated. In both sets of tests the body was present, but in one of these the forces on it were not included in the measurements. The results shown in Figure 3 show that excluding the body forces gave a small but significant increase in C_{ma}^* and in $-C_{mq}^*$. If this was allowed for in the NLL test, which was the only other one of the tests without body, there would be a slight improvement in the agreement of the C_{mq} measurements but not of the C_{ma} measurements shown in Figure 2.

In Figure 4 the tests made with the unsymmetrical sting mounting show values of the rolling moment due to pitching†. This derivative is due to the unsymmetrical support and, as the rolling moment axis is in this case $c/2$ away from the plane of symmetry,

$$C_{la} = \frac{c}{2} \frac{C_{La}}{b} = \frac{1}{8} C_{La}$$

$$\text{and } C_{lq} = \frac{c}{2} \frac{C_{Lq}}{b} = \frac{1}{8} C_{Lq}$$

Comparison with the ONERA measurements on C_{la} and C_{lq} in Figure 3 show good agreement with these formulae.

The yawing and rolling moment due to roll are shown in Figure 5. The tests at I.M.F.M. show appreciably larger values for $-C_{lp}$ and C_{np} than those at O.N.E.R.A. at small values of the frequency.

There seems to be no particular reason for this difference. For the unsymmetrically mounted model the IMFM tests show a steady reduction in C_{np} and $-C_{lp}$ with increase of the frequency parameters. This may be because these tests were made with a steady rate of roll. As discussed in Reference 4, this can give rise to large values of the helix angle, particularly near the tip of the model, which would not be present in an oscillating test at the same frequency parameter.

* Strictly these should be $(C_{ma} - k^2 C_{m\dot{q}})$ and $-(C_{mq} + C_{m\dot{a}})$; similarly C_{La} should be $(C_{La} - k^2 C_{L\dot{q}})$, $C_{Lq} = (C_{Lq} + C_{L\dot{a}})$, $C_{la} = (C_{la} - k^2 C_{l\dot{q}})$, $C_{lq} = (C_{lq} + C_{l\dot{a}})$.

† In Reference 4 these results are quoted incorrectly as values of rolling moment due to yaw.

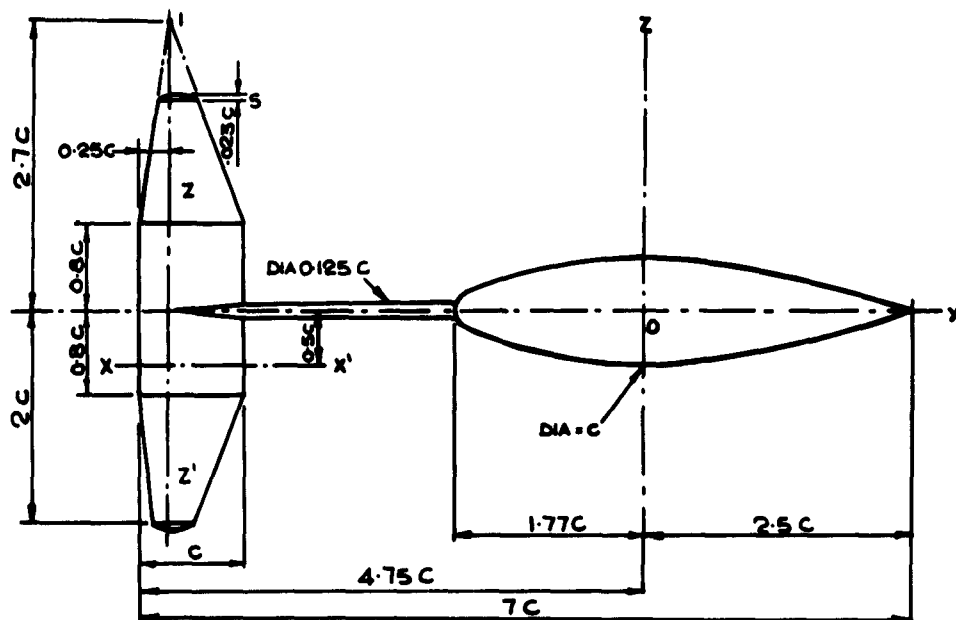
5. CONCLUSIONS

(i) Measurements of damping derivative on AGARD Model D made in four different low speed tunnels show reasonable agreement, though there is a considerable scatter in many of the results.

(ii) For an unsymmetrically mounted model, measurements made in steady roll show changes in C_{lp} and C_{np} with increase of frequency parameter. All other derivatives measured were substantially unaltered by change of frequency parameter.

REFERENCES

1. O.N.E.R.A. *Mesure des Dérivées Aérodynamiques en Incompressible à la Soufflerie D'Alger.* O.N.E.R.A. Fiche Documentaire Provisoire No.200, April 1958.
2. Yff, J. *Measurements of Some Low Speed Oscillatory Stable Derivatives of the AGARD Wing Model D.* N.L.L. (Amsterdam) TM F.195, December 1956.
3. Letko, W. *Wind Tunnel Investigation of Low-Speed Oscillatory Derivatives in Pitch and in Roll of AGARD Model D.* (Prepared for AGARD Panel meeting in Brussels, April 1956).
4. Valensi, J. *Détermination en Soufflerie des Dérivées Aérodynamiques de la Maquette Etalon AGARD D et Comparaison de Résultats avec ceux Obtenus à l'O.N.E.R.A.* Institut de Mécanique des Fluids de Marseille Rapport E.73, Juin 1957.
5. Valensi, J. *A Review of the Techniques of Measuring Oscillatory Aerodynamic Forces and Moments on Models Oscillating in Wind Tunnels.* Fifth Meeting of AGARD Wind Tunnel Panel, AGARD AG 15/P6, May 1954, pp.14-50, paragraph 5.



AXES OF ROTATION:

ROLLING, OX

(NOTE: ON THE FIGURE, THE WING IS REPRESENTED IN SYMMETRICAL MOUNTING.

FOR DISSYMMETRICAL MOUNTING OX' MOVES TO OX)
YAWING AND PITCHING, OZ .

WING PROFILE:

NACA 64 A1 012 .

WING TIPS:

$\frac{1}{2}$ BODIES OF REVOLUTION GENERATED BY THE
WING TIP PROFILE.

Fig.1 General configuration of AGARD Model D

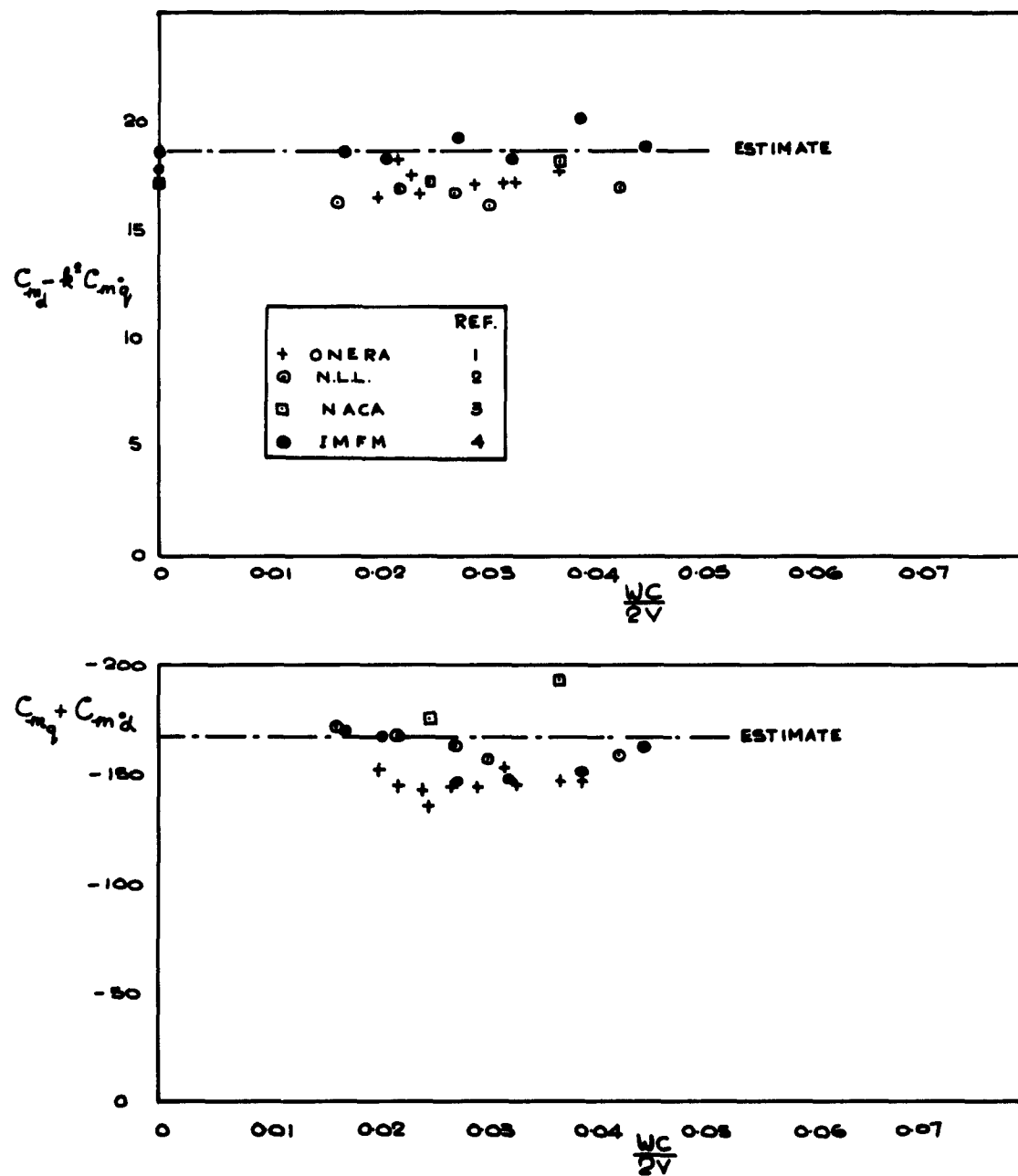


Fig.2 AGARD Model D. Pitching moment derivatives due to pitch

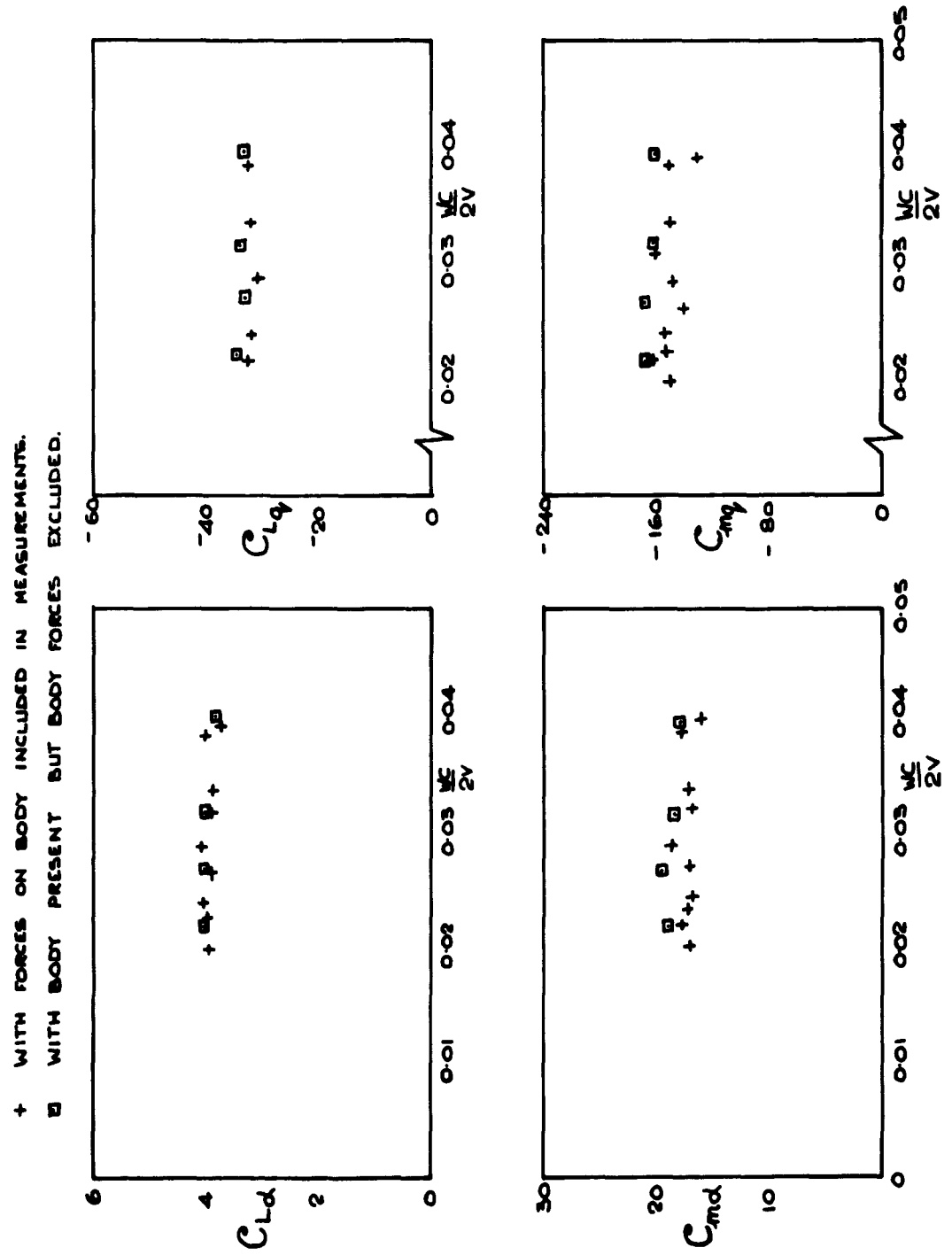


Fig.3 AGARD Model D. Lift and pitching moment derivatives with and without body

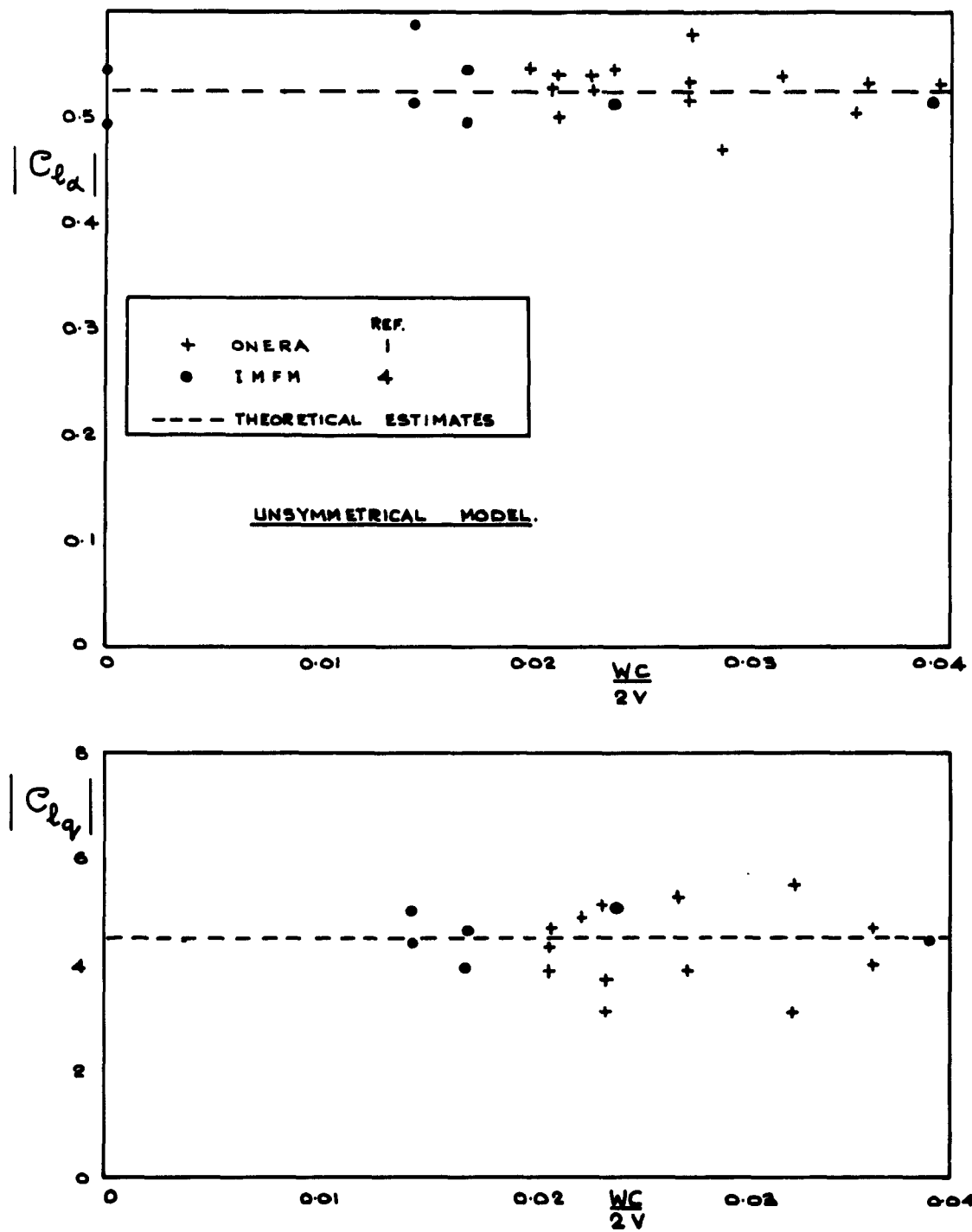


Fig. 4 AGARD Model D. Rolling derivatives due to pitch and rate of pitch

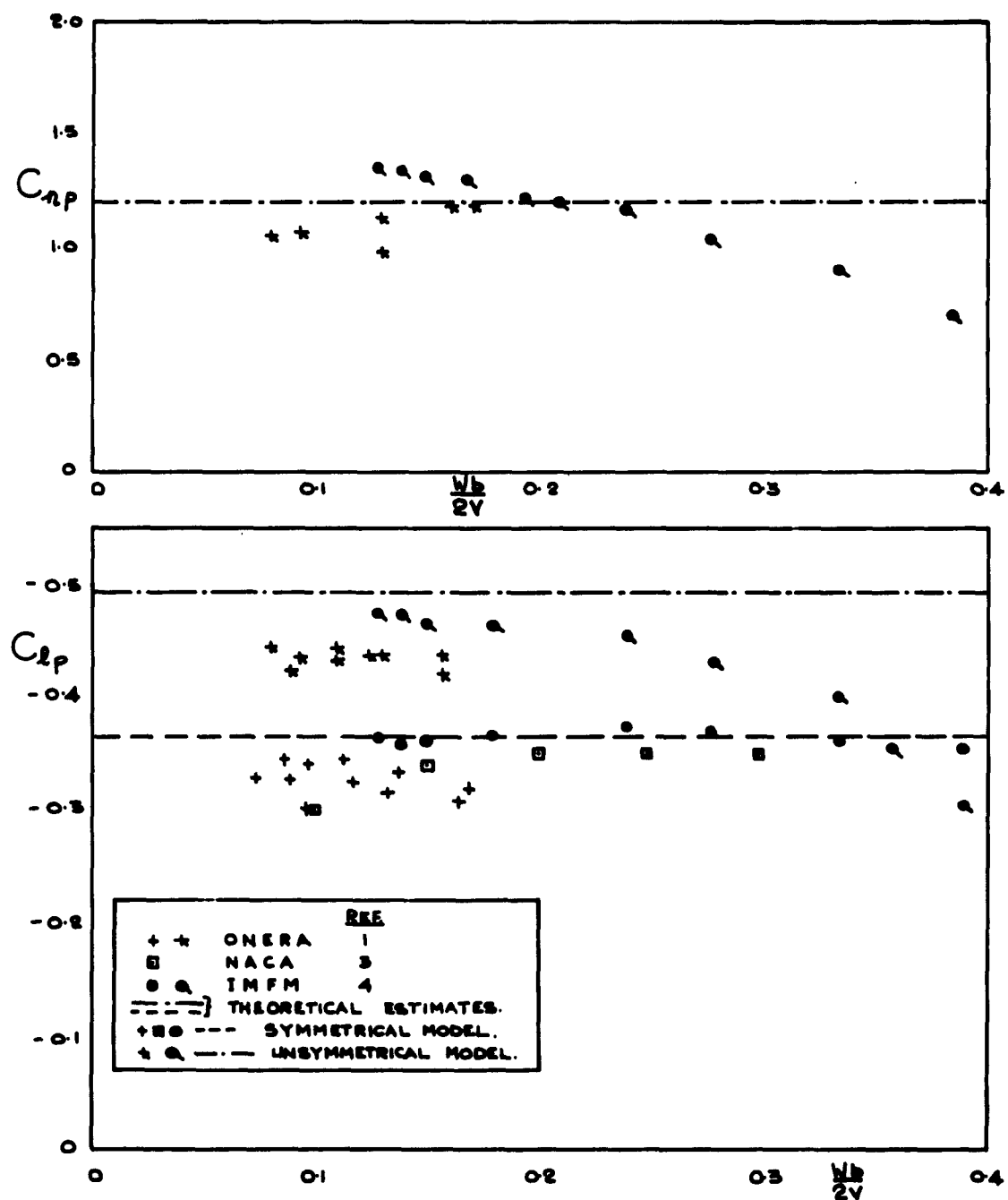


Fig.5 AGARD Model D. Rolling and yawing moment derivatives due to rate of roll

PART VI

TESTS ON AGARD MODEL E

by

R. Hills

Aircraft Research Association, Bedford, England

SUMMARY

Tests on hemispheres in various hypersonic facilities are summarized. Pressure distribution and heat transfer measurements are in reasonable agreement over the forebody, though there are some discrepancies in results over the afterbody. A few measurements of shock wave detachment distance are also compared with theoretical curves.

CONTENTS

	Page
SUMMARY	230
LIST OF FIGURES	232
NOTATION	233
1. INTRODUCTION	235
2. DRAG MEASUREMENTS	235
3. PRESSURE DISTRIBUTION	235
4. HEAT TRANSFER	235
5. SHOCK WAVE DETACHMENT DISTANCE	236
6. CONCLUSIONS	237
REFERENCES	237
FIGURES	239

LIST OF FIGURES

		Page
Fig.1	AGARD Model E. Drag coefficient for a hemisphere-cylinder. Comparison of theory and experiment (Fig.25 of Ref.1)	239
Fig.2	AGARD Model E. Hemisphere-cylinder pressure distribution. Comparison of theory and experiment (Fig.16 of Ref.1)	240
Fig.3	AGARD Model E. Stagnation point heat transfer rates on a hemisphere (Fig.4 of Ref.2)	241
Fig.4	AGARD Model E. Stagnation point heat transfer for a hemisphere-cylinder in Hotshot 1 (Fig.23 of Ref.1)	242
Fig.5	AGARD Model E. Heat transfer over a hemisphere cylinder	243
Fig.6	AGARD Model E. Comparison of shock detachment distance with theory and experiment (Fig.26 of Ref.1)	244
Fig.7	AGARD Model E. Variation of shock detachment distance with stagnation temperature (Fig.13 of Ref.5)	245

NOTATION

C_D	drag coefficient, = $\text{drag}/(\frac{1}{2}\rho V^2 \times \text{frontal area})$
D	body diameter
D_1	diffusion coefficient
k	thermal conductivity
K	density ratio across a normal shock wave
L	Lewis number, = $D_1 \rho C_p / k$
M	Mach number
p	static pressure
\dot{q}	heat transfer rate
R	hemisphere radius
s	distance along surface from stagnation point
T_0	stagnation temperature
δ	axial distance from upstream side of shock to model stagnation point
γ	ratio of specific heats

Suffixes

$_1$	denotes initial channel pressure in shock tube
$_e$	denotes local flow conditions
$_s$	denotes body stagnation point
$_\infty$	denotes free-stream conditions ahead of bow shock

TESTS ON AGARD MODEL E

1. INTRODUCTION

A hemisphere was selected as a suitable model for testing in various hypersonic facilities and it was suggested that measurements of pressure distribution, stagnation temperature, heat transfer and normal aerodynamic coefficients should be compared. Tests have been made on a hemispherical cylinder in Hotshot¹, in several shock tubes^{2,4,6}, in a light gas gun³, and in a shock tube tunnel using a reflected shock technique⁵. The flow over a hemisphere has been discussed in considerable detail in References 1 and 2 and this note merely summarizes some of the discussion in those two papers and adds a few further results.

2. DRAG MEASUREMENTS

Balance measurements of the drag of a hemisphere were made in Hotshot¹ using a strain-gauge balance. The model consisted of a hemisphere of 2 in. in diameter with a 2° flare 1 in. long at the rear. The model was made of fibre glass and light enough to give a frequency response of approximately 1 kc/s. The balance was viscously damped to 40% of critical damping.

The drag balance results (Fig.1) have not been corrected for base pressure drag, as this is estimated to contribute less than 1% to the overall drag. Comparison of the integrated pressure distribution with the measured drag shows a difference of about 10% which can be attributed mainly to skin friction. The simple Newtonian theory $C_D = \frac{1}{2}C_{pmax}$ gives an accurate estimate of the pressure drag at high Mach numbers. The Hodges experimental results¹⁰ are from ballistic range tests and show good agreement with the calculations due to Liu¹¹, who has worked out the forebody drag as that due to the local pressure behind a closely wrapped bow shock.

3. PRESSURE DISTRIBUTION

Figure 2 shows a collection of a number of measurements of the pressure distribution on a hemisphere from different hypersonic facilities, including conventional tunnels, shock tubes, Hotshot and a light gas gun tunnel. The Newton, Prandtl-Meyer theory matches the forebody pressure distribution accurately and there is reasonable agreement between all the different measured results at high Mach number on the forebody. The afterbody pressures are, however, appreciably affected by Mach number and further experimental results are required in this region.

4. HEAT TRANSFER

Heat transfer results from a number of measurements in shock tubes have been compared in Reference 2 and Figure 3 reproduces the analysis. In all these tests thin film platinum resistance thermometers have been used for the measurements, except in some of the tests in Reference 6 when a thin film surface thermocouple was used. The film thickness used in the NACA tests was 4×10^{-6} in.: in other cases it was not

recorded. The results are compared with the theoretical curves of Fay and Riddell¹² using a Lewis number of 1.4 and a Prandtl number of 0.71. An average for the results for the thin film gauges is about 20% below the theoretical curves. One set of tests⁴ made at AVCO with a thick film, 1×10^{-3} in. thick, of the calorimeter type of gauge, showed results very close to the theoretical curves. There is therefore an apparent difference in the results due to the method of measurements which has not yet been explained.

Figure 4 shows some measurements made in Hotshot¹. These were made with a Morgandyne gauge, which consists of a copper ring 0.01 in. thick with an outside diameter of 3.16 in., inductively coupled to an inner coil and excited at 20 kc/s. As the copper changes its resistance with the addition of heat, a signal is produced proportional to the total heat added to the copper. The results in Figure 4 are too scattered for any precise evaluation, but again show a tendency to fall below the values given by the Fay-Riddell equation.

The measured distribution of heat transfer over the hemisphere is compared with the curves for Lees theory¹³ in Figure 5. This theoretical curve has been obtained by using the experimental pressure distribution shown for Hotshot in Figure 2. The results are fairly scattered but are in reasonable agreement with the theoretical values for $\gamma = 1.4$. The few results from the light gas gun tunnel are appreciably higher than the other measurements.

5. SHOCK WAVE DETACHMENT DISTANCE

The shock wave detachment distance ahead of a hemisphere has been measured from schlieren photographs both in Hotshot¹ and in a reflected shock tunnel⁵. Figure 6 from Reference 1 shows the results from Hotshot plotted against Mach number, as compared with various measurements at lower Mach numbers and with calculations.

Figure 7 shows some corresponding results obtained in the reflected shock tunnel. Some of these results at the higher stagnation temperature were in fact obtained from direct luminosity photographs where schlieren was not possible. These results are compared with the simplified Serbin formula for the shock detachment distance¹⁴

$$\frac{\delta}{R} = \frac{0.67}{K - 1}$$

where K is the density ratio across a normal shock at the free stream Mach number. Estimates of K have been made in Reference 5 at the nominal $M = 10$ nozzle (a nozzle area ratio of 576) for flow in thermal equilibrium through the nozzle and for completely frozen nozzle flow. With frozen flow there is only a small change in K with increase of stagnation temperature but, with equilibrium flow, K increases fairly rapidly with increase in temperature. Figure 7 shows the corresponding estimate of shock wave detachment distance for the two cases and shows that most of the experimental results lie between the two curves.

6. CONCLUSIONS

(i) Measurements of pressure distribution on a hemisphere made in different types of hypersonic facilities showed reasonable agreement over the forebody but some differences over the afterbody.

(ii) Heat transfers measured with thin film gauges also showed reasonable agreement, but there is a discrepancy between these results and measurements with thick film calorimeter type gauges.

(iii) The few measurements of shock wave detachment distance are scattered. Further measurements may be useful in deciding whether the flow in any facility is in thermal equilibrium or frozen.

REFERENCES

1. Boison, J.C. *Experimental Investigation of the Hemisphere-Cylinder at Hypervelocities in Air.* Arnold Engineering Development Center, AEDC-TR-58-20, November 1958.
2. Henshall, B.D. *Stagnation Point Heat Transfer Rate Measurements in the Unexpanded Flow of the NPL Hypersonic Shock Tunnel* ARC 20,716, January 1959.
3. Cox, R.N. *The ARDE Gun Tunnels and Some Experimental Studies of Hypersonic Flow.* Armament Research and Development Establishment (UK), ARDE Memorandum (B) 70/59, October 1959.
4. Rose, P.H.
Stark, W.I. *Stagnation Point Heat Transfer Measurements in Dissociated Air.* AVCO Research Note 24, April 1957.
5. Nagamatsu, H.T.
et alii *Real Gas Effects in Flow Over Blunt Bodies at Hypersonic Speeds.* GRC Report 59-BL-2177, February 1959.
6. Sabol, A.P. *Measurements in a Shock Tube of Heat-Transfer Rates at the Stagnation Point of a 1.0-inch-diameter Sphere for Real-Gas Temperatures up to 7.900°R.* NACA TN 4354, August 1958.
7. Rose, P.H. *Physical Gas Dynamics Research at the AVCO Research Laboratory.* AVCO Research Note 37, May 1957.
8. Stine, H.A.
Wanlass, K. *Theoretical and Experimental Investigation of Aerodynamic-Heating and Isothermal Heat Transfer Parameters on a Hemispherical Nose With Laminar Boundary Layer at Supersonic Mach Numbers.* NACA TN 3344, December 1954.

9. Kubota, T. *Investigation of Flow Around Simple Bodies in Hypersonic Flow.* Guggenheim Aeronautical Laboratory, California Institute of Technology, CIT Memo 40, June 1957.
10. Hodges, A.J. *The Drag Coefficient of Very High Velocity Spheres.* Journal of the Aeronautical Sciences, Vol.24, October 1957, pp.755-758.
11. Liu, V.C. *On the Drag of a Sphere at Extremely High Speeds.* Journal of Applied Physics, Vol.29, February 1958, pp.194-195.
12. Fay, J.
Riddell, F.R. *Stagnation Point Heat Transfer in Dissociated Air.* AVCO Research Note 18, June 1956.
13. Lees, L. *Laminar Heat Transfer Over Blunt Nosed Bodies at Hypersonic Flight Speeds.* Jet Propulsion, Vol.26, April 1956.
14. Serbin, H. *Supersonic Flow Around Blunt Bodies.* Journal of the Aeronautical Sciences, Vol.25, January 1958, p.58.
15. Schwartz, R.N.
Eckerman, J. *Shock Location in Front of a Sphere as a Measure of Real Gas Effects.* Journal of Applied Physics, Vol.27, February 1956, pp.169-174.
16. Boison, J.C.
Curtiss, H.C. *Preliminary Results of Spherical-Segment Blunt Body Surveys in the 20-inch Supersonic Wind Tunnel at J.P.L.* AVCO RAD-2-TM-57-77, October 1957.
17. Oliver, R.E. *An Experimental Investigation of Flow Over Simple Blunt Bodies at a Nominal Mach Number of 5.8.* Guggenheim Aeronautical Laboratory, California Institute of Technology, CIT Memo 26, June 1955.
18. Lees, L. *Recent Developments in Hypersonic Flow.* Jet Propulsion, Vol.27, November 1957, pp.1162-1178.

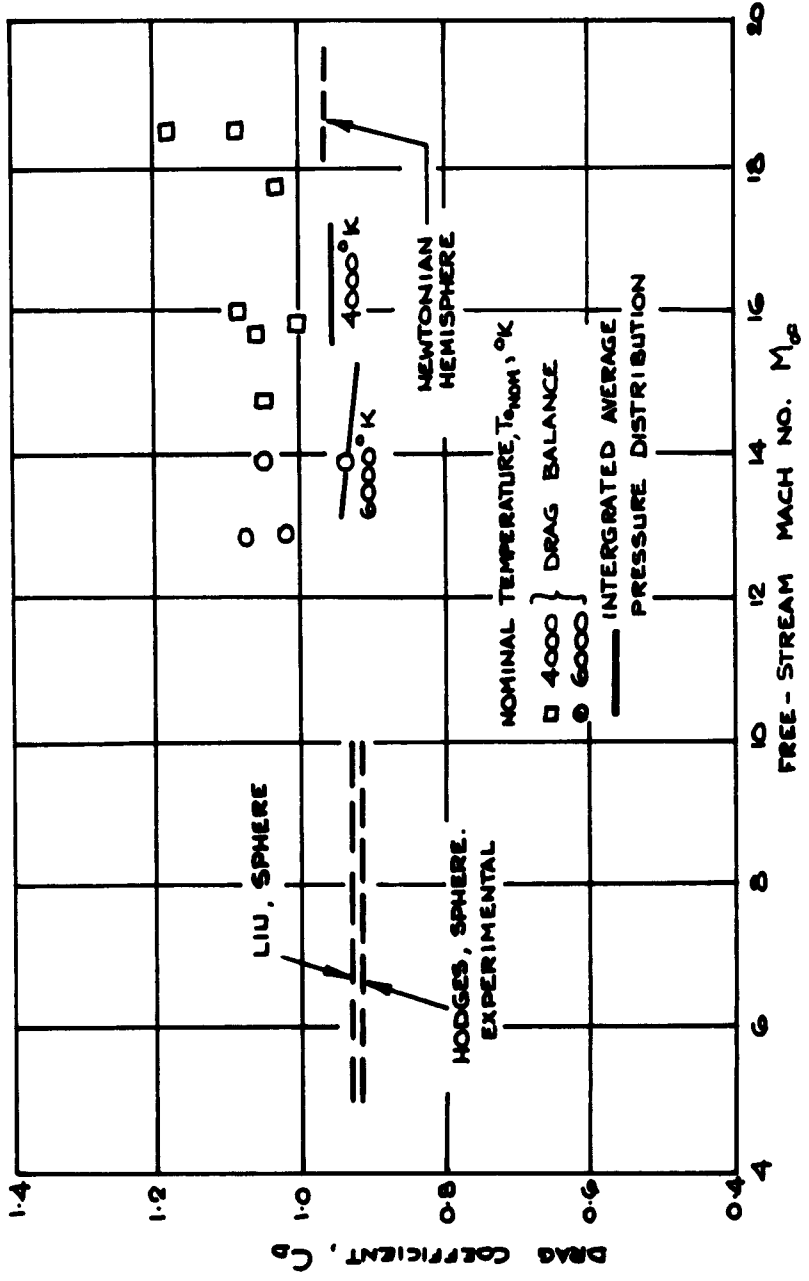


Fig. 1 AGARD Model E. Drag coefficient for a hemisphere-cylinder. Comparison of theory and experiment (Fig. 25 of Ref. 1)

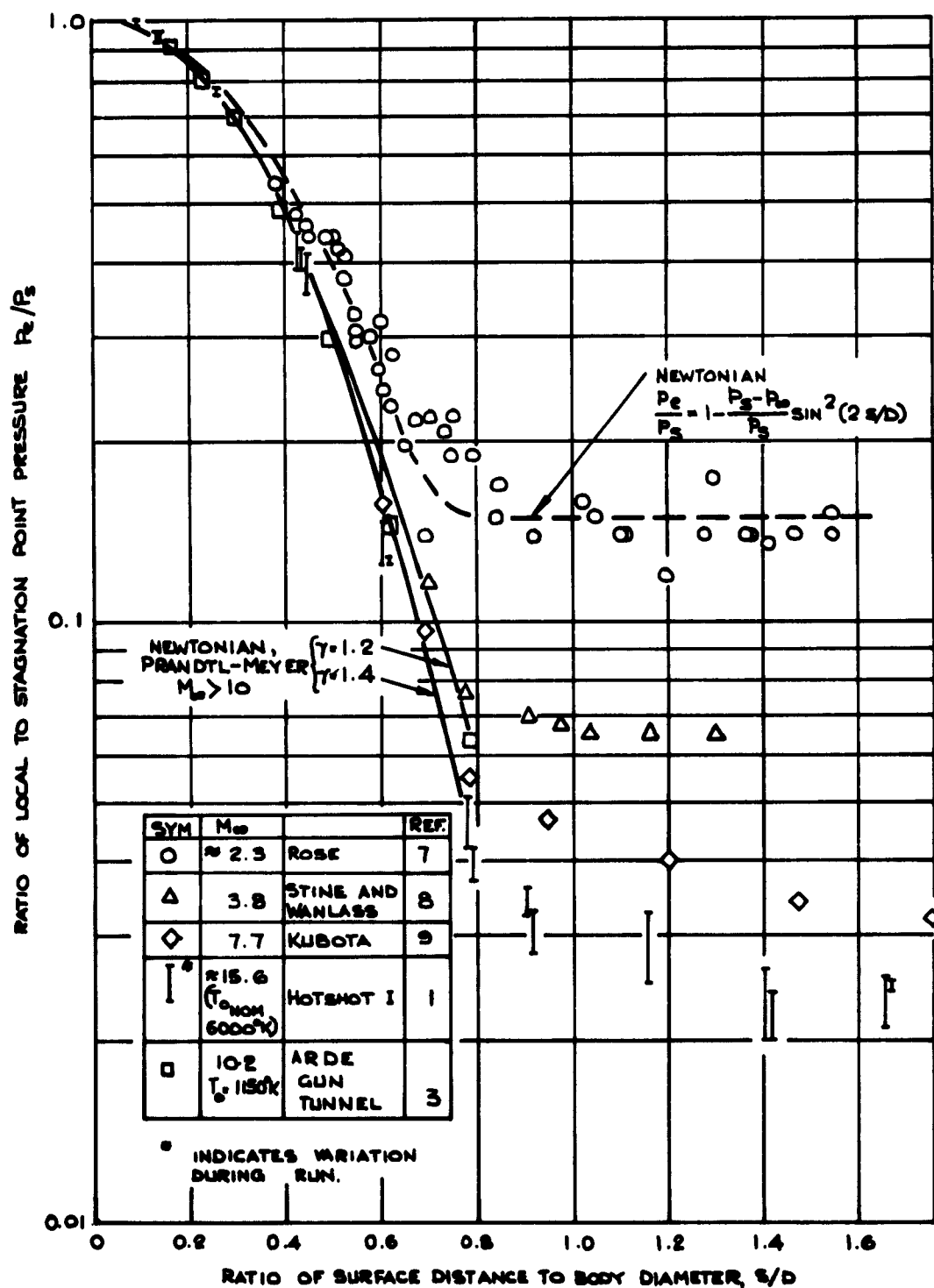
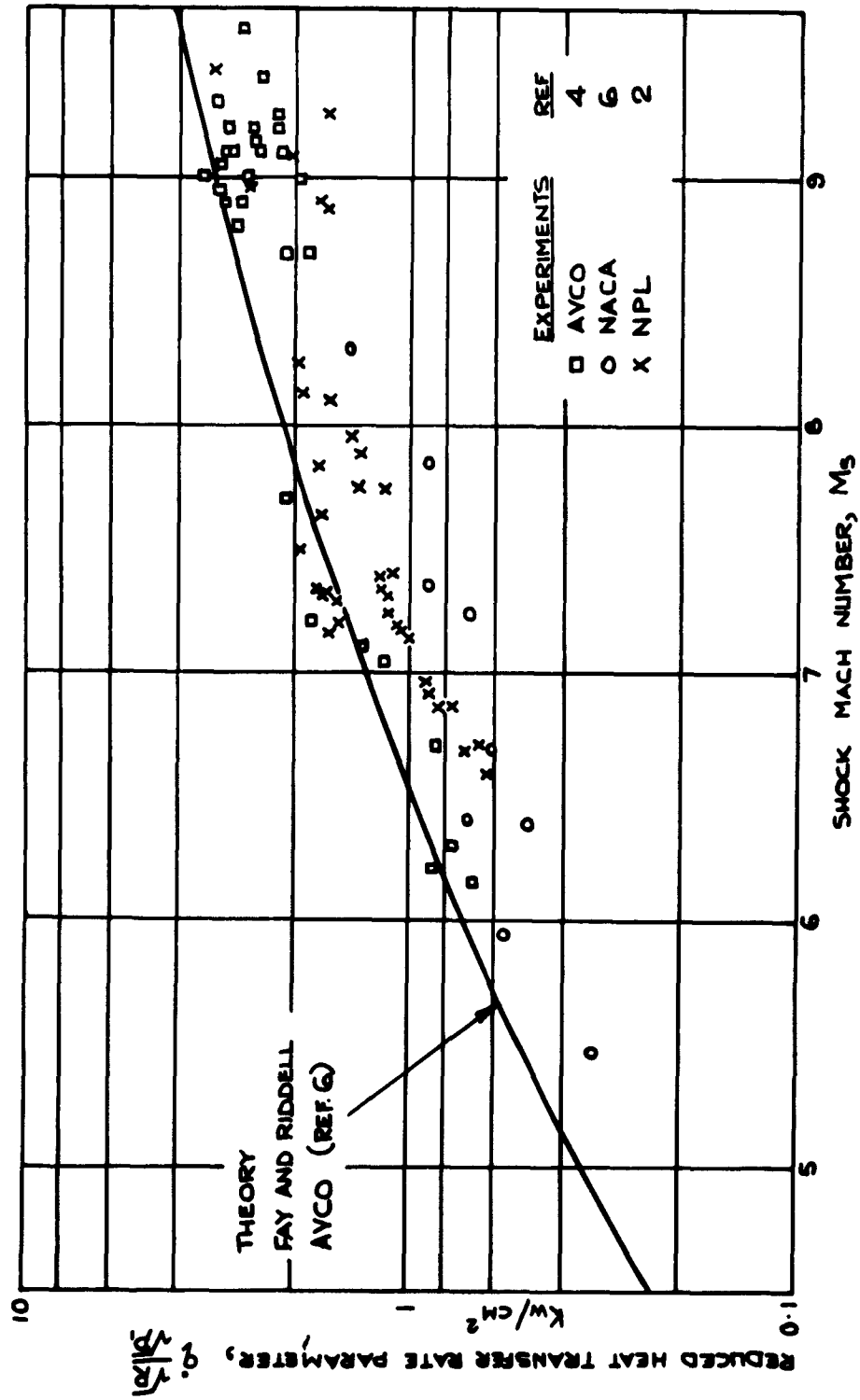


Fig.2 AGARD Model E. Hemisphere-cylinder pressure distribution. Comparison of theory and experiment (Fig.16 of Ref.1)



P_1 = CHANNEL PRESSURE (MM. OF MERCURY)
 R = MODEL NOSE RADIUS (MILLIMETRES)

Fig. 3 AGARD Model E. Stagnation point heat transfer rates on a hemisphere (Fig. 4 of Ref. 2)

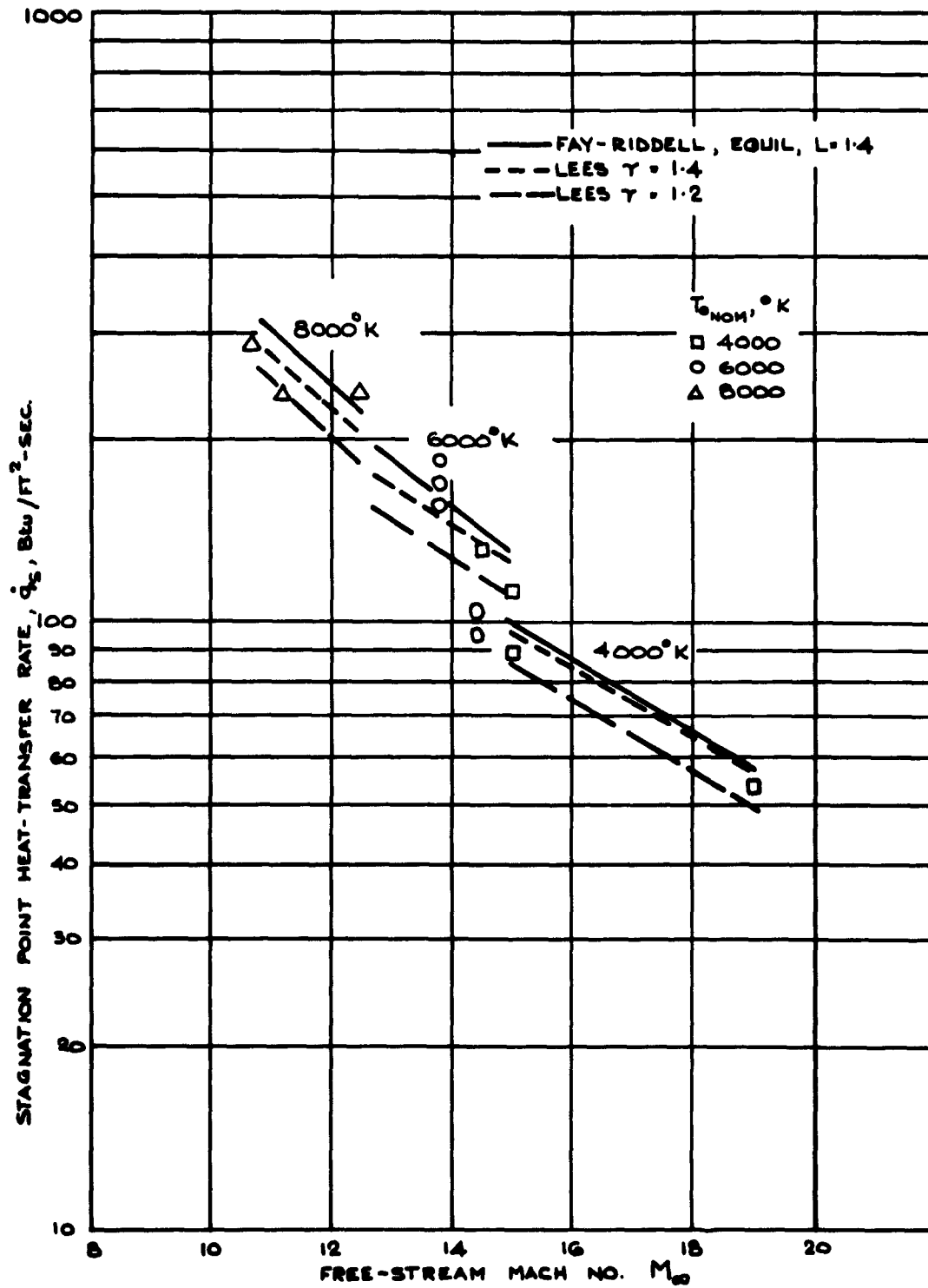


Fig. 4 AGARD Model E. Stagnation point heat transfer for a hemisphere-cylinder in Hotshot 1
(Fig. 23 of Ref. 1)

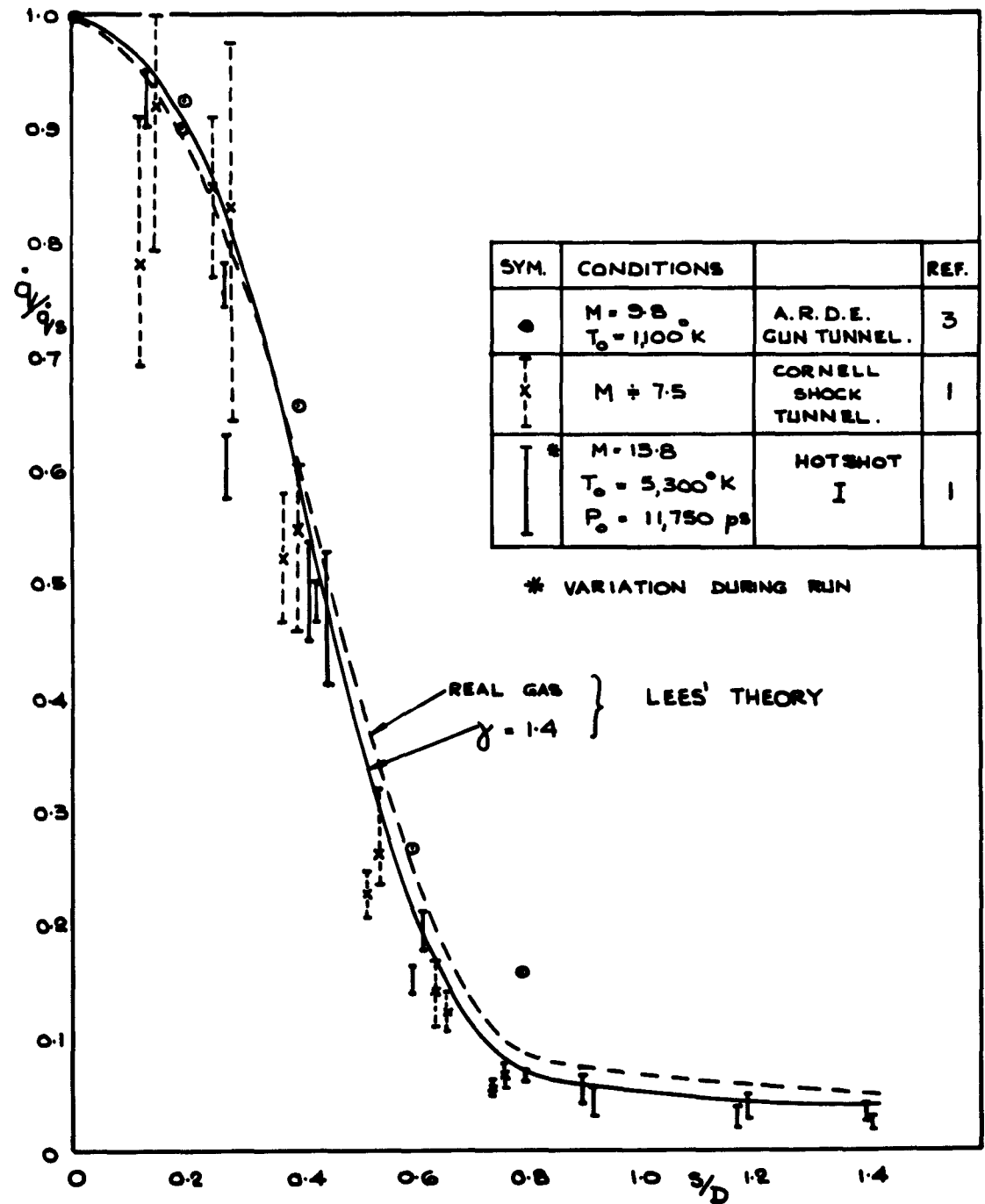


Fig.5 AGARD Model E. Heat transfer over a hemisphere cylinder

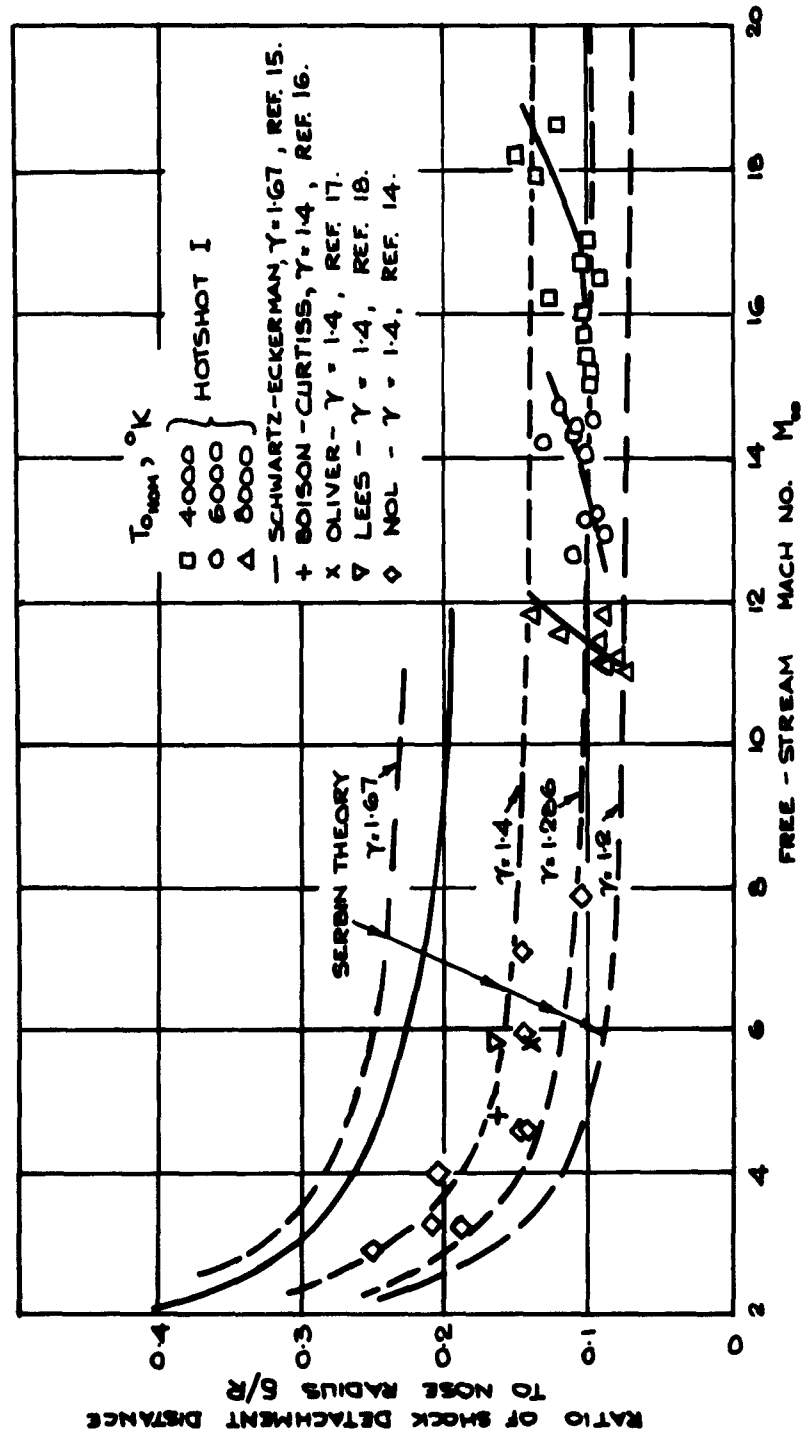


Fig. 6 AGARD Model E. Comparison of shock detachment distance with theory and experiment
(Fig. 26 of Ref. 1)

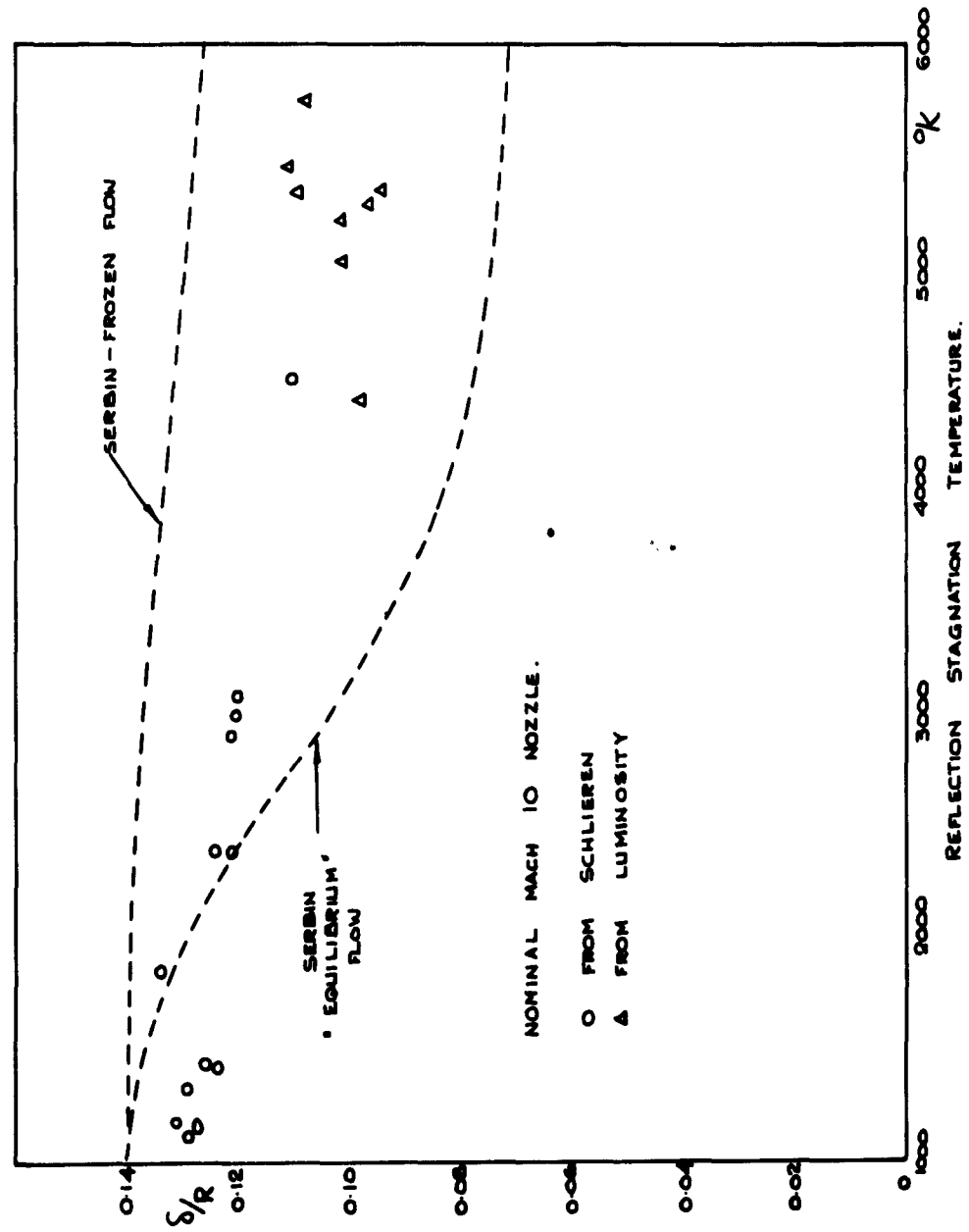


Fig.7 AGARD Model E. Variation of shock detachment distance with stagnation temperature
 (Fig.13 of Ref.5)

DISTRIBUTION

Copies of AGARD publications may be obtained in the various countries at the addresses given below.

On peut se procurer des exemplaires des publications de l'AGARD aux adresses suivantes.

BELGIUM BELGIQUE	Centre National d'Etudes et de Recherches Aéronautiques 11, rue d'Egmont, Bruxelles
CANADA	Director of Scientific Information Service Defense Research Board Department of National Defense 'A' Building, Ottawa, Ontario
DENMARK DANEMARK	Military Research Board Defense Staff Kastellet, Copenhagen Ø
FRANCE	O.N.E.R.A. (Direction) 25, Avenue de la Division Leclerc Châtillon-sous-Bagneux (Seine)
GERMANY ALLEMAGNE	Wissenschaftliche Gesellschaft für Luftfahrt Zentralstelle der Luftfahrtokumentation München 64, Flughafen Attn: Dr. H.J. Rautenberg
GREECE GRECE	Greek National Defense General Staff B. MEC Athens
ICELAND ISLANDE	Director of Aviation c/o Flugrad Reykjavik
ITALY ITALIE	Ufficio del Generale Ispettore del Genio Aeronautico Ministero Difesa Aeronautica Roma
LUXEMBURG LUXEMBOURG	Obtainable through Belgium
NETHERLANDS PAYS BAS	Netherlands Delegation to AGARD Michiel de Ruyterweg 10 Delft

<p>AGARDograph 64 North Atlantic Treaty Organization, Advisory Group for Aeronautical Research and Development A REVIEW OF MEASUREMENTS ON AGARD CALIBRATION MODELS Editor: R. Hills (Pt.I: R. Hills; Pt.II: H. Valk and J.H. van der Zwaan; Pt.III: J.P. Hartzuiker; Pt.IV: H. Valk; Pt.V: R. Hills; Pt.VI: R. Hills) 1961 245 pages incl. 112 refs., 79 figs.</p> <p>An analysis has been made of measurements in various wind tunnels of AGARD Calibration Models A, B, C, D and E. The analysis has shown con- siderable scatter of results, particularly at</p> <p>P.T.O.</p>	<p>533.6.072 3b6b</p>	<p>AGARDograph 64 North Atlantic Treaty Organization, Advisory Group for Aeronautical Research and Development A REVIEW OF MEASUREMENTS ON AGARD CALIBRATION MODELS Editor: R. Hills (Pt.I: R. Hills; Pt.II: H. Valk and J.H. van der Zwaan; Pt.III: J.P. Hartzuiker; Pt.IV: H. Valk; Pt.V: R. Hills; Pt.VI: R. Hills) 1961 245 pages incl. 112 refs., 79 figs.</p> <p>An analysis has been made of measurements in various wind tunnels of AGARD Calibration Models A, B, C, D and E. The analysis has shown con- siderable scatter of results, particularly at</p> <p>P.T.O.</p>	<p>533.6.072 3b6b</p>
<p>AGARDograph 64 North Atlantic Treaty Organization, Advisory Group for Aeronautical Research and Development A REVIEW OF MEASUREMENTS ON AGARD CALIBRATION MODELS Editor: R. Hills (Pt.I: R. Hills; Pt.II: H. Valk and J.H. van der Zwaan; Pt.III: J.P. Hartzuiker; Pt.IV: H. Valk; Pt.V: R. Hills; Pt.VI: R. Hills) 1961 245 pages incl. 112 refs., 79 figs.</p> <p>An analysis has been made of measurements in various wind tunnels of AGARD Calibration Models A, B, C, D and E. The analysis has shown con- siderable scatter of results, particularly at</p> <p>P.T.O.</p>	<p>533.6.072 3b6b</p>	<p>AGARDograph 64 North Atlantic Treaty Organization, Advisory Group for Aeronautical Research and Development A REVIEW OF MEASUREMENTS ON AGARD CALIBRATION MODELS Editor: R. Hills (Pt.I: R. Hills; Pt.II: H. Valk and J.H. van der Zwaan; Pt.III: J.P. Hartzuiker; Pt.IV: H. Valk; Pt.V: R. Hills; Pt.VI: R. Hills) 1961 245 pages incl. 112 refs., 79 figs.</p> <p>An analysis has been made of measurements in various wind tunnels of AGARD Calibration Models A, B, C, D and E. The analysis has shown con- siderable scatter of results, particularly at</p> <p>P.T.O.</p>	<p>533.6.072 3b6b</p>

<p>transonic speeds, on Models B and C. When transition is fixed on the models, scatter is reduced and, where possible, reference curves are given to enable comparison to be made with any future tests.</p> <p>This is one of a series of Wind Tunnel AGARDographs concerned with wind tunnel design, operation, and test techniques. Professor Wilbur C. Nelson of the University of Michigan is the editor of the Series.</p>	<p>transonic speeds, on Models B and C. When transition is fixed on the models, scatter is reduced and, where possible, reference curves are given to enable comparison to be made with any future tests.</p> <p>This is one of a series of Wind Tunnel AGARDographs concerned with wind tunnel design, operation, and test techniques. Professor Wilbur C. Nelson of the University of Michigan is the editor of the Series.</p>
<p>transonic speeds, on Models B and C. When transition is fixed on the models, scatter is reduced and, where possible, reference curves are given to enable comparison to be made with any future tests.</p> <p>This is one of a series of Wind Tunnel AGARDographs concerned with wind tunnel design, operation, and test techniques. Professor Wilbur C. Nelson of the University of Michigan is the editor of the Series.</p>	<p>transonic speeds, on Models B and C. When transition is fixed on the models, scatter is reduced and, where possible, reference curves are given to enable comparison to be made with any future tests.</p> <p>This is one of a series of Wind Tunnel AGARDographs concerned with wind tunnel design, operation, and test techniques. Professor Wilbur C. Nelson of the University of Michigan is the editor of the Series.</p>

NORWAY NORVEGE	Mr. O. Blichner Norwegian Defence Research Establishment Kjeller per Lilleström
PORTUGAL	Col. J.A. de Almeida Viana (Delegado Nacional do 'AGARD') Direcção do Serviço de Material da F.A. Rua da Escola Politecnica, 42 Lisboa
TURKEY TURQUIE	Ministry of National Defence Ankara Attn. AGARD National Delegate
UNITED KINGDOM ROYAUME UNI	Ministry of Aviation T.I.L., Room 008A First Avenue House High Holborn London W.C.1
UNITED STATES ETATS UNIS	National Aeronautics and Space Administration (NASA) 1520 H Street, N.W. Washington 25, D.C.



Printed by Technical Editing and Reproduction Ltd
95 Great Portland St. London, W.1.